



HAL
open science

Hydrogen-rich syngas from steam gasification of cellulose in a biorefinery approach

Majd Elsaddik

► **To cite this version:**

Majd Elsaddik. Hydrogen-rich syngas from steam gasification of cellulose in a biorefinery approach. Chemical and Process Engineering. Ecole des Mines d'Albi-Carmaux, 2022. English. NNT : 2022EMAC0016 . tel-04368491

HAL Id: tel-04368491

<https://theses.hal.science/tel-04368491v1>

Submitted on 1 Jan 2024

HAL is a multi-disciplinary open access archive for the deposit and dissemination of scientific research documents, whether they are published or not. The documents may come from teaching and research institutions in France or abroad, or from public or private research centers.

L'archive ouverte pluridisciplinaire **HAL**, est destinée au dépôt et à la diffusion de documents scientifiques de niveau recherche, publiés ou non, émanant des établissements d'enseignement et de recherche français ou étrangers, des laboratoires publics ou privés.

Université Fédérale



Toulouse Midi-Pyrénées

THÈSE

en vue de l'obtention du

DOCTORAT DE L'UNIVERSITÉ DE TOULOUSE

délivré par

IMT – École Nationale Supérieure des Mines d'Albi-Carmaux

présentée et soutenue par

Majd ELSADDIK

le 8 décembre 2022

Hydrogen-rich syngas from steam gasification of cellulose in a biorefinery approach

École doctorale et discipline ou spécialité :

MEGEP : Génie des Procédés et de l'Environnement

Unité de recherche :

Centre RAPSODEE, UMR CNRS 5302, IMT Mines Albi

Directeur de thèse :

Ange NZIHOU, Professeur, IMT Mines Albi

Autres membres du jury :

Laurence LECOQ, Professeure, IMT Atlantique, *Présidente*

Anne-Cécile ROGER, Professeur, Université de Strasbourg, *Rapporteuse*

Marco CASTALDI, Professeur, The City College of New York, *Rapporteur*

Maïté HURON, Responsable R&D, ETIA, *Examinatrice*

Guo-Hua DELMAS, Directeur scientifique, BioEB, *Examinateur*

Michel DELMAS, Professeur, Université de Toulouse, *Invité*

Acknowledgments

Ce travail a pu voir le jour grâce à des personnes à qui je souhaite ici rendre hommage et exprimer ma profonde gratitude.

Je voudrais tout d'abord remercier la Région Occitanie et BioEB d'avoir financé cette thèse de doctorat.

Mes remerciements les plus sincères et les plus distingués vont à mon directeur de thèse, Ange Nzihou. Il a toujours été à l'écoute de mes fréquentes questions et s'est toujours intéressé à l'avancée de mes travaux. Son attention méticuleuse et ses précieux conseils m'ont sans aucun doute permis d'enrichir considérablement mon travail et de préciser mes propos.

Les travaux présentés ont également pu être effectués grâce à la participation de la société BioEB, représentée à qui je souhaite exprimer ma profonde gratitude pour leurs apports sur le plan scientifique et technique. Je remercie chaleureusement Michel et Guo-Hua Delmas pour leur précieuse expertise en chimie végétale et pour les agréables discussions que nous avons partagées ensemble.

Pour l'honneur qu'ils m'ont fait en acceptant d'être rapporteurs de ce travail de recherche, je remercie Anne-Cécile Roger et Marco Castaldi . Je remercie également la présidente Laurence Lecoq et Maïté Huron pour l'intérêt qu'ils ont porté à mes travaux en les examinant et de participer au jury.

J'adresse aussi mes remerciements à l'ensemble des techniciens, enseignants-chercheurs et assistantes du centre RAPSODEE notamment ceux avec qui j'ai eu l'occasion de travailler et partager des bons moments. Céline, je te remercie pour ta disponibilité et ton aide dans les tests ATG. Je remercie également ta famille pour votre présence et vos encouragements. Merci à Louise pour son aide dans les analyses GC-MS et Karl Fischer. Mickaël et Pierre, merci de m'avoir aidé à résoudre les problèmes techniques du montage expérimentale aussi pour les discussions que nous avons eu dans la halle.

Je voudrais remercier particulièrement Maria Gonzalez Martinez pour sa contribution et son encouragement. C'était un grand plaisir de travailler et de rédiger la revue avec toi. Je remercie également F. Javier Escudero Sanz pour son aide concernant l'établissement du bilan matière du procédé de pyrogazéification. Je tiens également à remercier Fabienne Espitalier pour sa gentillesse et sa grande aide sur la partie simulation. Un grand

Acknowledgments

merci à Paul Gaborit pour son aide précieuse sur LaTeX. Je remercie les assistantes du laboratoire, Valérie et Chrtystel pour leur sympathie et leur aide dans la résolution des problèmes administratifs. Je désire grandement remercier les doctorants et les post-doc/ingénieurs de RAPSODEE pour la bonne ambiance de travail mais également pour les nombreux bons moments passés ensemble. Je souhaite remercier spécialement Lina et Séverin pour toute l'aide qu'ils ont su m'apporter.

Par ailleurs, je tiens également à adresser mes sincères remerciements à mes amis pour leur soutien durant ces trois années. Merci Lisa, Thomas, Elie et Asaad pour votre présence vos encouragements.

Pour ma sœur Chiraz et mon beau-frère Teseer qui m'ont apporté leur soutien moral et leur dévouement, je les en remercie sincèrement.

Pour son soutien inestimable depuis toutes ces années, je pense énormément à ma mère, à qui je souhaite dédier mon travail.

Pour clore ce préambule, mes remerciements affectueux vont aussi à mon père et mon frère dont leurs encouragements ont contribué à l'aboutissement de mes travaux.

Contents

<i>Acknowledgments</i>	iii
<i>Contents</i>	v
<hr/>	
French extended abstract / Résumé Long	1
Introduction	11
1 Literature review	19
1.1 Lignocellulosic biomass	20
Composition and structure	20
1.2 Biomass fractionation for a biomass-based biorefinery	23
1.2.1 Sulfur-bearing pulping	24
1.2.2 Sulfur-free pulping	25
1.3 Pyrogasification process of lignocellulosic materials	27
1.3.1 Pyrolysis	28
1.3.2 Gasification	29
1.3.3 Pyrogasification products	30
1.3.4 Pyrogasification technologies	32
1.4 Pyrogasification of biomass components	37
1.4.1 Pyrolysis	37
1.4.2 Gasification	39
1.4.3 Partial conclusion	42
1.5 Syngas cleaning and conditioning towards hydrogen applications	44
1.5.1 Syngas application and cleaning	44
1.5.2 Renewable hydrogen production	45
1.6 Motivation and objective of the study	50
2 Materials and Experimental Methods	53
2.1 Materials	54
2.2 Properties Characterization	54
2.2.1 Proximate and ultimate analysis	54
2.2.2 Macromolecular composition	56
2.2.3 Inorganic composition: quantitative analysis	57
2.3 Biomass pretreatment using LEEBIO process	58
2.3.1 Biomass pretreatment	58
2.3.2 Lab-scale pretreatment	58
2.3.3 Pilot scale pretreatment	60
2.3.4 Effectiveness of LEEBIO treatment	61
2.4 Pyrolysis and gasification behaviors and kinetics	63
2.4.1 Pyrolysis in TGA	63

2.4.2	Steam gasification in TGA	63
2.5	Lab scale fixed bed pyrogasification	65
2.5.1	Experimental setup	65
2.5.2	Experimental conditions and program	66
2.5.3	Pyrolysis products	66
2.5.4	Products quantification and analysis in steam gasification of char	70
3	Lignocellulosic biomass fractionation using LEEBIO technology	71
3.1	Introduction	71
3.2	Results and discussion	72
3.2.1	Optimization of pulping time at lab-scale	72
3.2.2	Acid treatment assessment	74
3.2.3	Effect of acid treatment on the inorganic composition	76
3.2.4	Validation of LEEBIO treatment at Pilot Scale	76
3.2.5	Alkaline treated pulp	80
3.3	Conclusion	81
4	Thermal degradation of LEEBIO cellulose pulp: effect of the composition and kinetics	83
4.1	Introduction	83
4.2	Kinetic analysis approach	84
4.3	Results and discussion	88
4.3.1	Pyrolysis characteristics	88
4.3.2	Fraser–Suzuki deconvolution and isoconversional kinetic study	91
4.4	Conclusion	99
	Appendix	101
5	TGA steam gasification of cellulose pulp biochar	103
5.1	Introduction	103
5.2	kinetic analysis approach	105
5.3	Results and discussion	106
5.3.1	Influence of the inorganic content on the cellulose pulp biochar reactivity	106
5.3.2	Gasification kinetics analysis	112
5.3.3	Kinetic model accuracy	117
5.3.4	Effect of silica elimination on biochar reactivity	119
5.4	Conclusion	120
6	Pyrogasification: pyrolysis and steam gasification of biochar	123
6.1	Introduction	123
6.2	Pyrolysis of cellulose: product distribution and characterization	124
6.2.1	Product distribution and gas composition	124
6.2.2	Characterization of the liquid products	125
6.3	Steam gasification of pyrolysis-derived biochar	127
6.3.1	Effect of steam/char ratio	130
6.3.2	Effect of Temperature	133
6.3.3	Effect of inorganic matter	136
6.4	Conclusion and perspectives	140
6.4.1	Conclusion	140
6.4.2	Hydrogen rich-gas production potential	141

7 Hydrogen production from steam gasification in a biorefinery approach: process assessment and heat integration	151
7.1 Introduction	151
7.2 Aspen Plus model development	152
7.2.1 Conceptual design	152
7.2.2 Methodology	153
7.2.3 Aspen Flowsheet and model description	153
7.2.4 Pinch analysis	159
7.3 Results and discussions	160
7.3.1 Char gasification: model validation and sensitivity analysis	160
7.3.2 Global material balance	162
7.3.3 Analysis of energy balance	164
7.4 Pinch analysis and heat integration	164
7.5 Conclusion	168
Conclusions and perspectives	169
Conclusions	169
Perspectives	171
<hr/>	
<i>List of Figures</i>	173
<i>List of Tables</i>	177
<i>Bibliography</i>	181
<i>Glossary</i>	211

French extended abstract / Résumé Long

L'Accord de Paris de 2015 a fixé un objectif de limitation du réchauffement climatique en dessous de 2 °C, et de poursuite des efforts pour le limiter à 1,5 °C. Pour atteindre cet objectif de température à long terme, les pays souhaitent parvenir à la neutralité carbone d'ici le milieu du siècle. Cependant, les émissions mondiales de gaz à effet de serre étant le principal facteur de réchauffement de la planète, elles sont actuellement loin d'atteindre l'objectif de 1,5 °C. Selon l'Agence internationale de l'énergie (AIE), les émissions mondiales de dioxyde de carbone liées à l'énergie ont rebondi de 6 % en 2021 pour atteindre le niveau annuel le plus élevé jamais enregistré. Elles ont été estimées à 34,9 $GtCO_2$ dont les combustibles fossiles représentent la part prédominante (IEA, 2021).

Il existe un consensus mondial sur le fait que la transition énergétique est essentielle pour atteindre l'objectif de température à long terme de l'accord de Paris. Dans son rapport annuel sur la transformation énergétique, l'Agence internationale pour les énergies renouvelables (IRENA) (IRENA, 2018) a déclaré :

- L'efficacité énergétique et les énergies renouvelables sont les principaux piliers de la transition énergétique;
- L'énergie renouvelable doit être développée massivement et plus rapidement;
- L'hydrogène produit à partir de ressources renouvelables pourrait être un levier essentiel de la transition énergétique.

Les sources d'énergie renouvelables comprennent l'énergie hydraulique, éolienne, solaire, géothermique et la biomasse. Le marché des systèmes d'énergie photovoltaïque et éolienne a joué un rôle clé dans le passage à la croissance verte par la production d'hydrogène vert. Pour ce faire, des électrolyseurs sont utilisés en utilisant de l'électricité et de l'eau renouvelables comme intrants. Cependant, la nature stochastique et intermittente de ces systèmes énergétiques constitue le principal défi pour un approvisionnement énergétique sûr et stable. En outre, l'hydrogène issu de l'électrolyse de l'eau ne permet pas de

répondre à la totalité de la demande d'hydrogène renouvelable. L'hydrogène issu de la biomasse pourrait potentiellement compléter l'électrolyse.

La biomasse est définie comme l'énergie dérivée de toute matière organique provenant de plantes et d'animaux. On considère qu'elle est disponible sur une base renouvelable ou récurrente puisqu'elle est créée par la conversion de l'eau atmosphérique et de l'énergie solaire par photosynthèse (Demirbaş, 2001). En 2021, le potentiel d'approvisionnement mondial en biomasse a été estimé à environ 100 EJ y^{-1} , ce qui représente 10% de l'approvisionnement énergétique mondial et 13% de l'énergie, et équivaut à la production totale d'énergie à partir de ressources renouvelables (Popp *et al.*, 2021).

La conversion de la biomasse en hydrogène peut être réalisée principalement par deux méthodes : la conversion biochimique et la conversion thermochimique. Lors de la conversion biochimique, les molécules de biomasse sont dégradées en molécules plus petites par l'activité des bactéries et des enzymes (Hongzhang Chen *et al.*, 2016). La principale technologie de conversion biochimique est la fermentation (rendement : 60–80 %) en plus de la digestion (anaérobie et aérobie) et de l'hydrolyse (acide). Cependant, l'échelle de développement de la production biologique d'hydrogène est encore faible (TRL 4).

La conversion thermochimique consiste à décomposer la biomasse en énergie directe ou en combustibles au moyen de la chaleur, avec ou sans oxydant. Les voies thermochimiques comprennent : la combustion directe (incinération), la torréfaction, la pyrolyse, la gazéification et le reformage. Les technologies thermochimiques comprennent les procédés hydrothermiques, à savoir la liquéfaction, la gazéification hydrothermale et la carbonisation hydrothermale. La gazéification et la pyrolyse présentent de nombreux avantages par rapport à la combustion. Les substrats de biomasse sont convertis par ces deux procédés non seulement en électricité, mais aussi en biocarburants liquides et gazeux et autres produits chimiques. Le processus de gazéification de base implique une pyrolyse, d'où le nom de "pyrogazéification" donné à cette technologie.

La pyrogazéification désigne le processus de décomposition des matières premières par oxydation partielle (air, vapeur, oxygène) pour obtenir des produits gazeux. Ces derniers, appelés gaz de synthèse, sont des vecteurs énergétiques composés de H_2 , CO , et de quantités abrégées de CO_2 , CH_4 et N_2 . Le gaz de synthèse peut être traité dans différentes étapes en aval de nettoyage et de purification pour éliminer les contaminants. Le produit de sortie final fournit le gaz hydrogène final.

Pour la production d'hydrogène, la gazéification de la biomasse est considérée comme une méthode potentielle, offrant des incitations exceptionnelles (Long *et al.*, 2013; Parthasarathy *et al.*, 2014) :

- Contrairement aux combustibles fossiles, la biomasse est une ressource naturelle mondialement et largement distribuée;

-
- La biomasse est neutre en carbone, le CO₂ libéré est absorbé par les plantes au cours de leur cycle de vie;
 - Les combustibles issus de la biomasse peuvent s'intégrer dans l'infrastructure existante de conversion des combustibles fossiles,
 - Par rapport aux voies biologiques, la gazéification de la biomasse est considérée comme plus efficace en termes de rendement et de coût de l'hydrogène, ainsi que de complexité du processus (Yadav *et al.*, 2021);
 - Le gaz de synthèse et l'hydrogène peuvent être utilisés dans un large éventail d'applications.

Néanmoins, la gazéification de la biomasse n'est toujours pas en mesure de produire de l'hydrogène à l'échelle industrielle à un prix compétitif. Des contraintes techniques, économiques et inhérentes rendent le processus non rentable et entravent la pénétration du marché. Outre la disponibilité saisonnière, d'autres problèmes doivent être soulignés dans la gazéification de la biomasse :

- Une part importante des coûts de production du gaz de synthèse est imputable au nettoyage et au conditionnement (Richardson *et al.*, 2012). Diverses substances indésirables sont générées, notamment du NO_x, du SO₂ et du goudron, qui entraînent des problèmes opérationnels et l'encrassement des équipements de traitement en aval;
- Le coût de la matière première représente 20 à 40 % du coût de production de l'hydrogène (Yukesh Kannah *et al.*, 2021);
- L'hétérogénéité de la matière première entraîne des différences dans la distribution et les propriétés des produits, ce qui complique les performances du processus.

Parallèlement au potentiel de développement de la gazéification de la biomasse pour la production de bioénergie, d'électricité et de carburants, les bioraffineries ont été perçues comme une solution prometteuse pour remplacer les raffineries de pétrole et réduire la dépendance aux combustibles fossiles dans différents domaines de production (Lersch, 2009).

Plusieurs définitions de la bioraffinerie ont été formulées au cours des dernières décennies. Selon l'Agence internationale de l'énergie (IEA), une bioraffinerie est conçue comme "la transformation durable de la biomasse en une gamme de produits commercialisables et en énergie" (Jong *et al.*, 2011). Ces produits comprennent des produits chimiques, des plastiques, des fibres et des biocarburants d'origine biologique. Les procédés chimiques utilisés dans l'industrie de la pâte et du papier sont traditionnellement utilisés pour

séparer les composants de la biomasse. Ces procédés présentent de sérieux inconvénients tels que la production de lignine contenant du soufre, ce qui limite leur application commerciale, ainsi que l'impact sur la pollution de l'air et de l'eau. Une approche plus prometteuse pour fractionner la biomasse est offerte par le procédé organosolv. Ce nouveau procédé de prétraitement fait appel à des solvants organiques/verts pour séparer la biomasse qui peut être convertie en produits biologiques de valeur. En raison de ses avantages inhérents, tels que la grande pureté des coproduits et la récupération des solvants, le prétraitement par organosolv peut être une force motrice pour établir des bioraffineries commerciales. Malgré son énorme potentiel, les procédés organosolv ne sont pas encore compétitifs en raison de la consommation d'énergie élevée pour le prétraitement et la récupération des solvants, ainsi que du coût élevé de ces derniers. Par conséquent, le développement d'un procédé organosolv opérant sous des conditions opératoires modérées ainsi qu'une récupération efficace des solvants sont les domaines de recherche recommandés pour la création de bioraffineries industrielles à base d'organosolv (Borand *et al.*, 2018).

Compte tenu du potentiel de la technologie de gazéification et du prétraitement des organosolv, il est intéressant de coupler les deux procédés dans un concept de bioraffinerie. Compte tenu d'un aperçu global du contexte énergétique et des défis de la production d'hydrogène à partir de la biomasse, cette thèse aborde le sujet de recherche de la production de gaz de synthèse riche en hydrogène à partir de la gazéification à la vapeur d'eau de la pâte de cellulose dans une approche de bioraffinerie. La principale nouveauté de ce travail réside dans le traitement en aval de la biomasse lignocellulosique à l'aide d'un procédé organosolv non dégradant et à faible consommation d'énergie et de solvants. Le procédé est basé sur la séparation chimique des résidus lignocellulosiques en cellulose, lignine, hémicelluloses et silice. Ce procédé utilise exclusivement de l'acide formique en dessous du point d'ébullition de l'eau et à la pression atmosphérique. Deux résidus de biomasse différents sont soumis à ce traitement. La performance du traitement est évaluée en termes de composition chimique de la pâte ainsi que de la teneur en espèces inorganiques qui peuvent être des précurseurs de contaminants dans le gaz de synthèse. Une approche de mise à l'échelle est réalisée pour le prétraitement de la biomasse à l'échelle laboratoire jusqu'à l'échelle pilote. La pyrogazéification de la pâte obtenue est étudiée à l'aide d'une analyse thermogravimétrique et d'un réacteur fixe à l'échelle du laboratoire, et les approches de cinétique et de rendement des produits, respectivement. **L'objectif ultime est d'intégrer la gazéification avec le prétraitement organosolv pour développer des bioraffineries autosuffisantes en énergie et économiquement viables.** La présente thèse se compose de sept chapitres divisés en sections.

Chapitre 1. Revue bibliographique

Ce chapitre a pour objectif de fournir une revue de la littérature permettant de mieux

comprendre ce travail de recherche. Tout d'abord, un historique de la biomasse lignocellulosique est présenté dans la section 1.1.

Ensuite, les méthodes de prétraitement chimique de la biomasse sont décrites dans section 1.2. Les deux catégories principales du fractionnement chimique de la biomasse sont présentées en mettant l'accent sur les procédés sans soufre notamment les traitements organosolv.

La section 1.3 intègre une description du procédé de pyrogazéification et les technologies de production à la vapeur d'eau. En outre du principe, des étapes et des réactions, les technologies de de pyrogazéification sont présentées. Dans ce travail, les procédés de pyrogazéification sont regroupés en deux types principaux : les gazéificateurs à une étape et les procédés multi-étagés notamment ceux qui sont consistant en des réacteurs séparés physiquement.

La section 1.4 présente l'état de l'art de la gazéification des constituants de la biomasse en mettant l'accent sur la production d'hydrogène. L'attention est portée sur la gazéification de la cellulose, les paramètres de fonctionnement et la production d'hydrogène.

Après, les applications du gaz de synthèse et les technologies d'épuration en vue de la production d'hydrogène sont présentées. Les technologies d'épuration du gaz de synthèse tel que le craquage thermique, l'adsorption et la séparation physique sont décrites. Ensuite, l'étape de water-gas-shift et de purification PSA (Pressure Swing Adsorption) sont présentées.

Traduit avec www.DeepL.com/Translator (version gratuite)

Enfin, la motivation et l'objectif de l'étude sont clairement définis.

Chapitre 2. Matériel et Méthodes

Ce chapitre fournit des détails sur le matériel et les méthodes expérimentales appliqués dans ce travail. Tout d'abord, les résidus lignocellulosiques sélectionnés, la paille de blé et la sciure de bois résineux ainsi que les techniques d'analyses de caractéristiques physico-chimiques sont soulignés dans 2.1 & 2.2.

Dans la section 2.3, le protocole expérimental de prétraitement de la biomasse par le procédé **LEEBIO** à différentes échelles, laboratoire et pilote, est présenté. Des tests à l'échelle du laboratoire ont d'abord été réalisés pour évaluer le traitement **LEEBIOTM** en utilisant différents résidus de biomasse et optimiser le temps de réaction. À la lumière des résultats obtenus, une opération à l'échelle pilote a été réalisée dans une approche de mise à l'échelle.

Par la suite, la section 2.4 décrit la procédure expérimentale d'analyse thermogravimétrique de la pyrolyse et de la gazéification. Pour la pyrolyse, une approche non-isotherme sous atmosphère inerte a été utilisée. Les tests ont été réalisés sous atmosphère

d'azote à différentes vitesses de chauffage de 2, 5 et 10 °C min⁻¹. Pour la gazéification, une approche isotherme a été menée. Le chauffage a été effectué à une vitesse constante jusqu'à la température de gazéification (750, 800 et 900 °C). Puis, l'atmosphère est passée à un mélange (N₂ + H₂O). Un test à blanc a été réalisé pour chaque condition expérimentale afin de supprimer. Pour chaque condition expérimentale, la répétabilité a été considérée comme satisfaisante, l'écart-type calculé de la perte de masse étant inférieur à 2%.

Pour la production du syngaz riche en hydrogène, le dispositif expérimental de pyrogazéification à la vapeur d'eau à l'échelle du laboratoire est décrit dans 2.5. Les tests de pyrogazéification du biochar ont été réalisés dans un réacteur à lit fixe semi-continu. Le procédé a été divisé en 2 étapes : dévolatilisation (ou pyrolyse) et gazéification du biochar. Les matières volatiles et le biochar sont produits dans l'étape de pyrolyse. Les matières volatiles ont été retirées du réacteur et ne sont pas prises en compte dans l'étape de gazéification. Le biochar obtenu a ensuite été gazéifié sous atmosphère de vapeur d'eau. Les gaz non condensables ont été échantillonnés en amont du train de condensation. Le volume des gaz de combustion a également été mesuré à l'aide d'un compteur de gaz. Les gaz incondensables à la sortie du four sont collectés à l'aide de sacs d'échantillonnage et analysés avec un micro-chromatographe en phase gazeuse. Les condensables échantillonnés sont analysés d'une part pour mesurer la teneur en eau, et d'autre part pour identifier et quantifier les composés organiques.

Chapitre 3. Séparation de la biomasse lignocellulosique par la technologie LEEBIO : du laboratoire à l'échelle pilote

Par conséquent, ce chapitre étudie le fractionnement de la paille de blé (WS) et de la sciure de résineux (SS) en utilisant le procédé LEEBIO. L'objectif ultime est d'obtenir une pâte de cellulose soumise à la pyrogazéification.

Dans une première série d'expériences, l'optimisation des conditions de traitement en termes de temps de réaction a été étudiée. L'impact des caractéristiques des matières premières sur les performances de fractionnement et l'effet de la mise en pâte acide sur la composition inorganique ont ensuite été abordés. Une autre étude a été entreprise à l'échelle pilote, en utilisant des SS, pour valider la technologie de fractionnement. Un bilan massique du procédé a ensuite été établi. Le but ultime est de préparer la pâte de cellulose qui sera soumise à la pyrogazéification.

La vitesse maximale de délignification des deux biomasses par de l'acide formique à 85 % en poids a été pratiquement achevée après près de 180 min. Les hémicelluloses ont été efficacement éliminées des deux matières premières. La lignine résiduelle de la sciure était relativement plus élevée en raison de la structure cellulaire du bois et du schéma de réaction de la mise en pâte. Des différences majeures dans la composition chimique entre la pâte et les matières premières ont été observées. La plupart des

éléments inorganiques notamment les métaux alcalins et alcalino-terreux (AAEM), ont été dissous tandis que le Si a été retenu dans la pâte résultante, précisément dans les cellules épidermiques.

La validation du procédé à l'échelle pilote, avec un facteur d'échelle de 1000, en réduisant en pâte de la sciure de bois résineux a donné lieu à des caractéristiques de pâte moléculaire similaires à l'échelle du laboratoire en termes de rendement en pâte, d'élimination de la lignine et des hémicelluloses ainsi que de composition minérale. Une étape supplémentaire de traitement alcalin de la pâte à l'échelle pilote a été réalisée avec succès pour éliminer le Si avec un taux d'élimination de 65 %.

Chapitre 4. Dégradation thermique de la cellulose LEEBIO : effet de la composition et de la cinétique

Ce chapitre a pour but de discuter de la dégradation thermique de la pâte extraite à l'aide de la TGA. D'abord, les caractéristiques de décomposition de la pâte en particulier l'effet de la composition. Ensuite, l'analyse cinétique non isotherme de la pâte de cellulose, selon un schéma de réaction parallèle, a été présenté. La méthode de Fraser-Suzuki a été adoptée pour déconvoluer les courbes TGA, suivie d'une procédure d'isoconversion intégrale et de la méthode "generalized master plots method".

Les premiers résultats ont montré que le comportement de décomposition thermique de la cellulose était significativement influencé par la composition. Une corrélation réussie a été obtenue entre les caractéristiques de dégradation thermique et les teneurs en composants. La température de dégradation a été déplacée vers des valeurs plus élevées avec l'augmentation de la teneur en lignine. Le taux de dévolatilisation augmentait avec la teneur en cellulose. L'effet du taux de chauffage sur le comportement thermique des échantillons a également été présenté. Les résultats montrent que la courbe TG et les températures maximales des courbes $d\alpha/dT$ se déplacent vers des températures plus élevées avec l'augmentation de la vitesse de chauffage. En outre, la hauteur du pic des courbes $d\alpha/dT$ la hauteur du pic des courbes $d\alpha/dT$ diminue avec l'augmentation de la vitesse de chauffe.

Une approche combinant la fonction de Fraser-Suzuki, la méthode d'isoconversion intégrale et la procédure des graphiques maîtres généralisés a été appliquée pour déterminer les paramètres cinétiques apparents. L'énergie d'activation s'est avérée être constante tout au long de la conversion. Les modèles "accélérateurs" tels que le mécanisme de nucléation et de croissance et la scission de chaîne ont pu décrire avec précision le comportement. Ces modèles ont été utilisés pour reconstruire les courbes expérimentales et la déviation était inférieure à 3,5 %.

Les résultats obtenus peuvent fournir des informations utiles pour la conception et la mise à l'échelle du réacteur pour la pyrolyse de la cellulose.

Chapitre 5. Gazéification à la vapeur d'eau de cellulose LEEBIO : analyse cinétique en mettant l'accent sur le rôle du silicium

Ce chapitre se concentre sur l'analyse de la cinétique de gazéification à la vapeur d'eau des chars de cellulose LEEBIO et de biomasse à travers une analyse thermogravimétrique isotherme. Une analyse de sensibilité sur la température de réaction et la pression partielle de la vapeur d'eau est réalisée.

Les résultats de la gazéification à la vapeur d'eau TGA ont révélé que la réactivité du biochar issu de la cellulose était 3 fois plus faible que celle du biochar issu de la biomasse brute, en raison de la différence de contenu inorganique, en particulier, AAEM et Si. La gazéification du biochar de cellulose a révélé l'effet négatif de Si ; la réactivité du biochar a diminué avec l'augmentation de la concentration de Si dans la cendre. Il est intéressant de noter que la structure morphologique a eu un impact à un faible taux de conversion, bien qu'elle ait été moins influente que la teneur en Si. Ainsi, un modèle cinétique pour décrire la cinétique de gazéification a été développé en utilisant la teneur en Si dans la cendre comme paramètre clé.

Une procédure basée sur les méthodes d'isoconversion et la méthode "generalized master plots method" est utilisée pour déterminer les paramètres cinétiques. Une nouvelle approche de modélisation basée sur la concentration en Si a été proposée pour prédire la cinétique de gazéification à la vapeur d'eau des biochars de la biomasse lignocellulosique et de la cellulose. Les données TGA et le modèle dérivé ont montré un accord satisfaisant. L'élimination des espèces Si par un lavage alcalin à base de NaOH a permis d'améliorer la gazéification du biochar de pâte de cellulose. Une réactivité plus élevée et un temps de réaction plus faible ont été observés pour la pâte lavée en milieu alcalin. Par conséquent, les résultats de la présente étude ont confirmé que la teneur en Si est un paramètre d'influence principal sur la cinétique du biochar.

Chapitre 6. Pyrogazéification : dévolatilisation et gazéification à la vapeur d'eau du biochar pour la production d'hydrogène

Dans ce chapitre, la pyrogazéification de la pâte à papier, de la sciure de résineux (SS) et de la cellulose kraft (ARC) a été étudiée dans un réacteur à lit fixe dans différentes conditions expérimentales.

Par rapport à la cellulose kraft, le rendement de la pyrolyse de la pâte de cellulose LEEBIO a été influencé par la lignine résiduelle, ce qui a donné lieu à une plus grande fraction de biochar et à des rendements plus élevés en H₂ et CH₄. À 750 °C, le rendement en bio-huile de la pyrolyse était supérieur à 50 %, ce qui peut être brûlé pour fournir de la chaleur aux étapes endothermiques du séchage et de la gazéification à la vapeur d'eau. Cet aspect a été développé en simulant le processus global couplant le prétraitement organosolv et la pyrogazéification de la pâte de cellulose.

Pour vérifier que le gaz est le seul produit dérivé de la gazéification du biochar et que l'étape de dévolatilisation est achevée, le bilan carbone des essais de gazéification est calculé. Les résultats confirment que le carbone contenu dans le biochar est converti en gaz non condensables, CO, CO₂, et CH₄. Cela confirme ainsi l'absence d'hydrocarbures et de goudrons dans les produits de la gazéification à la vapeur d'eau du biochar.

Traduit avec www.DeepL.com/Translator (version gratuite)

Les résultats de la gazéification à la vapeur d'eau du biochar ont montré l'effet de la température et du rapport vapeur d'eau/carbone sur les performances du procédé et la qualité du gaz. L'influence de ces paramètres sur la composition du gaz est décrite en termes de fractions et de ratios de gaz. En effet, $(H_2 + CH_4)/CO$, H_2/CO , H_2/CO_2 , CO/CO_2 , et H_2/CH_4 , sont sélectionnés comme indicateurs pour évaluer la qualité du gaz et son efficacité de production. Un rapport vapeur d'eau/carbone plus élevé a été bénéfique pour la qualité du gaz en augmentant le rapport H_2/CO par la promotion des réactions carbone-gaz et eau-gaz. La diminution de CO/CO_2 avec l'augmentation du rapport vapeur d'eau/carbone s'explique par la prédominance des réactions impliquant la vapeur d'eau sur la réaction de Boudouard. Le rendement en hydrogène a été amélioré en augmentant la température, ce qui a favorisé la réaction endothermique carbone-vapeur d'eau. Cependant, avec l'augmentation de la température, H_2/CO a été réduit en raison de la réaction inverse de déplacement de gaz vers l'eau tandis que H_2/CH_4 par la réactivité de la réaction de reformage du méthane à la vapeur.

Les résultats de l'essai de gazéification à 950 °C de la pâte de cellulose de LEEBIO ont montré un grand potentiel pour la production de gaz de synthèse riche en H₂ de haute qualité. On a obtenu un potentiel d'hydrogène et de H_2/CO de 52,9 g_{H₂} kg_{cellulose}⁻¹ et de 1,8, respectivement. Le rendement potentiel maximal en hydrogène obtenu dans cette étude correspond à 32 % du rendement théorique de la gazéification intégrale de la biomasse, ce qui équivaut à 166 g kg⁻¹ de matière première. Cette différence est attribuée à l'utilisation d'un schéma de gazéification en deux étages, où l'hydrogène n'est produit qu'à partir de la gazéification à la vapeur du biochar.

Les résultats ont démontré l'absence d'azote dans tout produit de gazéification du biochar de pâte à papier. En outre, les composés alcalins, en particulier le K, peuvent être capturés par la silice dans le solide, empêchant son chargement dans le gaz produit. En utilisant différents indices, les résultats montrent une faible tendance à l'encrassement et à l'agglomération pour la pâte de cellulose LEEBIO comparé à la biomasse brute. Par conséquent, la gazéification de la pâte de cellulose LEEBIO a montré un fort potentiel pour produire un gaz de synthèse plus propre.

Chapitre 7. Production d'hydrogène par la gazéification à la vapeur d'eau dans une approche de bioraffinerie : évaluation énergétique et intégration

de la chaleur

Ce chapitre est consacré à l'évaluation de la production d'hydrogène à partir de la pyrogazéification de la pâte à papier dans une approche de bioraffinerie intégrée. La technique d'intégration de la chaleur du procédé est réalisée à l'aide de la technique d'analyse Pinch. Le logiciel Aspen Plus V12 est utilisé à cette fin.

Le procédé est divisé en cinq étapes : traitement de la biomasse par la procédé LEEBIO, pyrogazéification, la réaction du gaz à l'eau, purification du H₂, et la combustion des volatiles de pyrolyse.

Une validation a été effectuée en comparant les résultats de la simulation et les données expérimentales à différentes conditions de fonctionnement. Une précision satisfaisante sur la composition et le rendement du gaz de synthèse a été obtenue à une température de gazéification de 950 °C.

Les résultats de la simulation ont montré que le prétraitement de la biomasse était l'étape du procédé qui demandait le plus d'énergie. L'analyse Pinch a montré que l'efficacité énergétique de la production d'hydrogène est fortement impactée par la consommation d'énergie de cette étape. Pour examiner l'impact du prétraitement de la biomasse sur l'efficacité du processus, l'efficacité de production de H₂ et la demande énergétique sont évaluées. Dans le cas du procédé global couplant le traitement de la biomasse et la pyrogazéification, le rendement énergétique de la production d'hydrogène et les besoins en énergie étaient respectivement de 26,5 % et 111,1 kWh kg_{H₂}⁻¹, respectivement. Ces valeurs se sont avérées inférieures aux valeurs rapportées pour les procédés de gazéification, qui vont de 35 à 65% et de 69 à 76 kWh kg_{H₂}⁻¹.

Une évaluation plus poussée en termes de récupération des solvants et des sous-produits ainsi qu'une analyse énergétique sont nécessaires pour améliorer la consommation d'énergie et réduire les besoins en services publics, rendant le procédé beaucoup plus compétitif.

Introduction

Energy is a foundation stone of socio-economic development and human well-being. It has a crucial role in the growth and survival of all living beings. Energy Safety and climate change tackling are the core elements of the current global energy landscape and policy. In 2021, 31.0% of the global marketed energy production came from fossil oil, 24.4% from coal, and 26.9% from natural gas. Of the 17.7% from low-carbon sources, renewables accounted for 13.5% and nuclear energy for 4.3% (bp, 2022). EIA (U.S. Energy Information Administration) projects a nearly 50% increase in world energy consumption by 2050 (Stephen Nalley *et al.*, 2021).

The Paris Agreement of 2015 set an objective to limit global warming below 2 °C and pursue efforts to limit it to 1.5 °C. To achieve this long-term temperature goal, countries aim to attain a climate-neutral world by mid-century. However, being the largest contributor to global warming, global greenhouse gas emissions are currently far to meet the 1.5 °C goal. According to the International Energy Agency (IEA), global energy-related carbon dioxide emissions rebounded by 6% in 2021 to reach their highest-ever annual level. They were estimated at 34.9 $GtCO_2$ of which fossil fuels account for the predominant share (IEA, 2021). These 2021 emissions used 8.7% of the remaining carbon budget to limit global warming to 1.5 °C, which would be used up in 9.5 years if current policy and technology trends continue (Z. Liu *et al.*, 2022).

There is a global consensus that energy transition holds key to achieving the Paris Agreement's long-term temperature goal. In their annual report on energy transformation, International Renewable Energy Agency (IRENA) (IRENA, 2018) stated:

- Energy efficiency and renewable energy are the main pillars of the energy transition;
- Renewable energy needs to be scaled up massively fast;
- Hydrogen from renewable resources has the potential to be a key driver of the energy transition.

Renewable sources of energy include hydro, wind, solar, geothermal, and biomass energy. The market of photovoltaic and wind energy systems has been playing a key role in the shift towards green growth through the production of green hydrogen. For this,

electrolysers are employed using renewable electrical power and water as inputs. However, the stochastic and intermittent nature of such energy systems is their main challenge for a safe and stable energy supply. In addition, hydrogen from water electrolysis cannot afford and cover the full demand for renewable hydrogen. Hydrogen from biomass could potentially supplement electrolysis.

Biomass is defined as the energy derived from any organic matter from plants and animals. It is considered to be available on a renewable or recurring basis since it is created by the conversion of atmospheric CO₂ water and sun energy through photosynthesis (Demirbaş, 2001). In 2021, global biomass supply potential was estimated at approximately 100 EJ y⁻¹ accounting for 10% of the global energy supply and 13% of energy, and equivalent to the total energy production from renewable resources (Popp *et al.*, 2021).

Biomass conversion into hydrogen can be mainly performed by two methods: biochemical conversion and thermochemical conversion. During biochemical conversion, biomass molecules are degraded into smaller molecules by the activity of bacteria and enzymes (Hongzhang Chen *et al.*, 2016). The main technology of biochemical conversion is fermentation (efficiency: 60–80 %) in addition to digestion (anaerobic and aerobic) and hydrolysis (acid). However, the scale of development of hydrogen biological production is still low (TRL 4).

The thermochemical conversion consists of biomass decomposition into direct energy or fuels employing heat with and without an oxidant. Thermochemical routes include: direct combustion (incineration), torrefaction, pyrolysis, gasification, and reforming. Thermochemical technologies include hydrothermal processes namely, liquefaction, hydrothermal gasification, and hydrothermal carbonization. A general presentation of thermochemical routes is illustrated in Figure 1. Gasification and pyrolysis have many advantages over combustion. Biomass substrates are converted via these two processes into not only electricity but also into liquid and gaseous biofuels and other chemicals. The basic gasification process involves pyrolysis, hence the technology is known as "pyrogasification".

Pyrogasification refers to the decomposition process of feedstocks by partial oxidation (air, steam, oxygen) to produce a gaseous product known as syngas. The latter is an energy carrier made of H₂, CO, and abbreviate amounts of CO₂, CH₄ and N₂. Syngas can be treated in different downstream steps of cleaning and purification to eliminate contaminants. The final output product delivers the final hydrogen gas.

Over the last decades, hydrogen production from biomass gasification has gained momentum. Web of Science Core Collection database was used to analyze the bibliometric data for the period between 2010 and 2022. The keywords searched in databases were ("biomass*" OR "biowaste*" OR "bioresource*") AND ("biofuel*" OR "Bioenergy*" OR "biogas" OR "syngas" OR "bio-oil"). Almost 45 000 research and conference papers were

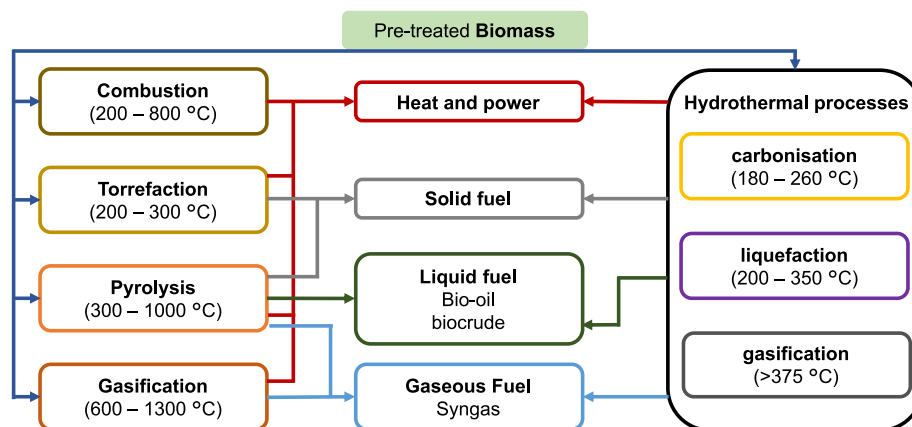


Figure 1: Thermochemical conversion pathways of biomass (Danso-Boateng *et al.*, 2022).

identified. VOSviewer software was used for the visualization of similarities by graphical mapping of the data. The analysis uses the co-occurrence of keywords in the title and abstract to generate Figure 2. Four clusters can be identified, denoted by different colors and by spatial groupings. Circles of the same color indicate a similar topic for these publications. As can be seen, the blue cluster focuses on thermochemical processes. Indeed, the keywords "hydrogen production" and "gasification" have similar strength. The distance between the two keywords reveals the strong link and topic similarity between both research areas.

As can be seen, different clusters of keywords are separated, among them, there is a cluster related to hydrogen production. Network connection visualizes that "hydrogen production" appears more frequently with "gasification", "pyrolysis" and "syngas production".

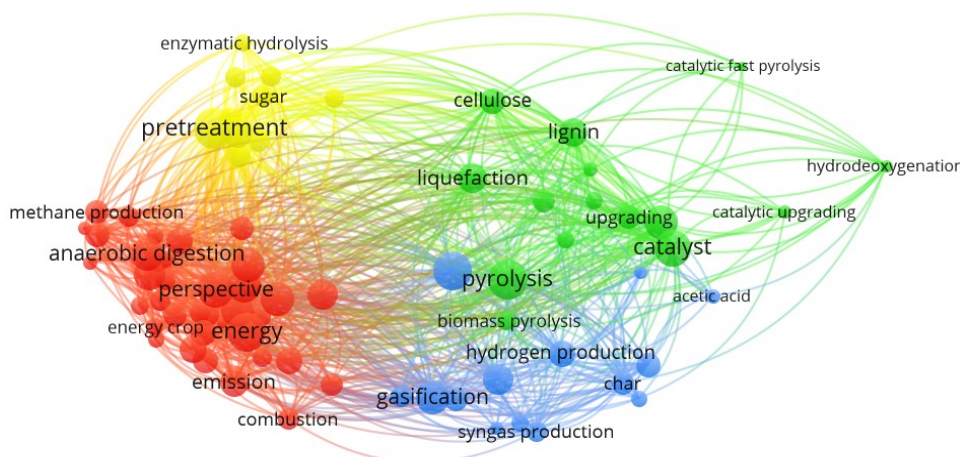


Figure 2: Co-occurrence map and link of the most frequent keywords in the title and abstract

For hydrogen production, biomass gasification is regarded as a potential method, offering outstanding incentives (Long *et al.*, 2013; Parthasarathy *et al.*, 2014) :

- Contrary to fossil fuels, biomass is a globally and widely distributed natural resource;
- Biomass is carbon neutral, the released CO₂ is absorbed by plants in the course of their life cycle;
- Biomass fuels can fit in the existing fossil fuels conversion infrastructure;
- Compared to biological routes, biomass gasification is believed to be more efficient in terms of hydrogen yield and cost as well as process complexity (Yadav *et al.*, 2021);
- Syngas and hydrogen can be used in a broad range of applications.

Nonetheless, biomass gasification is still unable to produce hydrogen on an industrial scale at a competitive price. Technical, economic, and inherent constraints make the process unprofitable and hinder market penetration. In addition to the seasonal availability, biomass gasification some other issues should be highlighted:

- A significant share of syngas production costs is accounted for by cleaning and conditioning (Richardson *et al.*, 2012). Different undesired co-products are generated including NO_x, SO₂ and tar which cause operational problems and fouling of downstream process equipment;
- The cost of the feedstock accounts for 20 to 40 % of hydrogen production cost (Yukesh Kannah *et al.*, 2021);
- The feedstock heterogeneity of yields to a difference in product distribution and properties, complicating the process performance.

Parallel to the potential of biomass gasification to expand in the production of bio energy, electricity, and fuels, biorefineries have been perceived as a promising solution to substitute petroleum refineries and reduce fossil fuels dependence in different area of production (Lersch, 2009).

Several definitions of biorefinery have been formulated over the past few decades. According to the international Agency of Energy (IEA), a biorefinery is intended as "the sustainable processing of biomass into a spectrum of marketable products and energy" (Jong *et al.*, 2011). These products include bio-based chemicals, plastics, fibers and bio-fuels.

Chemical processes used in the pulp and paper industry are conventionally used to separate biomass components. These processes have serious drawbacks such as the production of sulfur-containing lignin limiting its commercial application as well as the impact on air and water pollution. A more promising approach to fractionate biomass is offered by the organosolv process. This emerging pretreatment process involves organic/green solvents to separate biomass which can be converted into valuable bioproducts. Owing to its inherent advantages such as high-purity co-products and solvent recovery, organosolv pretreatment can be a driving force to establish commercial biorefineries. Despite their enormous potential, organosolv processes are not competitive yet due to high energy consumption for both pretreatment and solvent recovery in addition to the high cost of the solvent. Therefore, the development of low-temperature/atmospheric organosolv process as well as efficient solvent recovery are the recommended research areas for the creation of industrial organosolv-based biorefineries (Borand *et al.*, 2018).

Considering the potential of gasification technology and organosolv pretreatment, there is an interest in coupling both processes in a biorefinery concept.

Given a global overview of the energy context and the challenges of hydrogen production from biomass, this thesis tackles the research topic of hydrogen-rich syngas production from steam gasification of cellulose pulp in a biorefinery approach. The main novelty of the work lies in the downstream treatment of lignocellulosic biomass using non-degrading and low energy & solvent intensive organosolv process. The process is based on the chemical separation of lignocellulosic residues into cellulose, lignin, hemicelluloses, and silica. This process uses exclusively formic acid under mild conditions (below water boiling point, atmospheric pressure). Two different biomass residues are subjected to this treatment. The performance of the treatment is assessed in terms of pulp chemical composition as well as the content in inorganic species which can be contaminants precursors in syngas. A scaling-up approach is carried out for biomass pretreatment on a laboratory scale to a pilot scale. The pyrogasification of obtained pulp is investigated using thermogravimetric analysis and lab-scale fixed reactor to examine the kinetics and gasification performance, respectively. **The ultimate goal is coupling gasification with organosolv pretreatment to develop energy-self-sufficient and economically viable biorefineries.**

The present thesis consists of seven chapters divided into sections.

Chapter 1 is intended to provide a literature review. First of all, a background on lignocellulosic biomass is given. Then, the chemical pretreatment methods of biomass are described with a focus on organosolv processes. Next, the pyrogasification process, technologies, and state-of-the-art on pyrogasification of biomass constituents are reviewed with a focus on hydrogen production. Attention is given to cellulose gasification,

operating parameters, and hydrogen production. Finally, syngas applications and cleanup technologies for hydrogen production are presented.

Chapter 2 provides details on the material and experimental methods applied in this work. First, the selected lignocellulosic residues and the characterization techniques are outlined. The experimental protocol of biomass pretreatment using LEEBIO process is then presented. Next, the experimental procedures thermogravimetric analysis of pyrolysis and gasification are described. Finally, the lab-scale experimental setup of pyrogasification as well as product quantification and analysis methods are given.

Chapter 3 is dedicated to studying the organosolv treatment of biomass. The ultimate objective is to obtain cellulose pulp that is subjected to pyrogasification. The process optimization in terms of pulping time is investigated at the laboratory scale. The effects of the solvent on pulp composition and the process efficiency as well as on the mineral composition of the pulp are elucidated. A scaling-up approach for biomass pulping at a laboratory scale to a pilot scale was carried out.

Chapter 4 analyzes the thermal decomposition of cellulose pulps in an inert atmosphere using thermogravimetric analysis. The effect of the macromolecular composition of the pulp is investigated. A non-isothermal kinetic analysis of cellulose pulp is presented in a parallel-reaction scheme. A model-free, isoconversional method is used as a tool for providing apparent kinetic parameters.

Chapter 5 focuses on the analysis of steam gasification kinetics of pulp and biomass chars through an isothermal thermogravimetric analysis. A sensitivity analysis on the reaction temperature and steam partial pressure is performed. The main motives are to assess the gasification behavior of cellulose pulp and to predict its kinetic parameters with a focus on inorganic content. A combined isoconversional and generalized master plots procedure is employed to determine apparent kinetic parameters. A kinetic modeling approach based on the inorganic content is performed to predict char gasification.

Chapter 6 deals with the pyrogasification of cellulose pulp. The process is split into two steps: pyrolysis and char gasification. The effect of the macromolecular composition on pyrolysis characteristics in terms of product yield and composition is studied. Pyrolysis was followed by the steam gasification of biochar. The primary objective is to investigate the production of H₂-rich syngas from the pulp. The influence of the operating parameters such as steam flow rate, temperature, and the inorganic content is examined. The results of pulp gasification are compared with raw biomass and commercial kraft cellulose to assess the potential of the cellulose pulp as an energy source.

Chapter 7 is dedicated to mass and energy assessment of the global process for H₂ production. The process is designed in a concept of organosolv-based biorefinery coupled with pyrogasification. The process model consists of formic acid treatment,

pulp pyrogasification and, syngas upgrade and purification. The model is developed using the simulation software Aspen Plus (V12). Pinch analysis is applied to maximize internal energy recovery and analyze the energy integration possibilities.

Finally, the present work is rounded off with general conclusions, and insights are suggested for future research works to complete the current investigations.

1.1	Lignocellulosic biomass	20
	Composition and structure	20
1.2	Biomass fractionation for a biomass-based biorefinery	23
	1.2.1 Sulfur-bearing pulping	24
	1.2.2 Sulfur-free pulping	25
1.3	Pyrogasification process of lignocellulosic materials	27
	1.3.1 Pyrolysis	28
	1.3.2 Gasification	29
	1.3.3 Pyrogasification products	30
	1.3.4 Pyrogasification technologies	32
	Single-stage gasifiers	32
	Multi-stage gasifiers	34
1.4	Pyrogasification of biomass components	37
	1.4.1 Pyrolysis	37
	1.4.2 Gasification	39
	1.4.3 Partial conclusion	42
1.5	Syngas cleaning and conditioning towards hydrogen applications	44
	1.5.1 Syngas application and cleaning	44
	1.5.2 Renewable hydrogen production	45
1.6	Motivation and objective of the study	50

This chapter presents a literature review concerning the pyrogasification of lignocellulosic biomass and its constituents. The broad aspects of chemical pretreatment methods, used in biorefining are also presented. Therefore, the structure of this chapter is presented as follows:

- Section 1.1 presents lignocellulosic biomass in terms of types, composition, and structure.
- Section 1.2 gives a general description of integrated biorefineries. The chemical pretreatment methods are covered with an eye on organosolv treatment potential and challenges.
- Section 1.3 is dedicated to the description of the pyrogasification process in terms of steps, products, and technologies.
- Section 1.4 focuses on the pyrogasification of biomass single components. A state-of-the-art is reviewed with an emphasis on cellulose steam gasification.

- Section 1.5 gives insights on syngas applications and its value chain towards hydrogen production.
- Section 1.6 illustrates the motivation and objective of the study.

1.1 Lignocellulosic biomass

Biomass can be classified into different groups depending on its type and applications. Among plant-based materials that do not threaten the world food supply, lignocellulosic biomass is the most abundant and economical resource (Ephraim *et al.*, 2020a). It accounts for about 50 % of biomass on earth with a production rate of 200 billion tonnes a year (G.-H. Delmas *et al.*, 2021). It can be divided into woody and non-woody lignocellulosic biomass.

- Woody biomass can be classified into softwood and hardwood. The main difference between the two categories is the presence of pores or vessels that exist in hardwood which has a more complex cellular structure (Brandt *et al.*, 2013).
- Non-woody biomass includes mainly herbaceous biomass and agricultural residues such as straws of grain crops and processing residues such as husks and bagasse.

Physical properties and chemical composition are the major differences between the two categories.

Composition and structure

Lignocellulosic biomass consists mainly of organic compounds that contain carbon (C), oxygen (O), hydrogen (H) also nitrogen (N), sulfur (S) and chlorine (Cl) at lower extend. Besides the elemental composition, lignocellulosic biomass has a polymeric structure of an integrated network of three structural constituents:

Cellulose

Cellulose is the major constituent, comprising 50 % of dry biomass. Considered to be the skeleton of the cell wall, cellulose is a linear polysaccharide made of a long chain of glucose units. Cellulose from different biomass species is undifferentiable since it has the same molecular structure. The chemical formula can be expressed as $(C_6H_{10}O_5)_n$. The minor differences lie in the degree of polymerization and degree of crystallinity.

Hemicelluloses

Hemicelluloses are amorphous and branched hetero-polysaccharides that are distributed in the cell wall as a linking material. The polysaccharides are formed from sugar monomers such as glucose and xylose. Unlike cellulose, hemicellulose structure is heterogeneous within lignocellulosic terrestrial plants.

Table 1.1: Composition of different lignocellulosic biomass: macromolecules content (Baruah *et al.*, 2018; Ephraim *et al.*, 2020a; Hernández-Beltrán *et al.*, 2019; Howard *et al.*, 2003; Khalid *et al.*, 2017; Timilsina *et al.*, 2010) and elemental composition (Vassilev *et al.*, 2010)

	Softwood	Hardwood	Straws	Grasses
Composition dry basis (wt.%, dry basis)				
Cellulose	45 – 50	40 – 55	30 – 47	25 – 45
Hemicellulose	25 – 35	24 – 40	19 – 50	5 – 50
Lignin	25 – 35	18 – 25	10 – 24	10 – 30
Elemental composition (wt.%, dry and ash free basis)				
C	51 – 55	50 – 57	48 – 51	46 – 52
O	39 – 43	36 – 44	40 – 51	42 – 45
H	5.9 – 6.3	5.9 – 6.7	5.6 – 6.4	5.1 – 6.5
N	0.1 – 0.5	0.1 – 0.7	0.5 – 2.8	0.3 – 2.6
S	0.01 – 0.10	0.01 – 0.11	0.08 – 0.28	0.04 – 0.27

Lignin

Lignin can be considered the most complex compound among the three polymers. This amorphous tri-dimensional aromatic polymer is composed of three different phenolic alcohol units: Hydroxyphenyl (H-unit), Guaiacyl (G-unit), and Syringyl (S-unit). Lignin is found as a hard solid in the outer layer of the cell wall. It provides resistance and a structural framework for the plant.

The described polymers are strongly interconnected, resulting in a complex structure. Hydrogen bonds connect cellulose to lignin and hemicelluloses through hydrogen bonds, while lignin and hemicelluloses are connected through hydrogen and covalent bonds. A representation of lignocellulosic biomass composition and the structure of the biopolymers is illustrated in Figure 1.1. The proportion of the three polymers varies within plant species depending on the type and origin, as shown in Table 1.1. Besides the preceding three main components, biomass contains ash and extractives. Ash covers a broad range of mineral species such as alkali and alkali earth metals, phosphorus, and silicon. Ash can make up a minor proportion (Vassilev *et al.*, 2010) (0.1–8 wt.% for woody biomass, 1–10 wt. % for grasses, and 5–20 wt. % for straws). Extractives are comprised of alcohols, lipids, and waxes accounting for 4 wt. % in wood and \leq 15 wt. % in agricultural residues (Di Blasi *et al.*, 1999).

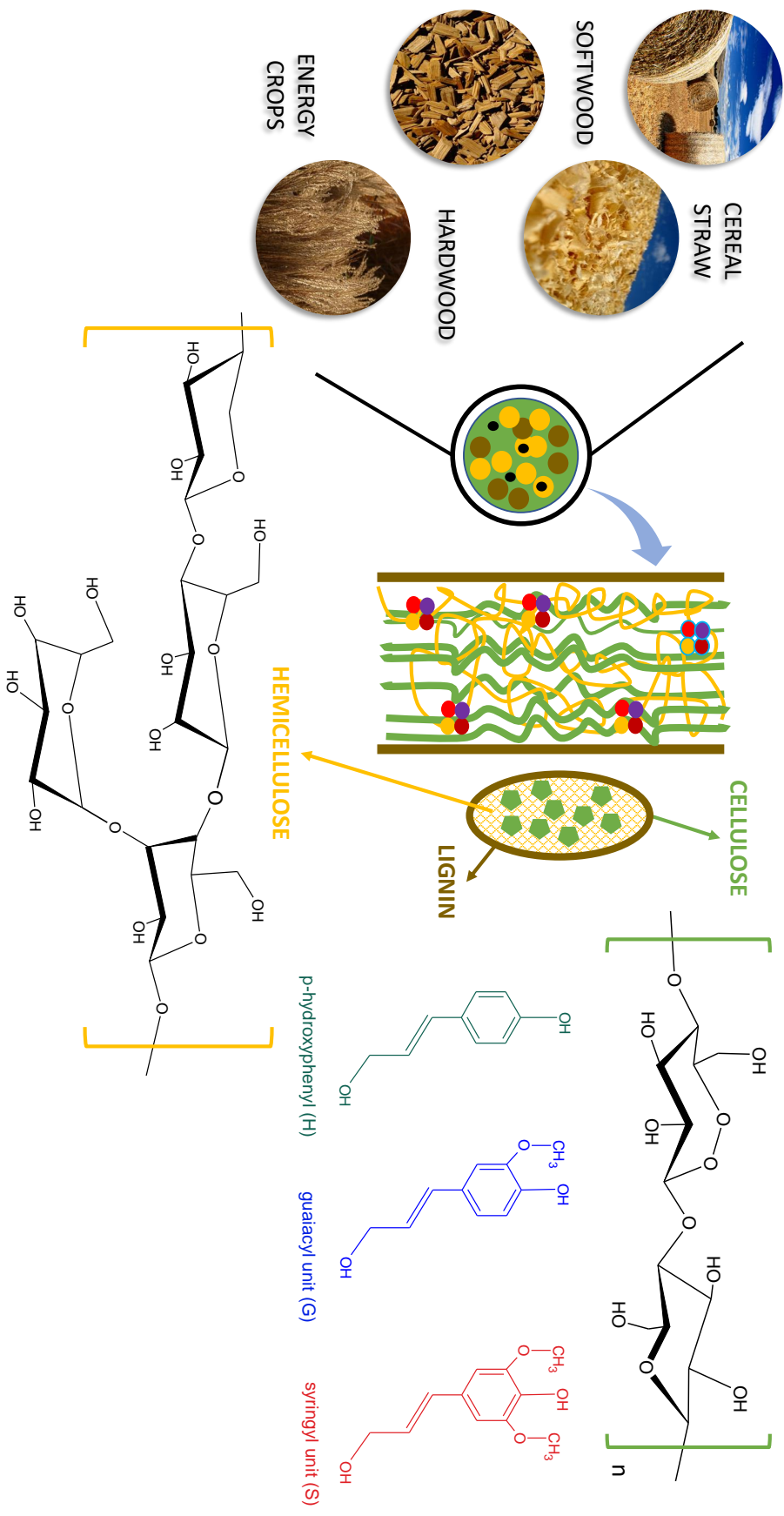


Figure 1.1: Schematic representation of biomass composition and structure

1.2 Biomass fractionation for a biomass-based biorefinery

Following a similar concept to crude oil refining, lignocellulosic biomass resources can be converted by different routes into marketable renewable fuels within the framework of an integrated biorefinery approach.

A biorefinery can be defined as a renewable alternative to petroleum refinery. It refers to the co-production of transportation biofuels, bioenergy, and marketable chemicals from renewable biomass sources (Cherubini *et al.*, 2010). It is also one of the main strategic keys to developing the circular economy. Biorefineries are classified into four major category groups based on their system components (Annevelink *et al.*, n.d.):

- *Feedstocks* can be sourced from dedicated feedstocks such as energy crops (sugar, starch, lignocellulosic crops) as well marine biomass. They can also be derived from lignocellulosic residues, oil-based residues, and organic waste.
- *Pretreatment and conversion processes* are grouped into four main categories: biochemical (digestion, fermentation), mechanical (blending, mechanical pulping), chemical (esterification, hydrolysis, chemical pulping) and thermochemical (pyrolysis, hydrothermal liquefaction)
- *Platforms* are the intermediates connecting biorefinery systems and their processes. They refer to the multi-functional groups that can be processed into other groups of useful molecules. For instance, lignin, biogas, bio-crude, syngas, and CO₂.
- *Products* are both energy and material products which include chemicals and composites and fibers materials as well as animal feed.

Nowadays, it is of great scope to develop integrated biorefineries to maximize biomass usage and to shift into more versatile and energy-self-sufficient systems. These facilities combine the production of bio-based products and energy. Among 803 mapped biorefineries in European Union in 2018, 177 are identified as integrated biorefineries (Parisi, 2018). Through integrated biorefinery processes, multiple added-value products can be obtained from a single lignocellulosic material through the use of different conversion processes. The pretreatment step is considered one of the main key elements to developing high-efficient integrated biorefineries. Biomass fractionation treatment is recognized to be suitable to overcome the challenges hindering the integration of biorefineries. This step allows the achievement of a maximum overall yield of the desired products and offer vital features such as closed-loop process operation. The step consists of increasing cellulose by separating or removing lignin and hemicelluloses. Biomass fractionation

can be achieved through four broad categories of pulping processes used in pulp and paper industries; among them, chemical pulping is the most common process. Chemical pulping involves cellulose extraction by isolating and dissolving lignin. It consists of using dissolving agents to break internal lignin and lignin–carbohydrate linkages and liberate pulp fibers. Lignin is therefore cleaved and dissolved while cellulose constitutes the solid fraction. Cellulose and lignin yields vary depending on operating conditions and biomass type. The chemical pulping can be classified into two categories (Mandlekar *et al.*, 2018): sulfur-bearing and free-sulfur processes.

1.2.1 Sulfur-bearing pulping

The sulfur-based processes are kraft and sulfite pulping. These technologies are used to treat wood chips. They entail several steps; cooking and washing are the two steps where chemical reagents are used. A brief description of each process type is presented as follows (Azadi *et al.*, 2013; Mathew *et al.*, 2018; Mboowa, 2021):

Kraft pulping

This process is currently the dominant chemical pulping method in paper making. Cellulose fibers are obtained by treating with a liquor containing sodium sulfide Na_2S and sodium hydroxide NaOH at $170\text{ }^\circ\text{C}$ for 1–2 h. Typical liquor: wood ratio is typically around 3–4 and pH of 13–14. The ions OH^- and H^+ react with lignin which undergoes degradation/depolymerization reactions into smaller water/alkali fragments.

Sulfite pulping

Sulfite pulping is one of the common pulping methods. This process uses aqueous sulfur dioxide such as bisulfite of sodium, magnesium, calcium, or ammonium, under different pH conditions. Delignification is achieved through two steps: sulfonation of lignin to form sulfonic acid which is cleaved to form soluble compounds. Typical sulfite pulping conditions are cooking temperature $120\text{--}180\text{ }^\circ\text{C}$; digestion time: 1–5 h. Similarly to the kraft process, this process is adapted for wood cooking.

Advantages and drawbacks

Kraft and sulfite processes are well established due to the ability to produce cellulose fibers with low lignin content and the chemical recovery of an inorganic pulping agent. Different existing kraft-based and sulfite-based biorefineries are commercial plants. For example, Domtar (USA) facility uses kraft pulping to produce noncrystalline cellulose, tail oil, and electricity. Alberta-Pacific Forest Industries developed a kraft-based refinery to produce pulp, methanol, and electricity. In Lenzing (Austria) and Borregaard (Norway) facilities wood is processed through sulfite pulping to produce various chemicals, materials, heat, and electricity..

The main shortcomings of sulfur-bearing pulping are the high energy consumption processes and pollution. Large amounts of polluting spent liquid are produced in the

cooking stage. Atmospheric and effluent emissions are one of the main issues resulting in health hazards and environmental risks (Hoffman *et al.*, 2017). The pollutants released from pulping and bleaching have been extensively investigated (Mandeep *et al.*, 2019; Singh *et al.*, 2019). The pollutants gases in the emissions are particulate matter, NO_x, SO₂, and other volatile sulfur compounds. Wastewater and black liquor contain different organic and inorganic pollutants which may lead to serious environmental implications on the food chain as well as aquatic and animal toxicity.

Moreover, product valorization is another main disadvantage of sulfur-based processes. Only 1 – 2 % of the lignin from the kraft process is used in commercial applications (Ruiz *et al.*, 2011). The presence of sulfur in the products limits the study of their chemistry and applications (J. Xu *et al.*, 2020). Lignin from Kraft and sulfite processes contain sulfur in their structure, 1 – 3 and 4 – 8 wt.% respectively (Azadi *et al.*, 2013). For instance, the gasification of black liquor was reported to produce syngas containing 0.6–2 vol. % H₂S (Berglin *et al.*, 1998; Dahlquist *et al.*, 2017; Wiinikka *et al.*, 2010) implying the addition of H₂S step downstream the shift reactor in hydrogen production process (Naqvi *et al.*, 2012).

1.2.2 Sulfur-free pulping

The main sulfur-free pulping methods are soda pulping and organosolv fractionation. Their concepts are described in the following section:

Soda pulping

This process is used to treat biomass residues with lower lignin content, typically agro-residues. Straws and bagasse are cooked with 10–15 % NaOH at about 150–160 °C to obtain sulfur-free lignin. The lower rate of delignification and the damage to lignin structure, compared to sulfur-bearing pulping, are the main limitation of this process (Azadi *et al.*, 2013).

Organosolv fractionation

Organosolv fractionation has been regarded as a promising alternative to the Kraft and sulfite processes, to fit well into the concept of sustainable biorefinery (Baruah *et al.*, 2018; J. Xu *et al.*, 2020). Organosolv processes enable the separation of biomass components with minor degradation, allowing their conversion into value products (Y.-H. P. Zhang, 2008).

In organosolv processes, lignocellulosic biomass is treated with a wide range of solvents to achieve separation of biomass components without forming inhibitory products (X. Zhao *et al.*, 2017). In organosolv treatment, lignin is dissolved by hydrolytic cleavage and hemicellulose is also hydrolyzed and solubilized to form the liquid phase, and the cellulose fraction is separated in the solid phase. Several reviews (K. Zhang *et al.*, 2016;

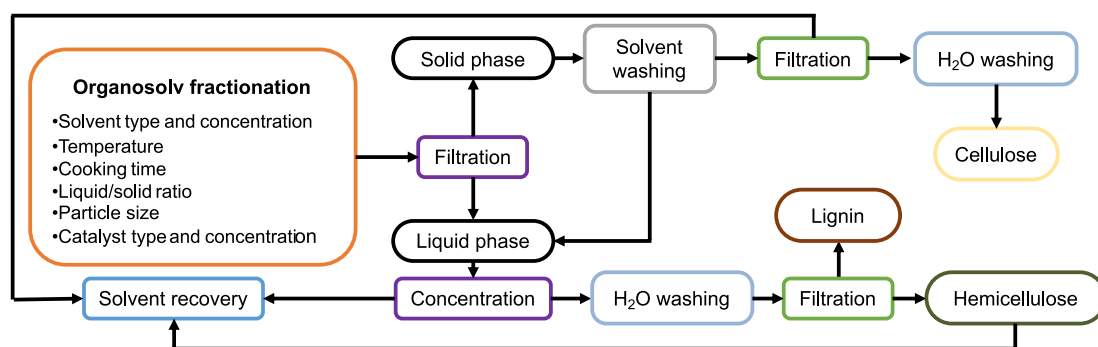


Figure 1.2: Flow scheme of the organosolv fractionation

Table 1.2: Product yields and conditions of Organosolv lignocellulosic biomass pretreatment

Biomass	Solvent	S/W	T	t	L/S	PY	DR	Ref
WS	Ethanol	50/50 ^a	210	90	10	48.6	59.1	(Wildschut <i>et al.</i> , 2013)
RS	Formic acid	90/10 ^b	100	60	12	44.4	63.1	(Hoang Quoc Lam <i>et al.</i> , 2001)
SB	Glycerol	80/20 ^b	198	150	15	54.4	81.4	(Novo <i>et al.</i> , 2011)

S/W solvent to water (v/v); T temperature (°C); t time (min); L/S liquid to solid(w/w); PY pulp yield; DR delignification rate; WS wheat straw; RS rice straw; SB sugarcane bagasse; ^a w/w; ^b v/v

Z. Zhang *et al.*, 2016) have discussed in detail different organic solvents that have been experimentally used. Various solvents have been studied including low-boiling-point solvents such as alcohols and high-boiling-point solvents, typically glycerol, as well as organic acids namely formic acid and acetic acid and others owing due to its low price, good solubility of lignin and ease of recovery (X. Zhao *et al.*, 2017). Table 1.2 illustrates the key factors of different organosolv processes utilized for the pretreatment of lignocellulosic materials.

Figure 1.2 shows the processing scheme of organosolv pretreatment. The pretreatment conditions are the main parameters that are included in the fine-tuning of organosolv pretreatment. These parameters: solvent to biomass ratio, reaction time, temperature, catalyst, and particle size (Ferreira *et al.*, 2020). The solid-to-liquid ratio (S/L) is considered a key parameter influencing the process efficiency in terms of cost and product yields. Thus, it is essential to determine the optimal S/L. Lower ratios improve the delignification rate (Vallejos *et al.*, 2015). S/L is typically between 1:3 and 1:10. Temperature is one of the most influential parameters since the solubility of lignin and solvent characteristics are strongly dependent on it. Operating temperature is in the range of 80–220 °C. Advantages of organosolv pretreatment include the production of

Table 1.3: Advantages and disadvantages of organosolv fractionation (Borand *et al.*, 2018; Wertz *et al.*, 2016)

Advantages	Disadvantages
Both woody and non-woody biomass can be used	High cost of solvent
Sulfur-free and high-quality lignin	Solvent recovery increases energy consumption
Smaller scale application is lower cost than other chemical pulping methods	High flammability and volatility of the organic solvents require the extreme attention of process control
Recovery of solvent is relatively easy	
By-products are converted to valuable products	

sulfur-free products, solvent recovery, and mild environmental conditions. The main advantages and disadvantages are summarized in Table 1.3.

Some of the existing organosolv-based biorefineries have been studied or are being developed for commercial establishment. The most common processes are alcohol-based such as the Alcell process (Canada), ECN (Netherlands), and Organocell (Germany) process. Organic acid-based processes include CIMV (France) and Chempolis (Finland).

Although the increasing amount of attention on organosolv pretreatment and its potential to provide a pathway for the biorefining of biomass, it is still facing some challenges hindering its commercialization. The high operating cost is the main obstacle hampering the commercial establishment of organosolv-based refineries. The solvents are expensive and their solvent recovery is energy-intensive. The development of low-cost processes using tunable solvents and moderate operating conditions (low temperature and atmospheric pressure) is one of the main research areas for their further development (Borand *et al.*, 2018; Z. Zhang *et al.*, 2016). The reduction of the operating cost and energy consumption can be achieved by optimizing vital features of the process such as using lower liquid-to-solid ratio as well as an operating temperature below the boiling point of water and lower energy technologies for solvent recovery.

1.3 Pyrogasification process of lignocellulosic materials

Pyrogasification is a thermochemical process that converts carbonaceous fuels like lignocellulosic material into useful gaseous fuel made of Hydrogen (H₂) and carbon monoxide (CO), called syngas (Basu, 2010). The chemistry of biomass pyrogasification

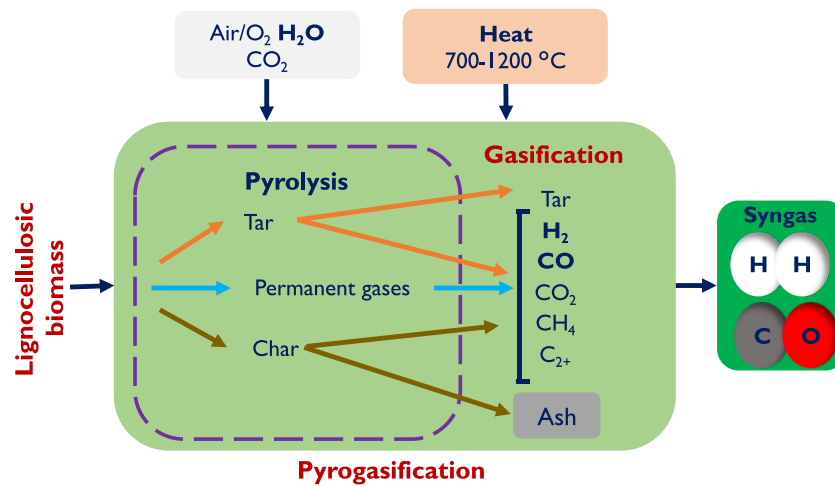


Figure 1.3: Pyrogasification process

is complex. As shown in Figure 1.3. It encompasses a pyrolysis step followed by a gasification step which is the main step. The so-called "gasification" processes are often in practice pyrogasification processes. Hence, the technology is known as "pyrogasification". An initial drying step is required. Drying consists of a loss of mass by evaporation of water in the biomass. Generally, this step is endothermic and takes place below 150 °C.

1.3.1 Pyrolysis

Pyrolysis is one of the main steps of pyrogasification, but can also be a remote thermochemical conversion route. This process, also called thermal devolatilization, is endothermic depolymerization in the absence of oxygen under a temperature ranging from 300 to 1000 °C that converts biomass into three fractions:

- *Gaseous and liquid products*, the major fraction of the pyrolysis gas comprises non-condensable gases such as CO, CO₂, CH₄, and a smaller proportion of other C₂₋₅H_m gases. The liquid product, also called bio-oil, groups tar and pyrolysis water.
- *Solid residue* called biochar, consisting of carbon and ash.

The product yield is strongly affected by operating conditions for a given biomass. Generally, lower temperatures and longer residence time are required if the target product is biochar. Higher temperatures and longer residence time promote gas production. Liquid production is favored under moderate temperatures and shorter vapor residence time (Y.-F. Huang *et al.*, 2016)

Pyrolysis technology can be grouped into different types following the operation conditions such as temperature, heating rate, residence time, pressure, and catalyst. Depending on the temperature and heating rate, pyrolysis technology can be grouped into

Table 1.4: Pyrolysis process conditions and product distribution (Bertero *et al.*, 2015; Danso-Boateng *et al.*, 2022; Demirbas *et al.*, 2002; Kin Wai Cheah *et al.*, 2022; Paasikallio *et al.*, 2013; Qureshi *et al.*, 2021).(desired product)

	Vacuum	Slow	Fast	Flash	Microwave	Catalytic
Temperature (°C)	350 – 600	400 – 650	400 – 1000	900 – 1200	150 – 850	350 – 750
Heating rate (°C s ⁻¹)	0.3 – 1	0.1 – 1	10 – 200	>1000	1 – 50	1 – 9
Residence time (s)	0.2 – 60	0.5 – 20	0.5 – 10	<0.1	0.5 – 0.8	3 – 10
Product distribution (wt.%)						
Biochar	16-30	20-35	10 – 25	10 – 15	20 – 40	12 – 43
Bio-oil	35 – 45	20 – 50	60 – 75	75	23 – 70	22 – 62
Gas	18 – 35	20 – 35	10 – 30	10 – 20	18 – 47	8 – 49

three main categories: slow, fast, and flash pyrolysis (Demirbas *et al.*, 2002). A broader classification would include vacuum, microwave, and catalytic pyrolysis (Danso-Boateng *et al.*, 2022). Contrary to atmospheric pressure, in vacuum pyrolysis to increase bio-oil selectivity towards more favorable properties (Banks *et al.*, 2016). Microwave pyrolysis involves microwave dielectric heating offering a more flexible and faster heating rate (Y.-F. Huang *et al.*, 2016). The operating parameters of pyrolysis processes and typical product yields are listed in Table 1.4.

1.3.2 Gasification

This step involves the conversion of pyrolysis products into gaseous fuel constituted mainly of CO and H₂. Gasification takes place at high temperatures (> 700 °C), in the presence of gasifying agents such as air, oxygen, steam carbon dioxide, or their mixture. The chemical reactions that occur during gasification are listed in Section 1.5. The main carbon-gas reactions as well as tar reforming and cracking are endothermic, requiring heat supply in the gasifier. The heat required can be autothermal or allothermal (Kaur *et al.*, 2019).

In an autothermal or direct gasification process, the heat is generated by burning a part of the feedstock or pyrolysis products in the gasifier. In a such process scheme, air, oxygen, steam, or a mixture of these are used as gasifying agent. The process can be represented by four main steps including oxidation, drying, pyrolysis, and biochar reduction with an additional step consisting of tar decomposition (Molino *et al.*, 2016). The main advantage is the high energy efficiency. This type of gasifier is inexpensive, easy to operate, and sustainable. However, the product gas has a low heating value

(4–6 MJ Nm⁻³) as nitrogen is used for air supply in combustion or as a diluent to control gasifier temperature (Couto *et al.*, 2013). Oxygen gasification can be an alternative to improve gas quality (10–18 MJ Nm⁻³) but it is limited by the high oxygen cost and risk (Moilanen *et al.*, 2011).

In allothermal or indirect heating, the heat required by endothermic processes is provided by external sources. Using only steam as a gasifying medium, hydrogen-rich syngas with higher heating value (14–18 MJ Nm⁻³) is produced. Another valuable advantage is the complete conversion of carbon avoiding problematic waste (Rauch *et al.*, 2014). Although the high quality of the gas, external heating can considerably increase the overall process cost (Gírio, 2019).

1.3.3 Pyrogasification products

The product distribution of the pyrogasification process varies depending on different parameters such as biomass composition, gasifying agent, and operating temperature. The main and desired product of gasification is the gaseous fraction called syngas, bio-syngas, or product gas. It consists mainly of CO and H₂ with smaller amounts of CO₂, and CH₄. Syngas from biomass pyrogasification can subsequently be converted to valuable industrial products, following different reaction paths. Syngas conditioning and applications are discussed in Section 1.5 with a focus on hydrogen. The other

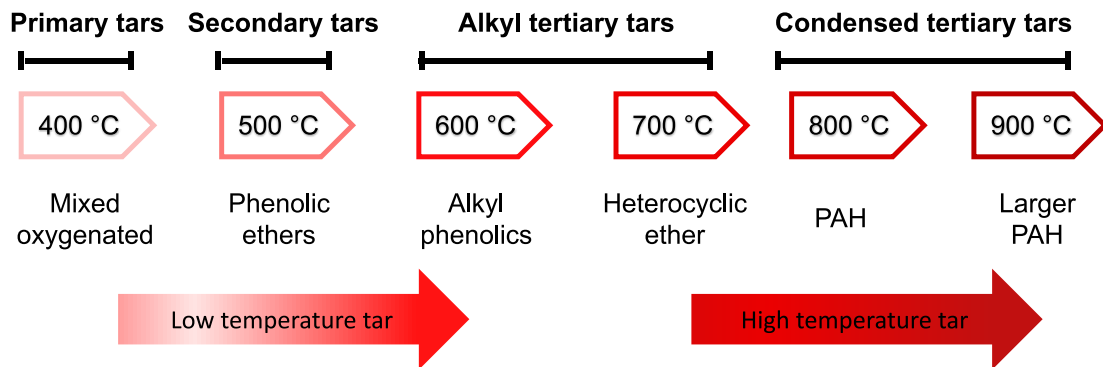


Figure 1.4: Tar groups as function of temperature (adapted from (Molino *et al.*, 2016))

products are unconverted condensable gases and unconverted biochar with residual ash. These products should be monitored, as they can be contaminants in certain syngas applications. The condensable phase contains water and tars. The European Commission for Standardization has defined tar as "all organic compounds present in the synthesis gas excluding gaseous hydrocarbons from C₁ to C₆" and also defined the main procedure for their measurement and analysis (CEN, 2006). In the gasification process, tars are formed as a result of complex reactions which depend strongly on the reaction conditions. Several authors have defined these undesired products differently. Milne and Evans (Milne *et al.*,

Table 1.5: Overview of the main chemical reactions of biomass gasification (Basu, 2010; Seo *et al.*, 2018)

Reaction type	Reaction	$\Delta_r H$ (kJ mol ⁻¹)
Oxidation reactions		
1 Carbon oxidation	$C + O_2 \longrightarrow CO_2$	-394
2 Carbon partial oxidation	$C + \frac{1}{2} O_2 \longrightarrow CO$	-111
3 Carbon monoxide oxidation	$CO + \frac{1}{2} O_2 \longrightarrow CO_2$	-284
4 Hydrogen oxidation	$H_2 + \frac{1}{2} O_2 \longrightarrow H_2O$	-242
5 Methane oxidation	$CH_4 + 2 O_2 \longrightarrow CO_2 + 2 H_2O$	-890
6 Methane partial oxidation	$CH_4 + O_2 \longrightarrow CO + 2 H_2O$	-36
Gasification reactions involving steam		
7 Water-gas reaction	$C + H_2O \longrightarrow CO + H_2$	+131
8 Water-gas reaction	$C + 2 H_2O \longrightarrow CO_2 + 2 H_2$	>0
9 Water-gas shift reaction	$CO + H_2O \rightleftharpoons CO_2 + H_2$	-41
10 Steam methane reforming	$CH_4 + H_2O \longrightarrow CO + 3 H_2$	+206
11 Steam reforming	$C_n H_m + n H_2O \longrightarrow n CO + (n + m/2) H_2$	> 0
Gasification reactions involving hydrogen		
12 Hydrogasification	$C + 2 H_2 \longrightarrow CH_4$	-73
13 Methanation	$CO + 2 H_2 \longrightarrow CH_4 + CO_2$	-247
14 Methanation	$CO + 3 H_2 \longrightarrow CH_4 + H_2O$	-206
15 Methanation	$CO_2 + 4 H_2 \longrightarrow CH_4 + 2 H_2O$	-165
Gasification reactions involving carbon dioxide		
16 Boudouard	$C + CO_2 \longrightarrow 2 CO$	+172
17 Dry reforming	$C_n H_m + n CO_2 \longrightarrow 2 n CO + m H_2$	> 0
Tar cracking		
18 Dehydrogenation	$p C_x H_y O_z \longrightarrow CO + CH_4 + H_2 + q C_n H_m + C$	> 0
19 Carbonization	$C_n H_m \longrightarrow n C + m/2 H_2$	> 0

1998) classified tars into 4 groups (3 classes): primary (derived from biomass polymers), secondary (phenolics and olefins), alkyl tertiary (methyl derivatives of aromatics) and condensed tertiary which are mainly polycyclic aromatic hydrocarbons PAH (benzene, naphthalene, acenaphthylene, anthracene/phenanthrene, pyrene). Figure 1.4 depicts a schematic overview of tar types as a function of temperature.

1.3.4 Pyrogasification technologies

Pyrogasification technologies can be divided into several categories according to different criteria. In this work gasifiers are grouped into two main types: single-stage and multistage gasifiers.

Single-stage gasifiers

In single-stage technology, the reactor configuration relies on contact between the feed material and the gasifying agent, heat transfer, and residence time of the feed material into the reaction zone. Fixed bed, fluidized bed, and entrained flow reactors are the most commonly used gasifiers. A brief description of each technology is reported below in the following section. Gasification technologies are reviewed in detail elsewhere (Meijden *et al.*, 2010; Mishra, 2021; Molino *et al.*, 2016; Molino *et al.*, 2018; Sansaniwal *et al.*, 2017; Williams *et al.*, n.d.).

Fixed bed

In a fixed bed reactor, the solid fuel is fed from the top and moves downwards, pyro-gasification reactions occur progressively. Fixed bed gasifiers are generally autothermal and come in two main configurations, based on the interaction between the gasifying agent and biomass solid: updraft and downdraft.

Updraft reactors are structurally simple, the oxidizing agent is fed from the bottom and the syngas produced moves upward. The high thermal efficiency, flexibility to handle different biomass varieties and low slag formation are their main strengths. Updraft gasifiers are more suitable for scale-up. On the other hand, the high concentration of tar in the syngas is the main obstacle limiting the use of this technology in many advanced applications (Ciferno, 2002). In a downdraft (co-current) gasifier, the oxidant enters from the top, and both solid and product gas move in the same direction and exit from the bottom passing the combustion zone. Downdraft gasifiers are characterized by low mineral content in the gas and low production of tar. However, the major drawback lies in their inability to handle low-density materials and high ash content fuel (Ren *et al.*, 2019).

Fluidized bed

Fluidized bed reactors are made of inert material which is stirred by the presence of the gas to hold on fluidization of biomass particles (< 10 mm). These gasifiers are

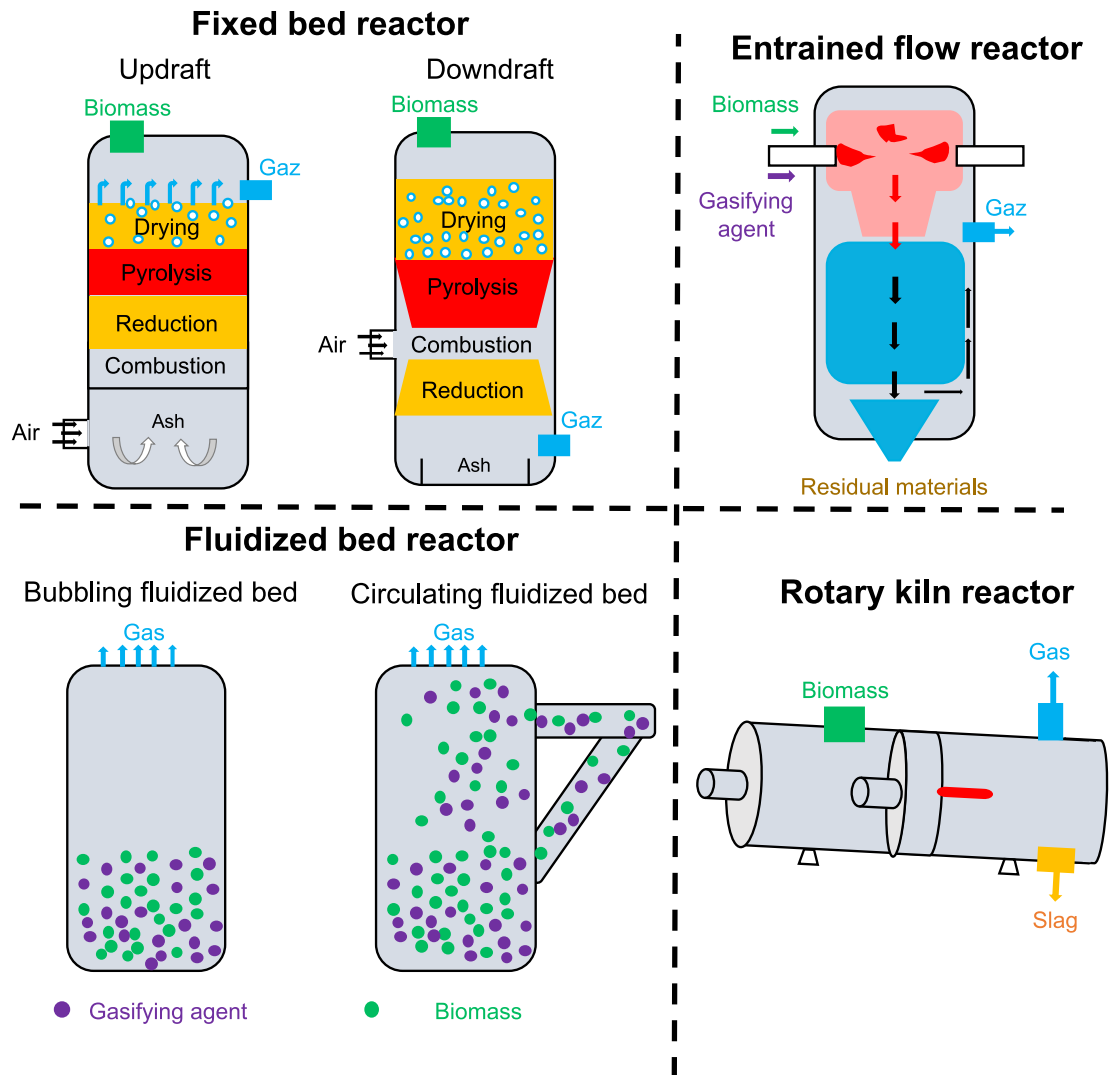


Figure 1.5: A schematic of different types of single-stage gasifiers (adapted from (Ren *et al.*, 2019))

recognized for their high mass and heat transfer rate, high mixing capability, and high efficiency for cold gas (Corella *et al.*, 2007). Restrictions on particle size and the high investments and maintenance costs are the main obstacles to the expansion of these technologies. Fluidized bed reactors are primarily classified into two families: bubbling and circulating. In a bubbling fluidized-bed gasifier, biomass is fed from the side and mixed with a gasification agent which is injected from the bottom of the bed to the top at the rate of $1\text{--}3\text{ m s}^{-1}$. The product gas exits through a cyclone to remove ash and particles while the remaining solid can be removed from the bottom.

Circulating fluidized bed reactors operate by higher gas velocities of $5\text{--}10\text{ m s}^{-1}$ allowing the dragging of the solid. The entrained particles are separated through a cyclone re-circulated in the reactor.

Entrained bed

In an entrained bed gasifier fine particles of biomass ($< 1\text{ mm}$) and the gasifying agent are introduced in co-current. The gasification is performed at high temperatures ($1200\text{--}1500\text{ }^{\circ}\text{C}$) which enhances tar cracking. These gasifiers are well-known for their high efficiency at a large scale (500 MWh). Their requirements for size reduction and heat recovery are the main disadvantages.

Rotary kilns

Rotary kiln reactors consist of a cylindrical chamber slightly inclined toward the discharge port ($1\text{--}3\text{ }^{\circ}\text{C}$). The cylinder rotates on its horizontal axis ($0.5\text{--}30\text{ rpm}$). The solid particles move from the inlet to the outlet, and the gas-solid contact takes place under the effect of rotation and gravitation. Rotary kilns have many characteristics such as the excellent capacity of handling biomass with different properties and low investment costs. However, these gasifiers are affected by the high content of dust and tar. Also, the low efficiency of heat and the limited flexibility are the main disadvantages of these reactors.

Multi-stage gasifiers

Processes using multi-stage concepts for pyrogasification are currently expanding. In this technology, pyrolysis and gasification are performed separately in two configurations (Heidenreich *et al.*, 2015):

- one unit with separated controlled pyrolysis and gasification zones
- separated pyrolysis and gasification units connected in series

This enables the thermoconversion step to take place under optimal operating conditions. The core reason to operate in a multi-stage process is to obtain clean syngas with a low tar content and enhance the overall process efficiency and throughput (Moreira, 2021).

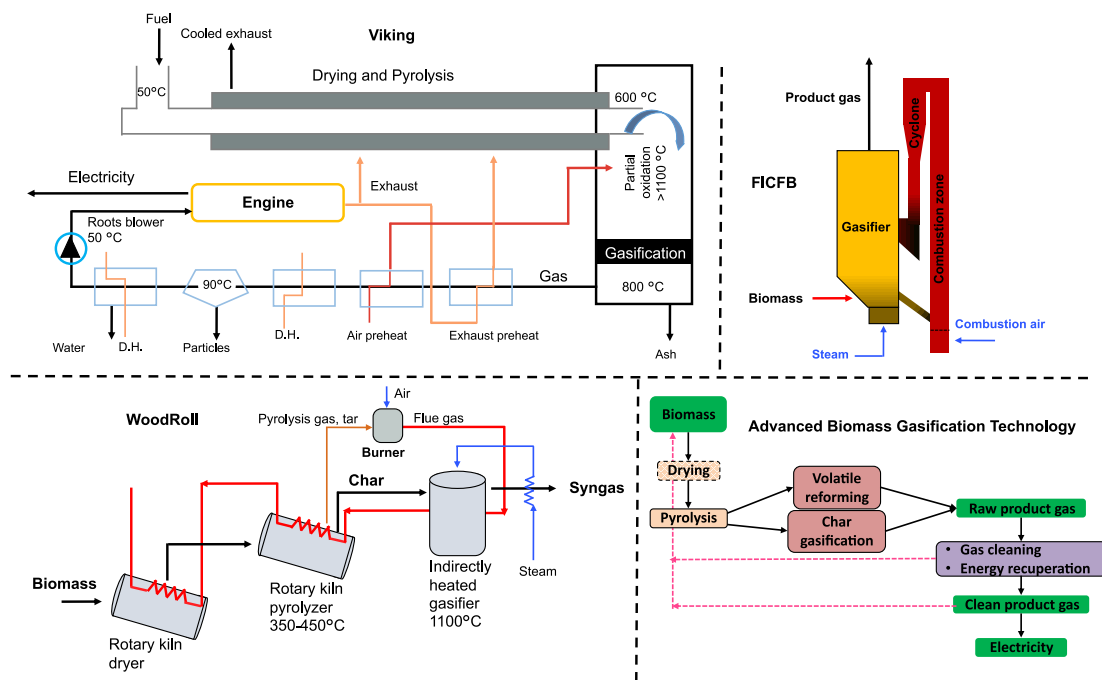


Figure 1.6: A schematic of multi-stage gasification technologies: Viking (Henriksen *et al.*, 2006), WoodRoll (Phounglamcheik *et al.*, 2017), FICFB (Pröll *et al.*, n.d.) and Advanced Biomass Gasification Technology (ARENA, 2018)

Nevertheless, separating pyrolysis and gasification in single controlled stages intensifies the process complexity.

The main multi-stage gasifiers with separated units are presented below. Details can be found in the reviews of Heidenreich *et al.* (2015) and Mednikov (Mednikov, 2018). Schematic presentation of described technologies is illustrated in Figure 1.6.

Viking process

Viking gasifier is a two-stage gasification process that has been developed by the Danish Technical University. The gasifier small-scale plant with a nominal thermal input of 70 kW (Gøbel *et al.*, 2002). The auto-thermal process consists of a screw pyrolysis reactor and a downdraft gasifier with an intermediate high-temperature tar cracking zone. Drying and pyrolysis are performed at 500–600 °C in the first reactor, heated by an external supply. The pyrolysis products are introduced in the second reactor operating at temperatures between 1100 and 1300 °C. By passing on the high-temperature partial oxidation zone, volatiles are oxidized to provide heat and gasifying medium for biochar gasification while tars are cracked. The heating value of the producer gas is approximately 6 MJ Nm^{-3} (Henriksen *et al.*, 2006) and tar content is lower than 15 mg m^{-3} (Mednikov, 2018).

WoodRoll technology

The WoodRoll technology is a three-stage gasification process. The technology was

initially developed as a test plant with a thermal capacity of 500 kW, by Cortus Energy, Sweden (Amovic *et al.*, n.d.). Drying and pyrolysis are performed separately in an indirect heated rotary kiln reactors at 105 and 360 – 400 °C, respectively. Produced pyrolysis volatiles are burned to generate heat for gasification and pyrolysis units. Biochar is gasified in an entrained flow reactor using steam as a gasifying medium, at ambient pressure and a temperature of 1100 °C. The high-grade product gas is the main advantage of WoodRoll technology. Pure syngas production at full-scale was deemed in 2020.

FICFB reactor

FICFB (fast internally circulating fluidized bed) process is a two-stage gasifier developed at the Technical University of Vienna, Austria Hofbauer *et al.*, 1997. The circulating fluidized bed consists of gasification and combustion zones. The biochar is gasified with steam. Similarly to WoodRoll, the product gas is nitrogen-free. The combustion zone supplies heat to the gasification unit via a circulating loop of the bed material. The technology was initially developed at a pilot scale with a thermal capacity of 100 kW and then scaled up. This gasifier is presently used as combined heat and power (CHP) plant and operates at about 8 MW with an electrical output of 2 MW_e Bolhàr-Nordenkamp *et al.*, 2003. FICFB CHP technology has been deployed in several of gasification installations in Europe.

Advanced Biomass Gasification Technology

Advanced biomass gasification technology in a three-stage gasifier for heat and CHP applications, developed by Curtin university and Renergi Pty Ltd., Australia (ARENA, 2018). This procedure is under development at a demonstration scale (100 kg h⁻¹ of biomass). Biomass moisture is removed in a drying unit by using heat recovered from the cooling of syngas. The dried biomass is then pyrolyzed in a separate pyrolysis unit. The gasification of volatiles and biochar is performed in different zones in the same reactor at 850–1000 °C (Jafri, n.d.). The product gas is cleaned in a hot gas cleaning and energy to meet the quality requirements of the endpoint applications.

A schematic view of the described multi-stage gasifiers is presented in Figure 1.6. In summary, single-stage technologies are conventionally used for biomass gasification. Recently, multi-stage processes have been gaining momentum since they allow the production of high-grade syngas. **In this research, steam gasification with a fixed bed reactor was used for hydrogen-rich syngas production.** Therefore, Table 1.6 summarized the final composition of syngas from steam gasification technologies. Regarding ongoing gasification projects and plants, several databases can be found in [IEA Bioenergy Task 33](#) and [Global Syngas Technologies Council](#).

Table 1.6: Gas composition from different gasification technologies

(vol. %)	Bubbling fluidized bed	Circulating fluidized bed	WoodRoll	FICFB
H ₂	52	34.2	55 – 58	35 – 45
CO	23	27.2	25 – 31	20-30
CO ₂	18	22.7	12 – 16	15 – 25
CH ₄	7	11.1	0 – 2	8-12
N ₂	n.d.	4.8	0	3 – 5
Tar (mg Nm ⁻³)	n.d.	n.d.	<30	<5
Ref.	(Couto <i>et al.</i> , 2013)	(Mednikov, 2018)	(Hofbauer <i>et al.</i> , 1997)	

1.4 Pyrogasification of biomass components

Pyrogasification of lignocellulosic biomass constituents has been widely covered in the literature. Most of the studies used pure cellulose, lignin, and xylan as model materials for biomass components. The ultimate motive has been to better understand the complex thermoconversion of biomass through the knowledge of the decomposition characteristics of the single components. In this section, a state-of-the-art review of pyrogasification of biomass constituents is provided, with an emphasis on steam gasification of cellulose.

Table 1.7: Ultimate and proximate analysis of pure biomass components lignin, cellulose and xylan (D. Lv *et al.*, 2010; Yang *et al.*, 2007; H. Yu *et al.*, 2018)

	Ultimate analysis (wt.%)					Proximate analysis (wt.%)			
	C	H	O	N	S	M	VM	FC	Ash
Cellulose	40–50	5–6	42–47	0–1	0-0.1	3–8	90–95	4.5–5.3	0–0.3
Xylan	35–45	5–7	38–43	0–0.1	0.05	4–14	65–80	14–16	2–5
Lignin	45–55	4–6	20–30	0.3–3	0.1–4	3–13	40–65	32–37	3–13

1.4.1 Pyrolysis

Most of the studies have focused on the pyrolysis of several milligrams of biomass components. The pyrolysis behavior of biomass components is different since inherent structures and chemical nature are different (Section 1.1) (Dorez *et al.*, 2014; D. Lv

Table 1.8: Pyrolysis characteristics of biomass three components: thermal behavior and product yields

	Thermal behavior		Products yields			Products composition	
	T range	Peak T	Biochar	Gas	Bio-oil	Gas	Bio-oil
Cellulose	307 – 404	342 ± 9	4 – 18	12 – 32	55 – 81	CO	Carbohydrates, furans, aldehydes, alcohols
Xylan	223 – 358	260 ± 9	19 – 27	38 – 48	44 – 58	CO ₂	Acids and ketones
Lignin	203 – 546	–	40 – 61	8 – 18	21 – 40	CH ₄	Phenols

Temperature unit is °C

et al., 2010; Jianqiao Wang *et al.*, 2019; S. Wang *et al.*, 2011; Yang *et al.*, 2007; Jie Yu *et al.*, 2017). Pyrolysis characteristics of the three components are summarized in Table 1.8.

From TGA, hemicellulose has a lower degree of polymerization compared to cellulose and lignin, therefore its decomposition is easier. It occurs at a lower temperature, in the range of 200–350 °C. The degradation of lignin is slower and is spread over a wider temperature range, 200 – 800 °C. Compared to lignin and hemicellulose, cellulose pyrolysis is faster and occurs at higher temperatures over a narrow temperature range, with a peak of decomposition at 350 – 380 °C.

The composition and formation mechanisms of pyrolysis products of the three components have been extensively studied (Giudicianni *et al.*, 2013; C. Li *et al.*, 2021; Qu *et al.*, 2011; Quan *et al.*, 2016; S. Wang *et al.*, 2011; C. Zhao *et al.*, 2017). Regarding the overall product distribution, cellulose is characterized by the lowest biochar yield while lignin pyrolysis produces the highest yield because of its higher carbon content and highly crosslinked nature. On the other hand, cellulose produces more bio-oil than hemicellulose and lignin. The yield of gas from hemicellulose is higher than cellulose and lignin. C. Zhao *et al.* (2017) reported that the high gas yield for hemicellulose is attributed to weak bond strengths in its chemical structures, and the micro-molecular volatiles can easily be degraded under the effect of temperature.

CO₂ and CO are the main gaseous products of all three components. A higher CO₂ yield is generated from hemicellulose due to the high carboxyl content in it. CO₂ is released by cracking and reforming of carbonyl and COOH. Cellulose pyrolysis owns the highest CO yield which is attributed to its higher carbonyl content. The largest volume fraction of CH₄ and H₂ is released from lignin pyrolysis to its higher content of aromatic ring and methoxyl–O–CH₃ functional groups.

The composition of organic bio-oil of the three components is different. Cellulose pyrolysis produces light-oxygenated species such as carbohydrates, aldehydes, acids, and alcohols. Levoglucosan is the main constituent of carbohydrates. Compared with that from cellulose, hemicellulose bio-oil derived contains markedly fewer saccharides and larger amounts of acids, ketones as well as furfurals. Lignin pyrolysis produces aromatic compounds, mainly phenols. Temperature, heating rate, as well as alkali and alkaline metals (AAEM) can significantly influence the distribution and properties of products (Hanping Chen *et al.*, 2021; Jie Yu *et al.*, 2017)

1.4.2 Gasification

The gasification has been studied under different experimental conditions at a lab scale. Differences in gasification performance were observed between the different biomass components. In general, steam gasification of lignin produces more hydrogen yield and higher H₂/CO than that of xylan and cellulose (Soomro *et al.*, 2018; T. Tian *et al.*, 2017; Wu *et al.*, 2013b). Recent findings on hydrogen yield in H₂/CO ratio in the gasification of different biomass components are shown in Table 1.9. Compared to that of hemicellulose and lignin, a higher carbon conversion is obtained in air-steam gasification of cellulose (Hanaoka *et al.*, 2005). According to H. Yu *et al.* (2018), lignin gasification was found to give the highest tar yield. They also observed some differences in tar composition (H. Yu *et al.*, 2014), resulting from differences in the molecular structures of the three components. Polycyclic aromatic hydrocarbons (PAH) represented the majority of tar. They reported that tar from lignin gasification generates more phenols and its derivatives in contrast to cellulose and xylan-derived tars which contain more miscellaneous and derivatives aromatics. As gasification is a complex series of thermochemical reactions. Operating conditions such as temperature, catalyst and gasifying agent have the potential to influence syngas production and characteristics.

Gasifying agent

The gasifying agent has a vital influence on the quality of syngas, in terms of composition and heating value (Section 1.3.2) (Molino *et al.*, 2018). The advantages and technical challenges of using different gasifying agents have been reviewed (J. Dong, 2016; Millan, 2018).

Yoon *et al.* (2012) made a comparison between air, air-steam, and steam as a gasification agent of the three biomass components and reported that air gasification produced more CO while steam gasification generates a higher amount of H₂ and CH₄. 1.3 and 15.9 L kg_{cellulose}⁻¹ were released when using air and steam as gasifying agents, respectively.

Increasing air ratio helps in cracking larger amounts of O₂ are available to react with tar molecules (H. Yu *et al.*, 2014). When using steam as a gasifying agent of cellulose, X. Zeng *et al.* (2021) reported that H₂ yield and concentration increased as steam to

carbon ratio increased, since **WGSR**, steam reforming of hydrocarbons and methane are promoted. However, excess addition of steam would decrease gasifier temperature and reduce residence time which manifests in lower tar cracking. A similar trend was observed in another study (Tang *et al.*, 2022a). Zou *et al.* (2016) reported that a low steam rate could cause carbon deposition on the catalyst and excessive steam injection weakened the catalyst performance. They identified an optimal steam flow rate for maximizing H₂ production. For cellulose CO₂ gasification, CO yield was considerably higher than that of H₂ on account of the Boudouard reaction (S. Zhang *et al.*, 2022).

Catalyst

The use of catalysts has been found to have a beneficial effect on hydrogen production from cellulose gasification. The catalyst may be inherently present or added. The effect of added catalyst on cellulose gasification is discussed in this section, while the effect of the inherent catalytic species on gasification kinetics is discussed in detail in Chapter 5.

Most of the studies used catalysts in the primary reactor (*in situ*) since their use can not only promote tar reforming but also can decrease the reaction temperature, and improve the carbon gasification rate and hydrogen selectivity. Alkali and alkaline earth metals (**AAEM**), transition metals, and metal oxide catalysts are the most used catalysts for cellulose gasification, as shown in Table 1.9. The use of **AAEM** can enhance heterogeneous biochar reforming reactions as well as homogeneous volatile reforming including water-gas shift, steam-tars reforming, and hydrocarbon reforming reactions. Jiang *et al.* (2018) investigated the effect of KCl yield and composition of gas and tar of the steam gasification of cellulose at a temperature range of 500–900 °C. The results showed that the presence of KCl increased the gas yield and promoted H₂ production. It also reduced the tar content and inhibited the formation of levoglucosan. Different studies investigated the use of Na-based catalysts for cellulose gasification (Su *et al.*, 2008; Shen Su *et al.*, 2010; H. Yu *et al.*, 2018).

Calcium oxide (CaO) has also been suggested since it was demonstrated that it can play a dual role as CO₂ sorbent (via carbonation reaction) and as a catalyst for tar reduction. In the experiment conducted by S. Zhang *et al.* (2022), cellulose was gasified at 650 °C in the presence of CaO in a CO₂ atmosphere. The yield of gas and H₂ increased almost 2 and 8 times, respectively, when CaO/cellulose mass ratio increased from 0 to 5. In another study (Magoua Mbeugang *et al.*, 2021), CaO was used for the steam gasification of cellulose. At 650 °C, H₂ content increased with increasing CaO/Cellulose; while that of CO decreased, resulting from the increase of CO₂ adsorption which would be helpful to further shift the equilibrium of **WGSR**. Similar trends were observed by Soomro *et al.* (2018), they studied the use of CaO catalyst for enhancing the steam gasification of cellulose and lignin. For both components, maximum H₂ concentration was obtained at 650 °C when CaO/cellulose and CaO/lignin was 1.5. At these conditions, H₂ yield of 12.37 and 33.48 mol kg⁻¹ was achieved for cellulose and lignin, respectively.

Nickel-based catalysts have also been suggested as a good choice for hydrogen production. Wu *et al.* (2013b) tested different Ni-based catalysts in cellulose steam gasification. It was found to be the most effective for H₂ production. The highest H₂ yield was achieved using Ni–Ca–Al (1:1) which showed high efficiency in reforming/cracking of PAH. Akubo *et al.* (2019) investigated a 10 wt. % Ni-based alumina catalyst. With the addition of the catalyst, H₂ concentration and yield increased from 26.48 and 6.06 to 56.43 % and 19.72 mmol g⁻¹, respectively. Other Ni-based catalysts showed good activity for hydrogen production (Inaba *et al.*, 2006; X. Zeng *et al.*, 2021; Zou *et al.*, 2016) and tar conversion (Y.-K. Park *et al.*, 2014).

Several other transition metals catalysts such as Fe-based (Tang *et al.*, 2022a; Tang *et al.*, 2022b; Zou *et al.*, 2018), and Rh-based catalysts (Asadullah *et al.*, 2002; Asadullah *et al.*, 2001) and natural mineral catalysts (Noda *et al.*, 2009) were also used for cellulose steam gasification.

Temperature

The reaction temperature is considered to be the most important factor affecting gasification performance. Generally, higher temperatures improve gas production and minimize tar content, as shown in Figure 1.7. According to Le Chatelier's principle, higher temperatures favor product formation in endothermic reactions such as carbon-gas reactions and tar reforming/cracking, therefore improving hydrogen production. H. Yu *et al.* (2014) reported that tar yield decreased and the fraction of light PAH increased with increasing temperature.

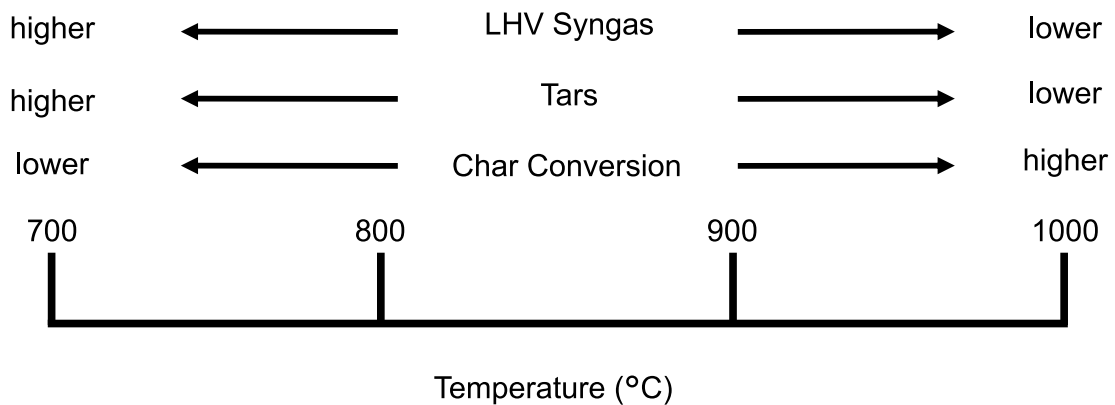


Figure 1.7: Influence of temperature on gasification process performance (Molino *et al.*, 2016).

T. Tian *et al.* (2017) pointed out in the study of cellulose steam gasification that an increase in temperature had a significant effect on increasing the gas yield and composition. H₂ concentration increased momentarily from 34.5 to 43.4 % and H₂ yield reached 0.27 Nm⁻³ kg with the increase of temperature from 920 to 1220 °C. Zou *et al.* (2018) studied cellulose gasification in a two-stage pyrolysis catalytic reforming fixed-bed reactor using a bi-metallic catalyst in the temperature range between 500 to 900 °C at

the step of 100 °C. The results demonstrated that higher temperatures contributed to higher gas yields and promoted tar decomposition. For hydrogen production, hydrogen concentration increased slightly when the temperature was increased from 500 to 700 °C. Nevertheless, the increase of hydrogen is not always directly correlated to the temperature. H₂ concentration decreased with further temperature increase which was attributed to the reverse WGSR. The same results were obtained in the study of Soomro *et al.* (2018), in which H₂ content in the gas tended to decrease when the temperature increased from 650 to 800 °C while hydrogen yield increased from 12.37 to 51.88 mol kg_{cellulose}⁻¹.

1.4.3 Summary and conclusion on biomass components pyrogasification

The results of different studies demonstrated that cellulose pyrogasification has the potential for hydrogen production. Therefore, cellulose is considered to be a promising energy resource. However, it must be pointed out that the main motive for using biomass pure components in pyrogasification was to predict biomass behavior and predict the interaction between its components. Moreover, most of the studies focused on pure components such as microcrystalline cellulose and alkali lignin which are derived from traditional biomass treatment, namely the kraft process with other additional treatments. It was mentioned that subsequent pretreatment of cellulose lowered hydrogen yield (Hassan *et al.*, 2020). In the case of alkali lignin, the presence of sulfur derived from the Kraft process was observed during gasification (Wu *et al.*, 2013b). In addition, the high cost of prepared cellulose limits its use in gasification at the production scale. Accordingly, the aforementioned depicts the importance of cellulose extraction method in terms of cleanliness and economic efficiency.

Table 1.9: Recent studies on gasification of biomass constituents and maximum H₂ production

Sample	Reactor type Operating conditions	Catalyst	H ₂ (mol kg ⁻¹)	H ₂ /CO (vol/vol)	Ref.
Waste wood	Fluidized bed 900 °C; steam	silica sand	59.0	2.6	(Fremaux <i>et al.</i> , 2015)
Pine sawdust	Fixed bed 900 °C; steam	dolomite	111.8	2.6	(S. Luo <i>et al.</i> , 2009)
Cellulose Lignin	Fluidized bed 800 °C; steam	CaO/feed = 1.5	41.6 51.9	2.7 2.1	(Soomro <i>et al.</i> , 2018)
Cellulose	Two-stage fixed-bed 650 °C; steam	CaO/feed = 4	12.8	1.8	(Magoua Mbeugang <i>et al.</i> , 2021)
Cellulose	Quartz tubular 650 °C; CO ₂	CaO/feed = 5	3.9	1.3	(S. Zhang <i>et al.</i> , 2022)
Cellulose			22.6	2.8	
Xylan Lignin	Two-stage fixed bed 800 °C; steam	Ni-Mg-Al	15.2 14.0	4.0 3.4	(Wu <i>et al.</i> , 2013a)
Cellulose		Ni-Ca-Al (1:1)	22.2	2.8	(Wu <i>et al.</i> , 2013b)
Cellulose	Cylindrical 800 °C; steam	Ni/Al ₂ O ₃ +KCl	28.5	2.3	(Zou <i>et al.</i> , 2016)
Cellulose			19.7	2.7	
Lignin		10 wt.% NiAl ₂ O	25.5	3.9	
Xylan Cellulose	Two-stage fixed bed 750 °C; steam		20.5 6.1	3.2 0.6	(Akubo <i>et al.</i> , 2019)
Lignin		Sand	7.0	1.4	
Xylan			6.4	0.7	
Cellulose	Two stage fixed-bed 800 °C; steam	CeO ₂ /Fe ₂ O ₃	28.6	2.8	(Zou <i>et al.</i> , 2018)
Cellulose	Fixed bed 900 °C; steam	Ca-Fe	12.9	0.6	(Tang <i>et al.</i> , 2022b)
		CaFe ₂ O ₄	10.9	0.7	(Tang <i>et al.</i> , 2022a)
Cellulose	Two-stage 500 °C; steam	Ca(OH) ₂ -Ni/Fe	27.4	6.3	(X. Zeng <i>et al.</i> , 2021)
Cellulose	Dual stage quartz 900 °C; steam	0.5 KCl	11.1	0.5	(Jiang <i>et al.</i> , 2018)
Cellulose	Fixed-bed 500 °C; O ₂ (90:10)	Ni/SiO ₂ Rh/Ce/SiO ₂	15.4 13.3	1.4 2.2	(Inaba <i>et al.</i> , 2006)

1.5 Syngas cleaning and conditioning towards hydrogen applications

1.5.1 Syngas application and cleaning

The syngas is a building block to the production of numerous biofuels and biochemicals as well as heat and power. A diagram highlighting syngas applications is shown in Figure 1.8. In general, there is no set of standard specifications on the syngas but H_2/CO ratio of the gas can give an insight into its possible valorization pathways. Detailed information on syngas applications can be found elsewhere (Boerrigter *et al.*, n.d.; Molino *et al.*, 2018; Rauch *et al.*, 2014; P. L. Spath *et al.*, 2003). The primary use of syngas is fuels production through Fischer-Tropsch and methanol synthesis. Fischer-Tropsch synthesis produces, through catalytic reactions, renewable fuels, such as gasoline, diesel, and kerosene.

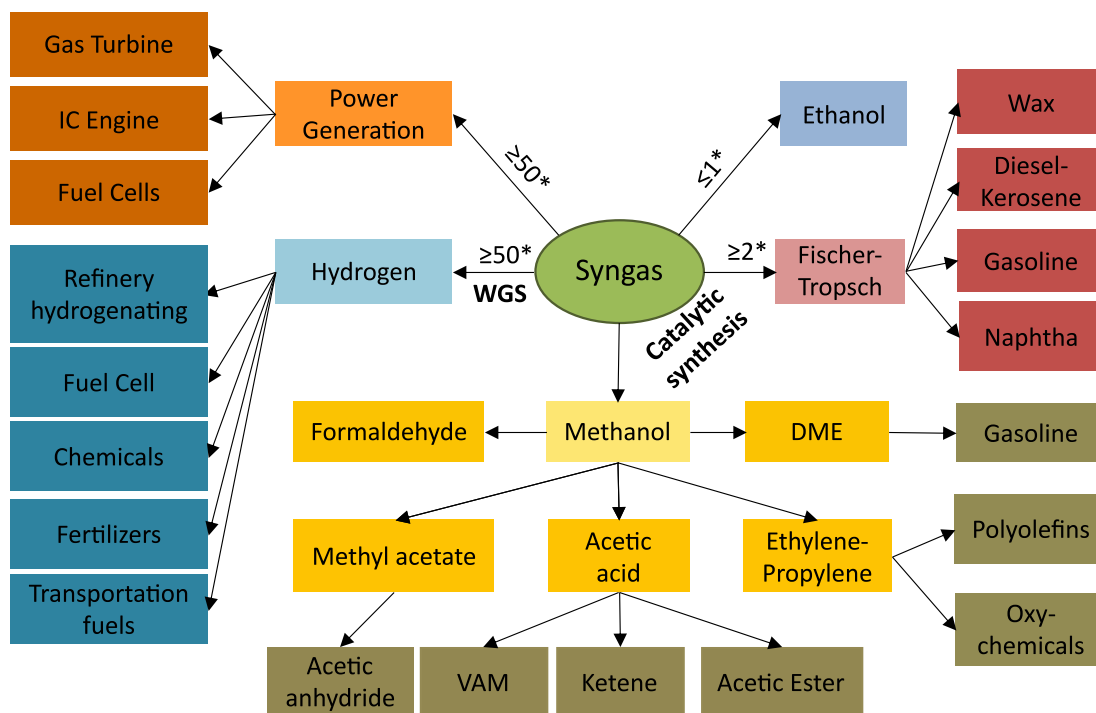


Figure 1.8: Application of syngas (* H_2/CO ratio) (adapted from (Hernández *et al.*, 2017))

Besides H_2 , CO , CO_2 , CH_4 , and N_2 (for air gasification), various impurities and contaminants found in the product gas are related to the feedstock and the production process. These pollutants are tars, particulate matter (PM), alkali metals, NH_3 , H_2S , HCl , SO_2 , and HCN . Many environmental concerns and technical issues in downstream equipment are associated with the presence of these impurities such as catalyst poisoning,

corrosion, and fouling (Abdoulmoumine *et al.*, 2015). The tolerance to pollutants and the cleanup method vary depending on the end-use technology and environmental emission regulations. For instance, for Fischer-Tropsch and methanol applications, the maximum allowable concentration of sulfur and nitrogen should be less than 1 and 0.1 ppm, respectively. Details on syngas specifications on impurities required for different applications can be found elsewhere (Asadullah, 2014; Ephraim *et al.*, 2020b; P. L. Spath *et al.*, 2003). Accordingly, these pollutants need to be gotten rid of to meet these stringent requirements.

Syngas cleaning is challenging and critical. Extensive research has been conducted on syngas cleanup in the last decades to meet cost goals and improve system performance. For instance, Abdoulmoumine *et al.* (2015) discussed the critical challenges in syngas cleanup and also summarized different hot gas cleanup technologies, while Chiche *et al.* (2013) presented a comprehensive review on trace contaminants removal from syngas for Fischer-Tropsch applications. Asadullah (2014) highlighted the advantages and disadvantages of different gas cleanup methods. Woolcock and Brown (Woolcock *et al.*, 2013) extensively reviewed cold, warm, and hot gas cleanup technologies for various contaminants. Other reviews have focused on removal technologies of the main significant pollutants (Torres *et al.*, 2007). Table 1.10 outlines the most common end-of-pipe technologies for syngas clean-up. Hot gas cleaning such as thermal cracking, adsorption, and physical separation is the common method owing to their higher thermal efficiency. On the other hand, in cold gas cleaning it is necessary to cool the gas down and then heat it to the desired temperature (Lotfi, 2021).

1.5.2 Renewable hydrogen production

By application, the chemical industry is the largest user of syngas while this H₂ is mainly produced from natural gas reforming. These last years have shown unprecedented momentum in hydrogen production from other routes including mostly water electrolysis and to a less extent, the pyrogasification of biomass. The literature shows a consensus that renewable hydrogen has the potential to be utilized in a variety of applications (Figure 1.8) or serve as a clean energy carrier. For hydrogen fuel applications, the international organization for standardization released ISO 14678:2019 classifying combustible hydrogen into three types: type I (gaseous), type II (liquid), and type III (solid) (ISO-14687, 2019). Each type requires a specific hydrogen purity depending on the endpoint applications. For example, hydrogen fuel with high purity grade (> 99.90) is required for industrial fuel applications (Aprea, 2014).

For this purpose, raw syngas is first upgraded to increase hydrogen content via water-gas shift reaction WGSR (Table 1.5). This subsequent step is achieved after the gas cleanup, CO is converted into a gas mixture in H₂ and CO₂. On an industrial scale, this step

Table 1.10: Overview of different syngas cleanup technologies

	Classification	Conditions-Reactions	RE (%)	
Tar	Hot	Thermal cracking	700 – 1300 °C	70-99
	Hot	Filters	400 – 1000 °C	50-98
		Cyclone	400 – 850 °C	<50-90
	Warm	OLGA technique	2 loop-oil scrubbing system	≤99
		Adsorption	80 °C – tar precipitation	50
	Cold	Wet scrubbers	Tar condensation	≤ 90
Particle matter	Hot-warm	Cyclone	900 °C	> 90-95
		Ceramic filters	400, 650, 850 °C	99
		Metallic filters	≤ 1000 °C	
		Granular bed filters	500-600 °C	>99.5
	Cold	Electrostatic precipitators	200 – 500 °C;1000 °C	
		Wet scrubbers		>95
H ₂ S	Cold	Chemical absorption	Amines scrubbing $H_2S + RNH_2 \rightleftharpoons RNH_3HS$	98-99
			K ₂ CO ₃ based process $H_2S + K_2CO_3 \rightleftharpoons KHCO_3 + KHS$	99.9
		Liquid redox process	RT $H_2S + 2 Fe^{3+} + \frac{1}{2} O_2 + H_2O + 2 Fe^{2+} + 2 OH^- + 2 Fe^{3+}$	99.9
			Physical absorption	-9 – 35 °C; 2-12 MPa
		Hybrid absorption	40 – 80 °C	99.99
		Hot	Adsorption	400 - 600 °C $MOx + xH_2S \longrightarrow MSx + xH_2O$ $MSx + 3 x/2 O_2 \longrightarrow MOx + xSO_2$
HCl	Cold	Caustic water/water absorption	$HCl + NaOH \longrightarrow NaCl + H_2O$	<93
	Hot	Adsorption	500-850 °C ;1 MPa $MO^+ + 2 HCl \longrightarrow MCl_2 + H_2O$ $MCO_3 + 2 HCl \longrightarrow MCl_2 + H_2O + CO_2$ $M_2CO_3 + 2 HCl \longrightarrow 2 MCl + H_2O + CO_2$	99-99.99
NH ₃	Cold	Water absorption	RT $2 NH_3 + NH_3 \longrightarrow N_2 + 3 H_2$	99
		Hot	Catalytic dehydrogenation	0.1 – 1 MPa; 700 - 800 °C $2 NH_3 \longrightarrow N_2 + 3 H_2$ $4 NH_3 + 3 O_2 \longrightarrow 2 N_2$
	Selective oxidation		2 MPa; 350-700 °C $4 NH_3 + 4 NO + O_2 \longrightarrow 4 N_2 + 6 H_2O$	60-99.99

RE: Removal Efficiency

is applied twice to ensure optimum conversion of CO. The first step is carried out at high temperature (HTS) close to equilibrium, typically at 300–450 °C, under the presence of an iron-chromium catalyst. Since WGS is exothermic and limited by the chemical equilibrium, a second step is applied at low temperature (LTS) to increase CO conversion. This step is run at about 180–250 °C and typically utilizes a copper catalyst. The concentration of residual CO at the outlet of HTS and LTS reactors is down to approximately 2.5 and 0.5% (Linde, 2022).

The gas mixture obtained after the shift contains a high concentration of H₂ and small quantities of CO₂, H₂O, CH₄, CO, and traces of other contaminants. The typical composition is 70–80 H₂, 15–25 CO₂, 3–6 CH₄, 1–3 CO (vol. %) (Nzihou *et al.*, 2021). To achieve high purity of hydrogen, different technologies currently exist for the purification of hydrogen streams. They can be broadly grouped into chemical, physical, and selective diffusion (Grashoff *et al.*, 1983). Physical purification methods comprise pressure swing adsorption, cryogenic separation, and metal hydride. Polymer membranes as well as metal membranes are the most used techniques of selective diffusion technique for hydrogen purification. The selection of the optimum purification techniques is based on the purity grade required by the end-pipe application and the viability of the purification technology (Dawood *et al.*, 2020).

A few comprehensive reviews about H₂ purification have been published in recent years. For instance, Du *et al.* (2021) presented an extensive and comprehensive review of hydrogen purification technologies for fuel cells. Dawood *et al.* (2020) summarized the state-of-the-art of hydrogen purification techniques. The advantages and limitations of the main purification technologies are summarized in the Table 1.11.

Pressure swing adsorption

Among the purification technologies, PSA is the dominant process where it is used in more than 85 % of industrial hydrogen production units at an industrial scale. PSA principle is based on the gas molecules binding ability to an absorbent material. The impurity molecules present stronger molecule/adsorbent interactions than hydrogen/adsorbent interactions, therefore are selectively retained (adsorbed) by the adsorbents. Hydrogen which cannot be adsorbed is recovered at the top of the adsorption columns at the pressure of the feeding flow (Chuah *et al.*, 2021). The gas stream leaving the PSA still contains unrecovered hydrogen and separated gases. Typically, several different micro- and mesoporous adsorbents are used in the form of successive layers, namely, silica gels, activated alumina, zeolites molecular sieves, and activated carbon (Besancon *et al.*, 2009). The use of multiple adsorbents, placed as layers in beds, allows the achievement of continuous flow systems and enhances PSA technology. The relative strength of various gases is shown in Figure 1.9. The cyclic nature of the process requires at least two vertical columns packed with adsorbents to operate simultaneously under four cyclic steps: adsorption, depressurization, purging, and repressurization. The performance

of the PSA cycle is measured in terms of two parameters, specifically, hydrogen purity and product throughput. The PSA process can exhibit a purity grade and a recovery rate of more than 99.999 % and 90 %, respectively. Air Liquide, Air Products, UOP, and Linde are the PSA suppliers for industrial purification of H₂.

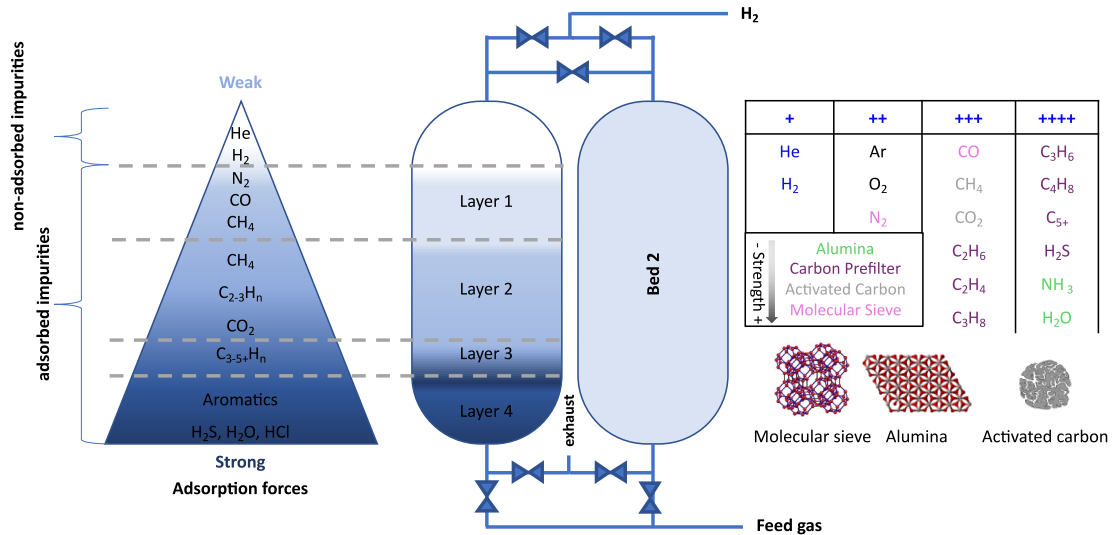


Figure 1.9: Flow scheme and relative strength of adsorption for different gas onto adsorbents used in PSA technology (Besancon *et al.*, 2009; Du *et al.*, 2021; Shah, 2021)

Table 1.11: Comparison of different features and aspects of hydrogen purification methods (Aasadnia *et al.*, 2021; Dawood *et al.*, 2020; Du *et al.*, 2021; Ebrahimi *et al.*, 2016; Grashoff *et al.*, 1983; C. Song *et al.*, 2019; Uehara, n.d.)

Type	Physical	Diffusion		
Technology	Pressure swing adsorption	Cryogenic separation	Polymer membrane	Palladium membrane
Principle	Separation under pressure according to the molecular characteristics and affinity for an adsorbent material	Stepwise condensation of gas feed at low temperatures	Gas molecules passage through the holes of permeable; membranes according to a solution-diffusion mechanism	
Conditions	2 – 15 MPa; RT	150 – 75 °C	2 – 20 MPa; 0 – 100 °C	< 2 MPa; 300 – 500 °C
H ₂ (vol. %)	50-90	50-90	70-95	> 98
Purity (%)	99-99.999	99-99.999	99.5%	99.99 – 99.999
H ₂ RR (%)	69-99.99.6	69-99.99.6	< 85	99
Scale	Large	Large	Small to large	Small to medium
Advantages	Low operation cost; Long service life; Fast process cycle; Large scale use	No chemical reagents or additives are used; Capability to produce liquid CO ₂	Novel separation concept; High selectivity; Low energy consumption; -Simple modular systems; No waste streams	
Drawbacks	Large floor area; Inflexibility; Low adaptability; Low selectivity; Suitable for CO ₂ low concentrations	Energy intensive; High capital cost	Sensitivity to Sulfur compounds and other trace elements; Fouling and low fluxes; Selectivity reduction by CO ₂ presence problems	
R&D	Enhance recovery rate; Removal of specific impurity	Enhance purity grade	Increasing H ₂ flux rates and purity grade; Improving durability; Reducing power requirement and cost	

1.6 Motivation and objective of the study

The literature review has highlighted the current status, challenges of pyrogasification technology, and thermochemical conversion of biomass components. Previous studies have outlined the potency of hydrogen production from cellulose gasification. Nevertheless, cellulose gasification has not been yet addressed as a potential pathway for green energy production. The main motive for using cellulose for gasification was to understand biomass behavior since its the main biomass constituent. Moreover, most of the previous studies used biomass components containing sulfur and generated from the sulfur-bearing process which is associated with air environmental risks. Even though organosolv fractionation can separate lignocellulosic into pure components to be used as added-value materials, it is a high-cost process.

In this context, BioEB has patented an innovative technology, for refining lignocellulosic material. Following a similar concept of crude oil refining, lignocellulosic biomass resources can be fractionated into their constituents that are further transformed by different routes into marketable renewable fuels and chemicals, as shown in Figure 1.10. The technology is branded as *LEEBIOTM* referring to **L**ow **E**nergy **E**xtraction of **B**IOmass. A wide range of residues can be treated including softwood, hardwood, straws, and energy crops.

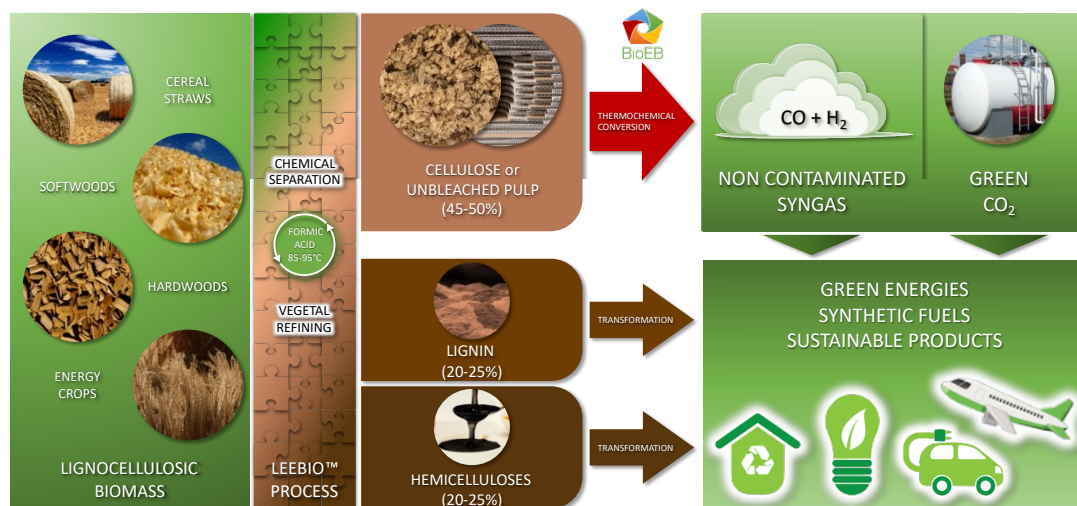


Figure 1.10: *LEEBIOTM* technology – Cellulose pulp, green energies, fuels, and products from biomass

The process consists of a non-degrading separation of lignocellulosic residues to cellulose, hemicelluloses, and lignin. This process uses only formic acid ($< 95\text{ }^{\circ}\text{C}$) at atmospheric pressure. The consequences of this chemical separation are very low energy consumption and a high separation efficiency. The profitability of this process is advocated by the fact that the extracted lignin and hemicelluloses can be introduced into industrial sectors

without changing the existing technologies infrastructures. The obtained cellulose pulp is sulfur-free and has a homogeneous inorganic composition and can be used as energy source, in addition to its conventional applications (G.-H. Delmas *et al.*, 2021).

Considering the potential of gasification technology and organosolv pretreatment, there is a great interest in coupling both processes in a biorefinery concept. The production of added-value products and a refined pulp via LEEBIO products entices to overcome gasification limitations in terms of feedstock price and syngas cleaning cost. On the other hand, gasification can be the driving force of this integration by producing energy to develop energy-self-sufficient biorefineries.

Therefore, the present work aims to investigate the gasification of an organosolv pulp in a biorefinery approach.

Materials and Experimental Methods

2

2.1	Materials	54
2.2	Properties Characterization	54
2.2.1	Proximate and ultimate analysis	54
	Proximate analysis	54
	Ultimate analysis	56
	High heating value analysis	56
2.2.2	Macromolecular composition	56
2.2.3	Inorganic composition: quantitative analysis	57
	Transmission Electron Microscopy	57
	Scanning Electron Microscopy	57
	X-ray powder diffraction	58
2.3	Biomass pretreatment using LEEBIO process	58
2.3.1	Biomass pretreatment	58
2.3.2	Lab-scale pretreatment	58
	Formic Acid treatment	58
	Residual lignin in the pulp	59
2.3.3	Pilot scale pretreatment	60
	Formic Acid Treatment	60
	Alkaline treatment	61
2.3.4	Effectiveness of LEEBIO treatment	61
2.4	Pyrolysis and gasification behaviors and kinetics	63
2.4.1	Pyrolysis in TGA	63
2.4.2	Steam gasification in TGA	63
2.5	Lab scale fixed bed pyrogasification	65
2.5.1	Experimental setup	65
2.5.2	Experimental conditions and program	66
2.5.3	Pyrolysis products	66
	Permanent gas quantification and analysis	66
	Pyrolysis oil quantification and analysis	68
	Analysis of tar composition	69
	Char quantification and analysis	70
2.5.4	Products quantification and analysis in steam gasification of char	70

The following chapter presents and describes the different materials and devices used in this work, as well as the experimental methods and protocols. It was split into several sections:

- Section 2.1 and 2.2 introduce the selected feedstocks and the characterization methods of their physico-chemical properties.
- Section 2.3 describes the extraction process of *LEEBIOTM* at the lab and pilot scale.
- Section 2.4 was dedicated to describing the experimental procedures of pyrolysis and gasification carried out using thermogravimetric analysis (TGA).
- Section 2.5 aims to describe lab-scale operating of steam gasification including the protocols, product sampling, and analysis methods.

2.1 Materials

In the context of *CELNER* project, straw and wood residues used in this work were selected based on their availability in *Occitanie* region (France). Wheat straw (*WS*) and softwood sawdust (*SS*) were opted as parent biomass samples for cellulose extraction and pyrogasification experiments. *WS* and *SS* crops were obtained commercially on the local market in bags of 10 liters. 100 kg of *SS* crops were provided from a local sawmill. *SS* was dried at 40 °C for 48 hours at RAGT-Energie Albi. A commercial microcrystalline cellulose (*MCC*) (catalog number 435236, Sigma Aldrich, CAS 9004-34-6) was purchased to represent cellulose in kinetic analysis during pyrolysis process. Commercial Cellulose fibers Arbocell (*ARC*) supplied from J. RETTENMAIER & SÖHNE GmbH was used in pyrogasification tests for comparison. The feedstocks are presented in Figure 2.1.

2.2 Properties Characterization

The physico-chemical properties of the selected materials, the cellulose pulp, and pyrogasification biochar were characterized.

2.2.1 Proximate and ultimate analysis

Proximate analysis

The proximate analysis includes the determination of the content of, volatile matter, ash, and fixed carbon. The first three properties were determined using EN ISO 18134-3, EN ISO 18122, and ISO 18123, respectively. The measurements were replicated three times. The fixed carbon content was calculated by difference:

$$100\% = \textit{Moisture} + \textit{Ash} + \textit{Volatile matter} + \textit{Fixed carbon}$$



(a) Raw WS



(b) Raw SS



(c) ARC pellets



(d) MCC

Figure 2.1: Selected feedstocks

Ultimate analysis

The quantification of the mass fractions of carbon (C), hydrogen (H), and nitrogen (N) was obtained by CHNS analysis using a Thermoquest NA 2000 elemental analyzer. Three replicates of the analysis were carried out following EN ISO 16948. The mass fraction of oxygen was calculated by difference:

$$100\% = C + H + N + S + O + Ash$$

High heating value analysis

The High Heating Value (HHV) was determined using an oxygen-automated bomb calorimeter (IKA C 5000). Roughly 400 mg of the sample powder was pressed to produce a tablet. The tablet was placed in the crucible which in turn was enclosed in the calorimeter bomb to undergo complete combustion. The HHV value was calculated by the calorimeter bomb.

2.2.2 Macromolecular composition

The macromolecular composition of the lignocellulosic materials was determined using a laboratory analytical and gravimetric procedure. The analyses were carried out by the technical staff of LGP2 UMR CNRS 5518 research center (Laboratoire Génie des Procédés Papetiers, Grenoble INP) based on the standards used in the paper industry. Prior to the determination of cellulose, hemicelluloses and, lignin content in the raw biomass and cellulose pulp samples were first crushed at 50 μm and dried for 12 h at 60 °C. In the next step, extractives were eliminated.

Extractives in biomass refer to the non-structural components such as fats, waxes, starch, sucrose, nitrate/nitrites, protein, and chlorophyll. Removal of extractives was carried out following the protocol described by Tanoh (Tchini Severin Tanoh, 2021). An acetone Soxhlet extraction system was employed to determine the extractives content. 3 g of the dried sample was added to a dried thimble which in turn was placed in the Soxhlet siphon tube for 6 h. 250 mL of acetone was added to the boiling flask. The solid residue was dried and then mixed with distilled water and boiled under reflux for 1 h. The fraction of extractives in the sample was calculated on a dry basis following Eq.2.1:

$$Extractives (\%) = \frac{(m_{initial\ dry\ sample} + m_{thimble}) - m_{thimble\ plus\ final\ sample}}{m_{initial\ dry\ sample}} \quad (2.1)$$

The extractive-free sample was used in the determination of lignin and polysaccharides.

The lignin content was determined by the sum of soluble and insoluble (Klason) lignin as described in TAPPI standard T222 om-83.

The elemental sugars content was measured for the biomass and cellulose pulp samples using ion chromatography after a two-stage sulphuric acid hydrolysis of samples, as described in TAPPI standard T249 cm-80. The neutral monosugars obtained were quantified by ion chromatography using a Dionex ICS5000 system equipped with the following components:

- Dual pump module pumps with an integrated degasser.
- Eluent generator in which a KOH cartridge generates OH^- ions by electrolysis.
- Detector/chromatography Module containing: guard and separator columns (CarboPac PA10), conductivity detectors, and electrochemical detectors.

The experiment was repeated twice to confirm the reproducibility.

2.2.3 Inorganic composition: quantitative analysis

The identification and quantification of the mineral species were performed using an inductively coupled plasma optical emission spectrometer (ICP - AES, HORIBA Jobin-Yvon Ultima 2). Before analysis, complete digestion of the solid was achieved using acid reagents, as described by (Pham Minh *et al.*, 2020). 150 mg of the dried and milled solid sample was placed in a closed Teflon PTFE vessel. 1.5 mL of H_2O_2 , 4 mL of HNO_3 , and 0.5 mL of HF were added. The system was heated at 220 °C for 1 h and 8 h for raw material and biochar, respectively. The obtained acid solution was then diluted with demineralized water to 50 mL. Finally, the solution was analyzed using the aforementioned technique.

Transmission Electron Microscopy

To examine the chemical structure at a nanometric scale, elemental composition, and mapping were performed using transmission electron microscopy (**TEM**) (JEOL cold-FEG JEM-ARM200F) at Centre de Microcaractérisation Raimond Castaing in Toulouse, France. **TEM** is coupled with energy-dispersive X-ray (**EDX**). For the measurements, powder samples with particle sizes below 50 μm were dispersed in ethanol and then deposited on a copper grid with a Lacey-type carbon film. The microscope was operated at 200 kV equipped with a probe Cs corrector reaching a spatial resolution of 0.078 nm. **EDX** spectra were recorded on a JEOL CENTURIO SDD detector.

Scanning Electron Microscopy

The morphology was observed using a Hitachi TM3030 Plus tabletop scanning electron microscope **SEM** with an accelerating voltage of 15 kV.

X-ray powder diffraction

X-ray powder diffraction **XRD** was used to examine the crystal structures. The powders were analyzed with an X'pert Pro MPD instrument (Panalytical). The Cu–K α radiation source ($\lambda = 1.542 \text{ \AA}$) operates at 5 kV and 40 mA. Diffraction peaks were recorded at $0.5 \text{ }^\circ \text{ s}^{-1}$ over a 2θ range from 10 to 100 $^\circ$. The **XRD** spectra were normalized to the 002 diffraction peak after baseline correction.

2.3 Biomass pretreatment using LEEBIO process

2.3.1 Biomass pretreatment

In the framework of this work, the extraction of cellulose was carried out at a lab and pilot scales following **LEEBIOTM** process steps. Lab-scale tests were performed first to assess **LEEBIOTM** treatment using different biomass residues and optimize reaction time. In light of the obtained results, a pilot-scale operation was carried out with a scaling-up approach.

The pulp samples were named as follows: As a reminder, the pulp was designated by: **Cell-Biomass-Scale**. Where, **Cell** refers to cellulose since it is the main constituent of the pulp solid; **Biomass** represents the treated biomass, **WS** and **SS**. **Scale** corresponds *L* lab scale tests and *P* for pilot scale test.

2.3.2 Lab-scale pretreatment

Formic Acid treatment

The extraction tests were performed at the RAPSODEE research center (Albi, France). Prior to the treatment, **WS** and **SS** were crushed into $< 5 \text{ mm}$ particles using a cutting Mill PULVERTSETTE 15. First, 40 g of dried biomass was loaded in a 0.5 L glass-jacketed reactor. Next, 200 g of an aqueous solution of formic acid (85 wt.%) (**FA**) were added to obtain a 5:1 liquid-to-solid ratio. Under medium stirring of 50 rpm (round per minute), using a mechanical stirrer with a Teflon anchor, the mixture was heated at 85 $^\circ\text{C}$. When the temperature was stabilized at 85 $^\circ\text{C}$, the chemical reaction started. Pulping/reaction time was varied from 2 to 4 h. After the desired reaction time, the mixture was cooled to room temperature. Then, the mixture was transferred into a Buchner filtration apparatus to separate the raw cellulose from the acid liquor 1. Acid liquor 1 was transferred into a glass beaker. After that, the remaining cellulose on the Buchner apparatus was gently washed with **FA** (85 wt. %), then filtered to remove the acid liquor 2 which was mixed with acid liquor 1 and the whole mixture was kept for further manipulations. Finally, the remaining pulp was washed with warm water (40-50 $^\circ\text{C}$) and filtered until a neutral pH of the filtrate was reached. The pulp was dried in the oven at 60 $^\circ\text{C}$ for 12 h. Graphs of the obtained pulps are depicted in Figure 2.2.

The volume of consumed potassium permanganate solution by lignin is determined following:

$$V = \frac{[(b - a) \times M]}{0.1} \quad (2.5)$$

Where a and b are the equivalent volume of sodium thiosulphate solution (mL) used for the determination of the sample and the blank solution, respectively. M is the molarity of sodium thiosulphate solution.

The Kappa number Kn is thus determined according to Eq. 2.6:

$$Kn = (V/m) * d \quad (2.6)$$

where m is the weight of the pulp sample and d refers to the correction factor which depends on the quantity of consumed $KMnO_4$; the values of d range from 0.958 to 1.044. The lignin content is calculated as follows:

$$Lignin = Kn \times 0.181 \quad (2.7)$$

2.3.3 Pilot scale pretreatment

Formic Acid Treatment

The operations were conducted at PIVERT-SAS in Compiègne, France. 40.2 kg of SS were pulped in ROSENMUND pilot filter/dryer RoLab 0.4 m² (Figure 2.3a). Prior to the acid pulping, the biomass was dried in a ventilated oven, for 3 h at 70 °C (30% air change), in order to reach the highest possible dry matter DM content. The final dry matter was 97.8 wt.%. The pilot extraction operations are summarized in the flowchart shown in Figure 2.4.

Acid treatment / Filtration

14 kg of the inlet biomass was loaded into the tank equipped with the 120 µm filtration cloth (Figure 2.3b). The equipment was closed and then the remaining 26.2 kg was introduced by suction. Of the total 40.2 kg of biomass, 206 kg of 85 wt. % formic acid (FA) (Fisher Chemical) were added through the Rolab liquid introduction line to obtain a 5:1 w/w liquid to solid ratio. Stirring was started at 30 rpm and the double jacket was heated to 90 °C. After 3 h, the temperature of the reaction medium reaches 85°C. This temperature was maintained for 3 h 30 before cooling the reaction medium (observation of a black coloration). The agitation was then slowed down to 7 rpm for 15 h, and the medium was pressurized to 1.5 bar to filter the liquor. The filtrate was stored in a 200 L plastic drum.

Acid wash / Filtration

134 kg of FA was introduced to the cellulose retained on the filter in 2 stages. 30.4 kg and 103.6 kg of the acid solvent were added for the first and second rounds, respectively. For each addition, the pulp in contact with the acid mixture was stirred for 5 min and then filtered at 1.5 bar on a 120 µm cloth. The filtered acid liquors were stored in containers.

Water washing / Filtration

The water washings were carried out in 3 times. Around 200 L of warm water (60 °C) was introduced in each addition to the Rolab. The mixture was stirred for 5 min and then filtered at 1 bar through a 120 µm filter cloth (Figure 2.3a). All filtrates were collected in a single storage.

Drying

After washing the cellulose, the Rolab filter tank was opened and the obtained pulp was placed in the Rolab drying tank. The drying tank has a larger heat exchange surface. The drying conditions were set at 70 °C, under agitation at 25 rpm and with a vacuum of 50 mbar in order to obtain a target DM around 90 wt. %. The obtained pulp, Cell-SS-P, is shown in Figure 2.3c.

Alkaline treatment

Cell-SS-A is the washed Cell-SS-P by sodium hydroxide solution. Alkaline treatment was performed to eliminate the remaining silicon in the cellulose pulp. 15 g of dried Cell-SS-P (> 95 %) are mixed with 150 mL of water. Approximately, 5 mL of 12 wt. % NaOH solution are then added until pH reaches a value of 11–12 at room temperature. Under stirring, the mixture was heated for 60 min until a stable temperature of 80 °C in the medium. Finally, the cellulose pulp is washed with hot water to reach pH 6–7 to ensure the removal of sodium hydroxide residues.

2.3.4 Effectiveness of LEEBIO treatment

After determining the optimal pulping time by measuring the kappa number, the effectiveness of both tests at the lab and pilot scale were assessed. The macromolecular composition of the pulp samples was determined using the analytical procedure described in Section 2.2.2.

Solid yield

The pulp yield is calculated as follows:

$$Y_{pulp} = \frac{m_{pulp}}{m_{biomass}} (\%) \quad (2.8)$$

where m_{pulp} and $m_{biomass}$ are the mass of dry and extractive-free pulp and biomass, respectively.

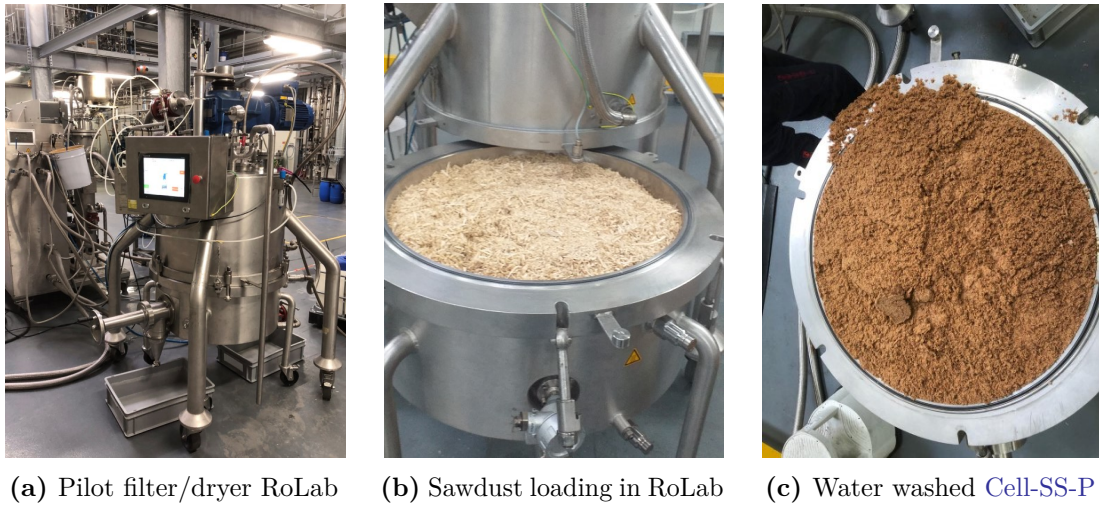


Figure 2.3: Cellulose extraction using RoLab 0.4 m²

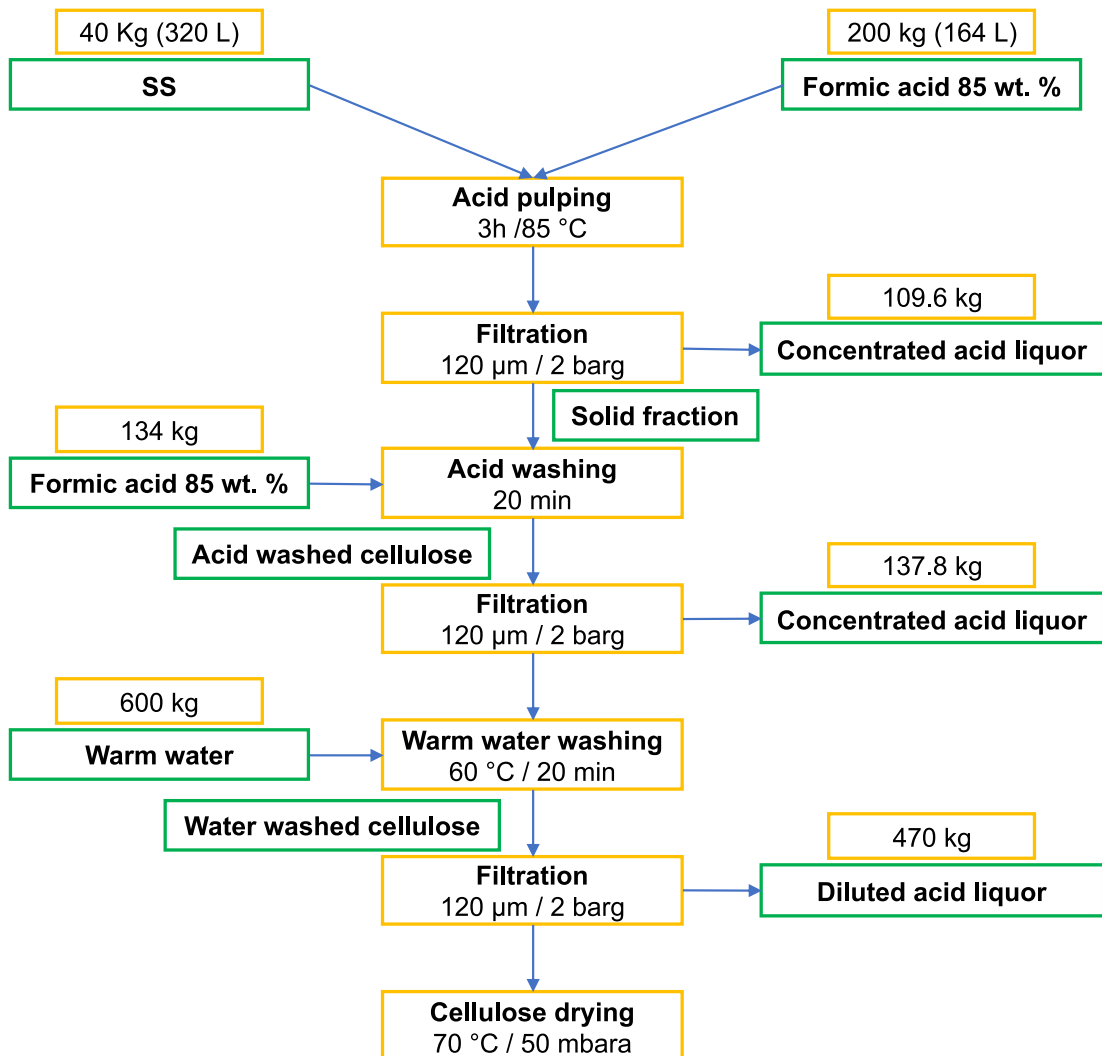


Figure 2.4: Flowchart of the SS extraction following the *LEEBIO*TM process

Elimination rate of lignin and hemicellulose

$$Y_i = \frac{W_{i, biomass} - W_{i, pulp} \times Y_{pulp}}{W_{i, biomass}} (\%) \quad (2.9)$$

wherein $W_{i, biomass}$ and $W_{i, pulp}$ is the mass fraction of corresponding components in biomass and pulp, respectively.

2.4 Pyrolysis and gasification behaviors and kinetics

In the present section, the main details of the experimental methods of pyrolysis and gasification using TGA are provided. The two processes were carried out in different analyzers, and different thermal approaches.

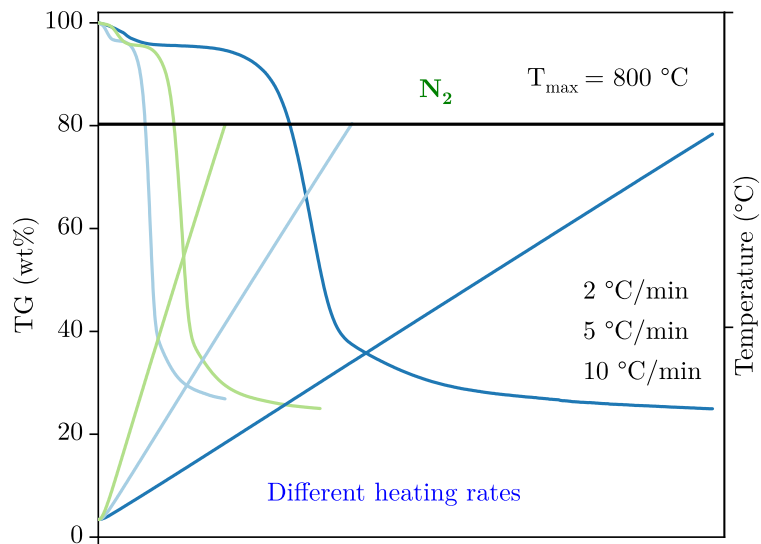
2.4.1 Pyrolysis in TGA

Non-isothermal experiments of slow pyrolysis experiments were conducted with TGA LabSys evo SETARAM. WS, Cell-WS-L, SS, Cell-SS-L, Cell-SS-P, and MCC were used in this study. The weight of the sample was ~ 10 mg in order to mitigate the heat and mass transfer limitations. The dried sample was placed in a platinum crucible and heated from room temperature to 800°C in an inert atmosphere at heating rates of 2, 5, and $10^\circ\text{C min}^{-1}$, respectively (Figure 2.5a). Pure nitrogen was used as a carrier gas to provide an inert atmosphere with a flow rate of 3 L h^{-1} . To remove buoyancy effects, a blank test was recorded before sample analysis for each heating rate program. The tests were performed in triplicate to verify their repeatability. The thermogravimetry (TG) and the Difference Thermo Gravimetry (dTG) curves were plotted by setting the weight of the sample at 150°C as the "zero point" of weight loss. The temperature range between 150 and 650°C was used in the kinetic study.

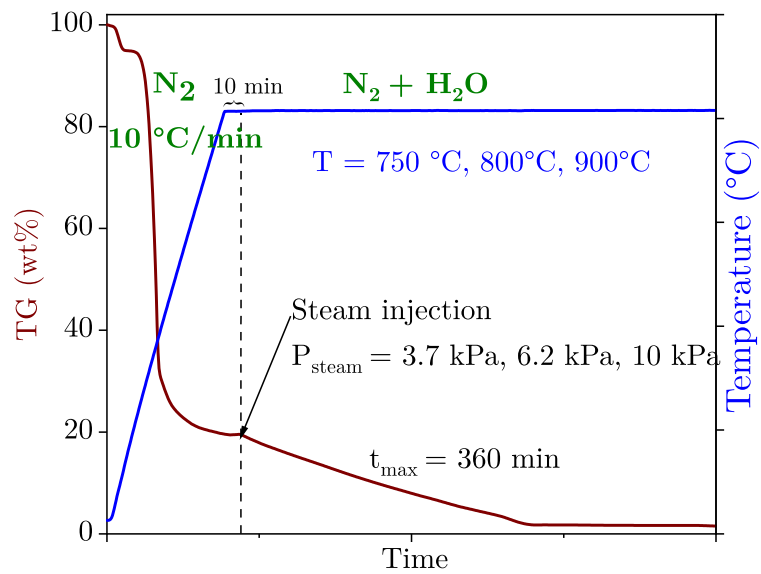
2.4.2 Steam gasification in TGA

A TG analyzer Seratam TG-ATD 92 thermal analyzer, coupled with a wet gas generator (Wetsys) was used to perform isothermal gasification experiments. WS, Cell-WS-L, SS and Cell-SS-P were used. 20 mg of each sample were placed in a cylindrical platinum crucible to experiment as follows (Figure 2.5):

1. Under a flow of 1 L h^{-1} of nitrogen, the sample was heated to be used to sweep the biochar sample during the heat-up period from room temperature to the gasification temperature (750 , 800 , and 900°C). The heat-up was carried out at a constant rate of $10^\circ\text{C min}^{-1}$.



(a) Pyrolysis



(b) Gasification

Figure 2.5: TGA experimental program of pyrolysis and gasification

2. The inert atmosphere was maintained at the desired temperature for 10 min to ensure complete pyrolysis. Thus, both temperature and mass were stabilized.
3. Afterward, the atmosphere was switched to the gasifying mixture ($N_2 + \text{Steam}$), with a steam flow rate of 3 L h^{-1} . The total flow rate was set to 4 L h^{-1} . Different partial steam pressures were used (3.7, 6.2, and 10 kPa) for the gasification of the pyrolysis char. The samples were then kept at the gasification temperature for 360 min. The medium was then cooled down to room temperature.

A blank test was conducted for each test condition to remove the buoyancy effect. The TGA experiments were reproduced to assess repeatability. The calculated standard deviation of the mass loss was below 2 %, which is considered to be satisfactory.

2.5 Lab scale fixed bed pyrogasification

2.5.1 Experimental setup

Pyrogasification tests were performed in a semi-continuous lab-scale fixed-bed at RAP-SODEE center. A photograph of the complete experimental setup is shown in Figure 2.7 and 2.6. It consists of four main parts:

1. The reactor
2. Heat and temperature control system
3. Inlet gas flow control which consists of two different panels: N_2 /air gas control and steam generator.
4. The gas sampling and analysis system.

The bed reactor is a stainless steel tube with an inner diameter of 6 cm and a length of 60 cm. It is electrically heated by a furnace. The thermal regulation is ensured by an 818 Eurotherm connected to K-thermocouple that is positioned at mid-height of the reactor. The temperature profile in the reactor is supervised by a series of 8 K-type thermocouples placed vertically on the outer wall of the reactor. The reactor is equipped with two frits placed on the bottom and the top. The first one is used to maintain the feedstock, while the top one is to prevent biochar particles escape.

The inlet gases are fed from the bottom of the reactor, under the bottom frit. The gases flow including N_2 and steam are controlled by mass flow controllers (BROOK Instrument, SLA 5800 Series). Nitrogen is delivered through a separate input for pyrolysis tests, while it is fed in a mixture with steam for gasification experiments. Steam was obtained

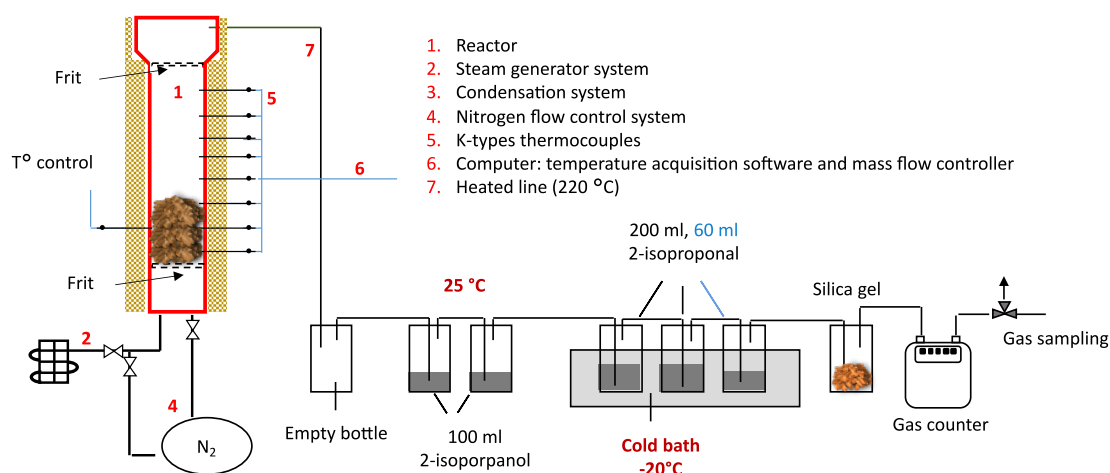


Figure 2.6: Schematic presentation of pyrogasification experimental setup

at 180 °C by a steam generator. Regarding the fluidization regime, preliminary tests were performed to ensure a fixed-bed regime during the experiments. Full information about the characterization of the fluidization regime in this reactor could be found by Klinghoffer (Klinghoffer, 2013) and Ducouso (Ducouso, 2015). In the present work, no inert bed material was involved in the tests.

Downstream, an electrical heating line is installed on the top exit of the reactor to maintain the temperature at 220 °C. The exit gas passes through a series of 7 impinger bottles to trap the condensates and clean the gas.

2.5.2 Experimental conditions and program

During the experiment, 90 g of the sample was heated under a nitrogen flow of 3.5 L min⁻¹ at a heating rate of 20 °C min⁻¹ to complete the pyrolysis step. After achieving the desired temperatures (750, 850, and 950 °C), the reactor was kept under an inert atmosphere for 15 min. After that, steam was continuously injected (isotherm for 1 h) with nitrogen to make up a mixture including 60 vol. %. At the end of the gasification step experiment, the heating was turned off and the atmosphere was switched to nitrogen until the room temperature was reached. For this study, Cell-SS-P SS, WS, SS, and ARC were used. The experimental program is presented in Figure 2.8.

2.5.3 Pyrolysis products

Permanent gas quantification and analysis

The non-condensable gases were sampled upstream of the condensation train. The volume of flue gas was also measured using a gas meter (Figure 2.6). The product gas was sampled offline, it was collected by a Tedlar bag Gas Sampling Bags. The



Figure 2.7: Fixed-bed reactor used in pyrogasification experiments

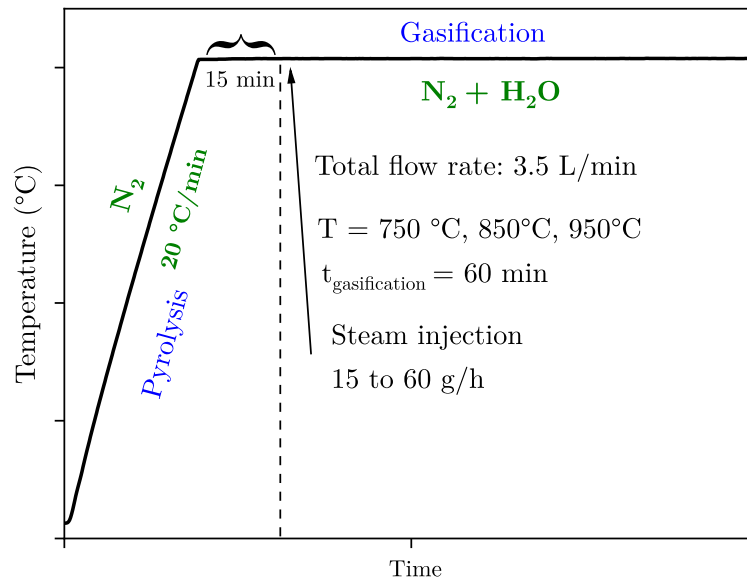


Figure 2.8: Experimental program of pyrolysis and gasification tests

concentration of H₂, N₂, CH₄, CO, CO₂, and C₂₋₃H_m was measured using a micro-gas chromatography (micro GC-3000A, Agilent). The flow rate of the permanent gases in the product gas was calculated from the composition of the analyzed gas and the material balance equation. It was calculated based on the known inlet flow rate of N₂ and its molar fraction in the product gas:

$$\dot{V}_{productgas} = \frac{\dot{V}_{N_2}}{Y_{N_2}} - \dot{V}_{N_2} \quad (2.10)$$

where, $\dot{V}_{productgas}$ denotes the volumetric flow rate of the product gas (L min⁻¹); \dot{V}_{N_2} represents the inlet flow rate of N₂; Y_{N_2} indicates the molar fraction of N₂ in the analyzed flue gas.

The mass flow rate of the product gas is calculated by Eq. 2.11:

$$\dot{m}_{productgas} = \dot{V}_{productgas} \times \rho_{productgas} \quad (2.11)$$

Pyrolysis oil quantification and analysis

Bio oil quantification

Condensates including tar and water were recovered through the condensation train placed upstream of the heated line as shown in Figures 2.6 and 2.9. The conditioning unit was adapted from tar protocol (CEN, 2006) using 6 impinger bottles containing iso-propanol. The two first bottles were placed at room temperature. Three other impingers were placed in a bath cooled to about -20 °C. The last one is filled with silica gel to trap the last traces of water and to protect the micro-GC. It is worth mentioning that a blank test of pyrolysis was carried out to ensure that iso-propanol contained does not evaporate during the experiment. The mass of iso-propanol remained constant. For each experiment, the bottles and pipelines were weighted to quantify the condensates. For pyrolysis tests, the condensates are composed of water and tar. The water content was immediately determined by the Karl Fischer method using V30 volumetric titrator (METTLER TOLEDO). The mass of the analyzed sample (iso-propanol + condensates) was ~ 0.5 g, where HYDRANAL composite 5 and dry methanol were used as titrant and solvent, respectively.

The weight of pyrolysis is determined at dry basis following:

$$m_{water} = m_{condensates} \times \left(1 + \frac{m_{isopropanol}}{m_{condensables}}\right) \times \%H_2O - m_{moisture} (wt. \%) \quad (2.12)$$

the weight of tar is thus calculated by difference:

$$m_{tar} = m_{condensates} - m_{water} \quad (2.13)$$



Figure 2.9: Collected condensates during pyrolysis stage

where $m_{condensates}$ stands for the weight of collected condensates, $m_{isopropanol}$ is the weight of iso-propanol, % H₂O represents the water content in the sample of iso-propanol and condensable matter is given by Karl-Fischer titrator. m_{water} means the weight of water in the total recovered liquid.

Analysis of tar composition

Qualitative analysis

The gas chromatography-mass spectrometry GC-MS (Shimadzu GCMS-TQ8030) instrument was used to analyze light compounds in bio-oil. The chromatographic separation was performed using a Rxi-5Sil MS column (30 m × 0.25 mm × 25 μm). Helium was used as carrier gas at a flow rate of 3 mL min⁻¹. A sample volume of 1 μL was injected in the split mode with a split ratio of 10:1. The injector was kept at a constant temperature of 250 °C. The GC oven temperature ramps for the work were as follows: begin heating at 40°C that was first held for 5 min, and then raised to 280 °C at a rate of 5 °C min⁻¹, and this final temperature was held for 2 min. The mass selective detector was operated in electron impact ionization mode (ionization energy of 70 eV). The transfer line and the ion source temperatures were kept at 260 and 200 °C, respectively.

Quantitative analysis

From the results of the qualitative analysis, 10 major compounds of bio-oil that displayed a relatively high content (based on the area %) were quantified by the external standard method. These compounds include benzene, toluene, m-xylene, m-xylene, styrene, m-cresol, phenol, naphthalene and fluorene. For each of the quantified compounds, calibration curves were prepared by the injection of 8 standard solutions (0.5, 2, 4, 8, 10, 15, 20, and 100 μg μL⁻¹). The results for the quantified pyrolysis compounds are then expressed as g kg⁻¹_{feedstock}.

Char quantification and analysis

Biochar was collected and weighed. The physio-chemical properties of biochar were analyzed using similar characterization tests applied to the feedstocks. The analytical techniques include: elemental, proximate analysis (2.2.1), ICP-OES, HHV, and TEM-EDX.

2.5.4 Products quantification and analysis in steam gasification of char

The product gas was measured using a similar protocol used for pyrolysis gas that is described in Section 2.5.3. Using the same approach of tar tapping, a condensation train was used for biochar gasification tests to condense the output steam.

Lignocellulosic biomass fractionation using LEEBIO technology: from laboratory to pilot-scale

3

3.1	Introduction	71
3.2	Results and discussion	72
3.2.1	Optimization of pulping time at lab-scale	72
3.2.2	Acid treatment assessment	74
3.2.3	Effect of acid treatment on the inorganic composition	76
3.2.4	Validation of LEEBIO treatment at Pilot Scale	76
3.2.5	Alkaline treated pulp	80
3.3	Conclusion	81

3.1 Introduction

Chapter 1 has pointed out the necessity of optimization of organic solvent pretreatment for commercialization biorefineries. As a consequence, this chapter investigates the fractionation wheat straw (WS) and softwood sawdust (SS) using LEEBIO process. In a first set of experiments, the optimization of treatment conditions in terms of reaction time was studied. The impact of feedstock characteristics on fractionation performance and the effect of acid pulping on the inorganic composition were then addressed. A further study was undertaken at a pilot scale, using SS, to validate the fractionation technology. A mass balance of the process was then established. The ultimate purpose is to prepare the pulp that will be subjected to pyrogasification. As a reminder, pulped biomass is called 'cellulose pulp' or 'pulp' following the nomenclature of the pulp and paper industry. The pulp is hence designated by: Cell-Biomass-Scale. Where, Cell refers to cellulose since it is the main constituent of the extracted solid; Biomass represents the treated biomass, WS and SS. Scale corresponds *L* lab scale tests and *P* the pilot scale test.

The results of the pilot-scale test, represented by Cell-SS-P, are shown with the findings of lab-scale tests, but they are discussed in a further section.

Table 3.1: Element and proximate analysis of feedstocks and pulp samples

		WS	Cell-WS-L	SS	Cell-SS-L	Cell-SS-P
Proximate analysis (dry basis, wt. %)	M	9.26	4.0	39.2	6.54	1.7
	VM	77.1	86.5	81.5	85.0	82.2
	FC	17.9	9.3	18.2	14.7	17.5
	A	5.0	4.2	0.3	0.3	0.3
Ultimate analysis (dry ash-free, wt. %)	N	0.9	0.1	0.1	0	0
	C	49.5	45.2	47.8	51.9	48.5
	H	6.8	6.4	6.2	6.0	6.1
	O*	42.8	48.3	45.9	42.1	45.4
	H/C	1.6	1.7	1.6	1.4	1.5
	O/C	0.6	0.8	0.72	0.6	0.7
	HHV	19.5	17.42	20.5	20.79	19.3

M: moisture; VM: volatile matter; FC: fixed carbon; A: ash; HHV unit is MJ kg⁻¹; * by difference

3.2 Results and discussion

Table 3.1 presents the elemental and proximate analysis of feedstocks and pulp samples. The present chemical data showed some differences related to biomass. For instance, WS are more enriched in ash while moisture content in SS is relatively high. These differences are generally related to agronomic practices such as types of soil, nutrient uptake, storage, and collection conditions. The pretreatment was performed on dried biomass at 85 °C and atmospheric pressure. Biomass was mixed with 85 wt. % formic acid (FA) at a 1:5 solid-to-liquid ratio. As can be seen, after acid treatment significant differences are apparent in the macromolecular composition between feedstock and pulp samples. This difference can be explained by the effect of FA on the chemical composition namely cellulose, lignin, and hemicellulose. These aspects as well as the effect of acid pulping on the inorganic composition are discussed in-depth in the next sections.

3.2.1 Optimization of pulping time at lab-scale

As mentioned above, LEEBIO process is operated at moderate conditions in terms of temperature and liquid-to-solid ratio. Pulping time refers to the reaction time between the solvent and biomass and depends on the aforementioned parameters. Generally,

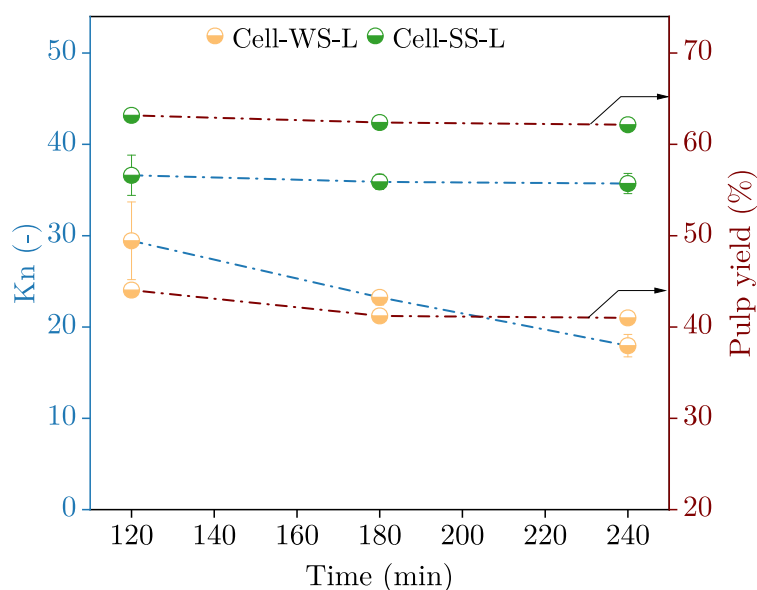


Figure 3.1: Effect of reaction time on pulp yield and kappa number

increasing reaction time tends to higher the extent of reaction, but increases the energy consumption. The optimization of pulping time can thus improve the efficiency of organosolv pretreatment.

Figure 3.1 shows the effect of cooking time on pulp yield and kappa number (Kn) on lab-scale tests. With extending the pulping time from 120 to 180 min, the pulp yield from and WS and SS decreased from 44.0 to 41.2 % and 63.2 to 62.4 %, respectively. Kn decreased from 29.4 to 23.3 and 36.6 to 35.9, respectively. Beyond 180 min, variations in the pulp yield of both samples were minimal. The observed trends are similar to those described in the literature (Baeza *et al.*, 1991; L. Hu *et al.*, 2019; Sinha, 2021; G. Yu *et al.*, 2013). Tu *et al.* (2008) tried different pulping time between 20 and 180 min for FA organosolv pretreatment. They found that the maximum delignification was mostly reached during the first 80 min of pulping. Moreover, cellulose degradation and lignin recondensation reactions can occur during long treatments (Dapiá *et al.*, 2002). Based on the above results, 180 min was selected as the optimum pulping time.

It is worth mentioning that the obtained cellulose pulp had a similar kappa number to others prepared using LEEBIO process (M. Delmas, 2019). Rice straw and birch were delignified to Kn 21 and 29 during 120 and 180 min of pulping, respectively. Compared to other pulps, higher yield, and kappa number were obtained from the softwood (SS) delignification. This difference is elucidated in the next section.

3.2.2 Acid treatment: effect on the chemical composition and fractionation effectiveness

Following the determination of the optimal pulping time, the effectiveness of LEEBIO treatment was assessed based on the chemical composition of pulp and biomass. The content of lignin and sugars were measured by gravimetric analysis. It must be pointed out that compared to the titrimetric analysis, the gravimetric analysis would display some differences since it is a destructive technique.

The FA treatment relies on the proton donor role of concentrated FA for various impacts (Quoc Lam *et al.*, 2001). This affects the hydrolysis of lignin through hydrolytic cleavage of ether bonds to form soluble fragments. It also affects the hydrolysis of hemicelluloses through the breakdown of glycosidic bonds to form soluble sugars (Jahan, 2006). In addition, lignin and hemicellulose are proposed to bind through electrostatic interactions rather than covalent linkages (Kang *et al.*, 2019). The action of FA can weaken these interactions and thus break these intermolecular links between lignin, cellulose, and hemicellulose. Therefore, this offers LEEBIO process the advantage to be a non-destructive method and operates at moderate experimental conditions (85 °C, 1 atm) compared to kraft pulping and other organosolv treatments. Furthermore, it was reported that harsh ethanol pulping conditions could lead to a significant amount of cellulose degradation (Lindemann *et al.*, 2017; Schmetz *et al.*, 2016).

Table 3.2 shows the chemical composition of feedstocks and pulp samples. The depicted results attest that the biomass fractionation was successfully performed in FA. As can be seen, after acid treatment, cellulose was the main component in the different pulps. The high hemicellulose rate of different samples shows the effect FA treatment on hemicellulose hydrolysis. On the contrary, the results displayed significant differences in delignification rate. For acid WS, Cell-WS-L was 2.5 times more delignified than those of SS. The results on WS pulping tie well with other studies, in terms of pulp yield and hemicellulose removal. However, it must be pointed out that the comparison of our results with other studies is limited. The treatment effectiveness significantly depends on different parameters including solvent concentration, liquid-to-solid ratio, temperature cooking time, and catalyst. In a recent study, Pathak *et al.* (2021) reported 97 % hemicellulose, 95 % lignin removal, and 86 % cellulose retention from sugarcane tops at 125 °C for 90 min with 85 % FA at 1:7.5 solid to liquid ratio. Hoang Quoc Lam *et al.* (2001) optimized the fractionation of rice straw in FA in terms of acid concentration, temperature, and cooking time. A delignification rate of 85 % and a pulp yield of 44.4 % were obtained by 60 min treatment in 90 % FA at 100 °C. M. Zhang *et al.* (2010) reported corncob using 80 % FA at 60 °C for 8 min achieved a 85 and 75 % of hemicellulose and lignin removal, respectively. G. Tian *et al.* (2019) investigated wheat straw fractionation and reported that 86 % of lignin can be removed by 20 min

Table 3.2: Macromolecular composition, pulp yield and removal rates of lignin and hemicelluloses

(wt. %)	WS	Cell-WS-L	SS	Cell-SS-L	Cell-SS-P
Cellulose	44.8	74.3	38.5	55.5	60.4
Lignin	21.2	11.7	31.6	32.5	32.5
Hemicelluloses	34.0	14.0	29.9	11.1	7.1
Glucomannan	0.9	0.0	22.6	5.9	2.1
Pulp yield		0.41		0.63	0.67
Hemicellulose removal rate		83.0		76.7	84.2
Delignification rate		77.4		33.2	31.3

at 130 °C using 90 % FA. Dapiá *et al.* (2002) preheated beech wood chips using 80 % FA for 3 h varying pulping temperature between 110 and 130 °C, efficiently removing 85 – 90 % of hemicellulose and 80 – 90 % of lignin and obtaining a pulp yield between 45 and 50 %.

Overall WS was more efficiently fractionated than SS. Since both feedstocks were treated under similar operating conditions, this can mainly be explained by the difference in the structure of the plant cell wall. The latter consists generally of three types of layers, namely the middle lamella (*M*), the primary wall (*P*), and the secondary wall (*S*). Cellulose, lignin, and hemicelluloses are differently distributed through these layers (Panshin, 1980). Lignin is highly concentrated in the center corner (*CC*) and its proportion decreases with increasing distance into the middle lamella (L. Dong *et al.*, 2015). According to literature, during organosolv treatment of straw and hardwood, lignin is removed in the order of $S \rightarrow M \rightarrow CC$ (I.-C. Wang *et al.*, 1993). In contrast to other biomass types, softwood delignification can be hindered by the preferential removal of lignin in *CC* and *M* regions (Paszner, 1989). Moreover, the high proportion of glucomannan in SS (Table 3.2) can also have an effect, limiting solvent penetration. It has been found that glucomannan is strongly bonded to cellulose in softwood cell walls, while lignin and hemicellulose are located between glucomannan-coated cellulose (Salmén, 2004; Salmén *et al.*, 2008).

The air present within wood capillaries is also an obstacle to liquid penetration of wood voids (Malkov, 2001). Compared to kraft pulping, the obtained lignin and hemicellulose removal rate seemed to be lower. This is due to the steaming and impregnation steps used in kraft pulping that were not applied in the present study. The first step aims to raise the temperature and expel the air from the inside of the wood chips (Broberg *et*

al., 2019). The second step consists of mixing the liquid and wood for several hours to ensure a uniform impregnation of water and reagents within the wood (Mortha *et al.*, 2016).

3.2.3 Effect of acid treatment on the inorganic composition

The concentration of different inorganic elements in treated feedstocks and pulps are illustrated in Figure 3.2. TEM-EDX mapping showing the distribution of inorganic elements presented in Figures 3.3 and 3.4

From TEM-EDX mapping, different metal oxides and other salts can be found in biomass. They include AAEM and other metals oxides such as K_2O , MgO , CaO , and Fe_2O_3 in addition to P_2O_5 and SiO_2 . As it can be seen in Figure 3.2, significant fractions of K, Na, Mg and Ca drastically decreased as a result of the dissolution of salts containing AAEM under acidic conditions. In addition, the concentration of P and S were also lowered, as well as that of N (Table 3.1).

In contrast, Si was the main inorganic constituent of pulp, indicating that Si derivatives are retained during acid pulping (Quoc Lam *et al.*, 2001). Si proportion in the inherent inorganic content was 52 % and 16 % for WS and SS, respectively while in the pulp was approximately 87 % and 50 % for Cell-WS-L and Cell-SS-L, respectively. These findings are directly in line with previous findings. Sinha (2021) reported that the amount of ash and Si retained in the pulp was very high, as % ash and % Si were 15.2 and 13.5, respectively. Pan *et al.* (2005) reported 83 % of Si in wheat straw remained in the pulp after acetic acid pulping. The aforementioned results are validated by TEM-EDX mapping, indicating that the majority of retained Si in the pulp is present in the form of SiO_2 , precisely in the epidermic cells (Patel *et al.*, 1991).

From TEM-EDX mapping, the presence of Ca in the cellulose pulp can be noticed, in contrast to other AAEM elements. As can be seen in Figure 3.2, Ca content did not change after the pulping which means that Ca salts were partially dissolved. Similar observations were made by Huang Quoc Lam *et al.* (2005). They reported that part of Ca content can remain in the pulp because of its weak solubility in acid media. Therefore, it can bond with Si to form calcium silicate ($SiCa_2$).

During thermochemical processes, slagging and fouling issues are related to these inorganics (Q. Liu *et al.*, 2017). They can also influence the gasification kinetics and products distribution. These aspects are discussed in Chapter 5 and 6.

3.2.4 Validation of LEEBIO treatment at Pilot Scale

To validate the performance of the process at a pilot scale, we conducted a fractionation test of SS at a scale factor of 1000. As the forest-wood industry plays a vital role in

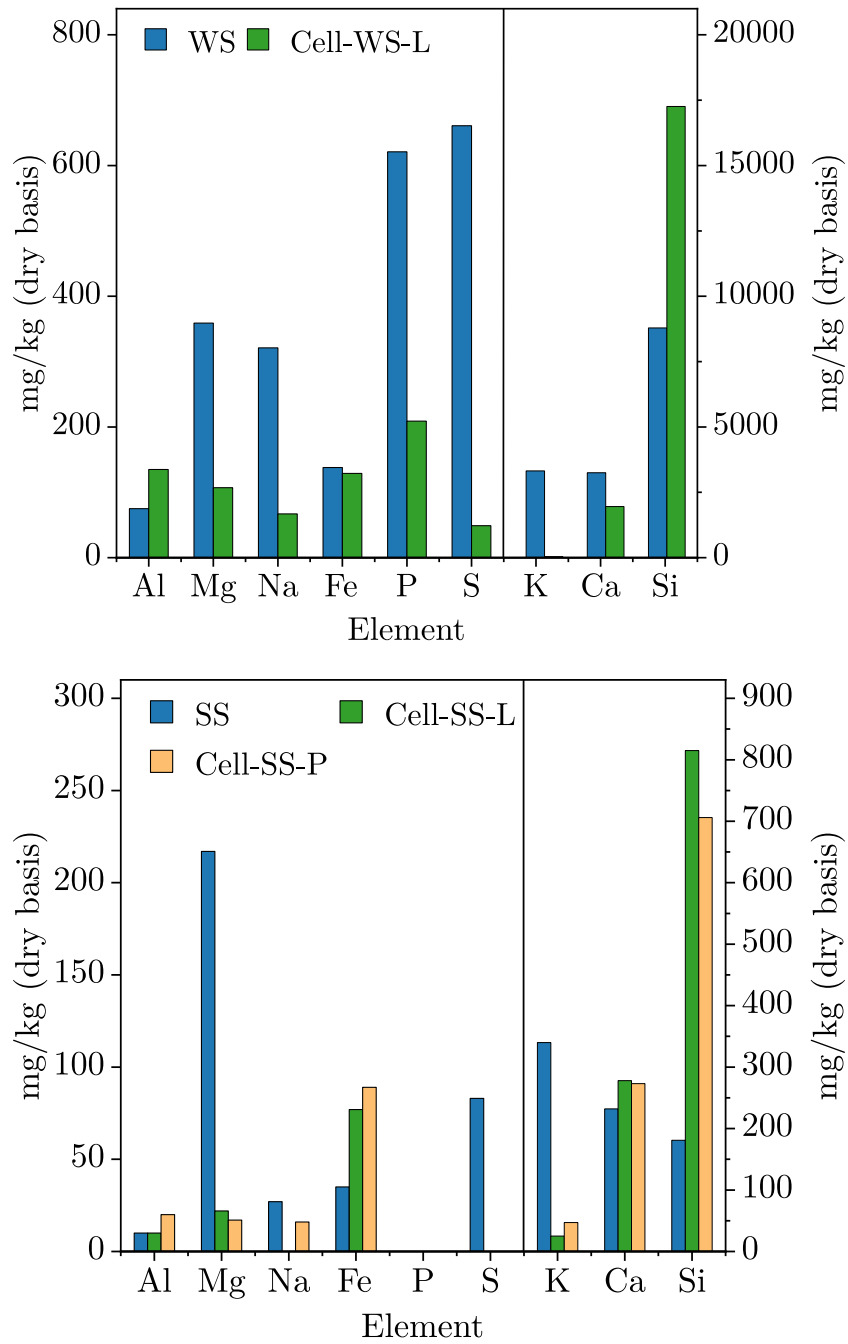


Figure 3.2: Inorganic composition of feedstocks and pulps

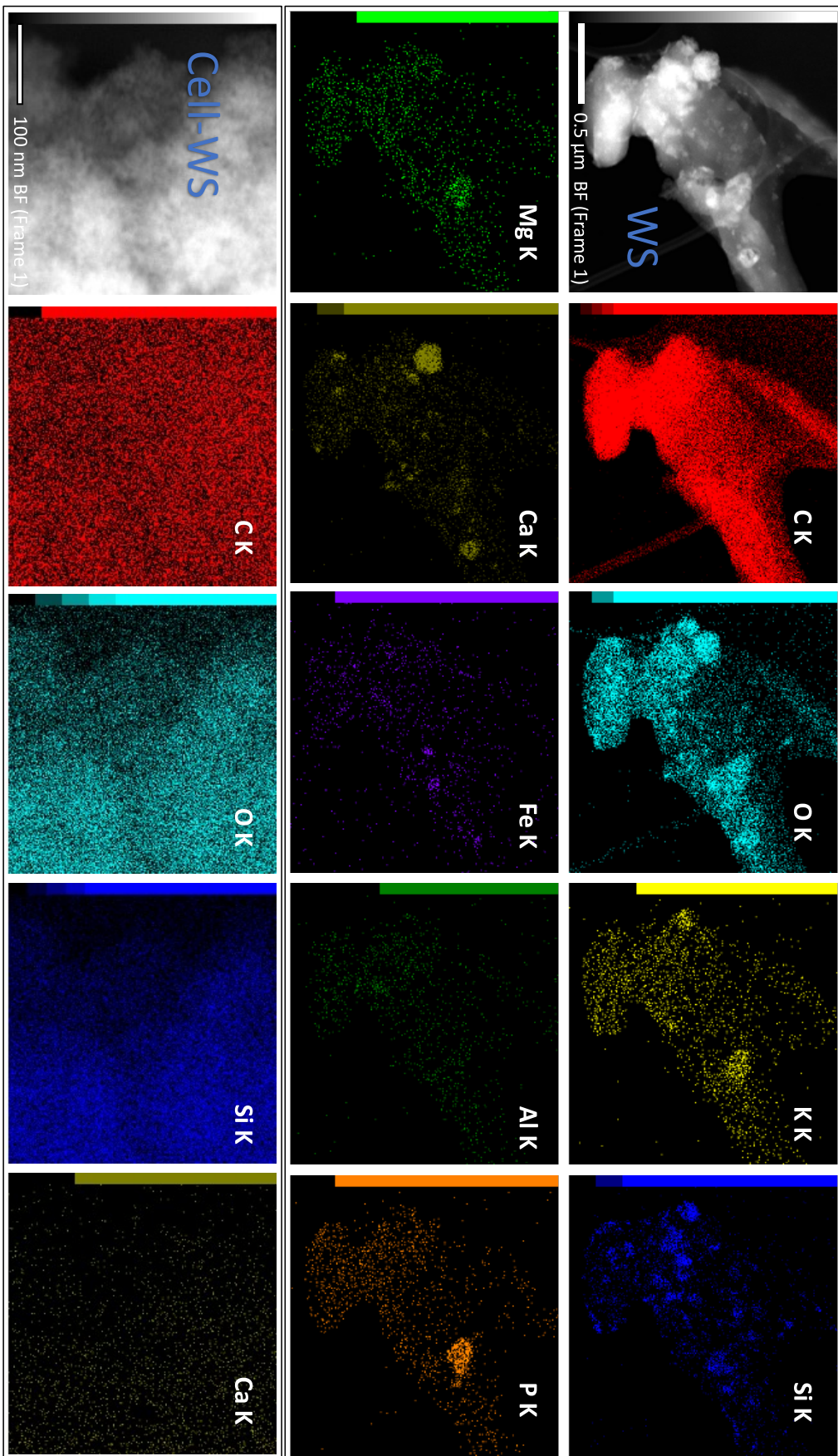


Figure 3.3: TEM image with energy-dispersive X-ray (EDX) mapping for WS and Cell-WS-L

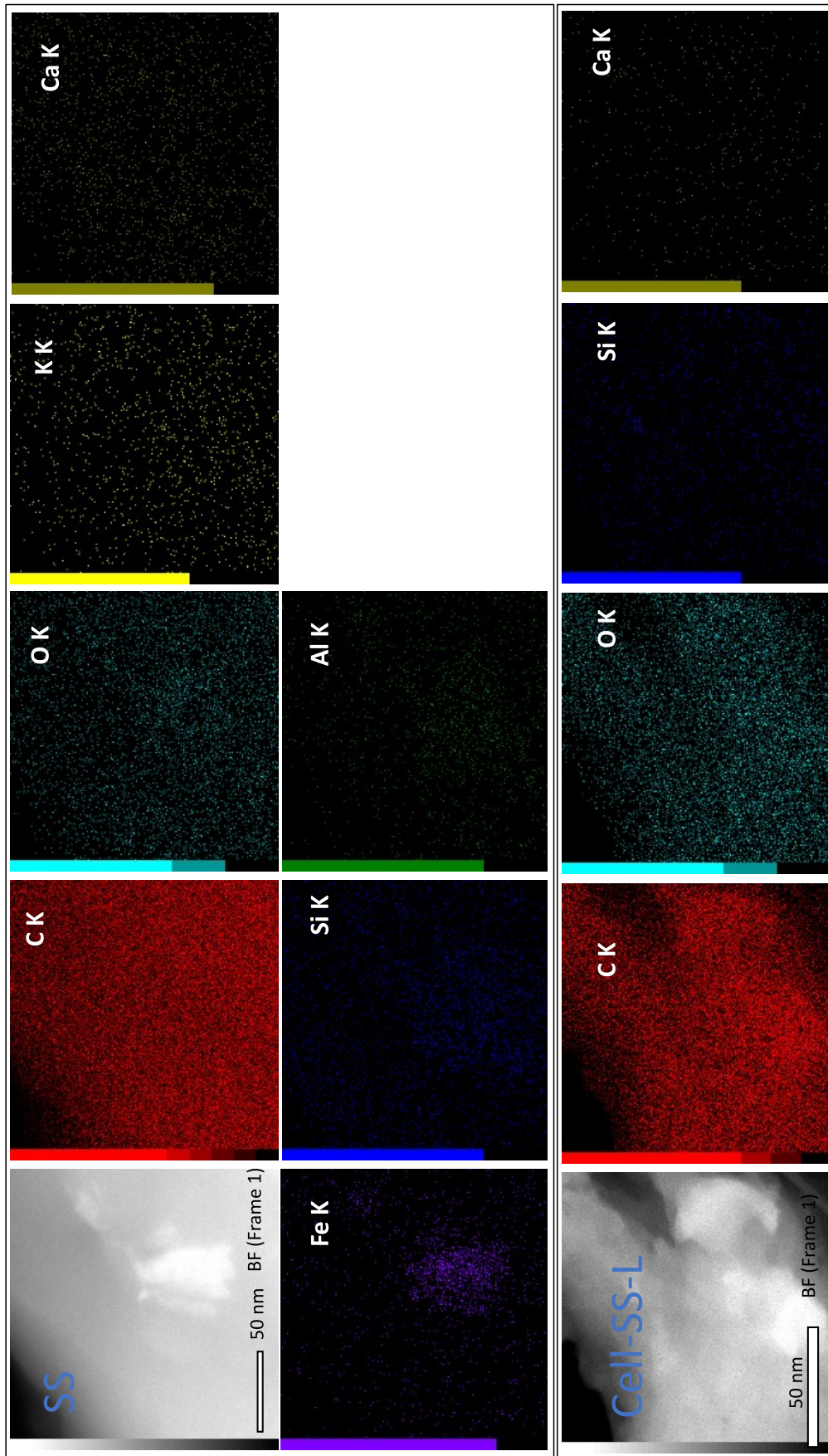


Figure 3.4: TEM image with energy-dispersive X-ray (EDX) mapping for SS, Cell-SS-L and Cell-SS-P

Table 3.3: Mass balance of pilot-plant acid pulping operation

		Weight (%DM)	Solid weight
	Treated SS	40.2 (97.8 %)	
Input	85 % FA for pulping	206	39.3
	85 % FA for acid washing	134.0	
Output	Acid liquor 1	109.6 (7.0 %)	
	Acid liquor 2	137.8 (2.8 %)	38.5
	Dried Cell-SS-P pulp	27.4 (98.3 %)	
Mass balance (kg)			-0.85

Weight unit is kg; DM: dry matter

the French economy and wood is one of the common raw materials used in gasification, we focused on softwood sawdust (**SS**). At the pilot scale, the same pulping conditions were maintained in terms of **FA** concentration, solid-to-liquid ratio, cooking time, and temperature.

Pulp yield, lignin and hemicellulose removal from the pilot scale test were comparable to those from lab-scale pulping, as shown in Table 3.2. This similarity in **SS** pulp properties confirms that the treatment effectiveness is mainly influenced by the wood cell structure, as aforementioned in Section 3.2.2. The results given in Figure 3.2 show that pulp from lab-scale and pilot-scale had similar mineral composition. The results confirm the action of **FA** on **AAEM** salts dissolution.

From a mass balance perspective, pilot scale operation offers a better and more reliable outlook than the laboratory scale. Table 3.3 summarizes the pilot-scale operation of **FA** treatment. In general, hemicelluloses are isolated during the cooking and the precipitated lignin is dissolved by the warm acid washing. Overall, these data are used as input in Chapter 7 for energy assessment and integration of biomass fractionation process coupled with pyrogasification of **Cell-SS-P** pulp.

3.2.5 Alkaline treated pulp

Elimination of Si from the pulp through alkaline treatment has two main purposes: on the one hand, silica has multifaceted applications in various industries, on the other hand, silica is well known for its inhibiting effect on biochar gasification (Nzihou *et al.*, 2013b). The inorganic composition of the pulp before (**Cell-SS-P**) and after alkaline treatment (**Cell-SS-A**) is given in Table 3.4. TEM -EDX cartography is given in Figure 3.5. The efficiency of the alkaline washing on the elimination of Si derivatives can be illustrated

Table 3.4: Main inorganic elements in SS pulp (pilot-scale) before and after alkaline treatment

mg kg ⁻¹	K	Na	Mg	Ca	Fe	P	S	Al	Si
Cell-SS-P	47	16	17	273	89	0	0	21	706
Cell-SS-A	34	208	419	1943	121	457	0	34	268

by a decrease of 65 % between Cell-SS-P and Cell-SS-A. However, the rise of AAEM content that was not present in the acid pulp may be due to the inorganic species in some impurities in the chemical itself. Moreover, the alkaline wash parts of the biomass elements are removed from the sample and the relative amount of these impurities increases.

It should be pointed out that alkaline treatment had also an influence on macromolecular composition by dissolving a fraction of residual lignin. This is the reason for the decrease in fixed carbon content, as shown in Table 3.1.

3.3 Conclusion

Wheat straw and softwood sawdust were successfully fractionated by a formic acid process at a lab scale. The maximum delignification rate of both biomass by 85 wt. % formic acid was practically completed after nearly 180 min. Hemicellulose was efficiently removed from both feedstocks. The residual lignin sawdust was relatively higher as a result of the wood cell structure and pulping reaction scheme. Major differences in the chemical composition between the pulp and the feedstocks were displayed. Most inorganic elements, namely alkali and alkaline earth metals were dissolved while Si was retained in the resultant pulp, precisely in epidermic cells.

The validation of the process at pilot scale, with a scaling factor of 1000, by pulping softwood sawdust, resulted in similar molecular pulp characteristics at lab-scale in terms of pulp yield, lignin, and hemicellulose removal as well as mineral composition. A further step of alkaline treatment of pilot-scale pulp was successfully achieved to eliminate Si with an elimination rate of 65 %.

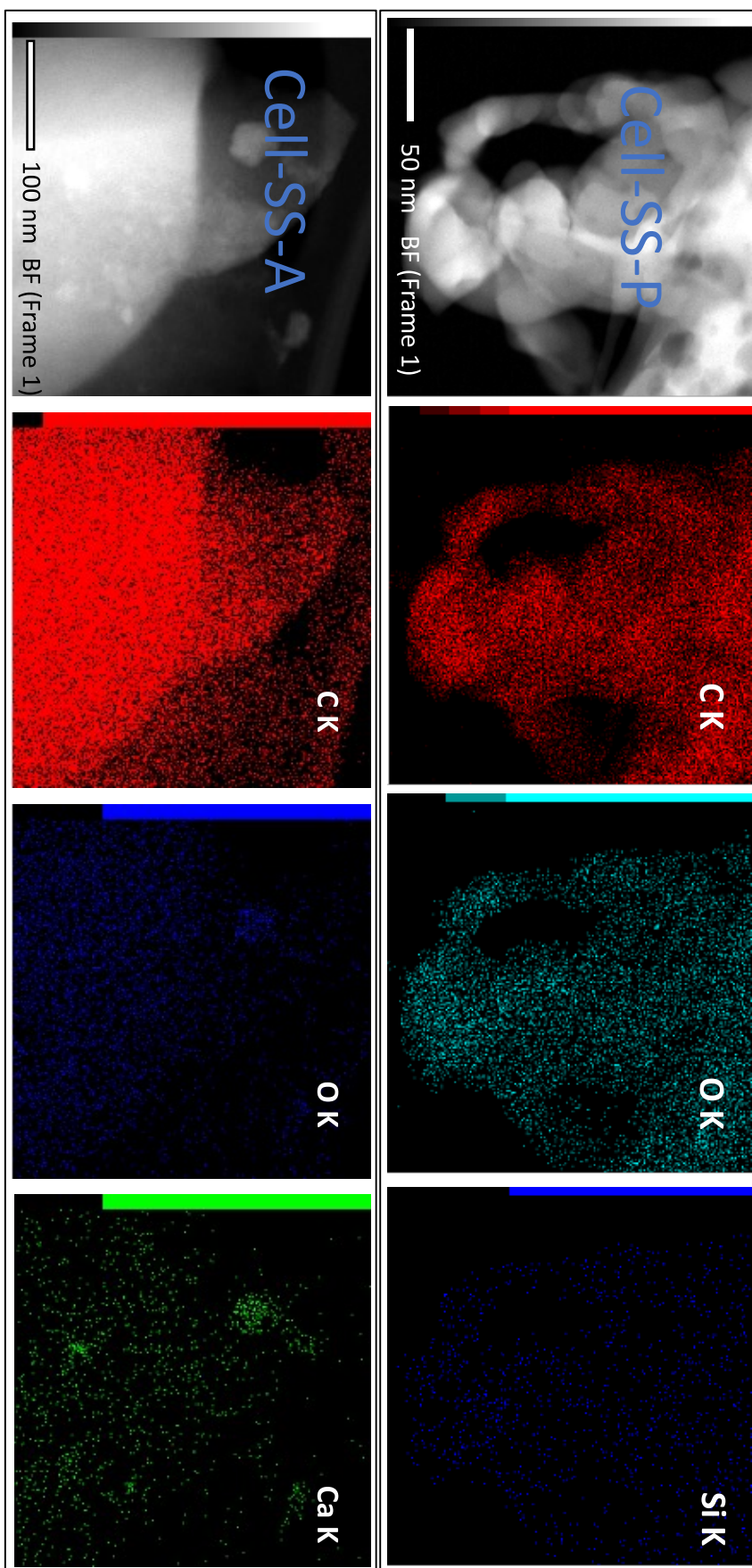


Figure 3.5: TEM mapping image with energy-dispersive X-ray (EDX) mapping for Cell-SS-P before and after alkaline treatment

Thermal degradation of LEEBIO cellulose pulp: effect of the composition and kinetics

4

4.1	Introduction	83
4.2	Kinetic analysis approach	84
	TGA kinetics	84
	Model with three independent reactions	85
	Peak deconvolution: Fraser–Suzuki function	85
	Triplet kinetic determination: isoconversional model-free approach	86
	Determination of reaction model: generalized master-plots	86
4.3	Results and discussion	88
	4.3.1 Pyrolysis characteristics	88
	TG and dTG profile	88
	Thermal stability	89
	Degradation rate	91
	Effect of heating rate	91
	4.3.2 Fraser–Suzuki deconvolution and isoconversional kinetic study	91
	Fraser–Suzuki deconvolution	91
	Activation energy estimation by KAS model-Free Kinetics	93
	Determination of the mechanism by master plots method	97
4.4	Conclusion	99
	Appendix	101

4.1 Introduction

This chapter is intended to discuss the thermal degradation of extracted pulp using TGA. The chapter is divided into two sections:

- Section 4.3.1 describes the decomposition characteristics of the pulp in particular the effect of the macromolecular composition.
- Section 4.3.2 discusses the non-isothermal kinetic analysis of cellulose pulp, under a parallel-reaction scheme. Fraser-Suzuki method was adopted to deconvolute TGA curves, followed by an integral isoconversional procedure and generalized master plots method.

According to ICTAC Kinetic committee (Vyazovkin *et al.*, 2011), isoconversional model-free methods are one of the main methods used for determining the kinetic parameters and mechanism during pyrolysis studies. Isoconversional methods have been recommended as a practical method capable of verifying the reliability of experimental data (Anca-Couce *et al.*, 2014). Differential and integral methods are the most popular isoconversional methods. They can be applied in both isothermal and non-isothermal approaches.

Accordingly, the integral isoconversional method Kissinger–Akahira–Sunose (KAS) in a non-isothermal approach was used for the kinetics analysis. The tests were performed under a temperature program of three different heating rates 2, 5, and 10 °C min⁻¹. Three different cellulosic materials were used:

- Pulp extracted from wheat straw at lab scale Cell-WS-L
- Pulp extracted from softwood sawdust at pilot scale Cell-SS-P
- Microcrystalline cellulose MCC was also used as a reference

4.2 Kinetic analysis approach

TGA kinetics

In non-isothermal TGA at linear heating rate, $\beta = dT/dt$, the reaction rate $d\alpha/dt$ can be expressed as follows:

$$d\alpha/dT = \left(\frac{A}{\beta}\right) \exp\left(\frac{-E_a}{RT}\right) f(\alpha) \quad (4.1)$$

where α represents the conversion, A (s⁻¹) is the pre-exponential factor, E_a (kJ mol⁻¹) is the apparent activation energy (kJ mol⁻¹), and R is the universal gas constant (8.314 J mol⁻¹ K⁻¹), and T is the gasification temperature. $f(\alpha)$ is a temperature-independent function representing the reaction mechanism. The degree of conversion α , calculated from measured mass loss, can be defined as:

$$\alpha = \frac{m_0 - m(t)}{m_0 - m_f} (\%) \quad (4.2)$$

Where m_0 is the mass of the dry sample, $m(t)$ is the sample mass at time t while m_f is the mass of the sample at the end of the pyrolysis reaction. $d\alpha/dT$ values are then calculated by dividing the change in α over that temperature step.

Model with three independent reactions

To describe LEEBIO pulp decomposition, three pseudo component model were considered, following a similar approach to that used for lignocellulosic biomass. This approach supposes that the decomposition occurs through three parallel reactions of pseudo-components which represent hemicelluloses, cellulose, and lignin present in the pulp. Thus, non-extracted hemicelluloses and lignin are taken into account in this approach. It should be pointed out that the proportion of pseudo-components should be in agreement with the macromolecular composition of the lignocellulosic material (Romero Millán *et al.*, 2017). The global reaction rate is then described by:

$$\frac{d\alpha}{dT} = \sum_{i=1}^3 c_i \frac{d\alpha_i}{dT} \quad (4.3)$$

In case of MCC, one pseudo component was considered, pseudo-cellulose.

Peak deconvolution: Fraser–Suzuki function

To separate the parallel decomposition of pseudo components, it is necessary to deconvolute all the above pseudo-components to obtain more information related to cellulose pyrolysis. In this study, the deconvolution procedure was achieved using Fraser-Suzuki Function (Cheng *et al.*, 2015):

$$\left. \frac{d\alpha}{dT} \right|_i = H_{p,i} \exp\left\{-\frac{\ln 2}{A_{s,i}^2} \ln\left[1 + 2A_{s,i} \left(\frac{T - T_{p,i}}{W_{hf,i}}\right)\right]\right\} \quad (4.4)$$

where H_p , A_s , T_p and W_{hf} are the parameters corresponding to the amplitude, asymmetry, peak position (K) and half-width of the curve (K). The obtained quality of fit between experimental and calculated curves were evaluated by the deviation $Dev(\%)$ (Eq. 4.5). The parameters of the Fraser-Suzuki Function were adjusted until obtaining the minimum $Dev(\%)$.

$$Dev(\%) = 100 \sum_{j=1}^N \frac{\sqrt{[(\frac{d\alpha}{dT})_{exp,j} - (\frac{d\alpha}{dT})_{calc,j}]^2 / N}}{(\frac{d\alpha}{dT})_{exp,max}} \quad (4.5)$$

where N is the number of experimental points employed. The conversion degree of each pseudo component can then be obtained from the integration of the separated $d\alpha/dT$ curve using Middle Riemann Sum method (Davis *et al.*, 2007):

$$\alpha_i = \sum_{j=1}^n \frac{1}{2} \left[\left(\frac{d\alpha}{dT}\right)_j + \left(\frac{d\alpha}{dT}\right)_{j-1} \right] [T_j - T_{j-1}] \quad (4.6)$$

Triplet kinetic determination: isoconversional model-free approach

The kinetics parameters were determined using an isoconversional model free-method, in particular, Kissinger–Akahira–Sunose (KAS). This integral isoconversional method assumes that the reaction rate at a constant conversion degree is only a function of temperature. Thus, the apparent energy E_a can be calculated without knowing the reaction mechanism (Pham Minh *et al.*, 2020). The KAS method is based on the following expression, obtained from the integral of Eq. 4.1:

$$\ln\left(\frac{\beta_i}{T^2}\right) = \ln\left(\frac{AR}{E_a g(\alpha)}\right) - E_a/RT \quad (4.7)$$

E_a (kJ mol^{-1}) can be obtained from a plot of (β_i/T^2) vs $1000/T$ at a given conversion degree. Three heating rates (β) were used: 2, 5 and $10 \text{ }^\circ\text{C min}^{-1}$. The values of E_a were determined in range of $\alpha = 0.05\text{--}0.90$ with a step of 0.05.

Determination of reaction model: generalized master-plots

The appropriate reaction model that describes the decomposition of cellulose can be determined by using generalized master plots method (Sánchez-Jiménez *et al.*, 2013). For non-isothermal conditions, the previous knowledge E_a is required (Gotor *et al.*, 2000). Using reference at point $\alpha = 0.5$ and E_a , the generalized master plots equation is expressed:

$$\lambda(\alpha) = \frac{f(\alpha)}{f(\alpha)_{0.5}} = \frac{d\alpha/dt}{(d\alpha/dt)_{0.5}} \frac{\exp(E_a/RT)}{\exp(E_a/RT_{0.5})} \quad (4.8)$$

The common reaction mechanisms used in kinetic analysis of solid-state reactions are listed in Table 4.1. The most suitable reaction mechanism is the one theoretical plot that gives the best match to the experimental plots, presented in Figure 4.1.

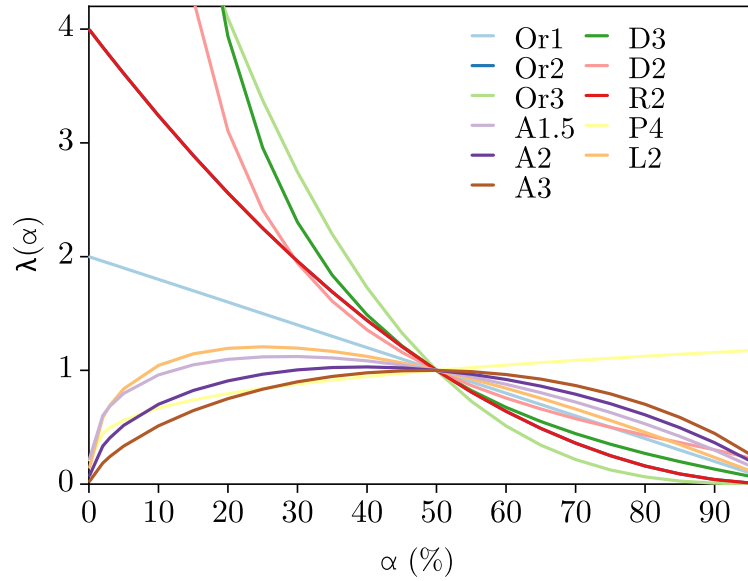


Figure 4.1: Generalized master plots of kinetic models listed in Table 4.1

Table 4.1: Most common reaction mechanisms in kinetics analysis for solid-state degradation processes (Brown, 1998; L. Luo *et al.*, 2021)

	Model	$f(\alpha)$
Order based	Or1 - first order	$1 - \alpha$
	Or-2 Second order	$(1 - \alpha)^2$
	Or3 - Third order	$(1 - \alpha)^3$
Diffusion	D1 - One dimensional	$1/(2\alpha)$
	D2 - Two dimensional	$[-\ln(1 - \alpha)]^{-1}$
	D3 - Three dimensional	$(3/2)(1 - \alpha)^{2/3}[1 - (1 - \alpha)^{1/3}]^{-1}$
Geometrical models	R2 - Contracting area	$2(1 - \alpha)^{1/2}$
Power law	Pn - Power law	$n(\alpha)^{(n-1)/n}$
Nucleation and Growth	An - Avrami-Erofeev	$n(1 - \alpha)[- \ln(1 - \alpha)]^{(n-1)/n}$
Random scission	L2	$2(\alpha^{1/2} - \alpha)$

4.3 Results and discussion

4.3.1 Pyrolysis characteristics

TG and dTG profile

Figure 4.2 shows the TG and $d\alpha/dT$ profiles of different samples. Three decomposition stages were identified, revealing the marked differences in the decomposition behavior between the cellulosic samples. Overall, the thermal decomposition of Cell-SS-P and Cell-WS-L pulps occurred over the three decomposition stages while MCC decomposed over the second stage. This thermal behavior of the pulp is primarily attributed to the presence of non-separated hemicelluloses and lignin which decomposed over the first and third stages, respectively. Similar results were obtained by Barneto *et al.* (2010) on pulp pyrolysis. Hemicelluloses are found to be less stable than cellulose, their decomposition starts at lower temperature (Giudicianni *et al.*, 2013; Zhou *et al.*, 2013). Lignin pyrolysis is slower than cellulose and occurs over a wide range of temperature leading to wider dTG curves (Yang *et al.*, 2007).

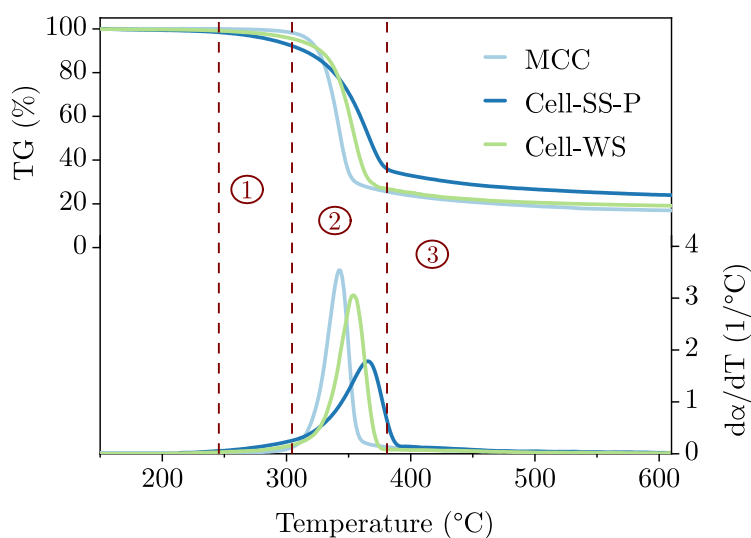


Figure 4.2: Comparison of TG and dTG profiles of different cellulose samples ($\beta = 10 \text{ }^\circ\text{C min}^{-1}$)

Another observation can be made regarding the effect of residual lignin on cellulose pyrolysis. The solid residue left was found to be proportional to lignin content. The highest solid content was obtained in pyrolysis of Cell-SS-P which has the highest lignin content while MCC presented the lowest solid yield. In agreement with the literature (D. Lv *et al.*, 2010), this difference in decomposition behavior is due to the difference in the inherent structure and chemical nature of cellulose and lignin. The first has a structure of a branching chain of polysaccharides which are easily volatilized. On the

Table 4.2: Crystallinity Index, lignin fraction and peak temperature ($\beta = 10 \text{ }^\circ\text{C min}^{-1}$)

	Cr.I. (%)	Lignin (wt. %)	T_{peak} ($^\circ\text{C}$)
MCC	80.0	0.0	343.5
Cell-WS-L	61.0	11.7	352.4
Cell-SS-P	49.0	32.5	367.0

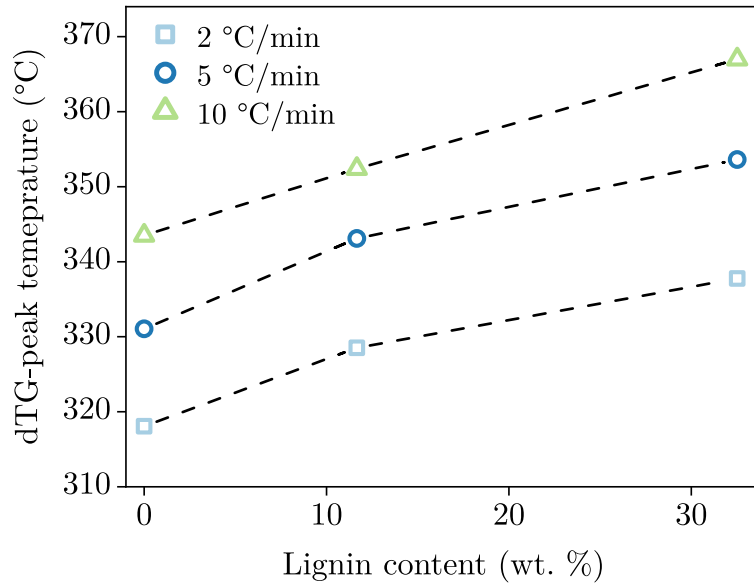
other hand, lignin consists of highly cross-linked and aromatic structures which are more thermally stable.

Thermal stability

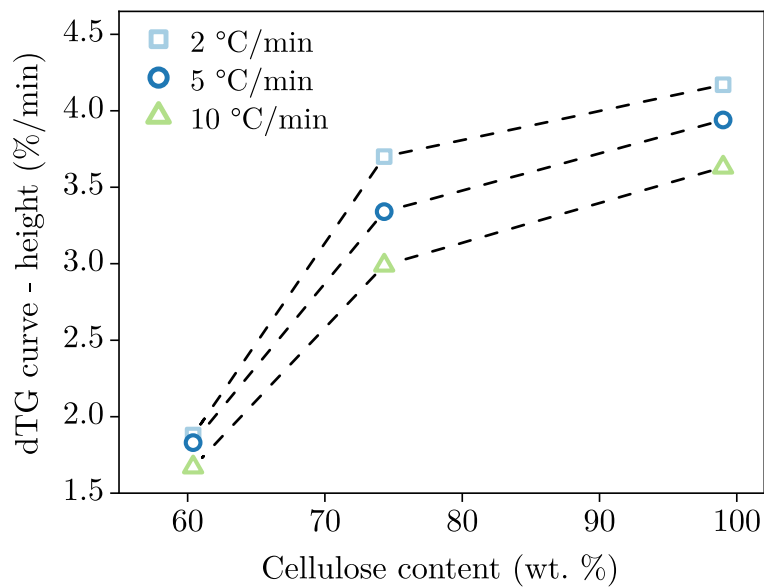
The thermal stability can be evaluated by the peak temperature of dTG curve. As seen in Figure 4.2, extracted cellulose had higher $d\alpha/dT$ -peak temperature than MCC. For cellulose, thermal stability can be affected by different parameters including crystallinity and the presence of lignin (S. Park *et al.*, 2010). An increase in the degree of crystallinity can shift the peak degradation temperature to higher values (Collard *et al.*, 2014). Higher lignin content leads to higher thermal stability (Ilyas *et al.*, 2017).

Table 4.2 illustrates the values of crystallinity index (CI) (Appendix 4.9), lignin content and $d\alpha/dT$ -peak temperature. CI of extracted cellulose samples was lower than MCC. For extracted cellulose, a lower CI is associated with a higher lignin proportion. Similar findings were obtained in the literature (Ilyas *et al.*, 2017; Owi *et al.*, 2016). Owi *et al.* (2016) showed that lignin removal led to an increment in the crystallinity of fibers.

In regards to the crystallinity effect on thermal stability, cellulose with lower CI exhibited higher degradation peak temperature. Hidenno (Hidenno, 2016) found that degradation temperature peaks were weakly related to the crystallinity of organosolv cellulose. On the other side, peak temperatures shift to higher values with higher lignin content. Figure 4.3a reports values of $d\alpha/dT$ peak temperatures as a function of lignin content. As it can be seen, a linear and direct relationship was found between the two parameters at different heating rates. Furthermore, the slope of the line is almost similar for all heating rates, though the intercept is different. The observed correlation coefficients (R^2) were all greater than 0.98. This result indicates that the thermal stability of rich cellulose material can be affected by lignin. According to literature (Jiawei Wang *et al.*, 2021), lignin has a significant role in the thermal degradation rate of cellulose and hemicelluloses in cell walls. Burhenne *et al.* (2013) showed that decomposition curves of biomass with a high lignin content shifted to a higher temperature compared to other feedstocks.



(a) Relationships between peak temperature of dTG curve and lignin content



(b) Relationships between dTG curve height and cellulose content

Figure 4.3: Influence of the composition contents on cellulose thermal decomposition

Degradation rate

The difference in the $d\alpha/dT$ curve height between samples is related to the difference in degradation rate. Cell-SS-P and Cell-WS-L decomposed slower than MCC and exhibited lower $d\alpha/dT$ curve-height. Cellulose pyrolysis is characterized by a high decomposition rate (Yang *et al.*, 2007). To investigate the influence of cellulose content on decomposition rate, Figure 4.3b presents the values of $d\alpha/dT$ curves height in the function of cellulose content at different heating rates. According to the depicted results, it can be noticed that there is a linear and direct relationship between degradation rate and cellulose content. The calculated correlation coefficients (R^2) were all higher than 0.87, indicating that TGA can be capable of characterizing cellulose pyrolysis. Gani *et al.* (2007) reported that the pyrolysis rate became faster with higher cellulose content. Different studies used TGA to study the thermal decomposition of cellulose and lignocellulosic material. A relationship, with a high correlation factor, between the cellulose content and dTG peak height, was found by Hideno (Hideno, 2016).

Effect of heating rate

The heating rate is one of the most influential parameters in TGA since it affects the thermal decomposition. Figure 4.4 shows TG et $d\alpha/dT$ of cellulosic materials at different heating rates. The results show that the TG curve and peak temperatures of $d\alpha/dT$ curves shift to higher temperatures with increasing the heating rate. In addition, the peak height of $d\alpha/dT$ curves decreased as the heating rate increased. These findings are in agreement with the literature (Z. Li *et al.*, 2008; Samuelsson, 2015; Shen *et al.*, 2009; Słopiecka *et al.*, 2012). This shift of peak temperature and the decrease of peak height are due to the combined effects of heat and mass transfer (M. Hu *et al.*, 2016). According to D. Chen *et al.* (2014), a higher heating rate increases the temperature gradients within the sample which can affect the inner temperature distribution, and the devolatilization rate is greater than the rate of volatile release. Hence, devolatilization takes place in different stages.

4.3.2 Fraser–Suzuki deconvolution and isoconversional kinetic study

Fraser–Suzuki deconvolution

As discussed in Section 4.2, extracted cellulose was considered to be represented by pseudo components representing cellulose, non-extracted hemicelluloses, and lignin. The results obtained from $d\alpha/dT$ curves deconvolution by applying the Fraser–Suzuki function (Eq. 4.4) are listed in Table 4.3. The deduced values of T_p , W_{hf} , A_s of $d\alpha/dT$ curve of pseudo-cellulose are in line with reported values in previous studies (M. Hu *et al.*, 2016; Romero Millán *et al.*, 2017; W. Wang *et al.*, 2022). Figure 4.5

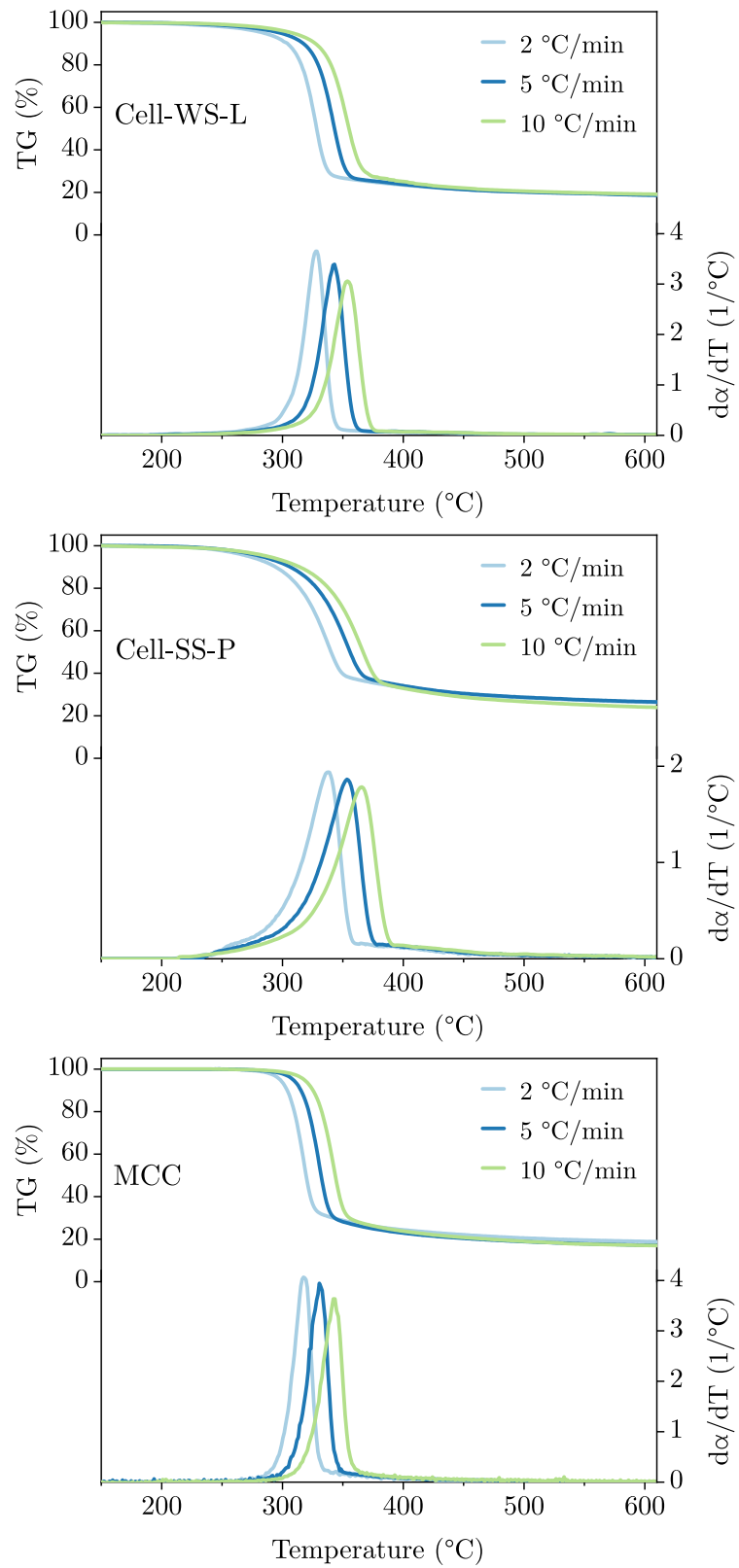


Figure 4.4: TG and $d\alpha/dT$ profiles of cellulose pyrolysis at different heating rates

Table 4.3: Fraser-Suzuki deconvolution parameters

		Pseudo-Cellulose		
β ($^{\circ}\text{C min}^{-1}$)		Cell-SS-P	Cell-WS-L	MCC
2	H_p	1.88	3.70	4.17
	T_p	337.8	328.5	318.1
	W_{hf}	29.0	19.0	17.4
	A_s	-0.40	-0.41	-0.40
	Dev (%)	2.62	1.36	1.64
5	H_p	1.83	3.34	4.20
	T_p	353.6	343.1	331.1
	W_{hf}	31.0	22.0	17.5
	A_s	-0.45	-0.41	-0.40
	Dev (%)	2.26	1.25	1.88
10	H_p	1.67	2.99	3.63
	T_p	365.0	355.4	342.8
	W_{hf}	31.5	22.0	19.5
	A_s	-0.43	-0.41	-0.40
	Dev (%)	1.26	1.25	1.57

shows an example of the deconvoluted curves and the comparison between the original experimental and calculated results. For extracted cellulose, three pseudo-component curves are deconvoluted, considering residual hemicelluloses and lignin, even though they do not represent the real composition (Romero Millán *et al.*, 2017). For MCC, composition and pyrolysis kinetics would not be affected by the deconvolution. The latter part of $d\alpha/dT$ curve was not considered since it corresponds to a second process that occurs at high conversion values and has a very limited contribution to the overall process (Sánchez-Jiménez *et al.*, 2011). The model fitting curves of the Fraser-Suzuki function were well matched to the experimental data with a deviation value lower than 3 % (Eq. 4.5).

Activation energy estimation by KAS model-Free Kinetics

For the current study, E_a of cellulose was obtained with the help of KAS integral method (Eq. 4.7). Figure 4.6 shows the KAS plots of $\ln(\beta/T^2)$ against $1000/T$ at different conversion degrees obtained using Middle Riemann Sum integral method (Eq. 4.6). E_a

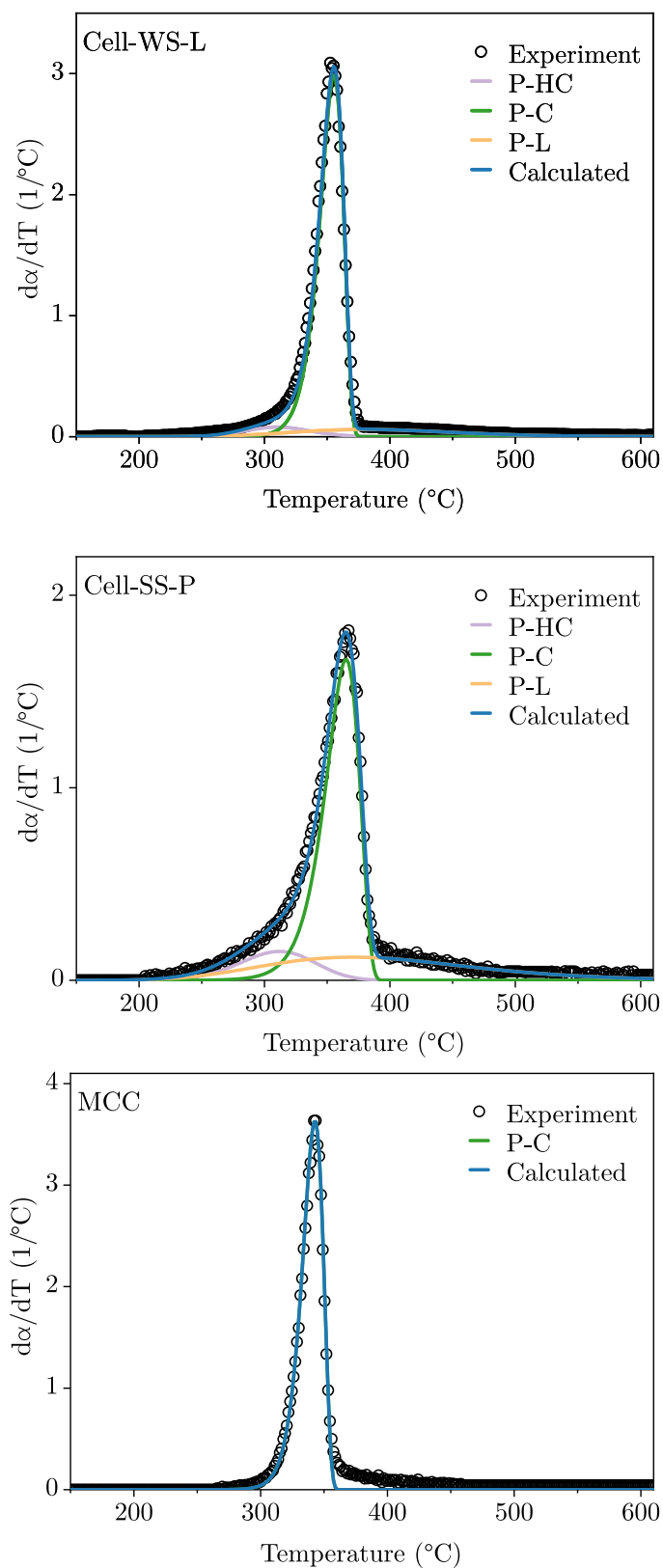


Figure 4.5: Deconvolution of $d\alpha/dT$ curves at $10^\circ\text{C}/\text{min}$ (P-HC pseudo-hemicellulose; P-C pseudo-cellulose; P-L pseudo-lignin; Calculated: sum of deconvoluted curves)

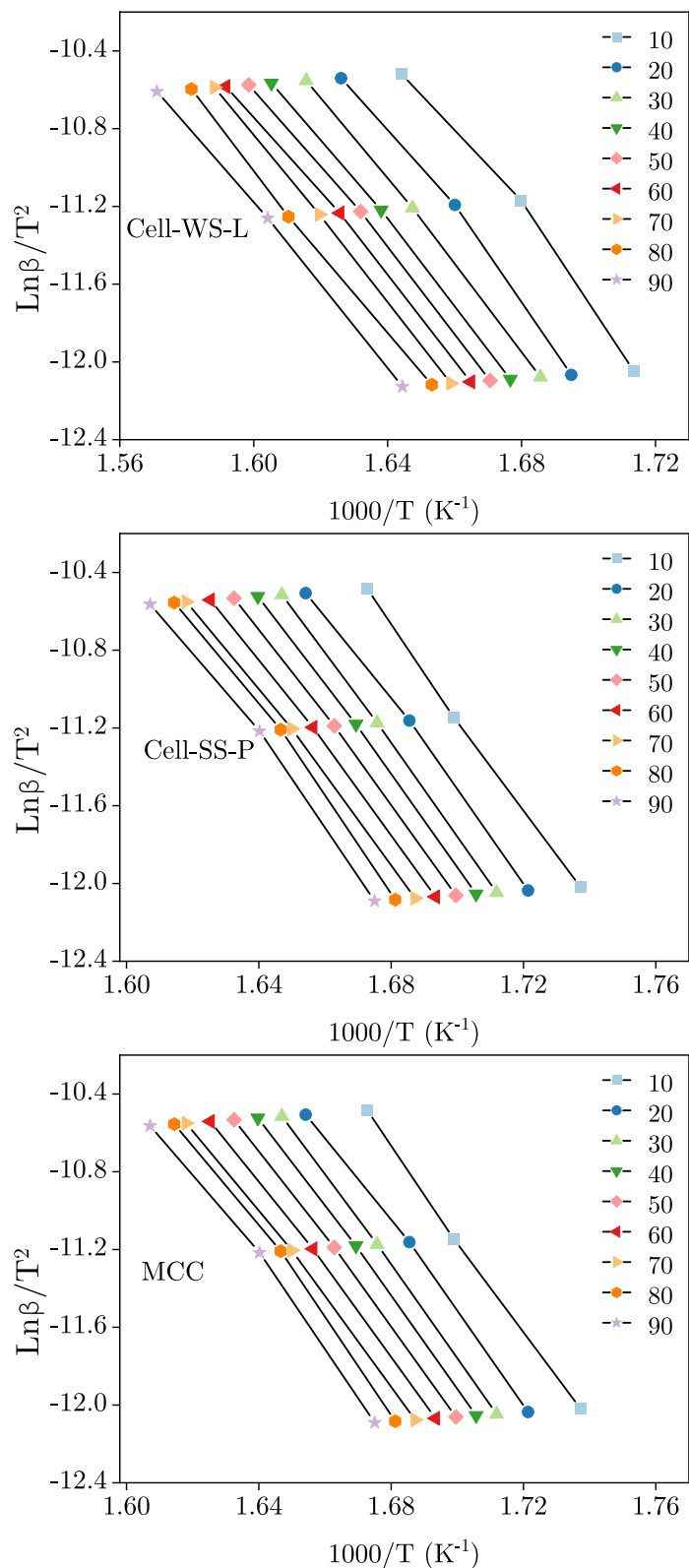


Figure 4.6: Kinetic plots for determination of activated energy using KAS model at different conversion (α step = 0.1)

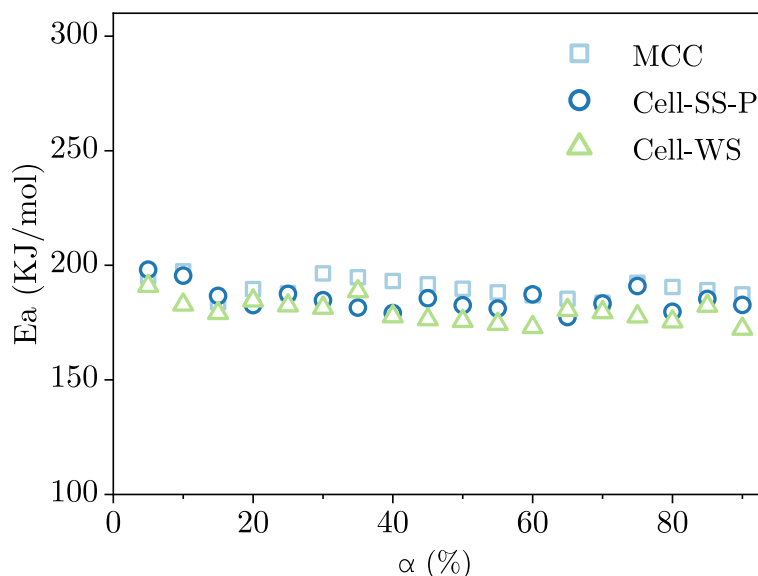


Figure 4.7: Variation of E_a as function of conversion degree for different cellulose samples

values at a specific conversion degree were obtained from the slope ($-E_a/R$) of each straight line. The obtained correlation coefficients (R^2) from linear fits for KAS are all greater than 0.9895 over the whole conversion range, reflecting that estimated E_a values were accurate and reliable.

Figure 4.7 illustrates the variation of E_a with conversion, obtained MCC and for pseudo-cellulose in Cell-WS-L and Cell-SS-P. It can be seen that calculated E_a was constant along the conversion range. The average E_a and A values are listed in Table 4.4. The small deviation ($< 3\%$) confirms that E_a is independent of α value, thus the pyrolysis of cellulose follows a single-process reaction mechanism (Vyazovkin *et al.*, 2011). Yeo *et al.* (2019) and Sánchez-Jiménez *et al.* (2013) reported that activation energy was constant along conversion, implying that the decomposition of cellulose can be represented by a single reaction mechanism. A slight difference was found between the activation energy of the material used in this study, where $E_{aMCC} > E_{aCell-SS-P} > E_{aCell-WS-L}$. According to Anca-Couce *et al.* (2014), such a trend is on account of two possible reasons, namely the interactions of cellulose with the other components and the activity of the mineral content. As shown in Table 4.4, the obtained activation energy values are close to the values reported in the literature for cellulose. Overall, the obtained results prove that KAS isoconversational method can accurately describe the kinetic behavior of these materials. A value of 185 kJ mol^{-1} can represent an average activation energy of cellulose pyrolysis.

Table 4.4: Average values of activation energy calculated over the whole conversion range

		Ea (kJ mol ⁻¹)	R ² min-max	Ref.
P-C	Cell-WS-L	179.9 ± 4.9	0.9895 - 0.9999	this study
	Cell-SS-P	185.1 ± 5.3	0.9919 – 1.000	
	MCC	190.2 ± 4.0	0.9952 – 1.000	
Average	185.0 ± 5.2	-		
	<i>Literature</i> ^a	187.9 ± 11.4	-	(Sánchez-Jiménez <i>et al.</i> , 2013; Şerbănescu, 2014; Yeo <i>et al.</i> , 2019)

P-C: Pseudo-cellulose; ^a values for MCC obtained from isoconversional methods

Determination of the mechanism by master plots method

Following the determination of the apparent activation energy, the generalized master plots method was employed to discriminate the mechanism function of the thermal decomposition. Using Eq. 4.8, experimental plots were built individually against α at different heating rates. Similarly, theoretical plots of listed models in Table 4.1 were constructed. Experimental and theoretical master plots were compared to each other as depicted in Figure 4.8. Since the generalized master plots are not influenced by the heating rate, experimental plots followed one reaction model under the different heating profiles. From Figure 4.8, the master plots of all samples follows a single mechanism over the whole conversion range, indicating that the pyrolysis process of pseudo-cellulose and MCC follow a single-step reaction.

Regarding the mechanism function $f(\alpha)$, Avrami-Erofeev (A2) equation best matched to pseudo-cellulose (P-C) in Cell-WS-L and MCC. This model has been considered in the literature to govern cellulose pyrolysis (Barud *et al.*, 2011; Capart *et al.*, 2004; Mamleev *et al.*, 2007). Avrami-Erofeev model is based on the nucleation and growth mechanism involving the formation of nuclei that react at an accelerating rate until their coalescence near reaction completion (Barneto *et al.*, 2009; Mamleev *et al.*, 2007). For pseudo cellulose in Cell-SS-P, the reaction followed the random-scission model. This model was proposed to describe cellulose decomposition by Sánchez-Jiménez *et al.* (2011). This model is based on random breakage of the polymeric cellulosic chains that correspond to fragmentation. This step is followed by the volatilization of the resulting fragments once they are short enough. Despite the difference between Avrami-Erofeev and the random-scission models from a mechanistic background, both of these "acceleratory" models were able to accurately describe the cellulose thermal degradation. In this regard,

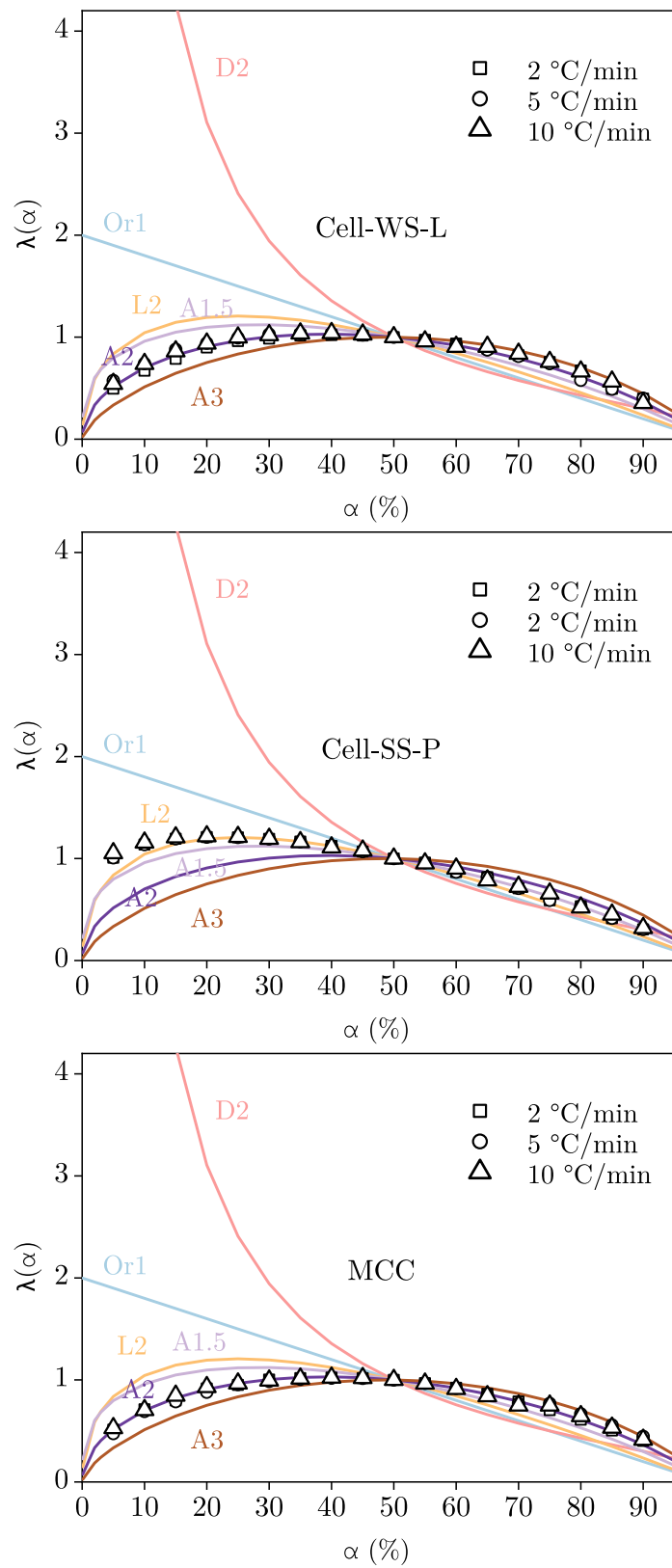


Figure 4.8: Experimental (symbols) and theoretical (lines) $\lambda(\alpha)$ master plot curves at different heating rates

Table 4.5: Pre-exponential factor values obtained by using KAS isoconversional method (calculated) and the adjusted values (solver)

		Ln(A) (min ⁻¹)		Ref.
		calculated	<i>Solver</i> ^b	
P-C	Cell-WS-L	28.5 ± 1.4	38.2	this study
	Cell-SS-P	27.5 ± 1.7	38.9	
	MCC	29.7 ± 1.1	40.1	
	Average	28.6 ± 1.1	39.0 ± 1	
	Literature ^a	37.1 ± 2.2		(Sánchez-Jiménez <i>et al.</i> , 2013; Şerbănescu, 2014; Yeo <i>et al.</i> , 2019)

P-C Pseudo-cellulose; ^a values for MCC obtained from different isoconversional methods

^b values was averaged over heating rates of 2, 5 and 10 °C min⁻¹

Romero Millán *et al.* (2017) reported that both of these models could be suitable for the description of cellulose pyrolysis material, considering that their theoretical plots are extremely similar.

Following the determination of the reaction model, the pre-exponential factor *A* was determined using Eq. 4.7. The calculated values are presented in Table 4.5. However, the values were relatively lower than the reported values in the literature. The optimal *A* values were calculated using Evolutionary Solving Method in Excel Squares regression by minimizing the deviation value in Eq. 4.5. An average value of *E_a* (185.0 kJ mol⁻¹) and an Avrami-Erofeev (A2) model were used. As shown in Table 4.5, the values of optimal *A* are roughly similar and in accordance to the literature. An average deviation of 36.6 % was found between the initial and the recalculated values of *A*. The reason for the lower value might be related to the thermal lag effects that become more significant at higher heating rates (Burnham *et al.*, 2015). The predicted curves by the model were in good agreement with the experimental data at all heating rates with a deviation of less than 3.5 %.

4.4 Conclusion

This chapter focuses on the thermal stability and pyrolysis behavior of a potential feedstock for thermochemical conversion. The obtained results can provide useful information for reactor design and scale-up for cellulose pyrolysis. Thermogravimetric analysis tests were performed under nitrogen atmosphere at different heating rates of 2, 5, and 10 °C min⁻¹. The main results are as follows:

- The first results showed that the thermal decomposition behavior of cellulose was significantly influenced by the composition. A successful correlation was obtained between thermal degradation characteristics and the component contents. The degradation temperature was shifted to higher values with increasing lignin content. The devolatilization rate increased with higher cellulose content. The effect of the heating rate on the thermal behavior of the samples was also presented.
- An approach combining Fraser-Suzuki function, integral isoconversional method, and generalized master plots procedure was applied for determining the apparent kinetics parameters. The activation energy was found to be constant along conversion. "Acceleratory" models such as nucleation and growth mechanism and chain scission were able to accurately describe the thermal decomposition behavior of extracted cellulose. The obtained kinetic triplet, summarized in Table 4.6 was used to reconstruct the experimental curves and the deviation was less than 3.5 %.

Table 4.6: Kinetic triplet for cellulose pyrolysis

Ea (kJ mol ⁻¹)	ln(A)(min ⁻¹)	f(α)
185.0	39.0	A2 - L2

Appendix

Crystallinity index (CI) of cellulose from the extracted pulp and MCC were calculated from the XRD spectra, from the height ratio between the intensity of the crystalline peak ($I_{002} - I_{AM}$) and total intensity (I_{002}) after subtraction of the background signal measured without the cellulose (S. Park *et al.*, 2010):

$$CI = \frac{I_{002} - I_{AM}}{I_{002}} (\%) \quad (4.9)$$

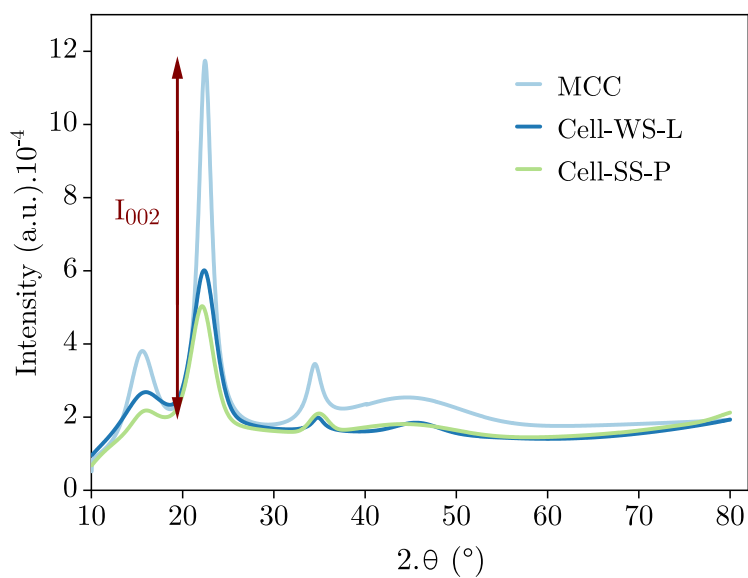


Figure 4.9: X-ray diffraction spectra of cellulose samples

TGA steam gasification of cellulose pulp biochar: insights on experimental and kinetic study with a focus on the role of Silicon

5.1	Introduction	103
5.2	kinetic analysis approach	105
	TGA kinetics	105
	Char reactivity measurements	105
	Gasification kinetic approach	105
5.3	Results and discussion	106
	5.3.1 Influence of the inorganic content on the cellulose pulp biochar reactivity	106
	5.3.2 Gasification kinetics analysis	112
	5.3.3 Kinetic model accuracy	117
	5.3.4 Effect of silica elimination on biochar reactivity	119
5.4	Conclusion	120

This chapter has been published as a research paper in an international journal, reference: Elsaddik, M., Nzihou, A., Delmas, M., & Delmas, G. H. (2023). Steam gasification of cellulose pulp char: Insights on experimental and kinetic study with a focus on the role of Silicon. Energy, Vol. 271, 126997. <https://doi.org/10.1016/j.energy.2023.126997>

5.1 Introduction

Results from Chapter 3 showed that acid treatment influenced the chemical composition of the pulp in particular ash content. Significant fractions of inorganic salts containing alkali and alkaline earth metals (AAEM) were dissolved under acidic conditions. Whereas, Si compounds remained in the pulp ash. In literature, there seems to be an agreement on the fact that biochar gasification reactivity is highly influenced by the inorganic matter present in the feedstock (Yuming Zhang *et al.*, 2020). It was

Table 5.1: Main inorganic elements in the biomass and cellulose pulp samples

mg kg (dry basis)	WS	Cell-WS-L	SS	Cell-SS-P	Cell-SS-A
AAEM	7248	2171	816	353	2713
Fe	138	129	35	89	121
P	621	209	0	0	457
Al	75	135	10	21	34
S	661	49	83	0	0
Si	8789	17259	186	706	268
K/Si					
	0.4	0.0	1.9	0.0	0.2
C.I. = (K+Ca+Na+Mg+Fe)/(Si+Al)					
	0.8	0.1	4.7	0.6	3.9
% Si					
	52	87	16	61	8

indicated that **AAEM**, such as Na, K, Mg and Ca have a catalytic impact that enhances biochar gasification (Nzihou *et al.*, 2013a). In contrast, other elements, namely Si has the opposite effect and may inhibit the gasification (Strandberg *et al.*, 2017). Therefore, the purpose of the present chapter is to: (1) study the gasification of **LEEBIO** cellulose pulp biochar; (2) understand the role of the inorganic on biochar reactivity with a focus on Si-content and propose a new approach to predict biochar gasification; (3) investigate the effect of Si elimination on pulp biochar gasification. Two pulp samples and their raw biomass selected: **Cell-WS-L** and **Cell-SS-P**, **WS** and **SS**. Alkaline washed pulp **Cell-SS-A** was also used to examine effect of Si elimination on biochar gasification behavior. The inorganic composition in terms of **AAEM**, Si and P contents of studied samples is presented in Table 5.1. Moreover, indices indicative of catalytic and inhibition activities are also calculated.

Steam gasification tests were conducted via thermogravimetric analysis (**TGA**), under different operating conditions, as presented in Chapter 2.

5.2 kinetic analysis approach

TGA kinetics

As already mentioned above, the gasification tests were performed isothermally. The biochar gasification rate is defined as the variation of the conversion degree α vs time:

$$r = \frac{d\alpha}{dt} \quad (5.1)$$

The degree of conversion α was calculated following:

$$\alpha = \frac{m_0 - m(t)}{m_0 - m_{ash}} \quad (5.2)$$

Where m_0 is the biochar mass at the end of the pyrolysis stage, m_{ash} is the sample ash content determined with TGA experiments, and $m(t)$ is the mass at a given time t of the analysis. $m(t)$ values were collected every 1.8 s.

Char reactivity measurements

The apparent reactivity $R(\alpha)$ in $\%.\text{min}^{-1}$ can be obtained from the conversion degree and the reaction rate following:

$$R(\alpha) = \frac{1}{1 - \alpha} \frac{d\alpha}{dt} \quad (5.3)$$

The average reactivity over a defined conversion range can be then expressed by the average of the apparent reactivities at each α .

Gasification kinetic approach

Typically, the overall biochar gasification rate can be expressed by:

$$r = \frac{d\alpha}{dt} = A \exp(-Ea/RT) \times h(P_{H_2O}) \times f(\alpha) \quad (5.4)$$

where A is the pre-exponential factor min^{-1} , Ea is the apparent activation energy (kJ mol^{-1}), and R is the universal gas constant ($8.314 \text{ J mol}^{-1} \text{ K}^{-1}$), and T is the gasification temperature. $h(P_{H_2O})$ describes the dependence on the partial pressure of the gasifying agent. It is assumed to follow a power law:

$$h(P_{H_2O}) = P_{H_2O}^m$$

Different partial steam pressures were used for gasifying the pyrolysis biochar: 3.7, 6.2, and 10 kPa.

Following a similar approach used in TGA pyrolysis kinetic analysis in Chapter 4 (Section 4.2), an approach using model-free isoconversional method was used to determine kinetic parameter. In this approach, the reaction rate is assumed to be only function of time at a constant conversion degree. Thus, the apparent energy E_a can be calculated without knowing the reaction mechanism (Pham Minh *et al.*, 2020), from the slope of the plot $\ln(t)$ vs T^{-1} at a given conversion degree. Three gasification temperatures were used: 750, 800 and 900 °C. The calculation of A depends on the previous knowledge of the reaction model.

For the reaction mechanism, several models can be used to describe biochar gasification rate. These models are widely used in gas-solid reactions. The mechanism of biochar gasification, $f(\alpha)$, can be determined using the generalized master-plots method. Isoconversional model-free methods and the generalized master-plots approach (Chapter 4, Section 4.2), can be determined from the experimental kinetic data:

$$\lambda(\alpha) = \frac{f(\alpha)}{f(\alpha)_{\alpha=0.5}} = \frac{d\alpha/dt}{(d\alpha/dt)_{\alpha=0.5}} \frac{\exp(E_a/RT)}{\exp(E_a/RT_{\alpha=0.5})} \quad (5.5)$$

For isothermal programs, the previous knowledge of the activation energy is not required (Sánchez-Jiménez *et al.*, 2013). Thus, the exponential terms in eq 5.5 can be canceled out. Hence, the experimental master plots can be established directly from an $d\alpha/dt$ curve. The most suitable reaction mechanism is the one theoretical plot that gives the best match to the experimental plots.

5.3 Results and discussion

5.3.1 Influence of the inorganic content on the cellulose pulp biochar reactivity

The conversion curves *vs* time of different biochar samples at different temperatures are shown in Figure 5.1. As expected, the gasification temperature has a significant impact on biochar reactivity. The temperature increase led to a considerable increase in reactivity, which reduces the reaction time. Table 5.2 provides an overview of reaction time, maximum conversion degree and the reactivity of all analyzed materials. A complete biochar conversion was obtained at 900 °C, while the full conversion at 800 °C and 750 °C after 300 min was below 60 % for Cell-SS-P and Cell-WS-L biochars. These findings are in agreement with previous studies on the reaction temperature effect for

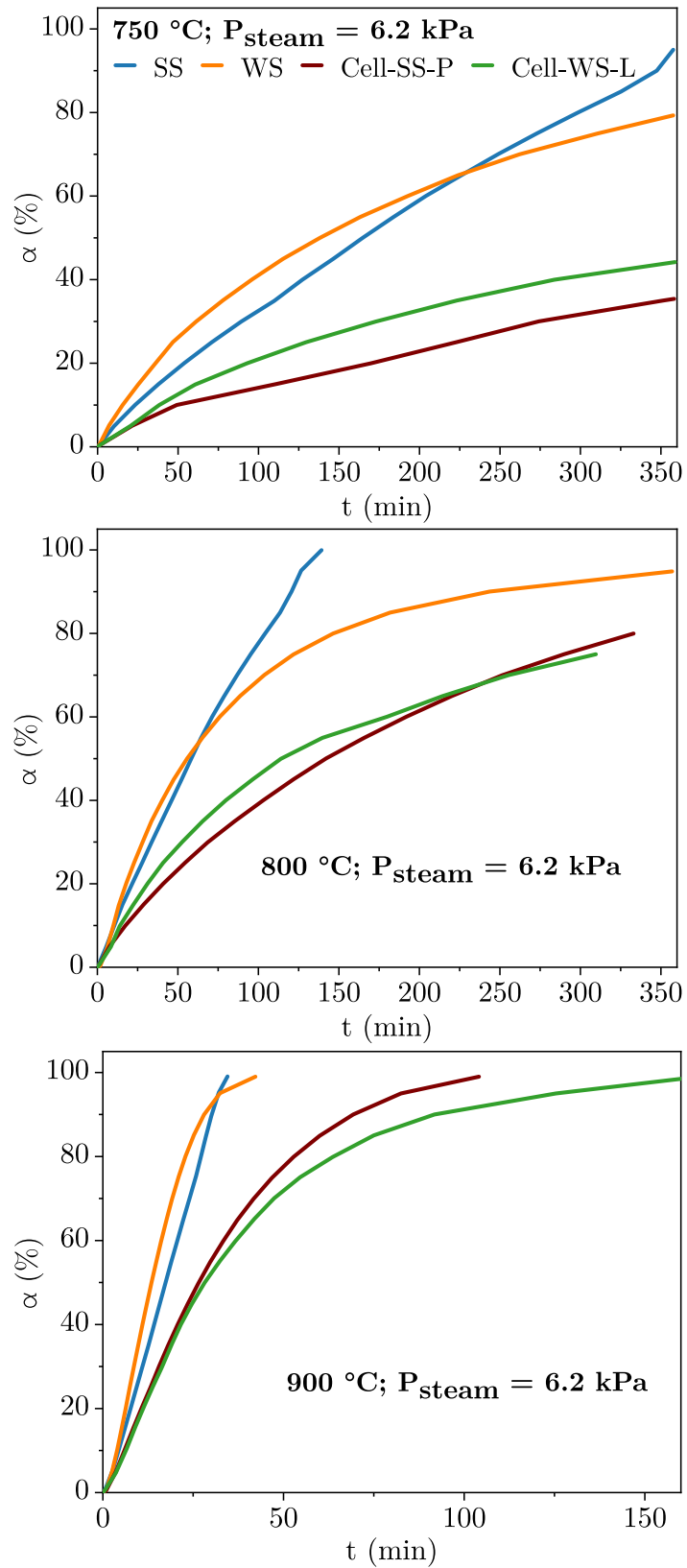


Figure 5.1: Conversion degree α vs time of different biochar samples at different temperatures with a partial steam pressure of 6.2 kPa

Table 5.2: Char steam gasification reactivity at 30 % conversion $R_{30\%}$, maximum conversion level after 360 min of reaction α_{max} , and its corresponding reaction time $t_{\alpha_{max}}$; partial steam pressure 6.2 kPa

		WS	Cell-WS-L	SS	Cell-SS-P
750 °C	$R_{30\%}$ (%.min ⁻¹)	0.55	0.07	0.30	0.09
	α_{max} (%)	79.3	44.2	95.0	35.4
	$t_{\alpha_{max}}$ (min)	$=360$ min			
800 °C	$R_{30\%}$ (%.min ⁻¹)	1.32	0.52	1.21	0.44
	α_{max} (%)	94.9	78.2	100	82.5
	$t_{\alpha_{max}}$ (min)	360	360	139.2	360
900 °C	$R_{30\%}$ (%.min ⁻¹)	6.2	2.69	4.33	2.98
	α_{max} (%)	$=100\%$			
	$t_{\alpha_{max}}$ (min)	53.2	178.8	34.5	117.3

both steam and CO_2 gasification of biomass biochars (Encinar *et al.*, 2021; Link *et al.*, 2010; T. Liu *et al.*, 2008).

From Figure 5.1, it is clear that the gasification behavior of cellulose pulp biochars is different from their raw biomass biochars. Table 5.2 reveals the difference in reactivities between cellulose pulp and raw biomass biochars at different temperatures. The pulp biochar displayed lower reactivity than the raw biomass biochars. A factor of 3 between the reactivities of raw biomass and cellulose pulp biochars at 800 °C was found. At 900 °C, the reaction time of Cell-SS-P and Cell-WS-L biochars is 117 min and 178 min, respectively, to obtain a 100 % biochar conversion. The reaction time of raw biomass biochars is 34 min and 42.2 min for SS and WS, respectively. This steep difference in the reaction time between the raw biomass and the cellulose pulp biochars could generate a significant difference at a large scale, particularly for the residence time in the gasification reactor.

Such difference cannot be explained by the difference in macromolecular composition in terms of lignin, cellulose and hemicelluloses (Dahou *et al.*, 2021; Gupta *et al.*, 2018). Gasification behavior seemed to be linked to the inherent inorganic elements in the lignocellulosic material, such as AAEM, Si, Al, and P. AAEM are known to be catalysts for the steam gasification reactions. The dominant catalytic effect is exhibited by K-species (Y. Huang *et al.*, 2009; Kajita *et al.*, 2010; Pflieger, 2021). In contrast, Si, Al, and P are reported to have inhibiting effect on the gasification. Specifically, inherent Si compounds such as SiO_2 tend to inhibit K-catalysis (Nzihou *et al.*, 2013b). Therefore, the raw biomass biochars, which contain AAEM species, had higher reactivities than

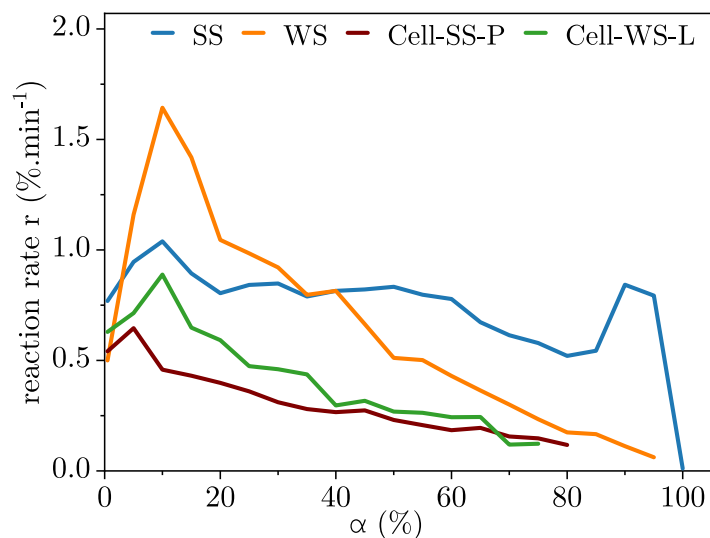


Figure 5.2: Experimental reaction rate as a function of conversion, at 800 °C with a partial steam pressure 6.2 kPa

pulp biochars. Since most of AAEM salts had been eliminated under acidic conditions during pulping, their concentration in the cellulose pulp was drastically reduced.

Different inorganic ratios have been used in the literature to highlight the catalytic effect of K and other AAEM species and the inhibitor effect of Si, as seen in Table 5.3. According to Dupont *et al.* (2016), the reaction rate was constant for biomass with $K/(Si+P) > 1$, in contrast the rate decreased along conversion for biomass with ratio $K/(Si+P) < 1$. Romero Millán *et al.* (2019) studied steam gasification on tropical biomass. A linear relationship was found between the biomass reactivity and the inorganic ratio $K/(Si+P)$ of samples, in the analyzed temperature range. Alkali or catalytic index (C.I.) has also been used to correlate the reactivity to the inorganic content. Other studies found a correlation between the reactivity and the content of K, Na, and Ca. However, the use of one of these inorganic ratios is limited in our case since there is a steep difference in K content between raw biomass and the cellulose pulp, as shown in Table 5.1. As mentioned above, Si is present in the ash from different materials and is the main element in pulp ash. Therefore, the %Si index calculated as follows was used in the analysis of the gasification kinetics:

$$\% Si = \frac{Si \text{ (mg kg}^{-1}\text{)}}{\text{Total major inorganic elements (mg kg}^{-1}\text{)}} \text{ (wt.\%)} \quad (5.6)$$

%Si for SS sample was 16 %, while that for WS, Cell-WS-L and Cell-SS-P samples were higher than 50 %. In order to verify the effect of Si, in particular on cellulose pulp gasification, the variation of reaction rate over the conversion is presented in Figure 5.2. The studied biochar samples can be classified into two groups:

Table 5.3: Char gasification studies taking into account inorganic elements (LB: Lignocellulosic Biomass; PC: Petroleum Coke)

Feedstock	Agent T (°C)	Main findings
K/(Si+P)		
LB MA	H ₂ O 800	K/(Si+P) > 1, constant reaction rate (Or0). K/(Si+P) < 1, decreasing reaction rate (Or1). (Dupont <i>et al.</i> , 2016)
LB Algae	H ₂ O 800	K/(Si+P) > 1, constant reaction rate; K/(Si+P) < 1, decreasing reaction rate; Si and P tend to encapsulate P species and limit its catalytic activity. (Hognon <i>et al.</i> , 2014)
LB	H ₂ O 750 – 950	Reactivity increases while reaction order decreased with increasing K/(Si+P); K/(Si+P) > 1, Or0; K/(Si+P) < 1 reaction order > 1 and can be a function of K/(Si+P). (Romero Millán <i>et al.</i> , 2019)
K/Si		
LB	H ₂ O 750 – 900	A factor of 3.5 is found between the average reaction rate of various wood biochars. Reaction rate is correlated to K/Si. (Dupont <i>et al.</i> , 2011)
LB	H ₂ O 650 – 800	Reactivity is correlated with K/Si for five of the six biochars. Ca content in the sixth sample is high. (Prestipino <i>et al.</i> , 2018)
Char	CO ₂ 800	X > 60 %, reactivity was influenced by the presence of K and Si. Reactivity was correlated to K/Si at X > 50 %. (Bouraoui <i>et al.</i> , 2016)
Catalytic Index (alkali index) C.I. = (K+Ca+Na+Mg+Fe)/(Si+Al)		
LB	CO ₂ 800	Reactivity increases with increasing C.I.. Average reaction rate is correlated to C.I. at higher conversion. (Bouraoui <i>et al.</i> , 2015)
LB	CO ₂ 800	Reactivity increases with increasing C.I. Modified random pore model can describe biochar gasification. (Gupta <i>et al.</i> , 2018)
LB Coal	CO ₂ 800	K has the major catalytic contribution. At T > 800 °C, K catalytic effect is reduced as it forms salts with Si and Al. (Thengane <i>et al.</i> , 2019)
LB	H ₂ O 900	Good correlation of biochar reactivity with (C.I.). Random pore model can describe kinetics using an additional term correlated to [Ca]. (López-González <i>et al.</i> , 2014)
LB- PC Coal	CO ₂ 850 – 1000	No relationship between the reactivity and alkali index of chars. (Huo <i>et al.</i> , 2014)
(K+Na+Mg)/(Si+Al+P+Ca)		
LB	H ₂ O 750 – 1000	This index is the most suitable to explain the reactivity among different index used. (González-Vázquez <i>et al.</i> , 2018)
(Na+Ca+K)		
LB	H ₂ O 900	3 groups are identified. Group I: [Na]+[K] > [Ca]; highest reactivity; Group II: [Ca] > [Na]+[K]; Group III: has the lowest reactivity due to the high silica content; A random pore model related to K content is used. (Zhang <i>et al.</i> , 2008)
LB	H ₂ O, CO ₂ 800 – 1300	Reactivity increases with increasing ([Na]+[K]). (Lin <i>et al.</i> , 2013)

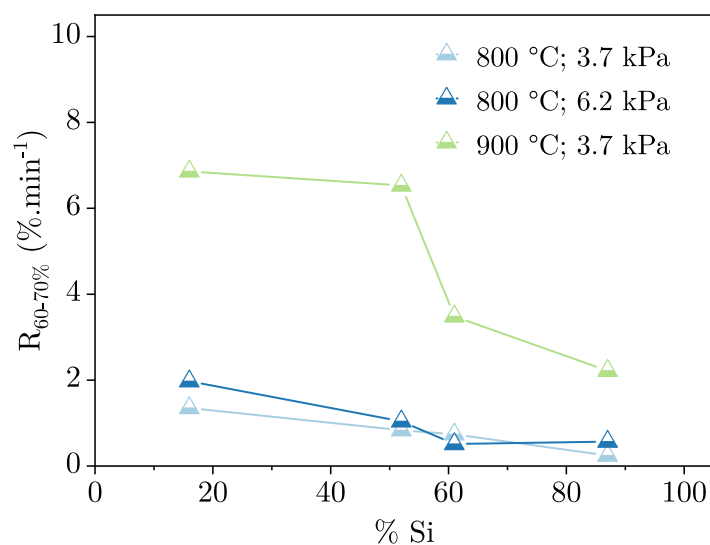


Figure 5.3: Average reactivity at selected conversion range as a function of %Si (curves are just shown to highlight the tendencies)

- This first group is represented by **SS** sample: the conversion increases as a straight line. The reaction rate is constant with increasing carbon conversion until about 80 %. Since its low content in **SS**, no inhibitory effect of Si on the gasification rate was identified. A significant increase in reaction rate was observed at higher conversion. This finding is in line with other studies using woody biomass with similar inorganic content (Bouraoui *et al.*, 2016; Hognon *et al.*, 2014). This trend was explained by the fact that **AAEM** are more concentrated at higher conversion which could enhance the catalytic effect (Dahou *et al.*, 2021).
- The second group includes **WS**, **Cell-WS-L** and **Cell-SS-P** samples: a maximum reaction rate at earlier conversion levels, then the conversion increases with a decreasing reaction rate. The decrease of reaction rate with conversion confirms the inhibitory effect of Si on biochar gasification. It should be underlined that the overall shape of the gasification rate profile was similar. After reaching the maximum at a lower conversion level, the reaction rate decreases with increasing conversion. As the carbon is consumed, Si concentration increases, leading to a steep drop in the reaction rate. According to literature, the decreasing rate is related to the tendency of silica to encapsulate **AAEM** species to form inactive silicate complex oxides, which are stable and non-catalytic compounds (Hognon *et al.*, 2014; Zhang *et al.*, 2008). However, these complexes are in much smaller amounts in the case of cellulose pulp biochar due to the reduced amount of **AAEM**. Two other different phenomena explaining the inhibitory effect were mentioned in the literature. Gupta *et al.* (2018) reported that the inhibition of biochar gasification can be caused by the bonding of silica with carbon. Lu *et al.* (2022)

reported that a high dispersion of Si on biochar can prevent the transformation of oxygen and slow the gasification down.

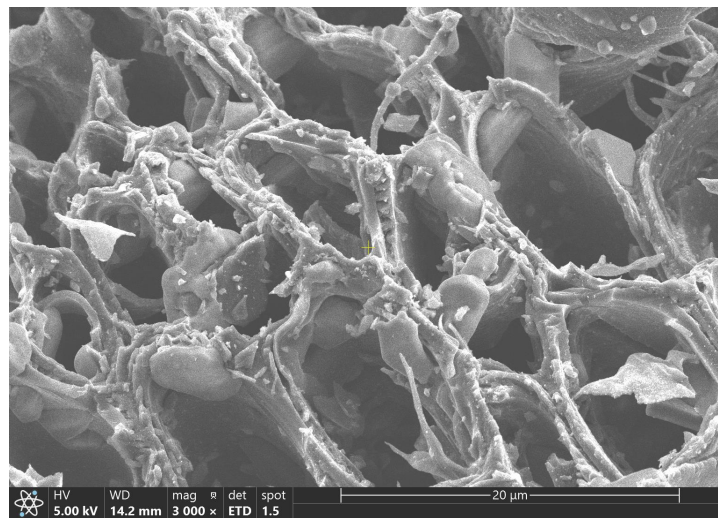
In order to validate our prediction, all the samples were combined by correlating %Si with the biochar reactivity. The average reactivity as a function of %Si is shown in Figure 5.3. As can be seen, a general trend for biochar gasification reactivity as a function of %Si can be established. The reactivity decreased with increasing %Si ratio. This confirms the inhibitory effect of Si and reveals that pulp biochar reactivity is governed by %Si.

Besides the effect of the inorganic composition, the morphological structure of biochar is another parameter that can also influence biochar reactivity. This parameter has been less covered in the literature than the inherent inorganic composition. SEM images of biomass biochar are shown in Figure 5.4. The morphological structure is particularly influenced by the release of the volatile species during the pyrolysis which is controlled by the heating rate (K. Zeng *et al.*, 2015). For slow heating rate as the one used in this study, no major modification occurs in the particle morphology (Rocca *et al.*, 1999), biochars from low heating rate pyrolysis keep their raw porosity. As shown in Figure 5.2, the reactivity of WS biochar is greater than that of SS. The same behavior was also observed when comparing Cell-WS-L and Cell-SS-P, considering that acid pulping does not have major effect on the morphological structure. This trend is reversed at subsequent stages of conversion and assessed with the inorganic content. Therefore, this result indicates that the biochar structure might have a slight effect on biochar reactivity at earlier stage of conversion. With increasing conversion, the concentration of inorganic elements increases, hence their catalytic or inhibitor effect is stronger, becoming the main parameter governing biochar gasification. In this regard, Di Blasi (Blasi, 2009) also reported that morphological structure seemed to be less affecting than the inorganic content.

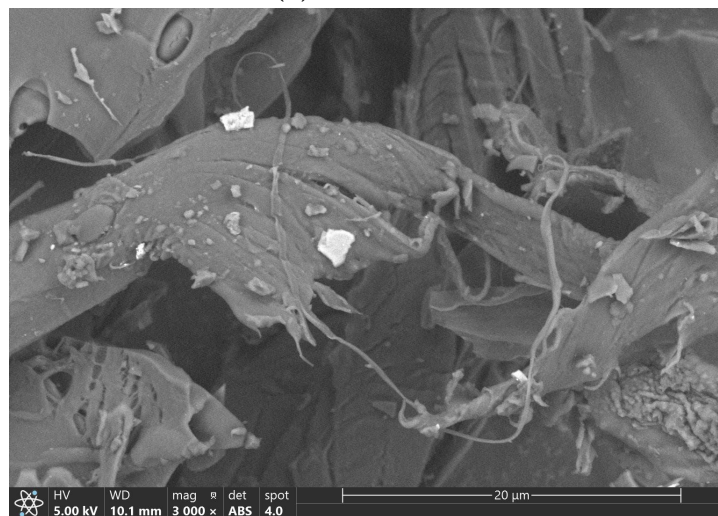
5.3.2 Gasification kinetics analysis

Prior to calculating E_a and A , the dependence on the partial pressure of the gasifying agent and the reaction mechanism were elucidated. The reaction order with respect to steam partial pressure is represented by the slope of the log-log plot of $d\alpha/dt$ vs partial steam pressure at fixed conversion. It was calculated at three different pressures. No significant variation with conversion was observed. As presented in Figure 5.5, the value was about 0.66, which ties well with the values reported in the literature (0.4 – 1) (Blasi, 2009).

$f(\alpha)$ is a function that is associated with a physical model that describes the kinetics of the solid-state reaction. Generally, n th-order models particularly the volumetric reaction



(a) WS biochar



(b) SS biochar

Figure 5.4: SEM images of SS and WS biochars

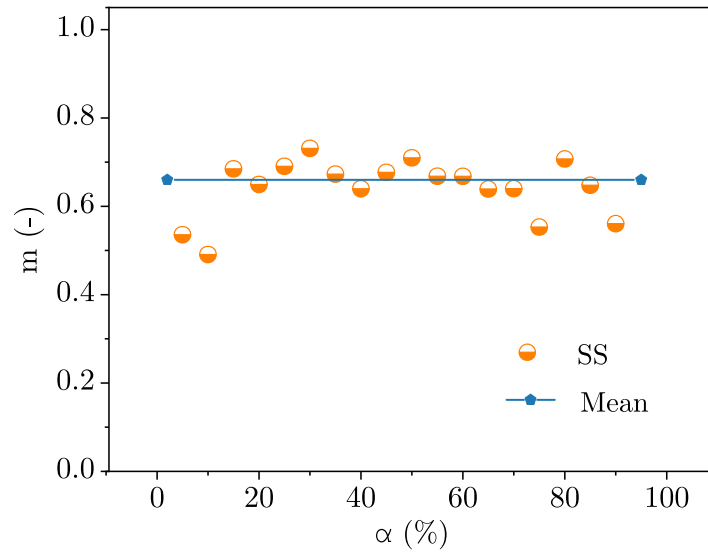


Figure 5.5: Dependence of the reaction rate on steam partial pressure

model, shrinking core model, and random pore model are the most commonly used applied kinetics models to describe heterogeneous gas-solid reactions (Tomaszewicz *et al.*, 2017). The above-mentioned models can be modified to take into account the effect of inorganic content. For instance, several kinetic models have been proposed taking into account inorganic content particularly K and Ca with and without considering Si. Volumetric models using $K/(Si+P)$ ratio have been used to predict steam gasification behavior of different biomass biochars (Dupont *et al.*, 2016; Romero Millán *et al.*, 2019). A random pore model with additional factor correlated to K content was used to describe steam gasification of biomass biochar (Kramb *et al.*, 2016; Zhang *et al.*, 2008). Grain model with additional factor function of (K/Si) (Dupont *et al.*, 2011), and Ca content (Kramb *et al.*, 2016; López-González *et al.*, 2014) was also used to describe steam gasification kinetics.

To determine the suitable kinetic model describing biochar gasification, generalized master plots were used. Theoretical master plots $f(\alpha)/f(\alpha)_{\alpha=0.5}$ for various kinetic models and experimental curves $\frac{d\alpha/dt}{(d\alpha/dt)_{\alpha=0.5}}$ against α are presented in Figure 5.6. As can be noted, no variation was observed in the kinetic model for all studied samples with temperatures and partial steam pressure. This confirms the independence of the decomposition mechanism from the operating conditions (Brown, 1998).

Regarding the kinetic model, it can be seen that n th-order based mechanisms could be noticed in the steam gasification of biomass and cellulose pulp biochars. The generalized master-plots curves show that the zero-order model is the most suitable mechanism model $f(\alpha)$ for SS biochar (group 1) with low Si content. The gasification rate is constant up to a conversion level of 80 %.

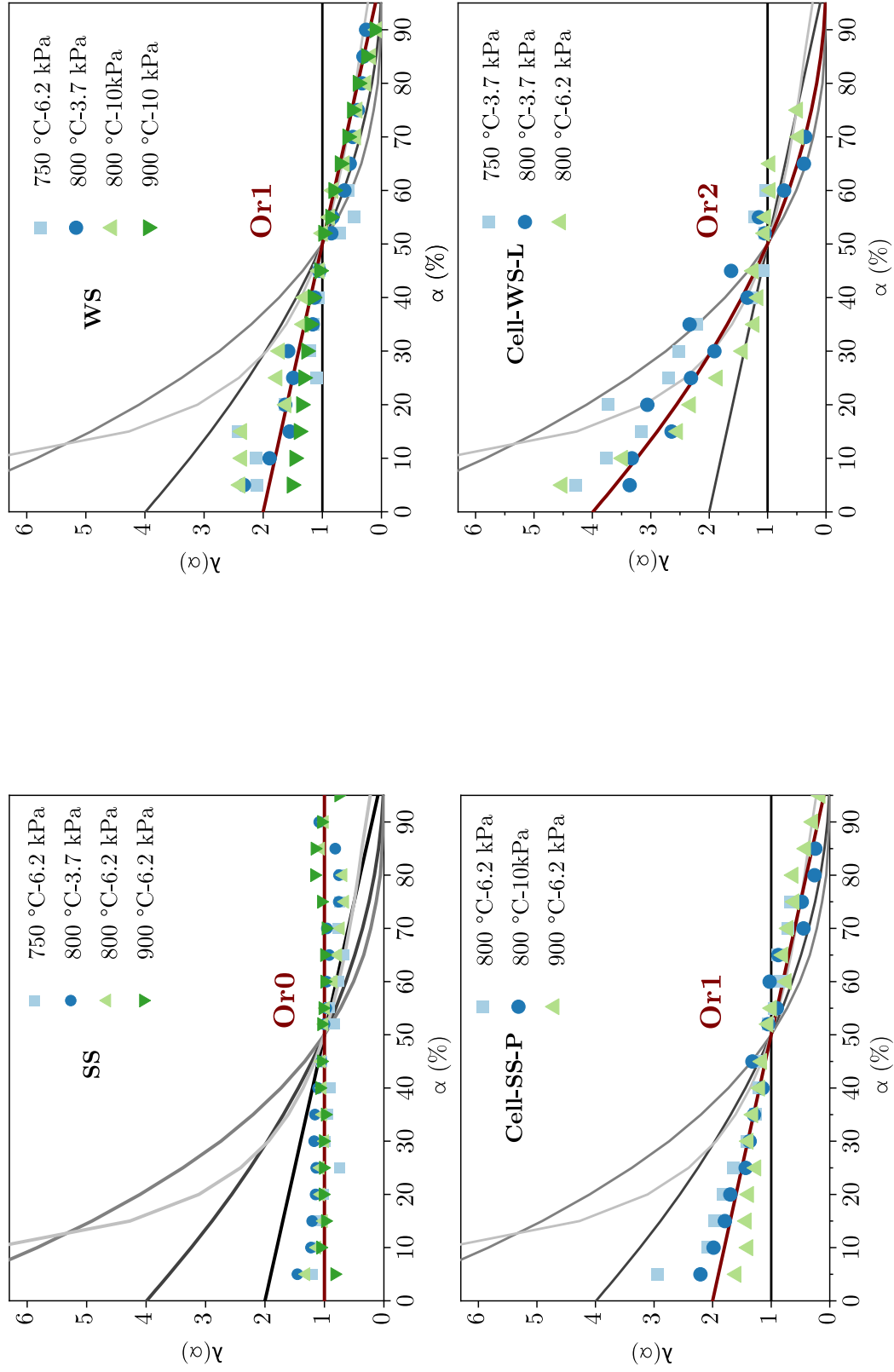


Figure 5.6: Comparison between theoretical master-plots and experimental plots against α for different samples

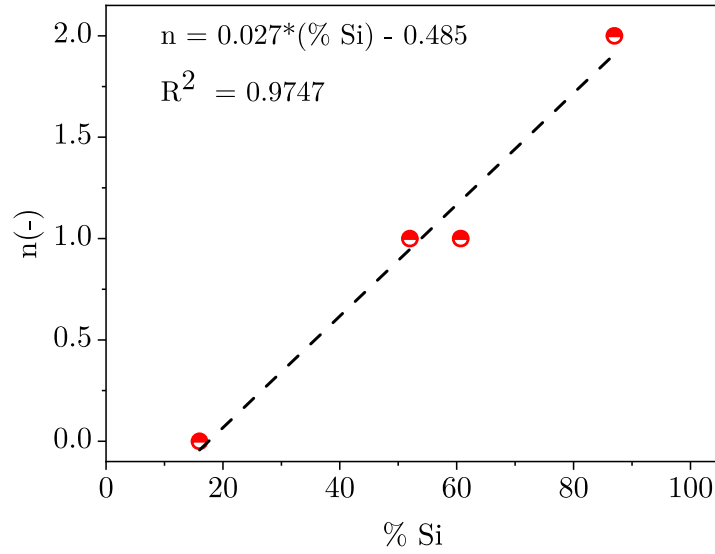


Figure 5.7: Reaction order n as a function of %Si

Table 5.4: Kinetic parameters of different biochar samples

	A (min kPa ^{-0.66})	Ea (kJ mol ⁻¹)
SS	4.0×10 ⁶	149.7±2.5
Cell-SS-P	2.4×10 ⁴	
WS	5.8×10 ⁴	
Cell-WS-L	4.8×10 ⁶	

On the other hand, it is apparent that the reaction mechanisms shift up to a higher reaction-order. The first-order mechanism gives the best match with the experimental data for **WS**. A first-order mechanism is also responsible for the **Cell-SS-P** gasification. This similar reaction order identified for the two samples can be explained by the similarity of %Si. The reaction mechanism of **Cell-WS-L** biochar gasification is close to second-order (Or2). This observation confirms the inhibitory effect of Si, where a decrease in the gasification rate is observed with increasing %Si.

From the data, a linear relationship between the reaction order n and %Si can be established, as shown in Figure 5.7. The reaction order increase with the increase of %Si. Consequently, the gasification behavior of the cellulose pulp biochar can be described using their silica content. The activation energy Ea was calculated from the slope of the plot $\ln(t)$ vs T^{-1} , for constant values of α . A mean value of 149.7 kJ mol⁻¹ was calculated for all biochar samples. These results are in accordance with results reported in the literature (Adamon *et al.*, 2019; Le *et al.*, 2015; Romero Millán *et al.*, 2019). Afterwards, the pre-exponential factor was determined using Eq. 5.4. The obtained

values are listed in Table 5.4. No apparent relationship was found between the kinetic parameters, A and E_a and the inorganic content. For biomass biochar, the value of A was higher for samples with low Si content. For cellulose biochars, the order of magnitude of this parameter was similar for the Cell-SS-P and Cell-WS-L, which have a low K concentration. Since the limited number of analyzed pulp biochar samples and their low K content, the kinetic parameter cannot be correlated to the inorganic content. The overall equation describing the gasification kinetic behavior rate was then expressed as follows:

$$\begin{aligned} \frac{d\alpha}{dt} &= A \times \exp\left(\frac{-149700}{RT}\right) \times P_{H_2O}^{0.66} \times (1 - \alpha)^n \\ n &= 0.027 \times (\%Si) + 0.48 \\ \%Si &= [0 - 100 \%]; P_{H_2O} = [3.7 - 10 \text{ kPa}] \end{aligned} \quad (5.7)$$

5.3.3 Kinetic model accuracy

To assess accuracy of the model, predicted reaction rate was compared with the experimental results. The deviation was quantified using Nonlinear Least Squares:

$$Dev (\%) = 100 \frac{\sqrt{\sum_{j=1}^n [\alpha_{exp,j} - \alpha_{calc,j}]^2}}{\sqrt{N} \alpha_{exp,max}} \quad (5.8)$$

where N is the number of experimental points employed; α_{exp} and α_{calc} are respectively the experimental and predicted model biochar conversion rates. The deviation (min-max) for SS, WS, Cell-SS-P and Cell-WS-L was respectively 1.6 – 5.2, 2.2 – 5.0, 1.9 – 5.0 and 2.4 – 9.1 % indicating that the model agrees well with the experimental results. Graphical comparisons between the breakthrough data and the data obtained from the model in Eq. 5.7 are given in Figure 5.8. As illustrated, the modeled data off all analyzed samples fitted sufficiently well with the experimental conversion profile vs time. This offers the potential of using Si content to describe the gasification behavior of a wide range of materials including cellulose pulp biochar. Most importantly, the gasification behavior of cellulose pulp biochars can be predicted despite the low content of AAEM species, particularly potassium. It should be emphasized that the linear relationship used to predict the reaction order from %Si was used to reproduce the results of other studies (Dupont *et al.*, 2016; Hognon *et al.*, 2014; Romero Millán *et al.*, 2019) in which they used inorganic ratios such K/Si and K/(Si+P). As it can be seen in Table 5.6, a very good agreement was found between the results for determining the reaction order except in the case of biomass having high phosphorous content.

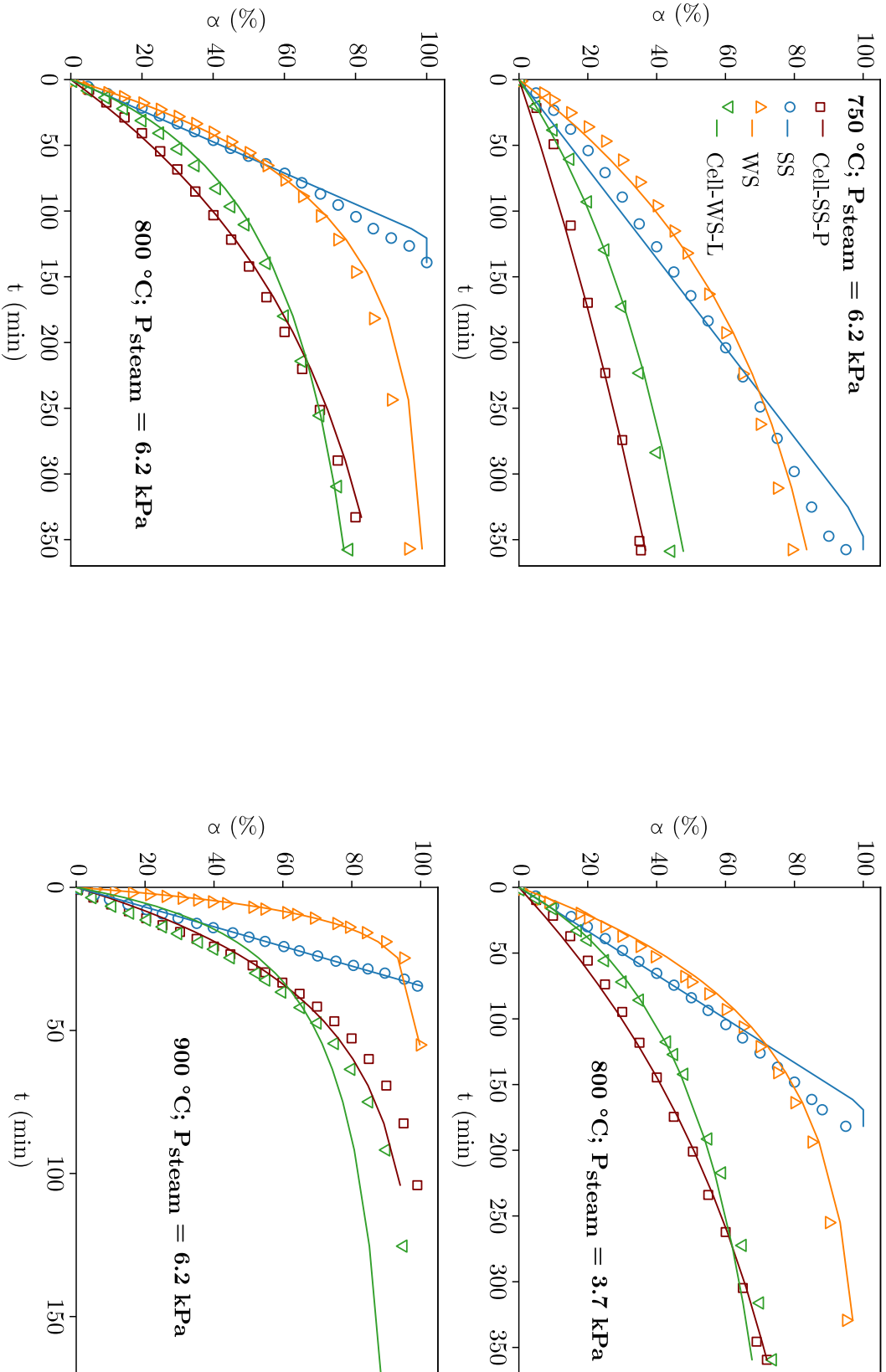


Figure 5.8: Comparison between experimental conversion data and the modeled conversion curves of all studied samples under different operating conditions. (scatter: experimental data; line: model-predicted results)

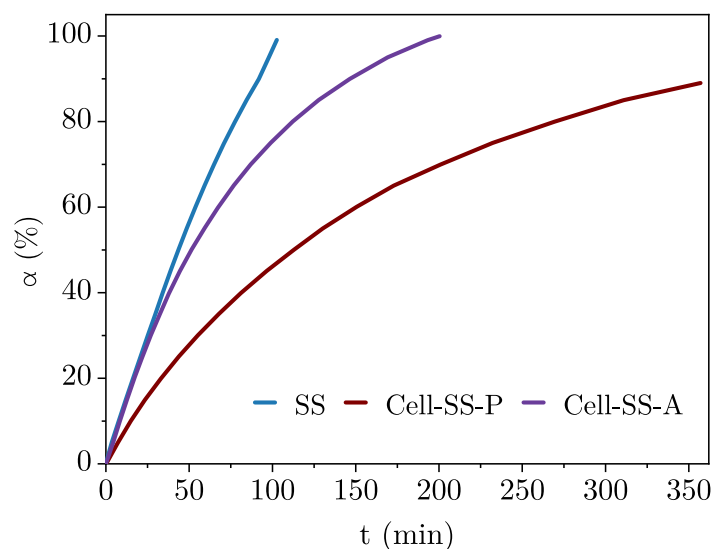


Figure 5.9: Conversion degree α vs time for of SS, Cell-SS, and Cell-SS-A biochars at 800 °C with a partial steam pressure of 10 kPa

5.3.4 Effect of silica elimination on biochar reactivity

The above results fully depict the significant difference in steam gasification behavior of the raw biomass and the cellulose pulp biochars. The pulp biochar gasification is governed by Si content. The severe inhibitory effect of Si on the pulp biochar gasification leads to lower reactivities which subsequently result in a more extensive reaction time. The elimination of Si is expected to increase the reactivity of pulp biochar. Figure 5.9 shows the comparison between the conversion profiles of raw biomass, cellulose pulp and the alkaline-washed pulp. Cell-SS-A showed higher reaction rate than Cell-SS-P, which Si is its main inorganic element. Si species, mainly found in the epidermic cells, are considerably removed through the alkaline treatment. Hence, biochar gasification reactivity increases. At low conversion, Cell-SS-A and SS biochars have almost similar reactivities. For the alkaline-washed pulp biochar, the trend of variation of reaction rate over the whole conversion range did not show any increase. The behavior of alkaline-washed pulp can be compared to other studies in which the effect of acid washed was elucidated in the absence of Si. Indeed, different studies have reported lower reactivities for acid washed biochar in absence of Si. Yip *et al.* (2010) found that the reactivity of acid-treated biochar had much lower reactivity than raw biochar, and its reactivity remained constant throughout the whole conversion range. Lower reactivities for raw biochars were reported for acid-washed biochars (Kajita *et al.*, 2010; Marquez-Montesinos *et al.*, 2002; Mitsuoka *et al.*, 2011).

In Table 5.5 the reactivity and reaction time at operating conditions are highlighted. The results provide important insights into the beneficial impact of Si removal on cellulose pulp biochar gasification. For instance, it can be noticed that the reactivity

Table 5.5: Gasification reactivity and the required time to achieve 70 % conversion at different operating conditions

$\alpha = 70 \%$	800 °C; 3.7 kPa		800 °C; 10 kPa		900 °C; 3.7 kPa		900 °C; 6.2 kPa	
	R	t	R	t	R	t	R	t
SS	1.51	126.0	2.84	64.8	8.06	28.8	9.74	24.0
Cell -SS-P	0.34	357.0	0.45	201.0	3.71	46.2	3.58	41.7
Cell-SS-A	0.87	139.2	1.35	87.0	4.87	36.0	6.14	28.5

R unit is $\%.\text{min}^{-1}$; t unit is min

increased 2.5 and 1.3 times at 800 and 900 °C with a partial steam pressure of 3.7 kPa, respectively. At 800 °C, the reaction time to achieve 70 % of biochar conversion was reduced from 357.0 and 201.0 min to 139.2 and 87.0 min with a partial steam pressure of 3.7 and 10 kPa, respectively. Hence, the required reaction time to achieve 70 % of conversion was reduced by 60 %. The same trend was observed at 900 °C where the reaction time was reduced by 22 and 32 % with a partial steam pressure of 3.7 and 10 kPa, respectively. The reduction of Si content leads to an increase in biochar reactivity and a decrease in the reaction time. *Cell-SS-A* biochar had a slightly lower reactivity than the raw biomass biochar.

5.4 Conclusion

In the this chapter, TGA steam gasification of LEEBIO cellulose pulps was investigated. The tests were performed using isothermal conditions. The results were compared to the raw biomass. The significant difference in AAEM and Si contents could lead to a major difference in gasification behavior. Slower gasification than the raw biomass biochar was observed. The gasification behavior of cellulose pulp biochar was predominantly governed by Si concentration. A less significant impact attributed to the morphological structure was also observed.

A new modeling approach based on Si concentration was proposed to predict the steam gasification kinetics of lignocellulosic biomass and pulp biochars. The TGA data and the derived model showed a satisfactory agreement. The elimination of Si species by NaOH based alkaline washing enabled the enhancement of pulp biochar gasification. A higher reactivity and lower reaction time were observed for alkaline-washed pulp. Hence, the results of the present investigation confirmed that Si content is a principal influencing parameter on biochar kinetics.

Table 5.6: Applicability of %Si in literature studies (order: study result; n reaction order determined using %Si)

	K/(Si+P)	%Si	order	n (-)	
(Romero Millán <i>et al.</i> , 2019)	100% CS	4	7	0.0	0.0
	100% BG	0.2	74	1.3	1.5
	100% OPS	0.2	78	1.4	1.6
	90%CS – 10%BG	1.2	35	0.0	0.4
	85%CS – 15%BG	0.9	42	0.1	0.7
	75%CS – 25%BG	0.6	52	0.7	0.9
	50%CS – 50%BG	0.4	65	1.0	1.3
	90%CS – 10%OPS	2.2	18	0.0	0.0
	85%CS – 15%OPS	1.7	23	0.0	0.1
	75%CS – 25%OPS	1.0	33	0.0	0.4
	50%CS – 50%OPS	0.6	52	0.7	0.9
	K/(Si+P)	%Si	order	n (-)	
(Dupont <i>et al.</i> , 2016)	Angelim	2.6	4	0	0.0
	Beech	4.8	3	0	0.0
	Faveira	0.2	61	1	1.2
	Maçaranduba	9.9	1	0	0.0
	Pine + Spruce	3.9	6	0	0.0
	SRC False acacia	3.8	4	0	0.0
	SRC Popular_1	2.6	4	0	0.0
	SRC Popular_2	2.5	2	0	0.0
	SRF Eucalyptus	4.6	4	0	0.0
	SRF Popular	1.3	8	0	0.0
	Alfalfa	7.3	1	0	0.0
	Barley straw	0.1	80	1	1.7
	Miscanthus	0.4	53	1	0.9
	Switchgrass	0.6	41	1	0.6
	Tall	2.5	20	0	0.1
	Triticale	0.7	47	1	0.8
	Wheat straw 1	0.8	42	1	0.6
	Wheat straw 2	0.1	77	1	1.6
	Chlamydomonas	0.2	0	1	0.0
	Spiruline	1.4	0	0	0.0
	K/(Si+P)	%Si	order	n (-)	
(Hognon <i>et al.</i> , 2014)	Miscanthus	0.4	52	1	0.9
	Beech	4.8	2.8	0	0.0
	Wheat straw	0.8	41	1	0.6

Pyrogasification: devolatilization and steam gasification of biochar for hydrogen production

6.1	Introduction	123
6.2	Pyrolysis of cellulose: product distribution and characterization	124
6.2.1	Product distribution and gas composition	124
6.2.2	Characterization of the liquid products	125
	Qualitative analysis	125
	Quantitative analysis	126
6.3	Steam gasification of pyrolysis-derived biochar	127
6.3.1	Effect of steam/char ratio	130
6.3.2	Effect of Temperature	133
6.3.3	Effect of inorganic matter	136
6.4	Conclusion and perspectives	140
6.4.1	Conclusion	140
6.4.2	Hydrogen rich-gas production potential	141

6.1 Introduction

According to the internal energy agencies, the current demand for hydrogen is majorly supplied by fossil fuels (International Energy Agency, 2019). Steam gasification has been regarded as an effective and economical route for hydrogen production leaving a minimal environmental footprint (Parthasarathy *et al.*, 2014). In the current energy and environmental context, the gasification of cellulose pulp is considered as a potential alternative to produce a sustainable hydrogen (G.-H. Delmas *et al.*, 2021). As a result, this chapter deals with the pyrogasification of LEEBIO cellulose pulp (Cell-SS-P). The primary objective is investigating the production of high-quality and H₂-rich syngas from steam gasification of pulp biochar.

Pyrogasification tests of biochar were performed in a semi-continuous fixed bed reactor in a multi-stage process approach. As already shown in Figure 2.8, the process was divided into 2 stages: devolatilization (or pyrolysis) and biochar gasification. Volatile matter and biochar are produced within the pyrolysis stage. Volatiles were removed

from the reactor and not taken into consideration in the gasification stage. The obtained biochar was then gasified under a steam atmosphere. Biochar gasification process has been widely used in literature (Muradov *et al.*, 2015; Ning *et al.*, 2018; Sattar *et al.*, 2014; Q. M. Waheed *et al.*, 2016; Jie Wang *et al.*, 2009). As presented in Chapter 1, WoodRoll technology is based on this concept for full-scale production of syngas.

Therefore, this chapter comprises two sections:

1. Pyrolysis characteristics of cellulose pulp with a focus on product distribution and composition
2. Biochar gasification with an emphasis on the effects of operating conditions on hydrogen production

6.2 Pyrolysis of cellulose: product distribution and characterization

Devolatilization experiments were performed under an inert atmosphere in a non-isothermal program using a linear heating rate of $10\text{ }^{\circ}\text{C min}^{-1}$ within the temperature range of 30 to $750\text{ }^{\circ}\text{C}$. At the end of the test, products have been grouped into three different fractions: biochar, tar, water, and gas (as described in Chapter 2). The mass balance for pyrolysis was calculated from the measured above-mentioned products. The product yield is calculated by the equation below:

$$Y_i = \frac{m_i}{m_{feedstock,daf}} (\%) \quad (6.1)$$

wherein m_i is the mass of corresponding products.

Mass balance range from 90 to 96 % which can be considered quite satisfactory for such an experimental setup. The reason for the non-closure of mass balance arises primarily from the fact that: (i) condensation of a slight fraction of volatiles would occur between the furnace outlet and tar trap, (ii) escape of light hydrocarbons in the gaseous product. The results of pyrolysis characteristics of [Cell-SS-P](#) and [ARC](#) are presented. The losses are therefore added to gas yield to bracket the mass balance 100 % closure.

6.2.1 Product distribution and gas composition

The yields of biochar, bio-oil and the distribution of H_2 , CO , CO_2 , CH_4 , and C_{2-3}H_n (gas analyzed using gas chromatography) products are shown in Table 6.1. Bio-oil or condensed liquid consists of tar and pyrolysis water.

Table 6.1: Product yields (wt. %) of pyrolysis products (dry basis)

	Biochar	Tar	Water	Gas	H ₂	CO	CO ₂	CH ₄	C _{2,3} Hn
Cell-SS-P	23.2	27.2	27.5	22.0	0.55	6.32	12.06	2.32	0.77
ARC	17.7	28.1	26.7	27.4	0.28	9.49	15.87	1.13	0.62

yield unit is in wt. %

Cell-SS-P pyrolysis produced more biochar, while ARC yielded a higher gas fraction. It has been shown in Chapter 3, Cell-SS-P contains mainly cellulose which is consisted of a branching chain of polysaccharides, which are highly volatile. In contrast, lignin is a full aromatic structural unit that are more thermally stable. In relation to the gaseous products, the yields of H₂ and CH₄ obtained from Cell-SS-P pyrolysis were nearly twice that for ARC which generated more CO and CO₂, in accordance with other studies (C. Li *et al.*, 2021; Quan *et al.*, 2016). The difference in polymeric structures and chemical nature possibly elucidates the different behaviors observed (D. Lv *et al.*, 2010). The higher CO and CO₂ yield from ARC are attributed to the higher content of carbonyl and carboxyl groups which undergo cracking and reforming (Qu *et al.*, 2011; Yang *et al.*, 2007).

6.2.2 Characterization of the liquid products

Besides water quantification, GC-MS was performed to provide insight into bio-oil composition. Qualitative and quantitative analyses of bio-oil were performed.

Qualitative analysis

The organic compounds were identified and grouped according to chemical types. The major categories of bio-oil are given in Figure 6.1. The identified components are listed in Table 6.11.

A variety of compounds were detected including saccharides, esters, ketones, furans, phenols, esters, and benzenes. The results of the quantitative analysis of bio-oils obtained from the pyrolysis of two cellulosic samples are given in Figure 6.1. In agreement with the literature (Qu *et al.*, 2011; C. Zhao *et al.*, 2017), acids, ketones, and furans were the main products of both cellulosic samples. According to the literature (Dufour, 2007; Morf Philipp Oliver, 2001), the presence of benzenes comes from the conversion of secondary tars, namely phenols, xylenes, and cresol. Cell-SS-P produced more phenols which is due to the content of lignin and its structural characteristics (Lyu *et al.*, 2015; Quan *et al.*, 2016). Hence, the higher phenol content possibly explains the higher benzene yield from Cell-SS-P pyrolysis.

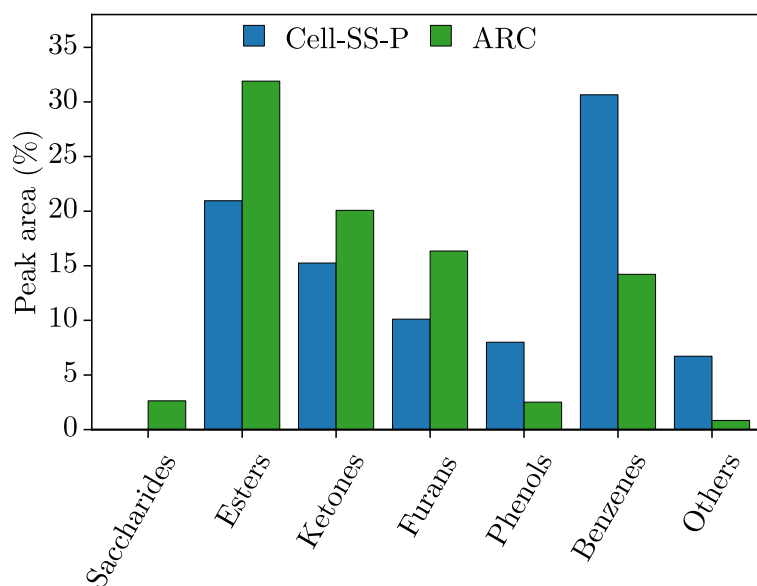


Figure 6.1: Chemical composition of pyrolysis bio-oils

Quantitative analysis

Given the results of the qualitative analysis, 7 major compounds are displaying a relatively high fraction (peak area) and are commonly identified in bio-oil from pyrolysis in the used temperature range. The analyzed compounds principally comprise secondary and tertiary tars. Consequently, the weight composition of bio-oil from Cell-SS-P is illustrated in Figure 6.2. As could be seen, the quantified tars account for 10.5 % of bio-oil and 21 % of total detected tars. The fraction of non-quantified tars mainly includes primary tars, namely mixed oxygenated compounds (acids and ketones). For ARC, quantified tars by GC-MS were 11 % of the total mass of sampled tars.

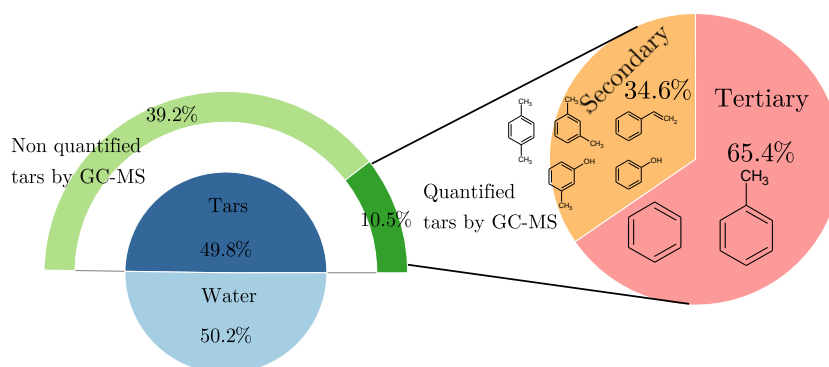


Figure 6.2: Composition of bio-oil from pyrolysis of Cell-SS-P

The yield of tars provided from the quantitative results are shown in Figure 6.3. In agreement with literature (Billaud, 2015; Dufour, 2007; Tchini Séverin Tanoh *et al.*, 2020), the mass yields of benzene, toluene, and phenol vary between 11–18, 7–19 and

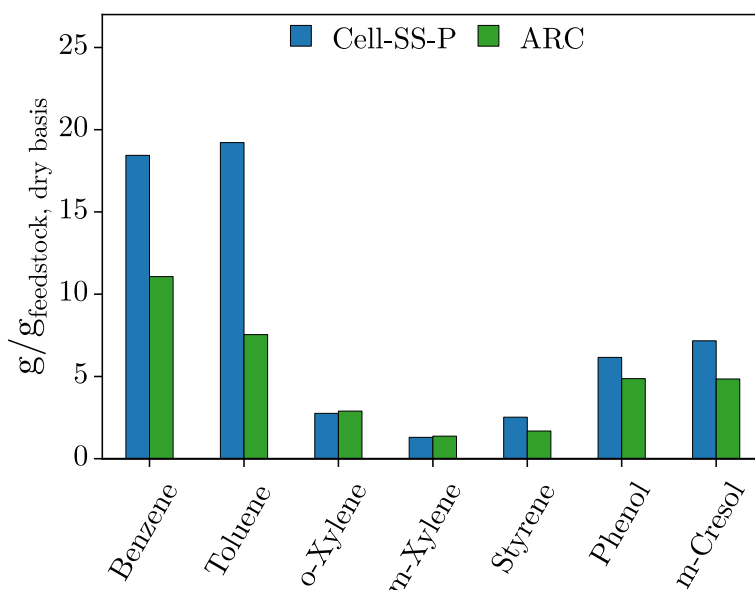


Figure 6.3: Yields of major tar compounds

4–6 g/kg (feedstock, db), respectively. Tchini Séverin Tanoh *et al.* (2020) reported that benzene yield increased while phenol yield decreased when increasing temperature from 700 to 800 °C. Dufour (2007) observed that aromatic compounds yields reached a maximum in the temperature range 800–900 °C, followed by a reduction with increasing temperature.

The results of pyrolysis product distribution and composition are used as input for the process modeling in Chapter 7. The pyrolysis step is followed by steam gasification of the obtained biochar.

6.3 Steam gasification of pyrolysis-derived biochar

Different factors influence the gasification performance for syngas production. The reaction temperature and steam-to-carbon ratio are the main influential operating parameters. Results reported in Chapter 5 showed that the gasification kinetics of cellulose pulp was different from the raw biomass and was explained by the difference in their inorganic content. The role of inherent minerals was therefore investigated. Finally, the potential of LEEBIO cellulose to produce sustainable hydrogen is evaluated. The pyrolysis biochar is used as feedstock for steam gasification. The properties of Cell-SS-P biochar are given in Table 6.2. Water gas reaction (WGR) (Eq. 6.2) alongside water gas shift reaction (WGSR) (Eq. 6.3), and Boudouard reaction (Eq. 6.4) is the main chemical reactions taking place during steam gasification of biochar. Steam methane

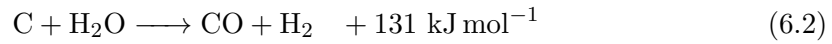
Table 6.2: Ultimate and proximate analysis at dry basis of different biochars

	Proximate analysis			Ultimate analysis				HHV (MJ kg ⁻¹)
	VM	FC*	A	C	H	N	O*	
Cell-SS-P	6.1	91.6	2.3	90.2	1.2	0.0	6.3	32.7
SS	9.0	89.7	1.4	90.8	1.2	0.1	6.5	32.1
ARC	4.5	91.5	4.0	85.0	1.6	0.0	9.6	31.5

* by difference

reforming (Eq. 6.6) and hydrogasification (Eq. 6.5) can equally occur; the effect of both reactions is less significant on hydrogen production and syngas composition.

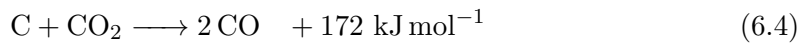
Water-gas reaction (WGR):



Water-gas shift reaction (WGSR):



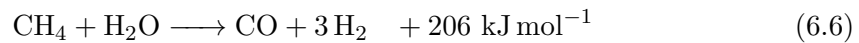
Boudouard reaction:



Hydrogasification reaction:



Steam methane reforming:



The gasification product yield as a function of the pyrolysis biochar and steam used in the gasification stage is calculated according to:

$$Y_i = \frac{m_i}{m_{\text{pyrolysis char}} + m_{\text{steam}}} (\%) \quad (6.7)$$

To evaluate the performance of the process, the below parameters are defined following:

Steam conversion:

$$X_{steam} = m_{steam} \left(1 - \frac{m_{condensed\ water}}{m_{steam}}\right) (\%) \quad (6.8)$$

where m_{steam} and $m_{condensed\ water}$ are respectively the mass of injected steam and the weight of trapped water that was measured gravimetrically. The recovered biochar was collected and weighed. The organic and mineral compositions were analyzed.

Carbon conversion:

$$X_C = m_{carbon\ in\ input\ char} \left(1 - \frac{m_{carbon\ in\ recovered\ char}}{m_{carbon\ in\ input\ char}}\right) (\%) \quad (6.9)$$

where the weight of carbon in biochar is $m_{biochar}(1 - X_{ash}) \times C\%$ (g)

$$m_{carbon\ in\ syngas} = \frac{V_{gas} (L) \times 1000 [CH_4\% + CO\% + CO_2\% + 2 \times C_2H_m] \times 12}{22.4} (g) \quad (6.10)$$

$$Dry\ gas\ yield = \frac{V_{dry\ gas}}{m_{dry-ash\ free\ feedstock}} (Nm^3\ kg^{-1}) \quad (6.11)$$

Cold gas efficiency:

$$CGE = \frac{LHV_{product\ gas} \times m_{product\ gas}}{LHV_{input\ char} \times m_{input\ char}} (\%) \quad (6.12)$$

To make sure that gas is the only product derived from biochar gasification and the devolatilization step is completed, the carbon balance of gasification tests is presented in Table 6.3. The data confirms that carbon in biochar is converted to non-condensable gases, CO, CO₂, and some CH₄ following the mentioned reactions. Thus, this result confirms the absence of hydrocarbons and tar; it indicates that condensates consist of non-reacted steam. A similar result was observed by (Jia *et al.*, 2017).

During biochar gasification process, the reaction temperature and the steam/carbon ratio (S/C) are vital parameters that have a strong impact on both H₂ yield and concentration in syngas (Florin *et al.*, 2007). Besides operating conditions, the inherent inorganic matter namely AAEM and other minerals can influence the gasification performance and impact the product distribution. The effects of each parameter on the product yields, gas yield as well as hydrogen production from biochar are investigated in the following sections. The influence of these parameters on gas composition is elucidated in terms of gas fractions and ratios. (H₂ + CH₄)/CO, H₂/CO, H₂/CO₂, CO/CO₂, and H₂/CH₄ have been selected as a scale to assess the gas quality and its production efficiency.

6.3.1 Effect of steam/char ratio

The S/C was varied by keeping biochar input constant, while steam was supplied into the reactor at the rates of 15, 30, 45, and 60 g h^{-1} . Table 6.4 summarizes the effect of S/C on steam gasification of Cell-SS-P biochar at 950 °C. The other results presenting the effect of S/C on gasification performance on biochar derived from raw biomass (SS) and ARC can be found in Table 6.9 and 6.10. The fractions of recovered char, condensates, and gas are calculated from their in gram per grams of the gasification stage input (pyrolysis biochar and injected steam). From the results, it is clear that the fraction of the recovered biochar was reduced with the raise of S/C . Biochar conversion continuously increased with an increase of S/C . This uptrend was expected given the presence of steam in the reactants of WGR (Eq. 6.2) which are promoted at high temperatures. This substantial raise is associated with an enhancement of the gas production of dry gas yield. The dry gas yield was improved from 0.4 to 0.9 $\text{Nm}^3 \text{kg}_{\text{cellulose pulp}}^{-1}$ when S/C was increased from 0.7 to 3.1. These findings seem to be consistent with other research (Xiao *et al.*, 2017).

It is reasonable to believe that the promotion of the biochar gasification process could be mainly caused by the steam addition. Nevertheless, the results indicate that biochar gasification can be divided into two stages, regarding the fraction of the gas in the product. With the initial increase in S/C from 0.7 to 1.5, the gas fraction augmented from 64.9 to 72.9 wt. %. This result can be explained by the higher reactivities of carbon-steam reactions, mentioned above. At this stage, the fraction of condensates was relatively insignificant, considering that the steam was converted to gas. When S/C was above 1.5, the gas fraction in the product slightly decreased and maintained at 66.6 wt. %. Excessive steam resulted in a decrease in steam conversion and a sharp upsurge in the condensate fraction. Similar findings were reported by Yan *et al.* (2010a), who suggested that the available biochar was not sufficient to react with all steam injected in the gasifier reactor. Hence, an excessive steam supply can lead to higher energy and operation cost.

Table 6.3: Experimental results of carbon during steam gasification of Cell-SS-P biochar ($T = 850$ °C)

Steam flow rate (g h^{-1})	15	30	45	60
Carbon balance (wt. %)				
Carbon in syngas	22.8	26.5	35.4	39.1
Carbon in biochar	75.4	74.2	66.2	60.1
Carbon balance	98.2	100.7	101.7	99.2

Table 6.4: The influence of steam flow rate on gasification of Cell-SS-P biochar at 950 °C

Steam flow rate (g h ⁻¹); 1 hour	15	30	45	60
S/C	0.7	1.5	2.3	3.1
Product distribution (wt. %)				
Gas	64.9	72.9	66.5	66.6
Biochar	33.9	19.1	7.3	2.7
Condensates	0.9	11.2	28.0	30.9
Material balance	99.7	103.2	101.9	100.2
Char conversion (%)	45.4	63.6	74.1	91.0
Steam conversion (%)	98.0	81.7	60.0	59.2
Gas production and hydrogen yield				
H ₂ (vol. %)	53.4	54.6	56.3	56.3
CO (vol. %)	39.0	36.0	31.8	30.4
H ₂ /CO	1.4	1.5	1.8	1.9
H ₂ /CO ₂	7.4	6.2	5.0	4.6
H ₂ /CH ₄	133.6	92.6	75.5	63.4
(H ₂ + CH ₄)/CO	1.4	1.5	1.8	1.9
CO/CO ₂	5.4	4.1	2.8	2.5
Dry gas yield (Nm ³ kg _{feedstock} ⁻¹)	0.4	0.7	0.8	0.9
H ₂ (g kg _{char} ⁻¹)	109.7	163.5	190.6	229.3
LHV (MJ Nm ³⁻¹)	10.9	10.7	10.4	10.3
CGE (%)	43.1	61.1	70.7	86.5

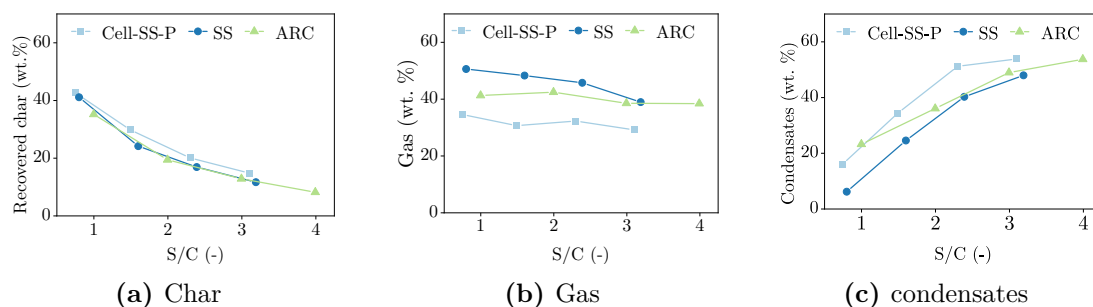


Figure 6.4: Product yield of different biochar samples as function as S/C at 850 °C

Consequently, the range of S/C between 1.5 and 2.3 was suitable for optimized biochar gasification at 950 °C. To validate this observation at a different temperature, the product evolution of the product distribution of different biochar samples (Cell-SS-P, SS, and ARC) at 850 °C were illustrated in Figure 6.4. Identical trends were observed regarding the fractions of recovered biochar and condensates. Taking into account different char samples, the gas fraction (Figure 6.4b) in the product displayed a decrease at S/C higher than 2.3. Considering these results, S/C was preferred to not exceed 2.3. The values reported in the literature were nearly between 2.475 and 3 (Ma *et al.*, 2013; Yan *et al.*, 2010a).

Besides its presence in the reactants in WGR, the steam flow rate can efficiently enhance the production of hydrogen via WGSR. Results indicate that hydrogen yield was significantly enhanced with more steam supply. The H_2 yield increased substantially from 109.7 to 190.6 $g\ kg_{char}^{-1}$ by changing S/C from 0.7 to 3.1. These findings seem to be consistent with other research (Turn *et al.*, 2007). Q. M. Waheed *et al.* (2016) suggested that the increase in H_2 yield was due to the promotion of the WGR and WGSR.

As far as the syngas composition is concerned, H_2 and CO_2 contents raised slightly while the concentration of CO decreased. The maximum H_2 fraction reached was 56.3 vol. %. The tendencies are in agreement with those in the literature (Salaudeen *et al.*, 2020; Turn *et al.*, 2007). This shows the benefit of steam injection on syngas quality as H_2/CO and $(H_2 + CH_4)/CO$. It is suggested that the increase of S/C increased the consumption of CO in WGSR (Eq. 6.3). Hence, its equilibrium shifts towards the rise of CO_2 and H_2 concentration. Compared to the aforementioned ratios, S/C showed a greater effect on CO/CO_2 which decreased significantly with increasing S/C . CO/CO_2 can be considered as a scale to evaluate the competition between WGSR and Boudouard reaction which is less dominant in such conditions. The significant decline in the H_2/CH_4 could be attributed to the reaction of hydrogasification (Eq. 6.5). The light drop in HHV with increasing the steam flow rate could be attributed to the increase of CO_2 concentration syngas. The increase of the dry gas yield under the effect of S/C led to significant improvement in CGE.

6.3.2 Effect of Temperature

The temperature is a crucial operating variable impacting the performance of biochar steam gasification. It directly influences the reaction rate and thermal equilibrium (Pinto *et al.*, 2003). Figure 6.5 depicts product distribution and gas yield during steam gasification. As expected, with increasing temperature, the gas fraction in the product increased and the solid and condensates decreased. With increasing temperature from 750 to 950 °C, the gas yield increased from 0.7 to 3.6 Nm³ kg⁻¹ of biochar for Cell-SS-P char, from 1.2 to 3.8 Nm³ kg⁻¹ of biochar for SS, from 1.5 to 4.3 Nm³ kg⁻¹ of biochar for ARC char. The yield of recovered biochar decreased by 73, 82, and 85% for the three biochar samples due to the improvement of carbon conversion. The yield of condensates displayed the same trend with a decrease of 49, 58, and 47 % for Cell-SS-P, SS, and ARC, respectively, with increasing temperature from 750 to 950 °C. The high gas yield reported for ARC could be due to the higher S/C compared to the other biochar samples.

The uptrend of gas yield and carbon and steam conversions with the increase in gasification temperature is related to endothermic reactions such as WGR (Eq. 6.2) and Boudouard reaction (Eq. 6.4) which are strengthened at a higher temperature. Several authors have highlighted the effect on gasification performance. Sattar *et al.* (2014) reported an increase in carbon conversion and gas yield with increasing temperature during the steam gasification of biochar derived from woody and herbaceous biomass.

The effect of temperature on the gas composition and hydrogen yield is presented in Figure 6.6. The evolution of carbon conversion and different gas ratios are listed in Table 6.5. Gasification temperature can impact the yields of syngas components, especially H₂ which is the main product of biochar gasification (T. Yu *et al.*, 2020). The maximum H₂ yield reached 190.6, 201.3, and 225.0 g kg_{char}⁻¹ at 950 °C for Cell-SS-P, SS, and ARC, respectively. These results were expected, considering hydrogen is one of the main products of the endothermic reaction of carbon with steam (WGR). This is consistent with what has been found in the literature. Indeed, full conversion of biochar and hydrogen yield of 197.8 g kg_{char}⁻¹ of biochar were achieved by Ning *et al.* (2018) at 900 °C. Ma *et al.* (2013) found that with temperature increase from 700 to 900 °C, both H₂ yield and carbon conversion increased from 28.68 to 83.3 mol kg_{char}⁻¹ and 49.29 to 90.42 %, respectively.

As observed, H₂ is the main component in syngas. The obtained values of H₂ content are in line with the values reported in the literature (Romero Millán *et al.*, 2021; Q. M. K. Waheed *et al.*, 2013; Jingbo Wang *et al.*, 2013). The results showed that the variation of gas concentrations was a monotonic trend. H₂ concentration in the gas mixture dropped gradually with temperature; at 950 °C, the concentration of H₂ was similar for different biochar samples, with an average of 57 vol. %. Hydrogen is mainly produced from

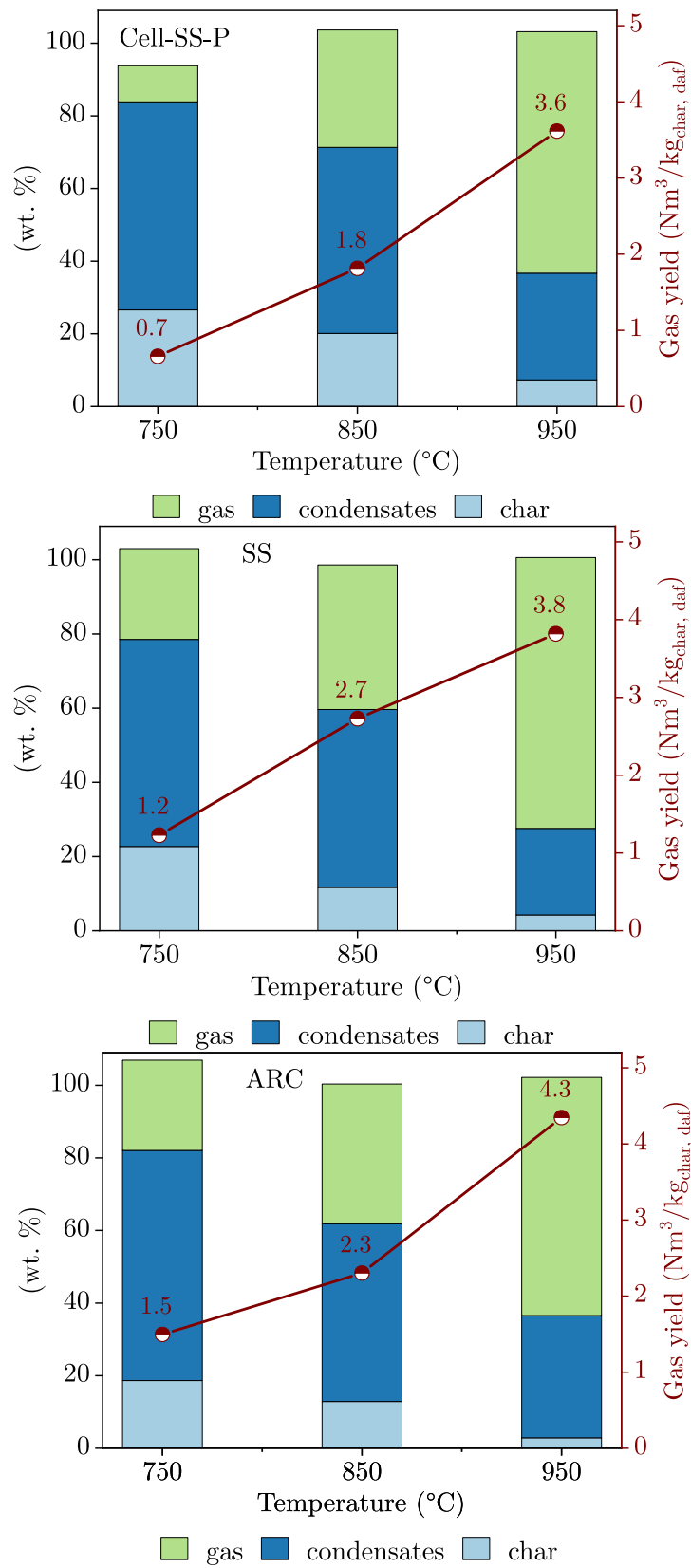


Figure 6.5: The influence of temperature on product yield ($\dot{m}_{steam} = 45 \text{ g h}^{-1}$)

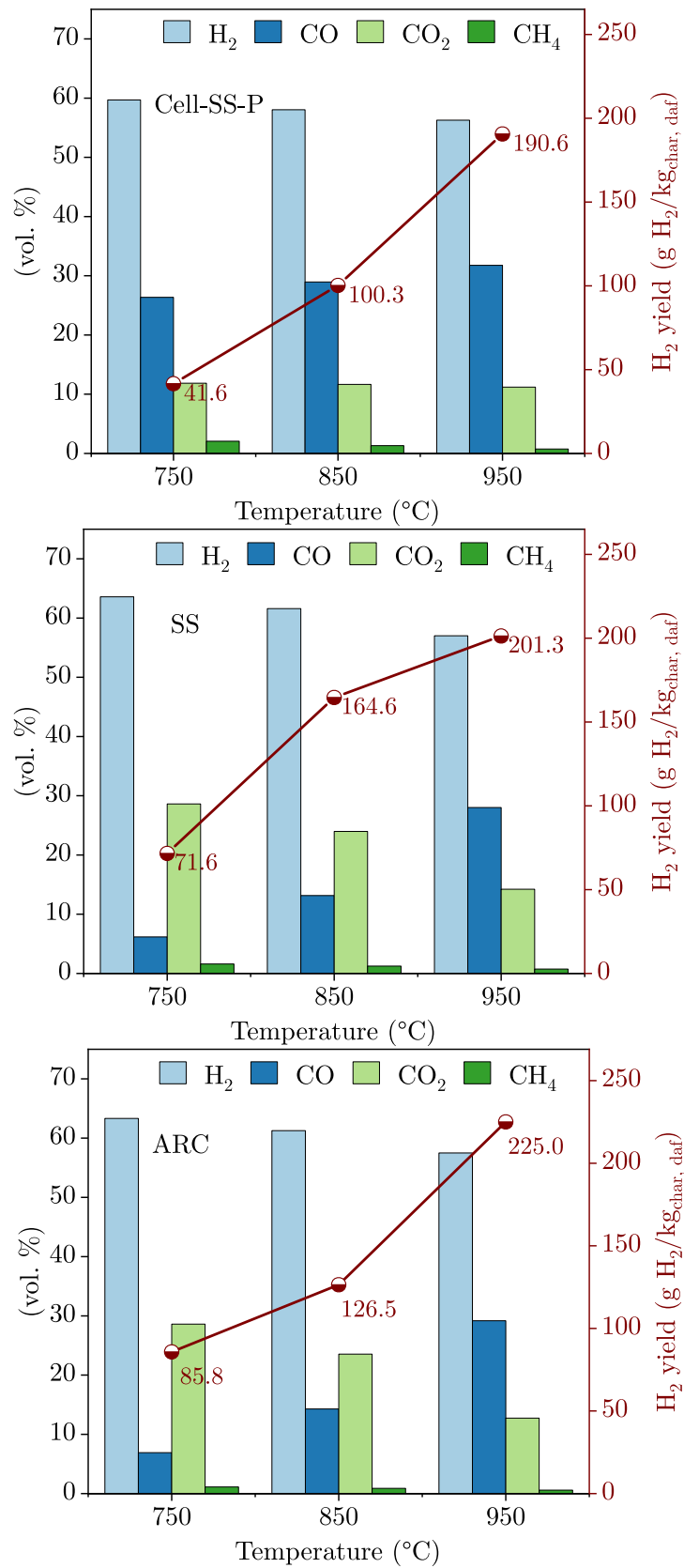


Figure 6.6: The influence of temperature on gas composition ($\dot{m}_{steam} = 45 \text{ g h}^{-1}$)

WGR (Eq. 6.2) and WGSR (Eq. 6.3). Hence, this decrease in H₂ fraction can be mainly attributed to the reactivity decrease WGSR (Eq. 6.3), which is slightly exothermic and starts to reverse at temperatures between 706 and 800 °C (Dupont, 2006; O'Hayre *et al.*, 2016). It was suggested that the Boudouard reaction can also contribute to the decrease of H₂ concentration since carbon is in the reaction of both (Ning *et al.*, 2018). However, this effect seemed to be minor, as H₂/CO₂ did not drop. The concentration of CO₂ decreased while the concentration of CO exhibited an upward trend with the increasing temperature. This reduction in CO₂ content was mainly a result of the endothermic Boudouard reaction (Eq. 6.4) and the reverse WGSR which are favored at higher temperatures. The temperature showed a great impact on the proficiency of syngas components ratios. As shown in Table 6.5, a marked decline of H₂/CO and a considerable increase of CO/CO₂ were displayed. Similar observations were obtained in the literature (T. Song *et al.*, 2012; Q. M. Waheed *et al.*, 2016). It was suggested by T. Song *et al.* (2012) that high temperature pushes the WGSR to the left hand at the expense of H₂; and the Boudouard reaction (Eq. 6.4) becomes dominant when the temperature exceeds 820 °C. Similar findings were reported by Franco *et al.* (2003). The CH₄ fraction gradually decreased to an average of 0.7 vol. % with the increase in temperature which might be linked to the low reactivity of the hydrogasification reaction (Eq. 6.5). This was translated by the sharp increase of H₂/CH₄, thus the effect of CH₄ fraction on (H₂ + CH₄)/CO was marginal. Yan *et al.* (2010a) concluded that WGR (Eq. 6.2), Boudouard reaction (Eq. 6.4) and methane steam reforming reaction (Eq. 6.6) played a more prevailing role and the reverse reaction of hydrogasification reaction (Eq. 6.5) might have occurred at higher temperatures.

6.3.3 Effect of inorganic matter

The results in the previous section showed that steam to carbon ratio S/C and temperature can strongly influence the steam gasification of the three biochar samples. The reactivity of biochar and the gas quality was strongly impacted by S/C and temperature. Carbon conversion showed an uptrend with a raise in reaction temperature and S/C. Regardless of the similar trend in product yield and gas composition, significant differences can be identified in steam gasification of Cell-SS-P biochar compared to other biochar samples in particular at temperatures lower than 950 °C.

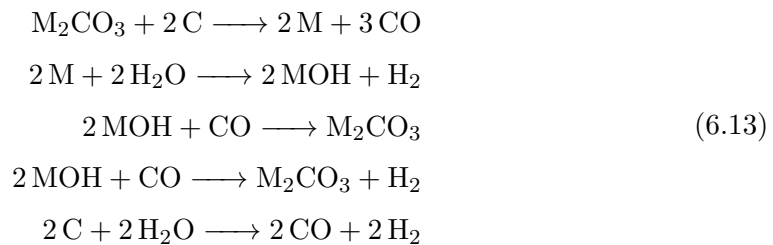
For instance, the gas yield from Cell-SS-P biochar gasification was found to be quite lower than other samples while the fraction condensates were quite higher at 750 °C, as seen in Figure 6.5. The results presented in Figure 6.6 reveal that hydrogen yield for steam gasification of Cell-SS-P biochar was 41.6 g kg_{char}⁻¹ of biochar, while yields of 71.3 and 85.8 g kg_{char}⁻¹ of biochar were obtained for SS and ARC char, respectively, at 750 °C. Furthermore, remarkable distinctions were noticed in CO and CO₂ contents in syngas produced from Cell-SS-P gasification. The obtained concentration of CO at 750 °C

Table 6.5: Carbon conversion and gas ratios in function of temperature and % Si content in raw material ($\dot{m}_{steam} = 45 \text{ g h}^{-1}$)

		Cell-SS-P	SS	ARC
Inorganic indices	K/Si	0.2	4.4	1.0
	%Si	61.1	5.5	17.4
		T (°C)		
X _c (%)	750	10.2	22.9	30.5
	850	35.4	48.7	47.7
	950	74.1	83.1	86.2
H ₂ /CO	750	2.3	10.3	9.2
	850	2.0	4.7	4.3
	950	1.8	2.0	2.0
H ₂ /CO ₂	750	5.0	2.6	2.2
	850	5.0	2.7	2.6
	950	5.0	4.0	4.5
H ₂ /CH ₄	750	29.0	39.8	57.5
	850	43.9	51.3	68.1
	950	75.5	81.4	95.8
(H ₂ + CH ₄)/CO	750	2.4	10.6	9.3
	850	2.0	4.8	4.3
	950	1.8	2.1	2.0
CO/CO ₂	750	2.2	0.2	0.2
	850	2.5	0.5	0.6
	950	2.8	2.0	2.3

was 26.4 vol. % for **Cell-SS-P** biochar while 6.2 vol. % for **SS** and 6.6 for **ARC**. The concentration of CO₂ followed the opposite trend. Similar observations can be made at 850 °C.

Such significant differences in gasification performance cannot only be linked to the macromolecular composition in terms of cellulose, lignin, and hemicelluloses, considering the fuel of steam gasification is pyrolysis char. These differences can be explained based on the difference in the inorganic matter in the feedstocks, which include **AAEM** and Si. As previously highlighted in Chapter 5, K is the main element in **SS** ash while the ash **Cell-SS-P** contains mainly Si since most of **AAEM** species were dissolved during acid pulping. The influence of inorganic matter on gasification reactivity product distribution has been underlined by several scholars in particular the catalytic role of K and the inhibitory effect of Si (Dahou *et al.*, 2021; Nzihou *et al.*, 2013b; Junqin Yu *et al.*, 2021). Table 6.5 represents K and Si contents in biochar samples, carbon conversion, and syngas characteristics at different temperatures. The differences in hydrogen yield and carbon conversion between **Cell-SS-P** and **SS** hydrogen yield obtained for **SS** at 750 and 850 °C permit us to point out the role of K in the enhancement of hydrogen production. According to literature (Matsukata *et al.*, 1988; McKee, 1983), the effect of K species on heterogeneous steam-carbon reaction (**WGR**, Eq. 6.2) can be described through an oxygen transfer mechanism in three steps from potassium carbonate, the catalytic intermediates of carbonate were metallic hydroxides and metals:



Thus, the increase in potassium content can remarkably influence carbon conversion and hydrogen production. In this regard, Yang Zhang *et al.* (2014) reported an increase in 60 % and 81 % in carbon conversion and H₂ yield, respectively, with the addition of K₂CO₃ at 700 °C. Nevertheless, this catalytic activity can be inhibited by Si which can encapsulate **AAEM** compounds (Hognon *et al.*, 2014) to form stable and non-catalytic **AAEM-silicates** (Boström *et al.*, 2012; Dahou *et al.*, 2021). However, the low carbon conversion of **Cell-SS-P** biochar cannot only be explained by assuming the encapsulation theory due to the reduced amount of **AAEM** that could react with Si. Different theories have been proposed explaining the inhibitory effect of Si. It has been reported by Gupta *et al.* (2018) that silica could bond to carbon which can hinder carbon conversion. Other theories have mentioned that the high dispersion of Si on biochar may prevent the transformation of oxygen (Lu *et al.*, 2022), and Si tends to form larger particles inside

the biochar structure (Bouraoui *et al.*, 2016). The results in Table 6.5 show the severe effect of Si in hindering biochar steam gasification. With a higher Si content, carbon conversion of Cell-SS-P biochar was comparatively lower than that of other biochars, at temperatures of 750 and 850 °C. The inhibitory effect of Si was less severe with increasing the temperature, as carbon conversion increased. Therefore, this indicates that Si can influence carbon-gas reactions such as WGR and Boudouard reaction.

The variation of listed gas ratios, in Table 6.5, permits us to elucidate the inhibiting effect of Si on the above-mentioned reactions. It is worth mentioning that H₂ concentration (Figure 6.6) in the producer gas for Cell-SS-P is relatively similar to other biochar samples, although the difference in carbon conversion. This can be explained by the reactivity of WGSR which is not directly affected by the catalytic and inhibiting inorganic species and shifts forward at lower temperatures. In this regard, it has been found that AAEM species had an insignificant catalytic effect on WGSR equilibrium (Yip *et al.*, 2010). H₂ is present in WGR (Eq. 6.2) and WGSR (Eq. 6.3) while CO₂ is present in Boudouard reaction (Eq. 6.4) and WGSR. Considering that WGSR is not directly influenced by the inorganic contents, H₂/CO₂ can be used as a benchmark to contemplate the competition of WGR/Boudouard. Higher H₂/CO₂ of syngas from Cell-SS-P, compared to that from other biochar, possibly indicates that Si hampering effect is stronger in the case of carbon steam reaction (WGR). This can be supported by the high CO/CO₂ in the case of Cell-SS-P, suggesting that CO₂ is exclusively consumed via Boudouard reaction to produce CO.

Moreover, the sharp difference in CO and CO₂ contents between Cell-SS-P biochar samples and other samples appears to not be a result of WGR and WGSR. As illustrated in Table 6.5, the higher CO/CO₂ ratio observed for rich silica char, namely Cell-SS-P char, suggests the dominance of Boudouard reaction. Lu *et al.* (2022) studied the gasification of Si rich coal biochar under two different atmospheres, steam (Lu *et al.*, 2022) and CO₂ (Lu *et al.*, 2021). It was reported that Si inhibitory effect was strongly severe in the steam atmosphere. The biochar showed a mesh structure and some small particles dispersed in the net, which was not observed in CO₂ atmosphere. In another study, P. Lv *et al.* (2018) reported that the reactivity of the gasified char after removal of AAEM had a higher reactivity in the CO₂ atmosphere than that gasified in the H₂O atmosphere. This was primarily attributed to the fact that the gasified char obtained in the CO₂ atmosphere has the lowest extent of aromatic condensation. Therefore, it is of paramount importance to carry out further characterization and analysis to promote these findings and establish the mechanism of Si inhibition effect.

6.4 Conclusion and perspectives

6.4.1 Conclusion

In this chapter, pyrogasification LEEBIO pulp, softwood sawdust (SS), and kraft cellulose (ARC) were studied in a fixed bed reactor under different experimental conditions.

Pyrolysis characteristics of extracted and kraft cellulose were mainly controlled by the chemical structure.

- Lignin in extracted pulp led to the production of a larger biochar fraction, hence lower gas yield. The higher gas yield was obtained from kraft cellulose pyrolysis.
- GC-MS analysis of bio-oil showed that acids, ketones, and benzenes are the major compounds. Benzenes are mainly formed by the conversion of phenols and xylenes.

Steam gasification of biochar obtained from cellulose pulp (LEEBIO cellulose or Cell-SS-P), softwood sawdust (SS), and kraft cellulose (ARC) was evaluated. The effect of the steam-to-carbon ratio, temperature, and inherent inorganic composition was studied. Syngas components ratios were used to assess the gas production quality and to assess the competition of the gasification reactions

- Increasing steam to carbon ratio boosted carbon conversion leading to enhancement in gas yield. Adding steam can improve hydrogen yield and concentration through water gas and water gas shift reactions, thus improving H_2/CO . The decrease of CO/CO_2 with increasing steam-to-carbon ratio, showed that the water-gas shift reaction is predominant over the Boudouard reaction. However, the excessive addition of steam is harmful to the gasification process. A steam-to-carbon ratio of 2.3 was found to be optimal for Cell-SS-P gasification.
- Higher temperature was beneficial for hydrogen production. Increasing temperature from 750 to 950 °C by strengthening endothermic water gas reaction. However, the hydrogen concentration in syngas and H_2/CO decreased at higher temperatures due to the reverse water gas shift reaction. The predominance of the Boudouard reaction at higher temperatures was expressed by the increase of CO/CO_2 .
- Compared with biomass and kraft cellulose chars, carbon conversion and hydrogen yield of LEEBIO cellulose pulp biochar were lower at 750 and 850 °C due to high content of Si. In contrast to alkali and alkaline earth metals, Si had a severe inhibitory effect on carbon-steam reactions.

6.4.2 Hydrogen rich-gas production potential

To evaluate the gasification performance of **Cell-SS-P** apart from the effect of Si, Table 6.7 gives an overview on steam gasification performance of different feedstocks at 950 °C. The present results provide a piece of evidence for the potential **Cell-SS-P** obtained following **LEEBIO** technology for hydrogen production. Indeed, dry gas and H₂ yields from cellulose pulp and the raw biomass are quite similar. This result ties well with previous studies (Jia *et al.*, 2017; Yan *et al.*, 2010b). However, the maximum potential hydrogen yield obtained in this study corresponds to 32 % of the theoretical yield of integral gasification of biomass, which is equivalent to 166 g kg_{feedstock}⁻¹, as shown in Table 6.6. This deficiency is attributed to the use of a multistage gasification scheme, where hydrogen is only produced from biochar steam gasification. Nevertheless, char gasification allows the production of cleaner syngas with lower tar content than that from a single-stage process, hence reducing cleaning costs and avoiding downstream problems.

Table 6.6: Theoretical yield of hydrogen from biomass steam gasification (full conversion of CO)

Gasification reaction	CH _{1.5} O _{0.7}	+	H ₂ O	→	CO	+	H ₂	g _{H₂} kg _{biomass} ⁻¹
(g mol ⁻¹)	24.7		5.4		28		2.1	85
WGSR	CO	+	H ₂ O	⇌	CO ₂	+	H ₂	g _{H₂}
(g mol ⁻¹)	28		18		44		2	81
Total g _{H₂} kg _{biomass} ⁻¹								166

Syngas can be subject to a wide range of applications including heat or power applications such as Integrated Gasification Combined Cycle (IGCC) to a variety of synthetic fuels and chemicals. The gaseous components ratios of syngas are the benchmark to determine its end-point applications. With a H₂/CO of 1.8, gas produced from **LEEBIO** pulp biochar(**Cell-SS-P**) at 950 °C would be suitable for Fischer-Tropsch applications (Butterman *et al.*, 2009), without further conditioning. As H₂/CO₂ is close to the required ratio value of 3–4 for methanation, the product gas can be used for methane production to substitute natural gas. High-efficiency combustion systems such as fuel cells, preceded by conditioning and purification steps, are also useful applications. The presence of CH₄ in the syngas can be critical depending on the targeted application. On the one hand, the low level of CH₄ (< 0.75 vol. %) is favorable for industrial applications because of the high energy demand for its removal and its risk in downstream applications. For instance, methane can cause carbon deposition and deactivation of catalysts (Phan *et al.*, 2018; Rego de Vasconcelos *et al.*, 2020). On the other hand, the presence of

Table 6.7: Comparison of steam gasification performance and hydrogen production from different biochar samples ($T = 950\text{ }^{\circ}\text{C}$, steam flowrate = 45 g h^{-1})

	Cell-SS-P	SS	ARC
H ₂ yield ($\text{g kg}_{\text{feedstock daf}}^{-1}$)	40	43.1	35.3
Potential H ₂ yield ($\text{g kg}_{\text{feedstock daf}}^{-1}$)	52.9	51.9	41
Dry gas yield ($\text{Nm}^3 \text{kg}_{\text{feedstock daf}}^{-1}$)	0.76	0.82	0.68
Potential dry gas yield ($\text{Nm}^3 \text{kg}_{\text{feedstock daf}}^{-1}$)	1	0.96	0.78
H ₂ +CO (vol. %)	88.1	85.0	86.7
H ₂ /CO	1.8	2.0	2.0
H ₂ /CO ₂	5.0	4.0	4.5
(H ₂ + CH ₄)/CO	1.8	2.1	2.4
LHV (MJ Nm^{-3})	10.4	10.2	10
CGE (%)	70.7	776	89.7

methane could enhance the energy content of the gas ($\text{H}_2 + \text{CH}_4$) to cover the high energy demand of an integrated LEEBIO-based biorefinery.

Gas cleaning is also a crucial step for the value chain of H₂-rich-syngas. Common impurities include fine particles, nitrogen-based compounds, sulfur-containing, and trace metals. The level of gas purity requirements and the tolerance to pollutants vary depending on the end-use technology. Figure 6.7 illustrates the distribution and variation of alkali metals to Si in the initial and recovered chars. The difference in nitrogen content between Cell-SS-P biochar and that of raw biomass (SS) reveals the profitability of LEEBIO technology. Indeed, cellulose pulp biochar is nitrogen-free which is beneficial for syngas. Literature on nitrogen content in feedstock has indicated that it appears in the syngas mainly in the form of NH₃, N₂ and some of HCN (Froment *et al.*, 2013; C. (Xu *et al.*, 2010). Besides being a precursor of NO_x emissions, ammonia is known as a catalyst poison. Despite their benefits on char conversion, AAEM present in ash are known to cause various operational problems such as fouling and slagging. This is due to the partial melting of ash particles to form a variety of deposit gaseous and liquid compounds. Empirical indices have been developed to predict ash behavior and deposition tendencies. AAEM elements, Fe in addition to Si are involved in the calculation of these indices. To evaluate char gasification Table 6.8 presents fouling and slag viscosity of biochar from LEEBIO cellulose pulp and raw SS. It can be observed that ash in SS falls within the range of medium fouling and high slagging ranges, due

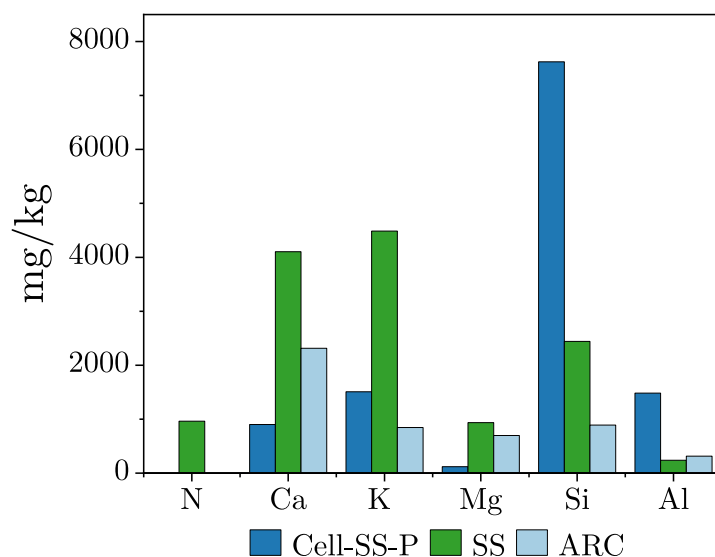


Figure 6.7: Contents of major inorganic elements in recovered biochar from steam gasification (recovered char: $T = 950\text{ }^{\circ}\text{C}$, $\dot{m}_{steam} = 15\text{ g h}^{-1}$)

to the high amount of **AAEM**. It can be noticed that the tendencies to slagging/fouling and agglomeration are significantly lower for ash in **LEEBIO**, as a result of formic acid pulping.

Table 6.8 also compares the results of alkali species to Si ratio in the input and recovered biochar during steam gasification. **AAEM** in particular K-compounds can cause hot erosion fouling and create deposits in downstream processes (Larsson *et al.*, 2021; Q. Liu *et al.*, 2017; Nutalapati *et al.*, 2007). It was reported that alkali release increased in the final stage of gasification (Ge *et al.*, 2022). It can be seen, the ratios of **AAEM** to Si remained constant during steam gasification of **Cell-SS-P** whereas a declining trend was observed for **SS** char, **AAEM** to Si ratio decreased by 74 %. This result indicates that despite its inhibiting effect, high silica content can retain metal species in the ash, thus preventing their loading in the syngas. The role of silica in capturing **AAEM** compounds has been highlighted in the literature. For example, Porbatzki *et al.* (2011) found that alkali retention was enforced for samples with low $(K+Na)/Si$ ratio. Andrea Jordan *et al.* (2012) reported that 30 % of the potassium was captured by aluminosilicates and was retained in the ash while more than 50 % of the alkali earth metals were released to the syngas. Knudsen *et al.* (2004) reported that biomass fuels with an appreciable content of silicate showed a lower release of potassium. Overall, compared to biomass fuel, moderate quantities of pollutants would be found in producer gas from **LEEBIO** cellulose biochar gasification with a low potential of problematic operation problems. Reduced clean-up and conditioning of producer gas would be required to fit the threshold of end-use processes.

Table 6.8: AAEM to Si ratio, slagging and fouling calculated according to char ash composition (AAEM species and Si are considered in the form of oxides)

	Cell-SS-P	SS
Fouling index, F_u (Garcia-Maraver <i>et al.</i> , 2017) $= \frac{B}{A} \times (\text{Na}_2\text{O} + \text{K}_2\text{O});$ < 0.6 low; 0.6–40 medium; > 40 high	0.0	2.5
Slag viscosity index, Sr (Rizvi <i>et al.</i> , 2015) $= \frac{\text{SiO}_2}{\text{SiO}_2 + \text{CaO} + \text{MgO} + \text{Fe}_2\text{O}_3}; \times 100$ > 72 low; 65–72 medium; < 65 high	83.7	8.3
K/Si <i>pyrolysis char</i>	0.2	4.4
K/Si <i>recovered char</i> *	0.2	1.8
Ca/Si <i>pyrolysis char</i>		
Ca/Si <i>recovered char</i> *	0.12	1.7
Mg/Si <i>pyrolysis char</i>	0.02	1.6
Mg/Si <i>recovered char</i> *	0.02	0.4

$$\frac{B}{A} = \frac{\text{FeO}_3 + \text{CaO} + \text{MgO}}{\text{SiO}_2 + \text{Al}_2\text{O}_3}; \text{ *}: 950 \text{ }^\circ\text{C}; \dot{m}_{\text{steam}} = 15 \text{ g h}^{-1}$$

Table 6.9: The influence of steam flow rate on gasification of SS biochar at 950 °C

Steam flow rate (g h ⁻¹); 1 hour	15	30	45	60
S/C	0.8	1.6	2.4	3.2
Product distribution (wt.%)				
Gas	63.0	76.2	73.0	69.6
Biochar	34.9	12.3	4.2	1.3
Condensates	0.0	15.2	23.4	29.9
Material balance	97.9	103.7	100.6	100.8
biochar conversion (%)	39.9	70.6	83.1	95.7
Steam conversion (%)	100.0	75.3	66.9	60.7
Gas production and hydrogen yield				
H ₂ (vol. %)	53.2	55.3	57.0	57.8
CO (vol. %)	37.6	32.50	28.8	25.8
H ₂ /CO	1.4	1.7	2.0	2.2
H ₂ /CO ₂	6.3	4.8	4.0	3.7
H ₂ /CH ₄	87.7	82.5	76.8	76.8
(H ₂ + CH ₄)/CO	1.4	1.7	2.1	2.3
CO/CO ₂	4.4	2.8	2.0	1.6
Dry gas yield (Nm ³ kg _{feedstock} ⁻¹)	0.4	0.7	0.8	1.0
H ₂ (g kg _{char} ⁻¹)	105.1	170.4	201.3	242.2
LHV (MJ Nm ⁻³)	10.8	10.4	10.0	9.8
CGE (%)	38.2	66.6	77.6	89.6

Table 6.10: The influence of steam flow rate on gasification of ARC biochar at 950 °C

Steam flow rate (g h ⁻¹); 1 hour	15	30	45	60
S/C	1.0	2.0	3.0	4.0
Product distribution (wt.%)				
Gas	70.5	74.1	65.6	59.3
Biochar	23.7	10.0	2.9	0.7
Condensates	6.9	20.9	33.7	41.0
Material balance	101.2	105.0	102.2	101.0
biochar conversion (%)	51.6	72.1	86.2	94.2
Steam conversion (%)	86.7	69.3	55.8	49.3
Gas production and hydrogen yield				
H ₂ (vol. %)	51.0	54.7	57.50	57.5
CO (vol. %)	36.2	32.4	29.2	27.2
H ₂ /CO	1.4	1.7	2.0	2.1
H ₂ /CO ₂	4.4	4.4	4.5	3.9
H ₂ /CH ₄	63.9	91.2	95.8	95.8
(H ₂ + CH ₄)/CO	1.4	1.7	2.0	2.1
CO/CO ₂	4.4	2.6	2.3	1.8
Dry gas yield (Nm ³ kg _{feedstock} ⁻¹)	0.4	0.6	0.7	0.8
H ₂ (g kg _{char} ⁻¹)	121.8	194.2	225.0	265.6
LHV (MJ Nm ⁻³)	10.6	10.3	10.2	9.9
CGE (%)	37.0	42.2	41.0	44.2

Table 6.11: Composition analysis of bio-oil obtained from pyrolysis of cellulose pulp

Group	Compound	MW	Formula	Cell-SS-P	ARC
				Area (%)	Area (%)
Saccharides	1,4:3,6-Dianhydro-.alpha.-d-glucofuranose	144	C ₆ H ₈ O ₄	-	0.92
	D-Allose	180	C ₆ H ₁₂ O ₆	-	1.71
	total			0	2.63
Esters	Propanoic acid, 2-hydroxy-, ethyl ester, (S)-	118	C ₅ H ₁₀ O ₃	16	22.83
	Propanoic acid, 2-oxo-, methyl ester	102	C ₄ H ₆ O ₃	-	2.69
	Methoxyacetic acid, 2-butyl ester	146	C ₇ H ₁₄ O ₃	-	0.91
	(S)-Isopropyl lactate	132	C ₆ H ₁₂ O ₃	4.26	5.47
	Isobutyl isopropyl carbonate	160	C ₈ H ₁₆ O ₃	0.69	-
total			20.95	31.90	
Ketones	2-Propanone, 1-hydroxy- (hydroxyacetone)	74	C ₃ H ₆ O ₂	9.46	14.08
	3-Penten-2-one, (E)-	84	C ₅ H ₈ O	1.84	1.29
	2-Propanone, 1-(acetyloxy)-	116	C ₅ H ₈ O ₃	0.81	1.37
	2-Cyclopenten-1-one, 2-methyl-	96	C ₆ H ₈ O	0.81	0.76
	1-Hydroxy-2-butanone	88	C ₄ H ₈ O ₂	-	0.91
	2-Cyclopenten-1-one	82	C ₅ H ₆ O	1.46	-
	1,2-Cyclopentanedione	98	C ₅ H ₆ O ₂	-	0.83
	2-Cyclopenten-1-one, 2-hydroxy-3-methyl-	112	C ₆ H ₈ O ₂	0.87	0.83
total			15.25	20.07	
Furans	Furan, 2,5-dimethyl-	96	C ₆ H ₈ O	4.11	-
	Furan, 2-ethyl-5-methyl-	110	C ₇ H ₁₀ O	-	1.5
	2-Furancarboxaldehyde, 5-methyl-	110	C ₆ H ₆ O ₂	1.58	1.41
	Furfural	96	C ₅ H ₄ O ₂	4.42	13.44
total			10.11	16.35	
Alcohols	Ethanol, 2-(1-methylethoxy)-	104	C ₅ H ₁₂ O ₂	2.57	3.12
Phenols	Phenol	94	C ₆ H ₆ O	1.63	0.98
	Phenol, 2-methyl- (o-cresol)	108	C ₇ H ₈ O	1	0.55
	Phenol, 3-methyl- (m-cresol)	108	C ₇ H ₈ O	1.73	0.98
	Phenol, 2-methoxy-	124	C ₇ H ₈ O ₂	0.76	-
	Phenol, 2,4-dimethyl-	122	C ₈ H ₁₀ O	0.82	-
	Creosol	138	C ₈ H ₁₀ O ₂	0.82	-
	Catechol	110	C ₆ H ₆ O ₂	1.24	-
total			8	2.51	
benzenes	Toluene	92	C ₇ H ₈	9.71	3.47
	o-Xylene	106	C ₈ H ₁₀	2.15	1.96
	Styrene	104	C ₈ H ₈	1.81	0.6
	Benzene	78	C ₆ H ₆	16.98	8.19
total			30.65	14.22	
Aldehydes	Pentanal	86	C ₅ H ₁₀ O	-	0.73
others	1,5-Heptadien-3-yne	92	C ₇ H ₈	5.55	-
	2,4-Hexanediene, 2,5-dimethyl-	110	C ₈ H ₁₄	1.17	0.84
total			6.72	0.84	

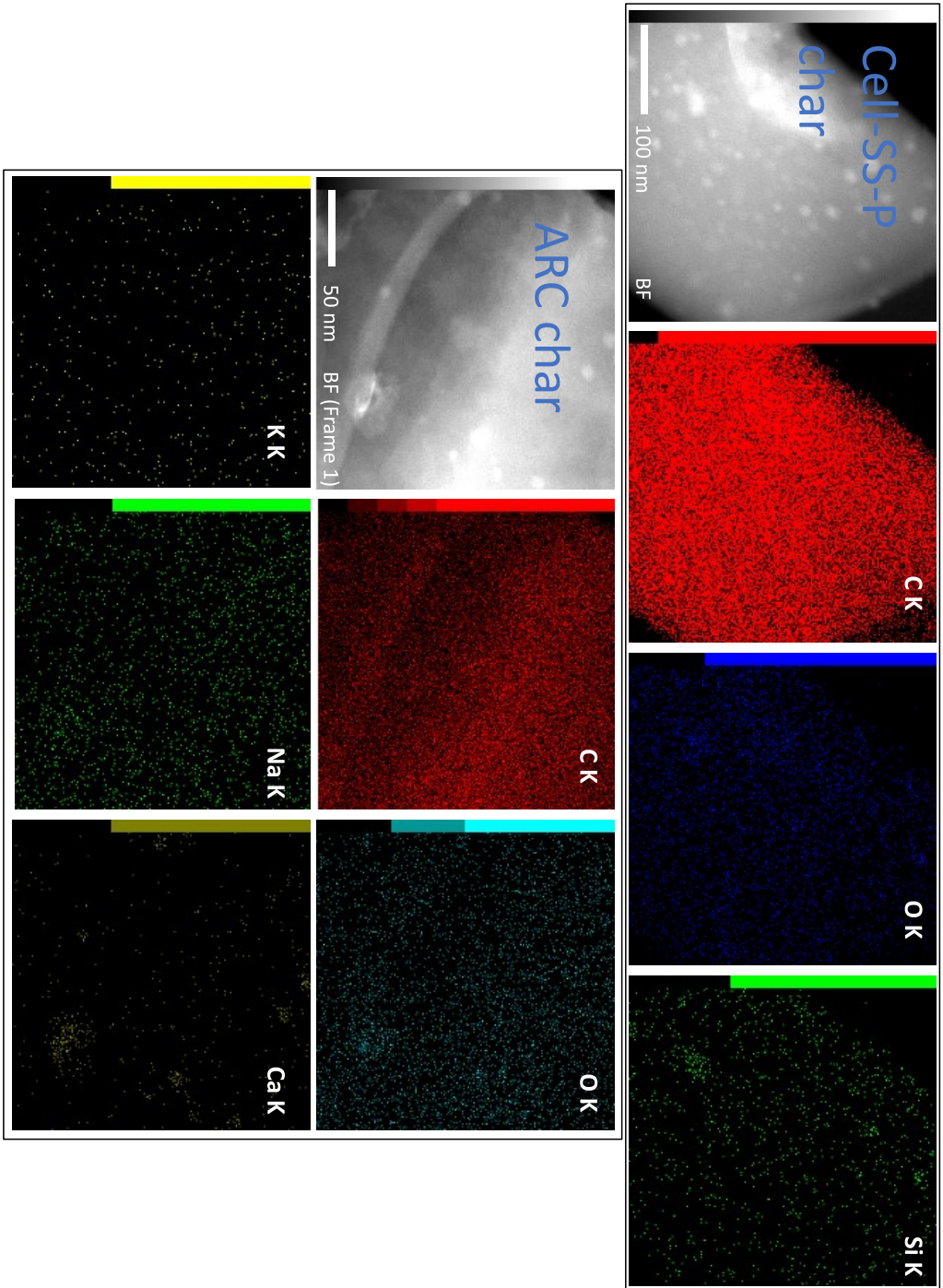


Figure 6.8: TEM mapping image with energy-dispersive X-ray (EDX) mapping for Cell-SS-P and ARC biochars

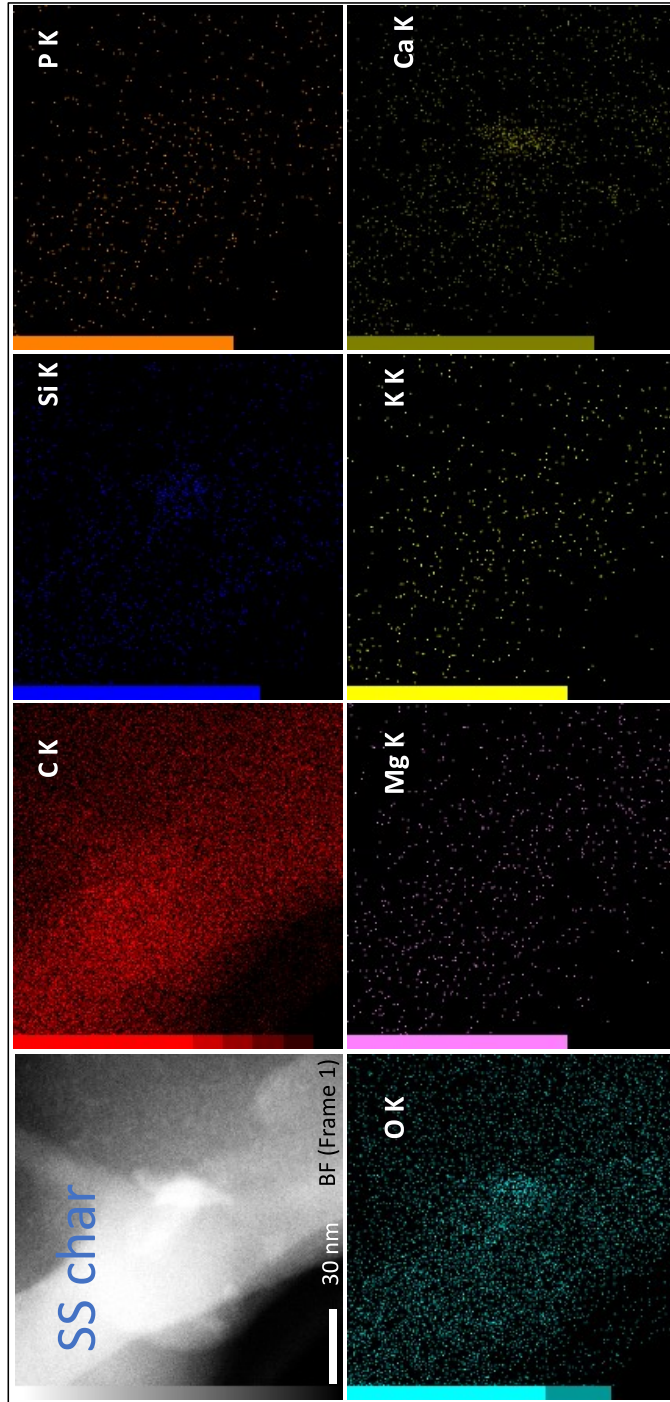


Figure 6.9: TEM mapping image with energy-dispersive X-ray (EDX) mapping for SS biochar

Hydrogen production from steam gasification in a biorefinery approach: process assessment and heat integration

7

7.1	Introduction	151
7.2	Aspen Plus model development	152
7.2.1	Conceptual design	152
7.2.2	Methodology	153
	Assumptions	153
	Definition of physical property method and operations units	153
7.2.3	Aspen Flowsheet and model description	153
	Biomass drying	154
	Biomass pretreatment	154
	Solid washing	154
	Drying	156
	Pyrolysis	156
	Volatiles combustion	156
	Char gasification	156
	Water-gas shift	158
	Pressure Swing adsorption (PSA)	159
7.2.4	Pinch analysis	159
7.3	Results and discussions	160
7.3.1	Char gasification: model validation and sensitivity analysis	160
7.3.2	Global material balance	162
7.3.3	Analysis of energy balance	164
7.4	Pinch analysis and heat integration	164
7.5	Conclusion	168

7.1 Introduction

This chapter is devoted to the evaluation of hydrogen production from pulp pyrogasification in an integrated biorefinery approach. The heat integration technique of the

process is performed using the pinch analysis technique. Aspen Plus V12 software is employed to this end.

Aspen Plus is the market-leading simulation tool that is used for process monitoring, conceptual design, and optimization. This multipurpose software uses steady-state models to predict process performance. It consists of three main components: (i) material and energy balance equations, (ii) physical and thermodynamic properties and mixture, (iii) models describing the unit operations. The simulation flowsheet is based on blocks of unit operations. Over the years, valuable biomass gasification models have been developed on Aspen Plus to assess the influence of operating conditions and process integration (Abdelouahed *et al.*, 2012; Gu *et al.*, 2019; Kaushal *et al.*, 2017; Nikoo *et al.*, 2008; Pala *et al.*, 2017). Biomass gasification models are divided into two types: kinetic model and an equilibrium model or a combination of both (Ahmad *et al.*, 2016).

7.2 Aspen Plus model development

7.2.1 Conceptual design

The global process involves five linked parts as shown in Figure 7.1 :

1. *LEEBIO pretreatment* Firstly, biomass is dried to reduce moisture content. Dried biomass is then treated with formic acid (FA). From this pretreatment step two streams are obtained: a liquid stream with lignin and hemicellulose dissolved in the solvent, and a solid stream with cellulose which is washed and dried.
2. *Pyrogasification* Extracted cellulose undergoes the devolatilization step to produce volatiles (gas and bio-oil) and biochar. These two products are separated. At this point, biochar is gasified with steam as a gasifying agent to produce hydrogen-rich syngas.
3. *Water-gas-shift reaction* The product syngas is upgraded in a shift reactor for additional hydrogen generation and to convert CO to CO₂.
4. *H₂ purification* A pressure swing adsorption (PSA) system to recover and purify the hydrogen present in the upgraded syngas.
5. *Combustion of volatiles from pyrolysis* This is done in a separated reactor to satisfy the heat demand of the pyrolysis and gasification reactors as well as pretreatment units.

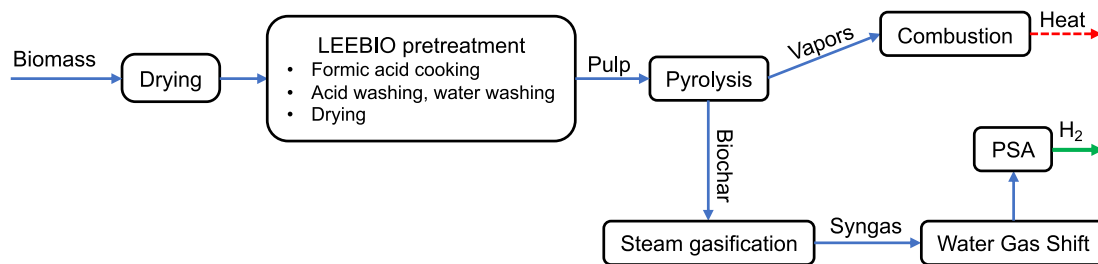


Figure 7.1: Simplified scheme of the model

7.2.2 Methodology

Assumptions

Process simulation was simplified, and the following assumptions were made:

- All units are operated at steady-state, isothermal, and isobaric conditions. Pyrolysis and gasification units are operated at 1 bar
- Drying and devolatilization occur instantly
- Ash are inert; catalytic and inhibiting effects are neglected
- Ideal gas considered
- Heat loss and pressure drops are neglected, temperature and pressure distribution within the units are uniform

Definition of physical property method and operations units

Biomass and its components as well as char and ash are defined as non-conventional solids in this process. Aspen Plus assumes that these components are heterogeneous solids and do not participate in phase equilibrium calculations. HCOALGEN and DGOALIGT library was used to determine the enthalpy and density based on their properties shown in Table 7.1. The MIXCINC stream class was used since both conventional and non-conventional solids are present, but there is no particle size distribution.

7.2.3 Aspen Flowsheet and model description

Figure 7.2 shows the Aspen Plus flowsheet process. Forty-five streams were used in the flowsheet. RAW-BIO, DRY-AIR, SOLVENT, WATER-1, WATER-2, AIR-COMB and WATER-3 were user-defined streams. The flowsheet comprises twenty-nine unit operation blocks, described in Table 7.2. The flow rate of inlet streams in biomass pretreatment steps is determined by a Calculator based on the experimental results presented in Chapter 3 and 6. To validate the present model, the experimental results of biochar gasification, a Design-Spec is carried out to ensure production of 90 g h^{-1} of Cell-Pulp in the PULP stream.

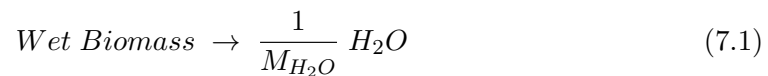
Table 7.1: Ultimate and proximate analysis at dry basis of different components

	Proximate analysis				Ultimate analysis			
	M	VM	FC*	A	C	H	N	O*
Raw biomass	39.2	85.5	18.2	0.3	47.8	6.2	0.1	45.9
Cell–Pulp	-	82.3	17.5	0.2	48.4	6.1	0	45.3
Char	-	6.1	91.6	2.3	90.2	1.2	0.0	6.3

* by difference

Biomass drying

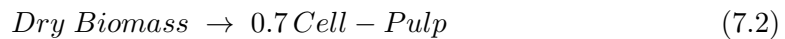
The raw biomass, represented by the stream RAW–BIO, with a moisture content around 39 % is dried with forced air at 70 °C. In this model, drying is carried out in a block DRYER in which moisture is evaporated and controlled by a Calculator to reduce the moisture content to 2 % in the dried biomass. The evaporated moisture is separated from the solid by FLASH1. Aspen plus considers that the molecular weight of a non-conventional solid is 1 g mol⁻¹. Therefore, the drying reaction of biomass is represented by the following equation:



The extent of the reaction in the RStoic is defined by: $\frac{H_2O_{in} - H_2O_{out}}{1 - H_2O_{out}}$

Biomass pretreatment

In the first step, the outlet stream DRY–BIO of FLASH1 moves into PULPING reactor. The stream SOLVPULP, consisting of a formic acid–water mixture (85 wt. % FA), is added to the organosolv reactor at 5:1 w/w as a solvent-to-wood ratio. The reactor was pressurized to 1.5 bar at 85 °C. During this process, the biomass is fractionated following Eq. 7.2. Separated lignin and hemicellulose are not represented in the obtained solid since they are dissolved.



Solid washing

Following that, the solid is cooled down and filtered by FILTER1 to separate dissolved lignin and hemicellulose. Next, the filtered solid is sent to an acid-washing stage to remove precipitated lignin. This step is represented by MIX1, in which 85 wt. % FA is mixed with the filtered solid at the liquid: solid ratio of 3.4. The mixture is then

Table 7.2: List of unit operations used in the flowsheet

Aspen ID	Model ID	Description and function
RStoic		Conversion reactor with known stoichiometry
	DRYER	Reduce of moisture content of wet biomass
	PULPING	Biomass fractionation into its main components
	REA-PYRO	Elemental decomposition of fuel and product distribution
	HTS	Simulates the water gas shift reaction at high temperature
	LTS	Simulates the water gas shift reaction at low temperature
RYield		Reactor with specifying reaction yields of each component
	DECOMP-C	Decompose the char into conventional components
RPlug		Plug flow reactor handles rate-based kinetic reactions only
	REA-GASI	Char steam gasification
RGibbs		Reactor with phase chemical equilibrium and composition
	COMBUST	Combustion of volatile from pyrolysis
Flash2	FLASH1,2	Vapor separations from liquid and solid streams
	FLASH3	Separation of pyrolysis vapors from biochar
Heater		Used to model: Heaters or coolers
	HEATER1	Pulp heating stream at 70 °C to evaporate water
	HEATER2,3	Water heating to generate steam at 180 °C
	COOLER1	Cooling down pulp and solvent mixture, cold T= 50°C
	COOLER2,3	Remove specified heat duty from gas streams
	COOLER4,5	Lowes the temperature of gas outlet from HTS and LTS
Flash2	FLASH1,2,3	Separating vapor from liquid and solid streams
Sep		Separates stream into 2 or more outlet streams
	CYCLONE	Separates solid and ash from the syngas
	TRAP1,2	Separates steam from syngas by condensation
	PSA1,2	Simulates pressure swing adsorption modules
Filter	FILTER1-3	Separation of liquids from solids
Mixer	MIX1-3	Combines streams into one outlet stream
FSplit	SPLIT1-3	Divides stream into 2 or more outlet streams
MCompr		Multistage polytropic compressor with an intercooler between each compression stage (Isentropic Eff.: 0.72)
	COMP1	Raises syngas pressure to 5 bar upstream of WGS
	COMP2,3	Raises syngas pressure to 30 bar upstream of PSA
Pump		Simulate a pump and calculate the outlet pressure
	PUMP1	Raises steam pressure to 5 bar upstream of WGS
Valve	VALVE1,2,3	Rigorous modeling of the pressure drop in control valves

filtered in FILTER1. Acid washing is followed by water washing (MIX2) and filtration (FILTER2) to clean the solid and remove FA. The required water rate is determined using a Calculator with a water: dried biomass ratio of 12.

Drying

Next, washed solid is dried to obtain a final moisture of 2.2 %. The step is carried out in HEATER1 to evaporate water and FLASH2 to separate water vapor from the solid.

Pyrolysis

The pyrolysis step is simulated using REA-PYRO reactor. Ext-Cell is converted to gases, bio-oil, and biochar. The product distribution information is derived from experimental data derived from Chapter 6. The following assumptions are made on volatile products:

- Gaseous products includes H₂, CO, CO₂, CH₄, and C₂H₄
- Bio-oil consists on water and tars which includes C₆H₆, C₇H₈, C₆H₆O and C₈H₁₀O₂

The reactor is operated at 700 °C and at atmospheric pressure; the yield distribution is determined through:

$$Cell\ Pulp \rightarrow \frac{1}{M_i} Component_i \quad (7.3)$$

where the M_i is the molecular weight of a single product; the conversion of each reaction is the yield of $Component_i$. From the REA-PYRO the product stream, PROD-PYR, enters FLASH3 for separating char in the stream SOLID and volatile products in the stream VAPORS.

Volatiles combustion

Volatiles obtained from pyrolysis are burned to provide heat for the endothermic steps. As mentioned in Chapter 1, this approach is used in the multi-stage gasification process, WoodRoll. The stream VAPORS and AIR-COMB are fed to the COMBUST reactor (Aspen ID: RGibbs). The heat of combustion fumes is recovered to achieve energy integration of the global process (COOLER3).

Char gasification

From FLASH3 the stream CHAR, is first fed into DECOMP-C to decompose char into conventional components (C_s, H₂ and O₂) and ash. The yield of the reactor is calculated according to the elemental composition of char given in Table 7.1.

The outlet stream CHAR is then mixed with steam provided by the superheated stream WATER-2. The total input enters the gasifier REA-GASI (Aspen ID: RPlug). In this study, the reactions included in the char gasification process are listed in Table 7.3

Table 7.3: Reactions implemented in the Aspen Plus model (Eikeland *et al.*, 2015; Solli *et al.*, 2018)

Reactions	Reaction rate (kmol m ⁻³ s), Ea (kJ mol ⁻¹)
C + H ₂ O ⇌ CO + H ₂	$r_{for} = 15.264 \times T \times \exp\left(\frac{-188.27}{RT}\right) [\text{H}_2\text{O}][\text{C}_{(s)}]$
	$r_{inv} = 3.88 \times 10^{-11} \times T^2 \times \exp\left(\frac{-52.54}{RT}\right) [\text{CO}][\text{H}_2][\text{C}_{(s)}]$
C + CO ₂ ⇌ 2 CO	$r_{for} = 15.264 \times T \times \exp\left(\frac{-188.27}{RT}\right) [\text{CO}_2][\text{C}_{(s)}]$
	$r_{inv} = 1.03 \times 10^{-12} \times T^2 \times \exp\left(\frac{-19.65}{RT}\right) [\text{CO}][\text{C}_{(s)}]$
0.5 C + H ₂ ⇌ 0.5 CH ₄	$r_{for} = 1.37 \times 10^{-5} \times T \times \exp\left(\frac{-97.16}{RT}\right) [\text{H}_2][\text{C}_{(s)}]$
	$r_{inv} = 1.25 \times T^{0.5} \times \exp\left(\frac{-112.89}{RT}\right) [\text{CH}_4]^{0.5}$
CO + H ₂ O ⇌ CO ₂ + H ₂	$r_{for}^* = 6.4 \times 10^8 \times T \times \exp\left(\frac{-304.62}{RT}\right) [\text{CO}]^{0.5} [\text{H}_2\text{O}]$
	$r_{inv} = 6.4 \times 10^6 \times T \times \exp\left(\frac{-326.41}{RT}\right) [\text{H}_2]^{0.5} [\text{CO}_2]$
CH ₄ + H ₂ O ⇌ CO + 3 H ₂	$r_{for} = 3.1 \times 10^3 \times \exp\left(\frac{-124.71}{RT}\right) [\text{CH}_4][\text{H}_2\text{O}]$
	$r_{inv} = 3.56 \times 10^{-6} \times T \times \exp\left(\frac{-124.71}{RT}\right) [\text{H}_2]^2 [\text{CO}]$

*adjusted constant ($K_0 = 7.68 \times 10^7$)

and initiated in REA–GASI block. It should be pointed out that the pre-exponential factor of forward **WGSR** is adjusted. This can be explained by the rapid kinetics of the reaction and the configuration of the lab-scale reactor used in the experimental study. Indeed, the temperature decreases gradually along the reactor which can promote the forward **WGSR**.

The reactor is about 6 cm in diameter and 60 cm in length and operates at different temperatures, 850 and 950 °C. The outlet gas steam of the gasifier enters CYCLONE for separating ash and residual carbon from the gas stream.

Water-gas shift

Afterward, the gas stream is then cooled down to 300 °C and separated from water through TRAP1. Before entering the water-gas shift, pressure the syngas (SYNGAS) to 5 bar. The compression is achieved by a multistage compressor COMP1. The steam input is supplied by pumping water (Water–3) up to 5 bar, then heated to 180 °C. The syngas and steam streams are fed the water-gas shift conditioning section which consists of two reactors, a high-temperature shift (HTS) and a low-temperature shift (LTS) reactor. The **WGSR** is exothermic and hence a lower temperature enhances CO conversion. At the industrial scale, the HTS generally operates at temperatures between

290 and 440 °C, and the LTS often operates between 160 and 210 °C. Syngas leaving the HTS and LTS shift reactors still contain 2 to 5 % and 0.6 to 1 % CO (Linde, 2022).

Both shift reactors are simulated as stoichiometric reactors (Aspen ID: RStoic) and the WGSR. CO conversion and steam injection flow rate (WATER-3) are adjusted indirectly. This adjustment is carried out using a Design-Spec to specify the residual % vol of CO at the leaving stream of each reactor. CO concentration in the outlet steam of HTS and LTS is fixed at 4 and 0.8 vol. %, respectively. The CO conversion from the global water-gas-shift system is thus around 80 %. The syngas and steam mixture is cooled down to 35 °C to separate water (TRAP2).

Pressure Swing adsorption (PSA)

The target of this stage is to obtain a high-quality hydrogen gas that can be used in subsequent applications. Gas cleaning is achieved by separating hydrogen from other gaseous species present in the syngas. The simulation of the PSA system is simplified by employing ideal separators representing two separation units. The system efficiency and conditions are adopted from literature (Gutiérrez Ortiz *et al.*, 2013). The stream CRUDE-H2 obtained from water-gas-shift is compressed at 30 bar and cooled down to 35 °C by a multistage compressor COMP2 to feed the PSA system. Within the first unit (PSA1), high-quality hydrogen (99.99 % purity) is separated with a specified recovery rate of 80 % and exists the PSA bed (PURE-H2) from the bottom stream at the same pressure of the inlet stream. The depressurization and pressurization of the tail gas streams are simulated by VALVE1,2,3 (1 bar) and COMP3,4,5 (30 bar). In the second PSA unit, CO is adsorbed and separated while CO₂ and CH₄ exit from the top stream for their subsequent sequestration.

7.2.4 Pinch analysis

In this study, Pinch analysis is used to examine the energy integration of the process. This methodology provides a rigorous, structured approach for determining energy targets and optimizing energy saving and usage (Kemp, 2007). The approach is based on thermodynamic principles. At the industrial scale, energy saving can be achieved by heat recovery from hot streams and duties which require cooling and hot steam and duties that need heating. A key tool of Pinch analysis is the graphic of composite curves which determines the minimum energy consumption. It illustrates the profiles of process heat availability (hot composite curve) and heat demands (cold composite curve). The energy targets are determined by overlapping the hot and cold composite curves separated by ΔT_{min} . The energy targets include the total recoverable heat, minimum hot utility requirement (Q_h), and minimum cold utility requirement (Q_c). ΔT_{min} refers to the minimum allowable temperature difference. This parameter is selected based on the shape of the composite curves and other factors related to the

process. $\Delta T_{min} = 50$ °C is considered for the analysis, according to National Renewable Energy Laboratory (NREL) for the design biomass gasification plant (P. Spath *et al.*, 2005).

7.3 Results and discussions

7.3.1 Char gasification: model validation and sensitivity analysis

To validate the simulation results, experimental data obtained in Chapter 6 were used. Figure 7.3 shows the comparison of the product gas composition and hydrogen yield between the present model and experimental data at two different gasification temperatures, 850 and 950 °C.

To evaluate the robustness of the model, the root-mean-square error (RMSE) was used to quantify the deviation from experimental results as follows:

$$RMSE = \sqrt{\frac{\sum_i^N (y_{exp,i} - y_{calc,i})^2}{N}} \quad (7.4)$$

where y and N are the mole fraction of syngas species and the count of data point sets, respectively.

It can be observed that the model predicted higher CO₂ concentration at 850 °C. In this set of experiments, CO and CO₂ showed higher errors, 12.3 and 10.7%, respectively. Besides, the simulation results were far from the experimental results for H₂ yield, with an error of 14.3 %. Since the errors related to kinetic constants were minimized (Section 7.2.3) the reason for this deviation could be that the inhibiting effect of Si on char gasification, discussed in Chapter 6, were not taken into consideration in the model.

The qualitative comparison (gas composition) of the simulation results of hydrogen molar ratio concerning the experimental data at a gasification temperature of 950 °C indicates that the predicted results are in good agreement with experimental data. It can also be noted, that the developed model results followed the trends shown by experimental results of char gasification. The obtained RMSE for H₂, CO, CO₂ and CH₄ were 1.5, 5.0, 4.0, and 0.4 %, respectively. Moreover, the results of the comparisons show good conformity for hydrogen yield.

Using the validated model, the gasification temperature was maintained at 950 °C. The steam input was specified by fixing a carbon conversion of 95 %. For hydrogen production, the gasification process was thus coupled to the subsequent steps of water-gas-shift and pressure swing adsorption steps.

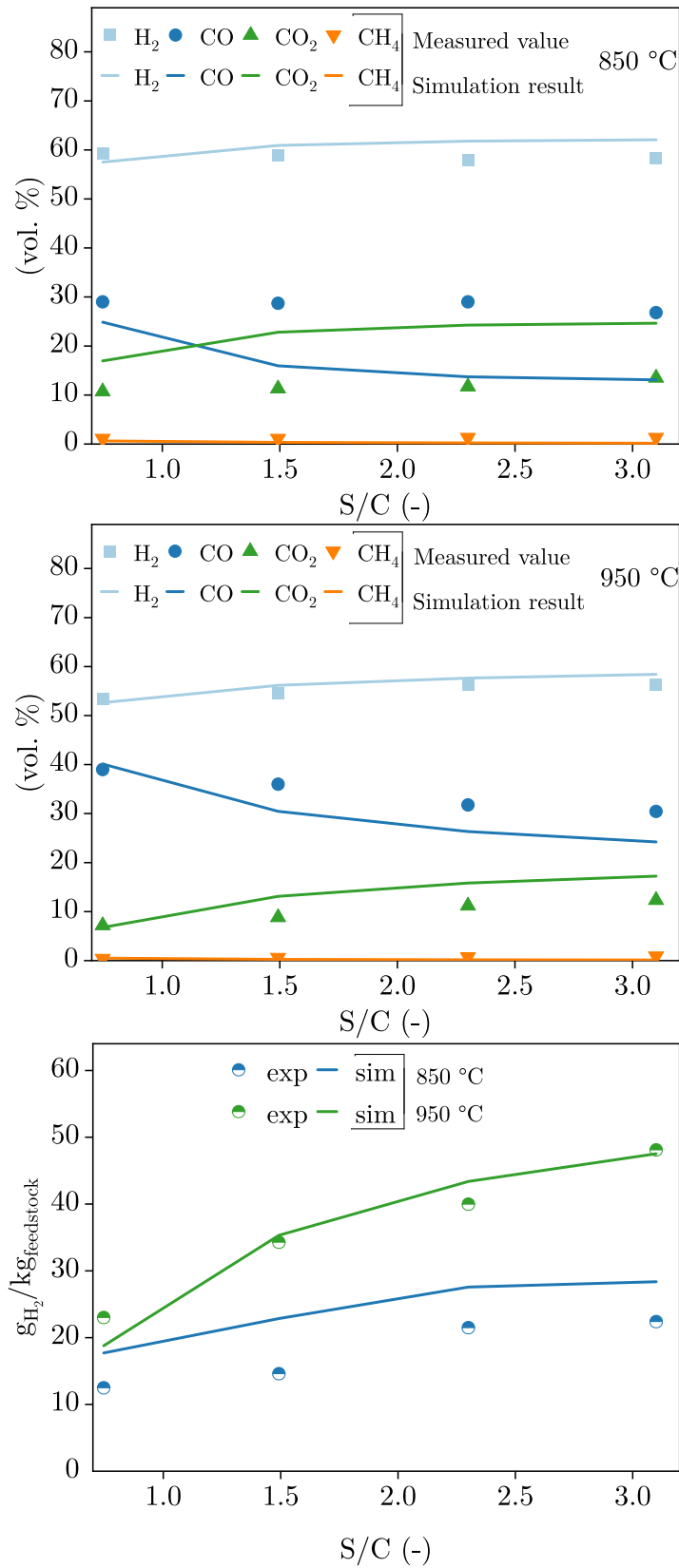


Figure 7.3: Effect of S/C ratio on gas composition and hydrogen yield at different temperatures: comparison between simulation and experimental data

7.3.2 Global material balance

The overall balance is a key element to evaluate the process in terms of economic potential. Table 7.4 illustrates raw materials and chemicals requirements for the global process of hydrogen production. The values of input and output flow rates were normalized to a hydrogen production basis of 1 kg h^{-1} (PURE-H₂). The operation conditions of hydrogen production, conditioning, and separation are summarized in Table 7.5. As mentioned before, gasification conditions were obtained from the experimental results while the operation conditions of HTS, LTS, and PSA units were based on the values applied at the industrial scale. The operation conditions and molar composition of the outlet stream from the char gasifier to the PSA unit are shown in Table 7.6.

Regarding the chemical demands, the production of 1 kg of H₂ in a biorefinery approach required a total formic acid consumption of 209 kg. This high consumption can lower the cost-effectiveness of the process. It should be emphasized that acid consumption can be considerably reduced by recycling formic acid (Hietala *et al.*, 2016). Similarly, water used in pulp washing can be recycled to reduce water requirements. In addition, the steps of lignin and hemicellulose recovery were simulated in the present study. The obtained lignin and hemicelluloses can be used in added-value materials and products, thus improving the efficiency of the process (G.-H. Delmas *et al.*, 2021).

As can be seen, the process allows the production of $1/27 \text{ kg}_{\text{H}_2} \text{ kg}_{\text{dry cellulose pulp}}^{-1}$. As mentioned in Chapter 6, hydrogen yield is relatively lower than the values reported in the literature, since hydrogen is only produced from char gasification. In this study, volatiles from pyrolysis was not considered in the steam gasification process to avoid tar-related problems and no catalyst was used. The pyrolysis volatiles, $18 \text{ kg kg}_{\text{H}_2}^{-1}$ are used as fuel for internal heating of other energy-demanding units. The combustion of volatiles from pyrolysis was carried out with excess air (Composition of combustion fumes in Table 7.11).

Table 7.4: Material balance of the global process

Hydrogen production basis: 1 kg h^{-1}			
Input	kg h^{-1}	Output	kg h^{-1}
Raw wet biomass	42.8	Dry biomass	26.9
Air (drying + combustion)	314.7	Pulp	18.8
Formic acid (85 wt. %)	208.9	Pyrolysis volatiles	14.4
Water (pretreatment)	322.3	Char	4.4
Steam	17.9	Ash	0.1

Table 7.5: Summary of operation conditions for different steps of H₂ production process

Block	T (°C)	P (bar)	Conversion, yield
Pyrolysis	700	1	$Y_{\text{char}} = 0.23$
Gasification	950	1	$X_{\text{C}} = 95.4 \%$
HTS	350	5	$X_{\text{CO}} = 80.1 \%$
LTS	210	5	$X_{\text{CO}} = 79.4 \%$
PSA	35	30	$RR_{\text{H}_2}^a = 80 \%$

^a Recovery rate**Table 7.6:** Molar composition, mass flow rate, temperature and pressure of gas streams at the outlet of different units

Block	T (°C)	P (bar)	Flow rate (kg h ⁻¹)	H ₂ vol. %	CH ₄ vol. %	CO vol. %	CO ₂ vol. %
Gasification	950	1	11.8	58.50	0.13	24.00	17.38
HTS	456	5	14.5	65.19	0.11	4.01	30.70
LTS	242	5	15.0	66.26	0.10	0.80	32.83
PSA, H ₂	35	30	1.0	99.99	0.00	0.00	0.01
PSA, CO ₂ -CH ₄	35	30	13.5	0.00	0.30	0.05	99.65

7.3.3 Analysis of energy balance

The hydrogen production process from cellulose pulp includes different steps, down and upstream pyrogasification. These steps are divided between endothermic requiring energy and exothermic releasing energy. On the one hand, the energy needs are identified as thermal under the form of heat and electricity. On the other hand, the recoverable energy is the available heat in hot streams.

The data of cold streams and units, obtained from simulation results are presented in Table 7.7. The units requiring energy supply include biomass and pulp drying, biomass pulping, steam superheating, pyrolysis, and char gasification in addition to the energy demand for the compressors and pump. As expected, biomass pulping is energy-intensive, having the highest heat requirement among the other energy-demanding units. The high energy consumption is one of the main obstacles preventing the expansion of organosolv treatment from a commercial point of view.

Four hot streams were available, as shown in Table 7.8. They include the recoverable heat from combustion gases and syngas in addition to the outlet streams from the HTS and LTS reactors. The recoverable heat from burning pyrolysis vapors had the major share of available heat. The cooling temperature of combustion gases was set at 200 °C to avoid vapor condensation. Overall, H₂ production at a basis of 1 kg h⁻¹ H₂, required 111.1 kW with 77.9 kW of available recoverable heat.

7.4 Pinch analysis and heat integration

Having identified the process stream heating and cooling information, Pinch analysis was applied to optimize the process. The electricity consumption was not considered. The cold and hot composite curves for the process were constructed at a minimum temperature approach, $\Delta T_{min} = 50$ °C. The results of the analysis are illustrated in Table 7.10. In regards to energy targets, the analysis shows that the hot duty available was mostly recovered, 77.3 from 77.9 kW, indicating the high potential for energy saving. The minimum hot utility requirement (Q_h) was 27.7 kW, while the cold utility requirement (Q_c) was negligible (0.6 kW). The Pinch was at 25 and 75 °C, for the cold and hot stream, respectively. Decreasing the ΔT_{min} towards the threshold value (10 °C) was possible, thus shifting the cold composite curve to the left side which would increase the hot utility requirement (Q_h) and cancel the cold utility requirement (Q_c). Hence, the ΔT_{min} was maintained at 50 °C, as Q_c was negligible.

The energy efficiency of hydrogen production is defined based on the first law of thermodynamics by the apparent thermal efficiency which is applied as follows:

Table 7.7: Energy consumption of different units of the global process (Hydrogen production basis: 1 kg h^{-1})

Thermal energy consumption	T_c ($^{\circ}\text{C}$)	T_h ($^{\circ}\text{C}$)	Q (kW)
Biomass drying	25	70	14.6
Biomass pulping	25	85	32.9
Pulp drying	25	70	14.1
Pyrolysis	70	700	12.2
Biochar gasification	309	950	17.1
Steam superheating	25	180	14.1
Total ①			105.0
Electricity consumption			Q (kW)
Compressors			6.1
Pump			0.002
Total ②			6.1
Total energy consumption ③ = ① + ②			111.1

Table 7.8: Hot streams data of the global process (Hydrogen production basis: 1 kg h^{-1})

Available energy for recovery	T_h ($^{\circ}\text{C}$)	T_c ($^{\circ}\text{C}$)	Q (kW)
Heat from pyrolysis volatiles combustion	1340	200	66.0
Cooling of syngas from gasification	950	350	6.3
Cooling of syngas from HTS	456	210	2.5
Cooling of syngas from LTS	242	35	3.1
Total			77.9

Table 7.9: The efficiency and energy consumption of hydrogen production routes (Dawood *et al.*, 2020; Staffell *et al.*, 2019)

	Efficiency (LHV) (%)	Energy requirement (kW h per kg _{H₂})
Methane reforming	65–75	46 (44–51)
Electrolysis	51–67	55 (50–65)
Coal Gasification	45–65	59 (51–74)
Biomass gasification	35–50	72 (69–76)

$$\eta_{EnH_2} = \frac{En_{H_2}}{En_{pulp} + En_{demand}} = \frac{\dot{m}_{H_2} \times LHV_{H_2}}{\dot{m}_{dry pulp} \times LHV_{pulp} + Q} \quad (7.5)$$

Where, \dot{m}_{H_2} and \dot{m}_{pulp} are respectively the mass flow rate of produced H₂ and pulp. LHV_{H₂} and LHV_{pulp} are respectively the low heating value of H₂ (120.9 MJ kg⁻¹) and cellulose pulp (18.1 MJ kg⁻¹); Q refers to the process energy input that was considered in two heat integration scenarios (case 1 and 2), as shown in Table 7.10. Case 1 gives an integrated process of pulp gasification with pretreatment. To examine the impact of biomass pretreatment on process efficiency, case 2 illustrates biomass pretreatment as a separate process physically removed from the gasification process. The obtained results of the nominal efficiency and energy requirements were compared with those of different hydrogen production methods summarized in Table 7.9.

In case 1, the energy efficiency of hydrogen production and the energy requirement was 26.5 % and 111.1 kW h per kg_{H₂}, respectively; These values were found to be lower than values reported for gasification processes, ranging from 35 to 65 % and 69 to 76 kW h per kg_{H₂}. In case 2, higher η_{EnH_2} was observed, reaching 42.1 %, hence revealing the energy-consuming nature of this organosolv pretreatment.

Table 7.10: Summary of Pinch analysis and energy efficiency results (hydrogen production basis: 1 kg h⁻¹)

Parameters	Value
Energy balance	
Total heat demand (kW) ①	105
Electrical energy (kW) ②	6.1
Heat available for recovery (kW)	77.9
Pinch analysis ($\Delta T_{min} = 50 \text{ }^\circ\text{C}$)	
Hot temperature pinch (T_{hPinch}) ($^\circ\text{C}$)	75.0
Cold temperature pinch (T_{cPinch}) ($^\circ\text{C}$)	25.0
Total recoverable heat (kW)	77.3
Minimum cold utility, Q_c (kW)	0.6
Minimum hot utility, Q_h (kW) ③	27.7
Material energy content	
H ₂ energy content (kW) ④	33.6
Dry pulp energy content (kW) ⑤	94.3
Energy efficiency	
1) η_{enH_2} with heat integration (%) ⑦ = ④/(⑤ + ③ + ②)	26.2
2) η_{enH_2} with heat integration and without considering pulping (%) ⑧ = ④/(⑤ + ③ + ② - $Q_{pulping}$ - $Q_{pulp\ drying}$)	41.5

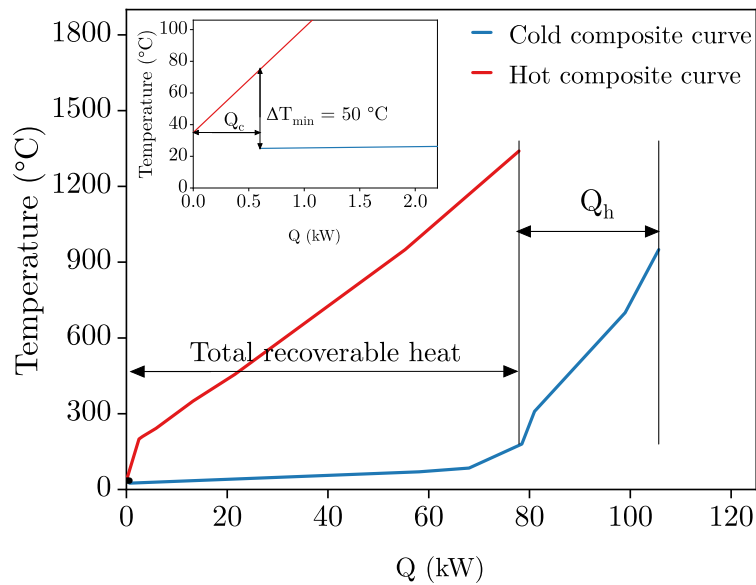


Figure 7.4: Hot and cold composite curves

7.5 Conclusion

In the present chapter, a comprehensive Aspen plus model was developed to assess hydrogen production from steam gasification in a biorefinery concept. A validation was conducted by comparing simulation results and experimental data at different operating conditions. A satisfactory accuracy on the syngas composition and yield was obtained at a gasification temperature of 950 °C.

The simulation results demonstrated that biomass pretreatment was the highest energy demand stage in the process. Pinch analysis showed that energy efficiency of hydrogen production is highly impacted by the energy consumption of this step. Further assessment in terms of solvent and by-products recovery as well as energy analysis is necessary to improve the energy consumption and reduce utilities requirements, making the process much more competitive.

Table 7.11: Combustion gas composition

Gas	H ₂	CO	CO ₂	H ₂ O	O ₂	N ₂	NO	NO ₂
vol. %	0.001	0.003	9.45	11.30	6.00	73.08	0.17	0.000

Conclusions and perspectives

Conclusions

With the urge to shift into global hydrogen production in the sustainable development scenario, steam gasification of lignocellulosic biomass has been regarded as an alternative energy source to fossil fuels and an important piece of the energy mix together with other renewable energy-based systems. In addition to its potentialities, biomass can be converted, in the same routes as that for fossil fuels (refinery), into a wide spectrum of marketable products and energy. This can be achieved using different conversion pathways through integrated biorefineries. While organosolv processes have been found highly efficient in ensuring maximum conversion of lignocellulosic material into added-value products, these processes are energy-intensive, implying a high operating cost. Integrating pyrogasification and organosolv treatment in a biorefinery approach can potentially improve the process's overall efficiency.

This thesis deals with hydrogen-rich syngas production from steam gasification of cellulose pulp obtained from a low-energy consumption organosolv process.

To meet this objective, two biomass residues, wheat straw (WS) and softwood sawdust (SS) were pulped at lab scale through formic acid pulping (LEEBIO process) with varying pulping time. The variations of the kappa number and pulp yield were minimal after 180 min, indicating that the delignification reaction was mostly reached. The results revealed that the WS was more efficiently fractionated, with higher rates of lignin and hemicellulose obtained. The structure of the plant cell wall was one of the most influencing parameters controlling solvent diffusion and lignin. Formic acid treatment significantly impacted the inorganic composition of the cellulose pulp. Most of AAEM salts were dissolved after formic acid pulping while Si in raw biomass ash remained in the pulp, namely in the epidermic cells. A scaling-up approach was carried out for SS fractionation from lab scale to pilot scale at a scale factor of 1000. The fractionation performance was consistent with that of the lab-scale test in terms of pulp yield, delignification rate, and mineral composition. In a subsequent step, an elimination rate of 65 % of Si from the pilot-scale pulp was achieved through alkaline treatment.

After formic acid pretreatment was conducted, the pyrogasification of cellulose pulp was studied using TGA and a lab-scale fixed bed reactor. The process was divided into

two stages: pyrolysis and steam gasification. Different commercial celluloses were used to assess cellulose pulp pyrogasification.

TGA tests were performed to understand the thermal stability and the kinetics of each process.

- Regrading thermal stability and pyrolysis behavior, the thermal decomposition of cellulose pulp was impacted by the macromolecular constituents and their inherent structure. Cellulose pulps with higher lignin content had a higher degradation temperature. Higher cellulose fraction led to an increase in the decomposition rate.
- The results of **TGA** steam gasification revealed that biochar reactivity from cellulose was 3 times lower than that of the raw biomass biochar as a result of the difference in the inorganic content, in particular, AAEM and Si. The gasification of cellulose char revealed the negative effect of Si; the biochar reactivity decreased with increasing Si concentration in the ash. It is worth noticing that the morphological structure was found to have an impact at a low conversion rate, although it was less influential than Si content. Thus, a kinetic model for describing the gasification kinetics was developed using the Si content in the ash as a key parameter.
- The gasification of alkaline-washed cellulose confirmed the inhibiting effect of Si on the gasification process. After the partial elimination of Si, the char reactivity increased 2.5 and 1.3 times at 800 and 900 °C, respectively.

Pyrogasification tests of cellulose pulp pyrogasification at a lab scale, to analyze the effect of operating parameters as well as product distribution composition.

- Compared to kraft cellulose, the product yield from the pyrolysis of **LEEBIO** cellulose pulp was influenced by the residual lignin, yielding a greater biochar fraction and higher H₂ and CH₄ yields. At 750 °C, the bio-oil yield from pyrolysis was more than 50 %, which can be burned to provide heat to the endothermic steps of drying and steam gasification. This aspect was developed by simulating the global process coupling organosolv pretreatment and pyrogasification of cellulose pulp.
- The results of steam gasification of biochar showed the effect of temperature and steam-to-carbon ratio and the process performance and gas quality. A higher steam-to-carbon ratio was beneficial to the gas quality by increasing H₂/CO through promoting carbon-steam and water-gas-shift reactions. The decreasing CO/CO₂ with increasing steam-to-carbon ratio, was explained by the dominance

of steam-involved reactions over the Boudouard reaction. Hydrogen yield was improved by raising the temperature, which enhanced the endothermic carbon-steam reaction. However, with increasing temperature, H_2/CO was reduced due to the reverse water-gas-shift-reaction while H_2/CH_4 by the reactivity of steam methane reforming reaction.

- The hydrogen yield and carbon conversion at 750 and 850 °C indicated that Si had a severe inhibitory effect on steam gasification of cellulose pulp biochar, particularly on Boudouard and water-gas reactions.
- Results of the gasification test at 950 °C of LEEBIO cellulose pulp showed great potential for high quality H_2 -rich syngas production. Potential hydrogen and H_2/CO of $52.9 \text{ g}_{H_2} \text{ kg}_{\text{cellulose pulp}}^{-1}$ and 1.8 were obtained, respectively.
- The results demonstrated the absence of nitrogen in any gasification product of LEEBIO pulp biochar. In addition, alkali compounds, in particular, K can be captured by silica in the solid preventing its loading in the producer gas. Hence, the gasification of LEEBIO cellulose pulp showed a strong potential to produce cleaner syngas.

As mentioned earlier the ultimate purpose of this work is the establishment of an integrated biorefinery coupling steam gasification and organosolv treatment. The process was modeled to examine the overall performance and evaluate the heat integration. Using pinch analysis, we were able to set targets for minimum energy consumption. The results revealed the energy-intensive nature of organosolv pretreatment. The hydrogen production efficiency was calculated, at 26.5 and 42.1 % with and without integrating biomass organosolv treatment, respectively.

Perspectives

The present study evidenced the potential of hydrogen production from an organosolv cellulose pulp in a biorefinery approach. In light of those challenges, several questions are worth further investigation:

- The integral fractionation of biomass should be investigated including the separation of hemicelluloses and lignin. This would be helpful for mass and energy assessment of the pretreatment process. To improve the effectiveness of formic acid pulping, using LEEBIO process, further steps should be applied to enhance solvent penetration in the plant cell wall. Concerning the effect of acid pretreatment on the inorganic composition, the pulping tests should be extended to other high-mineral content biomass containing syngas precursors species such Cl and S.

- Besides the major effect of Si and AAEM species, the results showed that the morphology of biochar could also influence the steam gasification reactivity. TGA gasification tests should be extended to other biochars with different morphological properties and inorganic composition. Therefore, the proposed semi-empirical model can be modified by combining both parameters to develop a unified phenomenological model.
- Concerning the inhibition effect of Si on carbon-gas reactions, it is of paramount importance to perform further gasification tests in CO₂ and a H₂O/CO₂ atmospheres. The characterization of the recovered char using BET and the measurement of gaseous and liquid products could elucidate the mechanism of action of Si in the gasification kinetics.
- The elimination of Si was found to be beneficial for biochar gasification. In the case of Si-rich cellulose pulp, namely from straws residues, alkaline treatment would be advantageous. First, it would allow reducing the inhibiting effect of Si, secondly separated silica is an important platform chemical that can potentially be converted into added-value products.
- In relation to the energy assessment of the overall hydrogen production process, experimental data from lignin and hemicellulose separation as well as the solvent recovery are required to complete the flowsheet configuration. Subsequently, the technical design and economic evaluation can be conducted to better assess the costs of the organosolv-based biorefinery producing chemicals and hydrogen.

List of Figures

1	Thermochemical conversion pathways of biomass	13
2	Co-occurrence map and link of the most frequent keywords in the title and abstract	13
1.1	Schematic representation of biomass composition and structure	22
1.2	Flow scheme of the organosolv fractionation	26
1.3	Pyrogasification process	28
1.4	Tar groups as function of temperature	30
1.5	A schematic of different types of single-stage gasifiers	33
1.6	A schematic of multi-stage gasification technologies	35
1.7	Influence of temperature on gasification process performance	41
1.8	Application of syngas	44
1.9	Flow scheme and relative strength of adsorption for different gas onto adsorbents used in PSA technology	48
1.10	<i>LEEBIOTM</i> technology – Cellulose pulp, green energies, fuels, and products from biomass	50
2.1	Selected feedstocks	55
2.2	Cellulose pulp from different WS and SS	59
2.3	Cellulose extraction using RoLab 0.4 m^2	62
2.4	Flowchart of the SS extraction following the <i>LEEBIOTM</i> process	62
2.5	TGA experimental program of pyrolysis and gasification	64
2.6	Schematic presentation of pyrogasification experimental setup	66
2.7	Fixed-bed reactor used in pyrogasification experiments	67
2.8	Experimental program of pyrolysis and gasification tests	67
2.9	Collected condensates during pyrolysis stage	69
3.1	Effect of reaction time on pulp yield and kappa number	73

3.2	Inorganic composition of feedstocks and pulps	77
3.3	TEM-EDX mapping images for WS and Cell-WS-L	78
3.4	TEM-EDX mapping images for SS and Cell-SS-L	79
3.5	TEM-EDX mapping images for Cell-SS-P before and after alkaline treatment	82
4.1	Generalized master plots of kinetic models listed in Table 4.1	87
4.2	Comparison of TG and dTG profiles of different cellulose samples	88
4.3	Influence of the composition contents on cellulose thermal decomposition	90
4.4	TG and $d\alpha/dT$ profiles of cellulose pyrolysis at different heating rates .	92
4.5	Deconvolution of $d\alpha/dT$ curves at $10^\circ\text{C}/\text{min}$	94
4.6	Kinetic plots for determination of activated energy using KAS model at different conversion	95
4.7	Variation of E_a as function of conversion degree for different cellulose samples	96
4.8	Experimental (symbols) and theoretical (lines) $\lambda(\alpha)$ master plot curves at different heating rates	98
4.9	X-ray diffraction spectra of cellulose samples	101
5.1	Conversion degree <i>vs</i> time of different biochar samples at different tem- peratures	107
5.2	Experimental reaction rate as a function of conversion, at 800°C with a partial steam pressure 6.2 kPa	109
5.3	Average reactivity at selected conversion range as a function of %Si (curves are just shown to highlight the tendencies)	111
5.4	SEM images of SS and WS biochars	113
5.5	Dependence of the reaction rate on steam partial pressure	114
5.6	group figs	115
5.7	Reaction order n as a function of %Si	116
5.8	Comparison between experimental conversion data and the modeled conversion curves	118
5.9	Conversion degree α <i>vs</i> time for of SS, Cell-SS, and Cell-SS-A biochars at 800°C with a partial steam pressure of 10 kPa	119
6.1	Chemical composition of pyrolysis bio-oils	126
6.2	Composition of bio-oil from pyrolysis of Cell-SS-P	126

6.3	Yields of major tar compounds	127
6.4	Product yield of different biochar samples as function as S/C at 850 °C	132
6.5	The influence of temperature on product yield	134
6.6	The influence of temperature on gas composition	135
6.7	Contents of major inorganic elements in recovered biochar from steam gasification	143
6.8	TEM mapping image with energy-dispersive X-ray (EDX) mapping for Cell-SS-P and ARC biochars	148
6.9	TEM mapping image with energy-dispersive X-ray (EDX) mapping for SS biochar	149
7.1	Simplified scheme of the model	153
7.2	Simulated ASPEN Plus flowsheet	157
7.3	Effect of S/C ratio on gas composition and hydrogen yield at different temperatures: comparison between simulation and experimental data .	161
7.4	Hot and cold composite curves	168

List of Tables

1.1	Chemical, elemental and proximate composition of different lignocellulosic biomass	21
1.2	Product yields and conditions of Organsolv lignocellulosic biomass pre-treatment	26
1.3	Advantages and disadvantages of organsolv fractionation	27
1.4	Pyrolysis process conditions and product distribution	29
1.5	Overview of the main chemical reactions of biomass gasification	31
1.6	Gas composition from different gasification technologies	37
1.7	Ultimate and proximate analysis of pure biomass components lignin, cellulose and xylan	37
1.8	Pyrolysis characteristics of biomass three components: thermal behavior and product yields	38
1.9	Recent studies on gasification of biomass constituents and maximum H ₂ production	43
1.10	Overview of different syngas cleanup technologies	46
1.11	Comparison of different features and aspects of hydrogen purification methods	49
3.1	Element and proximate analysis of feedstocks and pulp samples	72
3.2	Macromolecular composition, pulp yield and removal rates of lignin and hemicelluloses	75
3.3	Mass balance of pilot-plant acid pulping operation	80
3.4	Main inorganic elements in SS pulp (pilot-scale) before and after alkaline treatment	81
4.1	Most common reaction mechanisms in kinetics analysis for solid-state degradation processes	87
4.2	Crystallinity Index, lignin fraction and peak temperature	89
4.3	Fraser-Suzuki deconvolution parameters	93

4.4	Average values of activation energy calculated over the whole conversion range	97
4.5	Pre-exponential factor values obtained by using KAS isoconversional method (calculated) and the adjusted values (solver)	99
4.6	Kinetic triplet for cellulose pyrolysis	100
5.1	Main inorganic elements in the biomass and cellulose pulp samples . . .	104
5.2	Char steam gasification reactivity at 30 % conversion $R_{30\%}$, maximum conversion level after 360 min of reaction α_{max} , and its corresponding reaction time $t_{\alpha_{max}}$; partial steam pressure 6.2 kPa	108
5.3	Char gasification studies taking into account inorganic elements	110
5.4	Kinetic parameters of different biochar samples	116
5.5	Gasification reactivity and the required time to achieve 70 % conversion at different operating conditions	120
5.6	Applicability of %Si in literature studies	121
6.1	Product yields of pyrolysis products	125
6.2	Ultimate and proximate analysis at dry basis of different biochars	128
6.3	Experimental results of carbon during steam gasification of Cell-SS-P biochar (T = 850 °C)	130
6.4	The influence of steam flow rate on gasification of Cell-SS-P biochar at 950 °C	131
6.5	Carbon conversion and gas ratios in function of temperature and % Si content in raw material ($\dot{m}_{steam} = 45 \text{ g h}^{-1}$)	137
6.6	Theoretical yield of hydrogen from biomass steam gasification	141
6.7	Comparison of steam gasification performance and hydrogen production from different biochars samples	142
6.8	AAEM to Si ratio, slagging and fouling calculated according to char ash composition	144
6.9	The influence of steam flow rate on gasification of SS biochar at 950 °C	145
6.10	The influence of steam flow rate on gasification of ARC biochar at 950 °C	146
6.11	Composition analysis of bio-oil obtained from pyrolysis of cellulose pulp	147
7.1	Ultimate and proximate analysis at dry basis of different components . .	154
7.2	List of unit operations used in the flowsheet	155
7.3	Reactions implemented in the Aspen Plus model	158

7.4	Material balance of the global process	162
7.5	Summary of operation conditions for different steps of H ₂ production process	163
7.6	Molar composition, mass flow rate, temperature and pressure of gas streams at the outlet of different units	163
7.7	Energy consumption of different units of the global process	165
7.8	Hot streams data of the global process	165
7.9	The efficiency and energy consumption of hydrogen production routes (Dawood <i>et al.</i> , 2020; Staffell <i>et al.</i> , 2019)	166
7.10	Summary of Pinch analysis and energy efficiency results	167
7.11	Combustion gas composition	168

Bibliography

- (Aasadnia *et al.*, 2021) Majid Aasadnia, Mehdi Mehrpooya, and Bahram Ghorbani. “A Novel Integrated Structure for Hydrogen Purification Using the Cryogenic Method”. *Journal of Cleaner Production* 278 (Jan. 2021), p. 123872 (cit. on p. 49).
- (Abdelouahed *et al.*, 2012) L. Abdelouahed, O. Authier, G. Mauviel, J. P. Corriou, G. Verdier, and A. Dufour. “Detailed Modeling of Biomass Gasification in Dual Fluidized Bed Reactors under Aspen Plus”. *Energy & Fuels* 26.6 (June 21, 2012), pp. 3840–3855 (cit. on p. 152).
- (Abdoulmoumine *et al.*, 2015) Nourredine Abdoulmoumine, Sushil Adhikari, Avanti Kulkarni, and Shyamsundar Chattanathan. “A Review on Biomass Gasification Syngas Cleanup”. *Applied Energy* 155 (Oct. 2015), pp. 294–307 (cit. on p. 45).
- (Adamon *et al.*, 2019) David G. F. Adamon, Latif A. Fagbémi, Ammar Bensakhria, and Emile A. Sanya. “Comparison of Kinetic Models for Carbon Dioxide and Steam Gasification of Rice Husk Char”. *Waste and Biomass Valorization* 10.2 (Feb. 2019), pp. 407–415 (cit. on p. 116).
- (Ahmad *et al.*, 2016) Anis Atikah Ahmad, Norfadhila Abdullah Zawawi, Farizul Hafiz Kasim, Abrar Inayat, and Azduwin Khasri. “Assessing the Gasification Performance of Biomass: A Review on Biomass Gasification Process Conditions, Optimization and Economic Evaluation”. *Renewable and Sustainable Energy Reviews* 53 (Jan. 2016), pp. 1333–1347 (cit. on p. 152).
- (Akubo *et al.*, 2019) Kaltume Akubo, Mohamad Anas Nahil, and Paul T. Williams. “Pyrolysis-Catalytic Steam Reforming of Agricultural Biomass Wastes and Biomass Components for Production of Hydrogen/Syngas”. *Journal of the Energy Institute* 92.6 (Dec. 2019), pp. 1987–1996 (cit. on pp. 41, 43).
- (Amovic *et al.*, n.d.) Marko Amovic, Pawel Donaj, Baldesca Moner, Ram Alzuheri, and Rolf Ljunggren. ”Fuel testing procedure for pyrolysis and gasification of biomass using TGA and WoodRoll test plant (Bransletest- metod for pyrolysis och forgasning av biomassa med anvandande av TGA och WoodRolls testanlaggning)” (), p. 47 (cit. on p. 36).
- (Anca-Couce *et al.*, 2014) Andrés Anca-Couce, Anka Berger, and Nico Zobel. “How to Determine Consistent Biomass Pyrolysis Kinetics in a Parallel Reaction Scheme”. *Fuel* 123 (May 2014), pp. 230–240 (cit. on pp. 84, 96).

- (Andrea Jordan *et al.*, 2012) C. Andrea Jordan and Galip Akay. “[Speciation and Distribution of Alkali, Alkali Earth Metals and Major Ash Forming Elements during Gasification of Fuel Cane Bagasse](#)”. *Fuel* 91.1 (Jan. 2012), pp. 253–263 (cit. on p. 143).
- (Annevelink *et al.*, n.d.) Bert Annevelink, Lesly Garcia Chavez, René van Ree, and Iris Vural Gursel. “Global Biorefinery Status Report 2022” (), p. 94 (cit. on p. 23).
- (Aprea, 2014) José Luis Aprea. “[Quality Specification and Safety in Hydrogen Production, Commercialization and Utilization](#)”. *International Journal of Hydrogen Energy* 39.16 (May 2014), pp. 8604–8608 (cit. on p. 45).
- (ARENA, 2018) ARENA. *An Advanced Biomass Gasification Technology Project Results*. 2018 (cit. on pp. 35, 36).
- (Asadullah, 2014) Mohammad Asadullah. “[Biomass Gasification Gas Cleaning for Downstream Applications: A Comparative Critical Review](#)”. *Renewable and Sustainable Energy Reviews* 40 (Dec. 2014), pp. 118–132 (cit. on p. 45).
- (Asadullah *et al.*, 2002) Mohammad Asadullah, Shin-ichi Ito, Kimio Kunimori, Muneyoshi Yamada, and Keiichi Tomishige. “[Energy Efficient Production of Hydrogen and Syngas from Biomass: Development of Low-Temperature Catalytic Process for Cellulose Gasification](#)”. *Environmental Science & Technology* 36.20 (Oct. 1, 2002), pp. 4476–4481 (cit. on p. 41).
- (Asadullah *et al.*, 2001) Mohammad Asadullah, Keiichi Tomishige, and Kauro Fujimoto. “A Novel Catalytic Process for Cellulose Gasification to Synthesis Gas”. *Catalysis Communications* (2001), p. 6 (cit. on p. 41).
- (Azadi *et al.*, 2013) Pooya Azadi, Oliver R. Inderwildi, Ramin Farnood, and David A. King. “[Liquid Fuels, Hydrogen and Chemicals from Lignin: A Critical Review](#)”. *Renewable and Sustainable Energy Reviews* 21 (May 2013), pp. 506–523 (cit. on pp. 24, 25).
- (Baeza *et al.*, 1991) Jaime Baeza, Silvio Urizar, Norma de Magalhães Erismann, Juanita Freer, Eckhard Schmidt, and Nelson Durán. “[Organosolv Pulping — V: Formic Acid Delignification of Eucalyptus Globulus and Eucalyptus Grandis](#)”. *Bioresource Technology* 37.1 (Jan. 1991), pp. 1–6 (cit. on p. 73).
- (Banks *et al.*, 2016) S.W. Banks and A.V. Bridgwater. “[Catalytic Fast Pyrolysis for Improved Liquid Quality](#)”. *Handbook of Biofuels Production*. Elsevier, 2016, pp. 391–429 (cit. on p. 29).
- (Barneto *et al.*, 2009) Agustín García Barneto, José Ariza Carmona, José E. Martín Alfonso, and Luís Jiménez Alcaide. “[Use of Autocatalytic Kinetics to Obtain Composition of Lignocellulosic Materials](#)”. *Bioresource Technology* 100.17 (Sept. 2009), pp. 3963–3973 (cit. on p. 97).

-
- (Barneto *et al.*, 2010) Agustín García Barneto, José Ariza Carmona, José E. Martín Alfonso, and Rafael Sánchez Serrano. “[Simulation of the Thermogravimetry Analysis of Three Non-Wood Pulps](#)”. *Bioresource Technology* 101.9 (May 2010), pp. 3220–3229 (cit. on p. 88).
- (Baruah *et al.*, 2018) Julie Baruah, Bikash Kar Nath, Ritika Sharma, Sachin Kumar, Ramesh Chandra Deka, Deben Chandra Baruah, and Eeshan Kalita. “[Recent Trends in the Pretreatment of Lignocellulosic Biomass for Value-Added Products](#)”. *Frontiers in Energy Research* 6 (Dec. 18, 2018), p. 141 (cit. on pp. 21, 25).
- (Barud *et al.*, 2011) Hernani S. Barud, Clóvis A. Ribeiro, Jorge M. V. Capela, Marisa S. Crespi, Sidney. J. L. Ribeiro, and Younes Messadeq. “[Kinetic Parameters for Thermal Decomposition of Microcrystalline, Vegetal, and Bacterial Cellulose](#)”. *Journal of Thermal Analysis and Calorimetry* 105.2 (Aug. 2011), pp. 421–426 (cit. on p. 97).
- (Basu, 2010) Prabir Basu. *Biomass Gasification and Pyrolysis - 1st Edition*. 2010 (cit. on pp. 27, 31).
- (Berglin *et al.*, 1998) N Berglin and T Berntsson. “CHP in the Pulp Industry Using Black Liquor Gasi@cation: Thermodynamic Analysis”. *Applied Thermal Engineering* (1998), p. 15 (cit. on p. 25).
- (Bertero *et al.*, 2015) Melisa Bertero and Ulises Sedran. “[Coprocesing of Bio-oil in Fluid Catalytic Cracking](#)”. *Recent Advances in Thermo-Chemical Conversion of Biomass*. Elsevier, 2015, pp. 355–381 (cit. on p. 29).
- (Besancon *et al.*, 2009) Brian M. Besancon, Vladimir Hasanov, Raphaëlle Imbault-Lastapis, Robert Benesch, Maria Barrio, and Mona J. Mølnvik. “[Hydrogen Quality from Decarbonized Fossil Fuels to Fuel Cells](#)”. *International Journal of Hydrogen Energy* 34.5 (Mar. 2009), pp. 2350–2360 (cit. on pp. 47, 48).
- (Billaud, 2015) Joseph Billaud. « [Gazéification de la biomasse en réacteur à flux entraîné : études expérimentales et modélisation](#) ». PhD thesis. Ecole des Mines d’Albi-Carmaux, Dec. 2, 2015 (cit. on p. 126).
- (Blasi, 2009) Colomba Di Blasi. “Combustion and Gasification Rates of Lignocellulosic Chars”. *Progress in Energy and Combustion Science* (2009), p. 20 (cit. on p. 112).
- (Boerrigter *et al.*, n.d.) H Boerrigter and R Rauch. “Review of Applications of Gases from Biomass Gasification” (), p. 34 (cit. on p. 44).
- (Bolhàr-Nordenkampf *et al.*, 2003) M Bolhàr-Nordenkampf, R Rauch, K Bosch, and C Aichernig. “Biomass CHP Plant Güssing – Using Gasification for Power Generation” (2003), p. 7 (cit. on p. 36).
- (Borand *et al.*, 2018) Merve Nazlı Borand and Filiz Karaosmanoğlu. “[Effects of Organosolv Pretreatment Conditions for Lignocellulosic Biomass in Biorefinery Applications: A Review](#)”. *Journal of Renewable and Sustainable Energy* 10.3 (May 2018), p. 033104 (cit. on pp. 4, 15, 27).

- (Boström *et al.*, 2012) Dan Boström, Nils Skoglund, Alejandro Grimm, Christoffer Boman, Marcus Öhman, Markus Broström, and Rainer Backman. “Ash Transformation Chemistry during Combustion of Biomass”. *Energy & Fuels* 26.1 (Jan. 19, 2012), pp. 85–93 (cit. on p. 138).
- (Bouraoui *et al.*, 2016) Zeineb Bouraoui, Capucine Dupont, Mejdı Jeguirim, Lionel Limousy, and Roger Gadiou. “CO₂ Gasification of Woody Biomass Chars: The Influence of K and Si on Char Reactivity”. *Comptes Rendus Chimie* 19.4 (Apr. 2016), pp. 457–465 (cit. on pp. 110, 111, 139).
- (Bouraoui *et al.*, 2015) Zeineb Bouraoui, Mejdı Jeguirim, Chamseddine Guizani, Lionel Limousy, Capucine Dupont, and Roger Gadiou. “Thermogravimetric Study on the Influence of Structural, Textural and Chemical Properties of Biomass Chars on CO₂ Gasification Reactivity”. *Energy* 88 (Aug. 2015), pp. 703–710 (cit. on p. 110).
- (bp, 2022) bp. “Statistical Review of World Energy 2022” (2022), p. 60 (cit. on p. 11).
- (Brandt *et al.*, 2013) Agnieszka Brandt, John Gräsvik, Jason P. Hallett, and Tom Welton. “Deconstruction of Lignocellulosic Biomass with Ionic Liquids”. *Green Chemistry* 15.3 (2013), p. 550 (cit. on p. 20).
- (Broberg *et al.*, 2019) Henrik Broberg, Raquel Bohn Stoltz, Anders Hjort, and Monica Ek. “Steaming of Wood Chips; Experimental Determination of Heating Times and Effect of Different Parameters” (2019), p. 39 (cit. on p. 75).
- (Brown, 1998) Michael E. Brown. *Handbook of Thermal Analysis and Calorimetry: Principles and Practice*. Elsevier, Sept. 7, 1998. 725 pp. Google Books: 33_3DBLGzMYC (cit. on pp. 87, 114).
- (Burhenne *et al.*, 2013) Luisa Burhenne, Jonas Messmer, Thomas Aicher, and Marie-Pierre Laborie. “The Effect of the Biomass Components Lignin, Cellulose and Hemicellulose on TGA and Fixed Bed Pyrolysis”. *Journal of Analytical and Applied Pyrolysis* 101 (May 2013), pp. 177–184 (cit. on p. 89).
- (Burnham *et al.*, 2015) Alan K. Burnham, Xiaowei Zhou, and Linda J. Broadbelt. “Critical Review of the Global Chemical Kinetics of Cellulose Thermal Decomposition”. *Energy & Fuels* 29.5 (May 21, 2015), pp. 2906–2918 (cit. on p. 99).
- (Butterman *et al.*, 2009) Heidi C. Butterman and Marco J. Castaldi. “CO₂ as a Carbon Neutral Fuel Source via Enhanced Biomass Gasification”. *Environmental Science & Technology* 43.23 (Dec. 1, 2009), pp. 9030–9037 (cit. on p. 141).
- (Capart *et al.*, 2004) Richard Capart, Lotfi Khezami, and Alan K. Burnham. “Assessment of Various Kinetic Models for the Pyrolysis of a Microgranular Cellulose”. *Thermochimica Acta* 417.1 (July 2004), pp. 79–89 (cit. on p. 97).
- (CEN, 2006) CEN. “Tar Measurement in Biomass Gasification, Standardisation and Supporting R&D” (2006) (cit. on pp. 30, 68).

-
- (D. Chen *et al.*, 2014) Dengyu Chen, Jianbin Zhou, and Qisheng Zhang. “Effects of Heating Rate on Slow Pyrolysis Behavior, Kinetic Parameters and Products Properties of Moso Bamboo”. *Bioresource Technology* 169 (Oct. 2014), pp. 313–319 (cit. on p. 91).
- (Hanping Chen *et al.*, 2021) Hanping Chen, Ziyue Tang, Biao Liu, Wei Chen, Junhao Hu, Yingquan Chen, and Haiping Yang. “The New Insight about Mechanism of the Influence of K₂CO₃ on Cellulose Pyrolysis”. *Fuel* 295 (July 2021), p. 120617 (cit. on p. 39).
- (Hongzhang Chen *et al.*, 2016) Hongzhang Chen and Lan Wang. *Technologies for Biochemical Conversion of Biomass*. Academic Press, Dec. 14, 2016. 292 pp. (cit. on pp. 2, 12).
- (Cheng *et al.*, 2015) Zhicai Cheng, Weixuan Wu, Peng Ji, Xiaotong Zhou, Ronghou Liu, and Junmeng Cai. “Applicability of Fraser–Suzuki Function in Kinetic Analysis of DAEM Processes and Lignocellulosic Biomass Pyrolysis Processes”. *Journal of Thermal Analysis and Calorimetry* 119.2 (Feb. 2015), pp. 1429–1438 (cit. on p. 85).
- (Cherubini *et al.*, 2010) Francesco Cherubini and Sergio Ulgiati. “Crop Residues as Raw Materials for Biorefinery Systems – A LCA Case Study”. *Applied Energy* 87.1 (Jan. 2010), pp. 47–57 (cit. on p. 23).
- (Chiche *et al.*, 2013) D. Chiche, C. Diverchy, A.-C. Lucquin, F. Porcheron, and F. Defoort. “Synthesis Gas Purification”. *Oil & Gas Science and Technology – Revue d’IFP Energies nouvelles* 68.4 (July 2013), pp. 707–723 (cit. on p. 45).
- (Chuah *et al.*, 2021) Chong Yang Chuah, Xu Jiang, Kunli Goh, and Rong Wang. “Recent Progress in Mixed-Matrix Membranes for Hydrogen Separation”. *Membranes* 11.9 (Aug. 30, 2021), p. 666 (cit. on p. 47).
- (Ciferno, 2002) Jared P Ciferno. “Benchmarking Biomass Gasification Technologies” (June 2002), p. 65 (cit. on p. 32).
- (Collard *et al.*, 2014) François-Xavier Collard and Joël Blin. “A Review on Pyrolysis of Biomass Constituents: Mechanisms and Composition of the Products Obtained from the Conversion of Cellulose, Hemicelluloses and Lignin”. *Renewable and Sustainable Energy Reviews* 38 (Oct. 2014), pp. 594–608 (cit. on p. 89).
- (Corella *et al.*, 2007) José Corella, José M. Toledo, and Gregorio Molina. “A Review on Dual Fluidized-Bed Biomass Gasifiers”. *Industrial & Engineering Chemistry Research* 46.21 (Oct. 1, 2007), pp. 6831–6839 (cit. on p. 34).
- (Couto *et al.*, 2013) Nuno Couto, Abel Rouboa, Valter Silva, Eliseu Monteiro, and Khalid Bouziane. “Influence of the Biomass Gasification Processes on the Final Composition of Syngas”. *Energy Procedia* 36 (2013), pp. 596–606 (cit. on pp. 30, 37).
- (Dahlquist *et al.*, 2017) Erik Dahlquist, Muhammad Naqvi, Eva Thorin, Jinyue Yan, Konstantinos Kyprianidis, and Philip Hartwell. “Experimental and Numerical Inves-

- tigation of Pellet and Black Liquor Gasification for Polygeneration Plant”. *Applied Energy* 204 (Oct. 2017), pp. 1055–1064 (cit. on p. 25).
- (Dahou *et al.*, 2021) T. Dahou, F. Defoort, B. Khiari, M. Labaki, C. Dupont, and M. Jeguirim. “Role of Inorganics on the Biomass Char Gasification Reactivity: A Review Involving Reaction Mechanisms and Kinetics Models”. *Renewable and Sustainable Energy Reviews* 135 (Jan. 2021), p. 110136 (cit. on pp. 108, 111, 138).
- (Danso-Boateng *et al.*, 2022) Eric Danso-Boateng and Osei-Wusu Achaw. “Bioenergy and Biofuel Production from Biomass Using Thermochemical Conversions Technologies—a Review”. *AIMS Energy* 10.4 (2022), pp. 585–647 (cit. on pp. 13, 29).
- (Dapiá *et al.*, 2002) S Dapiá, V Santos, and J.C Parajó. “Study of Formic Acid as an Agent for Biomass Fractionation”. *Biomass and Bioenergy* 22.3 (Mar. 2002), pp. 213–221 (cit. on pp. 73, 75).
- (Davis *et al.*, 2007) Philip J. Davis and Philip Rabinowitz. *Methods of Numerical Integration*. Courier Corporation, Jan. 1, 2007. 626 pp. Google Books: [gGCKdqka0HAC](#) (cit. on p. 85).
- (Dawood *et al.*, 2020) Furat Dawood, Martin Anda, and G.M. Shafiullah. “Hydrogen Production for Energy: An Overview”. *International Journal of Hydrogen Energy* 45.7 (Feb. 2020), pp. 3847–3869 (cit. on pp. 47, 49, 166).
- (G.-H. Delmas *et al.*, 2021) Guo-Hua Delmas, Joseph H. Banoub, and Michel Delmas. “Lignocellulosic Biomass Refining: A Review Promoting a Method to Produce Sustainable Hydrogen, Fuels, and Products”. *Waste and Biomass Valorization* (Nov. 10, 2021) (cit. on pp. 20, 51, 123, 162).
- (M. Delmas, 2019) Michel Delmas. “A Low Energy Production Process for Producing Paper Pulp from Lignocellulosic Biomass”. Pat. BIOEB. Aug. 22, 2019 (cit. on p. 73).
- (Demirbas *et al.*, 2002) Ayhan Demirbas and Gönenc Arin. “An Overview of Biomass Pyrolysis”. *Energy Sources* 24.5 (May 2002), pp. 471–482 (cit. on p. 29).
- (Demirbaş, 2001) Ayhan Demirbaş. “Biomass Resource Facilities and Biomass Conversion Processing for Fuels and Chemicals”. *Energy Conversion and Management* 42.11 (July 2001), pp. 1357–1378 (cit. on pp. 2, 12).
- (Di Blasi *et al.*, 1999) Colomba Di Blasi, Gabriella Signorelli, Carlo Di Russo, and Genaro Rea. “Product Distribution from Pyrolysis of Wood and Agricultural Residues”. *Industrial & Engineering Chemistry Research* 38.6 (June 1, 1999), pp. 2216–2224 (cit. on p. 21).
- (J. Dong, 2016) Jun Dong. “MSWs Gasification with Emphasis on Energy, Environment and Life Cycle Assessment”. Theses. Ecole des Mines d’Albi-Carmaux ; Zhejiang University. Institute for Thermal Power Engineering, Nov. 2016 (cit. on p. 39).
- (L. Dong *et al.*, 2015) Lei Dong, Xuebing Zhao, and Dehua Liu. “Kinetic Modeling of Atmospheric Formic Acid Pretreatment of Wheat Straw with “Potential Degree of Reaction” Models”. *RSC Advances* 5.27 (2015), pp. 20992–21000 (cit. on p. 75).

-
- (Dorez *et al.*, 2014) G. Dorez, L. Ferry, R. Sonnier, A. Taguet, and J.-M. Lopez-Cuesta. “Effect of Cellulose, Hemicellulose and Lignin Contents on Pyrolysis and Combustion of Natural Fibers”. *Journal of Analytical and Applied Pyrolysis* 107 (May 2014), pp. 323–331 (cit. on p. 37).
- (Du *et al.*, 2021) Zhemin Du, Congmin Liu, Junxiang Zhai, Xiuying Guo, Yalin Xiong, Wei Su, and Guangli He. “A Review of Hydrogen Purification Technologies for Fuel Cell Vehicles”. *Catalysts* 11.3 (Mar. 19, 2021), p. 393 (cit. on pp. 47–49).
- (Ducouso, 2015) Marion Ducouso. “Gasification Biochar Reactivity toward Methane Cracking”. PhD thesis. Ecole des Mines d’Albi-Carmaux, Nov. 5, 2015 (cit. on p. 66).
- (Dufour, 2007) Anthony Dufour. “Optimisation de la production d’hydrogène par conversion du méthane dans les procédés de pyrolyse/gazéification de la biomasse”. thesis. Institut national polytechnique de Lorraine, 2007 (cit. on pp. 125–127).
- (Dupont, 2006) Capucine Dupont. “Vapogazéification de La Biomasse : Contribution à l’étude de La Phénoménologie Entre 800 et 1000 °C”. These de doctorat. Lyon 1, Jan. 1, 2006 (cit. on p. 136).
- (Dupont *et al.*, 2016) Capucine Dupont, Sylvain Jacob, Khalil Ould Marrakchy, Céline Hognon, Maguelone Grateau, Françoise Labalette, and Denilson Da Silva Perez. “How Inorganic Elements of Biomass Influence Char Steam Gasification Kinetics”. *Energy* 109 (Aug. 2016), pp. 430–435 (cit. on pp. 109, 110, 114, 117, 121).
- (Dupont *et al.*, 2011) Capucine Dupont, Timothée Nocquet, José Augusto Da Costa, and Christèle Verne-Tournon. “Kinetic Modelling of Steam Gasification of Various Woody Biomass Chars: Influence of Inorganic Elements”. *Bioresource Technology* 102.20 (Oct. 2011), pp. 9743–9748 (cit. on pp. 110, 114).
- (Ebrahimi *et al.*, 2016) Hadi Ebrahimi and Mohammad Rahmani. “A New Design for CO₂ Capture and Usage in a Syngas Production Unit by Carbonate Chemical Looping”. *Journal of Natural Gas Science and Engineering* 36 (Nov. 2016), pp. 241–251 (cit. on p. 49).
- (Eikeland *et al.*, 2015) Marianne S. Eikeland, Rajan K. Thapa, and Britt M. Halvorsen. “Aspen Plus Simulation of Biomass Gasification with Known Reaction Kinetic”. The 56th Conference on Simulation and Modelling (SIMS 56), October, 7-9, 2015, Linköping University, Sweden. Nov. 25, 2015, pp. 149–156 (cit. on p. 158).
- (Encinar *et al.*, 2021) José María Encinar, Juan Félix González, and Sergio Nogales-Delgado. “Thermogravimetry of the Steam Gasification of Calluna Vulgaris: Kinetic Study”. *Catalysts* 11.6 (May 22, 2021), p. 657 (cit. on p. 108).
- (Ephraim *et al.*, 2020a) Augustina Ephraim, Patricia Arlabosse, Ange Nzihou, Doan Pham Minh, and Patrick Sharrock. “Biomass Categories”. *Handbook on Characterization of Biomass, Biowaste and Related By-products*. Ed. by Ange Nzihou. Cham: Springer International Publishing, 2020, pp. 1–29 (cit. on pp. 20, 21).

- (Ephraim *et al.*, 2020b) Augustina Ephraim, Rajesh Munirathinam, Ange Nzihou, Doan Pham Minh, and Yohan Richardson. “Syngas”. *Handbook on Characterization of Biomass, Biowaste and Related By-products*. Ed. by Ange Nzihou. Cham: Springer International Publishing, 2020, pp. 1113–1171 (cit. on p. 45).
- (Ferreira *et al.*, 2020) Jorge A. Ferreira and Mohammad J. Taherzadeh. “Improving the Economy of Lignocellulose-Based Biorefineries with Organosolv Pretreatment”. *Bioresource Technology* 299 (Mar. 2020), p. 122695 (cit. on p. 26).
- (Florin *et al.*, 2007) N Florin and A Harris. “Hydrogen Production from Biomass Coupled with Carbon Dioxide Capture: The Implications of Thermodynamic Equilibrium”. *International Journal of Hydrogen Energy* 32.17 (Dec. 2007), pp. 4119–4134 (cit. on p. 129).
- (Franco *et al.*, 2003) C Franco, F Pinto, I Gulyurtlu, and I Cabrita. “The Study of Reactions Influencing the Biomass Steam Gasification Processq” (2003), p. 8 (cit. on p. 136).
- (Fremaux *et al.*, 2015) Sylvain Fremaux, Sayyed-Mohsen Beheshti, Hojat Ghassemi, and Rasoul Shahsavan-Markadeh. “An Experimental Study on Hydrogen-Rich Gas Production via Steam Gasification of Biomass in a Research-Scale Fluidized Bed”. *Energy Conversion and Management* 91 (Feb. 2015), pp. 427–432 (cit. on p. 43).
- (Froment *et al.*, 2013) K. Froment, F. Defoort, C. Bertrand, J.M. Seiler, J. Berjonneau, and J. Poirier. “Thermodynamic Equilibrium Calculations of the Volatilization and Condensation of Inorganics during Wood Gasification”. *Fuel* 107 (May 2013), pp. 269–281 (cit. on p. 142).
- (Gani *et al.*, 2007) Asri Gani and Ichiro Naruse. “Effect of Cellulose and Lignin Content on Pyrolysis and Combustion Characteristics for Several Types of Biomass”. *Renewable Energy* 32.4 (Apr. 2007), pp. 649–661 (cit. on p. 91).
- (Garcia-Maraver *et al.*, 2017) Angela Garcia-Maraver, Jesus Mata-Sanchez, Manuel Carpio, and Jose A. Perez-Jimenez. “Critical Review of Predictive Coefficients for Biomass Ash Deposition Tendency”. *Journal of the Energy Institute* 90.2 (Apr. 2017), pp. 214–228 (cit. on p. 144).
- (Ge *et al.*, 2022) Yaxin Ge, Saiman Ding, Xiangrui Kong, Efthymios Kantarelis, Klas Engvall, and Jan B.C. Pettersson. “Real-Time Monitoring of Alkali Release during CO₂ Gasification of Different Types of Biochar”. *Fuel* 327 (Nov. 2022), p. 125102 (cit. on p. 143).
- (Gírio, 2019) Francisco Gírio. “Innovation on Bioenergy”. *The Role of Bioenergy in the Bioeconomy*. Elsevier, 2019, pp. 405–433 (cit. on p. 30).

-
- (Giudicianni *et al.*, 2013) Paola Giudicianni, Giuseppe Cardone, and Raffaele Ragucci. “Cellulose, Hemicellulose and Lignin Slow Steam Pyrolysis: Thermal Decomposition of Biomass Components Mixtures”. *Journal of Analytical and Applied Pyrolysis* 100 (Mar. 2013), pp. 213–222 (cit. on pp. 38, 88).
- (Gøbel *et al.*, 2002) B. Gøbel, Claus Hindsgaul, U. Henriksen, and Jesper Ahrenfeldt. “High Performance Gasification with the Two-Stage Gasifier”. *12th European Biomass Conf.* (Jan. 1, 2002) (cit. on p. 35).
- (González-Vázquez *et al.*, 2018) M.P. González-Vázquez, R. García, M.V. Gil, C. Pevida, and F. Rubiera. “Unconventional Biomass Fuels for Steam Gasification: Kinetic Analysis and Effect of Ash Composition on Reactivity”. *Energy* 155 (July 2018), pp. 426–437 (cit. on p. 110).
- (Gotor *et al.*, 2000) Francisco J. Gotor, José M. Criado, Jiri Malek, and Nobuyoshi Koga. “Kinetic Analysis of Solid-State Reactions: The Universality of Master Plots for Analyzing Isothermal and Nonisothermal Experiments”. *The Journal of Physical Chemistry A* 104.46 (Nov. 1, 2000), pp. 10777–10782 (cit. on p. 86).
- (Grashoff *et al.*, 1983) G J Grashoff, C E Pilkington, and C W Corti. “The Purification of Hydrogen” (1983), p. 13 (cit. on pp. 47, 49).
- (Gu *et al.*, 2019) Haidong Gu, Yuanzheng Tang, Jian Yao, and Feng Chen. “Study on Biomass Gasification under Various Operating Conditions”. *Journal of the Energy Institute* 92.5 (Oct. 2019), pp. 1329–1336 (cit. on p. 152).
- (Gupta *et al.*, 2018) Ankita Gupta, Sonal K. Thengane, and Sanjay Mahajani. “CO₂ Gasification of Char from Lignocellulosic Garden Waste: Experimental and Kinetic Study”. *Bioresource Technology* 263 (Sept. 2018), pp. 180–191 (cit. on pp. 108, 110, 111, 138).
- (Gutiérrez Ortiz *et al.*, 2013) F.J. Gutiérrez Ortiz, A. Serrera, S. Galera, and P. Ollero. “Methanol Synthesis from Syngas Obtained by Supercritical Water Reforming of Glycerol”. *Fuel* 105 (Mar. 2013), pp. 739–751 (cit. on p. 159).
- (Hanaoka *et al.*, 2005) Toshiaki Hanaoka, Seiichi Inoue, Seiji Uno, Tomoko Ogi, and Tomoaki Minowa. “Effect of Woody Biomass Components on Air-Steam Gasification”. *Biomass and Bioenergy* 28.1 (Jan. 2005), pp. 69–76 (cit. on p. 39).
- (Hassan *et al.*, 2020) N. S. Hassan, A. A. Jalil, D. V. N. Vo, and W. Nabgan. “An Overview on the Efficiency of Biohydrogen Production from Cellulose”. *Biomass Conversion and Biorefinery* (Nov. 12, 2020) (cit. on p. 42).
- (Heidenreich *et al.*, 2015) Steffen Heidenreich and Pier Ugo Foscolo. “New Concepts in Biomass Gasification”. *Progress in Energy and Combustion Science* 46 (Feb. 2015), pp. 72–95 (cit. on pp. 34, 35).

- (Henriksen *et al.*, 2006) Ulrik Henriksen, Jesper Ahrenfeldt, Torben Kvist Jensen, Benny Gøbel, Jens Dall Bentzen, Claus Hindsgaul, and Lasse Holst Sørensen. “[The Design, Construction and Operation of a 75kW Two-Stage Gasifier](#)”. *Energy* 31.10-11 (Aug. 2006), pp. 1542–1553 (cit. on p. 35).
- (Hernández *et al.*, 2017) Simelys Hernández, M. Amin Farkhondehfal, Francesc Sastre, Michiel Makkee, Guido Saracco, and Nunzio Russo. “[Syngas Production from Electrochemical Reduction of CO₂: Current Status and Prospective Implementation](#)”. *Green Chemistry* 19.10 (May 22, 2017), pp. 2326–2346 (cit. on p. 44).
- (Hernández-Beltrán *et al.*, 2019) Javier Ulises Hernández-Beltrán, Inty Omar Hernández-De Lira, Mónica María Cruz-Santos, Alexia Saucedo-Luevanos, Fernando Hernández-Terán, and Nagamani Balagurusamy. “[Insight into Pretreatment Methods of Lignocellulosic Biomass to Increase Biogas Yield: Current State, Challenges, and Opportunities](#)”. *Applied Sciences* 9.18 (Sept. 6, 2019), p. 3721 (cit. on p. 21).
- (Hideno, 2016) Akihiro Hideno. “[Comparison of the Thermal Degradation Properties of Crystalline and Amorphous Cellulose, as Well as Treated Lignocellulosic Biomass](#)”. *BioResources* 11.3 (June 13, 2016), pp. 6309–6319 (cit. on pp. 89, 91).
- (Hietala *et al.*, 2016) Jukka Hietala, Antti Vuori, Pekka Johnsson, Ilkka Pollari, Werner Reutemann, and Heinz Kieczka. “[Formic Acid](#)”. *Ullmann’s Encyclopedia of Industrial Chemistry*. Ed. by Wiley-VCH Verlag GmbH & Co. KGaA. Weinheim, Germany: Wiley-VCH Verlag GmbH & Co. KGaA, Mar. 21, 2016, pp. 1–22 (cit. on p. 162).
- (Hofbauer *et al.*, 1997) H. Hofbauer, G. Veronik, T. Fleck, R. Rauch, H. Mackinger, and E. Fercher. “[The FICFB — Gasification Process](#)”. *Developments in Thermochemical Biomass Conversion*. Ed. by A. V. Bridgwater and D. G. B. Boocock. Dordrecht: Springer Netherlands, 1997, pp. 1016–1025 (cit. on pp. 36, 37).
- (Hoffman *et al.*, 2017) Emma Hoffman, Judith R. Guernsey, Tony R. Walker, Jong Sung Kim, Kate Sherren, and Pantelis Andreou. “[Pilot Study Investigating Ambient Air Toxics Emissions near a Canadian Kraft Pulp and Paper Facility in Pictou County, Nova Scotia](#)”. *Environmental Science and Pollution Research* 24.25 (Sept. 2017), pp. 20685–20698 (cit. on p. 25).
- (Hognon *et al.*, 2014) Céline Hognon, Capucine Dupont, Maguelone Grateau, and Florian Delrue. “[Comparison of Steam Gasification Reactivity of Algal and Lignocellulosic Biomass: Influence of Inorganic Elements](#)”. *Bioresource Technology* 164 (July 2014), pp. 347–353 (cit. on pp. 110, 111, 117, 121, 138).
- (Howard *et al.*, 2003) R.L. Howard, E. Abotsi, van Rensburg E.L. Jansen, and S. Howard. “[Lignocellulose Biotechnology: Issues of Bioconversion and Enzyme Production](#)”. *African Journal of Biotechnology* 2.12 (Dec. 31, 2003), pp. 602–619 (cit. on p. 21).
- (L. Hu *et al.*, 2019) Liqiu Hu, Haishun Du, Chao Liu, Yuedong Zhang, Guang Yu, Xinyu Zhang, Chuanling Si, Bin Li, and Hui Peng. “[Comparative Evaluation of the Efficient Conversion of Corn Husk Filament and Corn Husk Powder to Valuable Materials](#)”.

-
- via a Sustainable and Clean Biorefinery Process”. *ACS Sustainable Chemistry & Engineering* 7.1 (Jan. 7, 2019), pp. 1327–1336 (cit. on p. 73).
- (M. Hu *et al.*, 2016) Mian Hu, Zhihua Chen, Shengkai Wang, Dabin Guo, Caifeng Ma, Yan Zhou, Jian Chen, Mahmood Laghari, Saima Fazal, Bo Xiao, Beiping Zhang, and Shu Ma. “Thermogravimetric Kinetics of Lignocellulosic Biomass Slow Pyrolysis Using Distributed Activation Energy Model, Fraser–Suzuki Deconvolution, and Iso-Conversional Method”. *Energy Conversion and Management* 118 (June 2016), pp. 1–11 (cit. on p. 91).
- (Y.-F. Huang *et al.*, 2016) Yu-Fong Huang, Pei-Te Chiueh, and Shang-Lien Lo. “A Review on Microwave Pyrolysis of Lignocellulosic Biomass”. *Sustainable Environment Research* 26.3 (May 2016), pp. 103–109 (cit. on pp. 28, 29).
- (Y. Huang *et al.*, 2009) Yanqin Huang, Xiuli Yin, Chuangzhi Wu, Congwei Wang, Jianjun Xie, Zhaoqiu Zhou, Longlong Ma, and Haibin Li. “Effects of Metal Catalysts on CO₂ Gasification Reactivity of Biomass Char”. *Biotechnology Advances* (2009), p. 5 (cit. on p. 108).
- (Huo *et al.*, 2014) Wei Huo, Zhijie Zhou, Xueli Chen, Zhenghua Dai, and Guangsuo Yu. “Study on CO₂ Gasification Reactivity and Physical Characteristics of Biomass, Petroleum Coke and Coal Chars”. *Bioresource Technology* 159 (May 2014), pp. 143–149 (cit. on p. 110).
- (IEA, 2021) IEA. “International Energy Agency (IEA), Global Energy Review 2021” (2021), p. 36 (cit. on pp. 1, 11).
- (Ilyas *et al.*, 2017) R. A. Ilyas, S. M. Sapuan, M. R. Ishak, and E. S. Zainudin. “Effect of Delignification on the Physical, Thermal, Chemical, and Structural Properties of Sugar Palm Fibre”. *BioResources* 12.4 (Oct. 4, 2017), pp. 8734–8754 (cit. on p. 89).
- (Inaba *et al.*, 2006) Megumu Inaba, Kazuhisa Murata, Masahiro Saito, and Isao Takahara. “Hydrogen Production by Gasification of Cellulose over Ni Catalysts Supported on Zeolites”. *Energy & Fuels* 20.2 (Mar. 1, 2006), pp. 432–438 (cit. on pp. 41, 43).
- (International Energy Agency, 2019) International Energy Agency. “The Future of Hydrogen” (June 2019), p. 203 (cit. on p. 123).
- (IRENA, 2018) IRENA. “The International Renewable Energy Agency-Global Energy Transformation: A Roadmap to 2050” (2018), p. 76 (cit. on pp. 1, 11).
- (ISO-14687, 2019) ISO-14687. “ISO 14687:2019 - Hydrogen Fuel Quality - Product Specification” (2019) (cit. on p. 45).
- (Jafri, n.d.) Yawer Jafri. “Emerging Gasification Technologies for Waste & Biomass” (), p. 83 (cit. on p. 36).
- (Jahan, 2006) M Sarwar Jahan. “Formic Acid Pulping of Bagasse”. *Bangladesh Journal of Scientific and Industrial Research* 41.3 (2006), pp. 245–250 (cit. on p. 74).

- (Jia *et al.*, 2017) Shuang Jia, Siyun Ning, Hao Ying, Yunjuan Sun, Wei Xu, and Hang Yin. “[High Quality Syngas Production from Catalytic Gasification of Woodchip Char](#)”. *Energy Conversion and Management* 151 (Nov. 2017), pp. 457–464 (cit. on pp. 129, 141).
- (Jiang *et al.*, 2018) Long Jiang, Changyi Liu, Song Hu, Yi Wang, Kai Xu, Sheng Su, and Jun Xiang. “[Catalytic Behaviors of Alkali Metal Salt Involved in Homogeneous Volatile and Heterogeneous Char Reforming in Steam Gasification of Cellulose](#)”. *Energy Conversion and Management* 158 (Feb. 2018), pp. 147–155 (cit. on pp. 40, 43).
- (Jong *et al.*, 2011) E. de Jong, H. Langeveld, and R. van Ree. “IEA Bioenergy Task 42 Biorefinery” (2011), p. 28 (cit. on pp. 3, 14).
- (Kajita *et al.*, 2010) Makiko Kajita, Tokuji Kimura, Koyo Norinaga, Chun-Zhu Li, and Jun-ichiro Hayashi. “[Catalytic and Noncatalytic Mechanisms in Steam Gasification of Char from the Pyrolysis of Biomass [†]](#)”. *Energy & Fuels* 24.1 (Jan. 21, 2010), pp. 108–116 (cit. on pp. 108, 119).
- (Kang *et al.*, 2019) Xue Kang, Alex Kirui, Malitha C. Dickwella Widanage, Frederic Mentink-Vigier, Daniel J. Cosgrove, and Tuo Wang. “[Lignin-Polysaccharide Interactions in Plant Secondary Cell Walls Revealed by Solid-State NMR](#)”. *Nature Communications* 10.1 (Dec. 2019), p. 347 (cit. on p. 74).
- (Kaur *et al.*, 2019) Ravneet Kaur, Poonam Gera, Mithilesh Kumar Jha, and Thallada Bhaskar. “[Thermochemical Route for Biohydrogen Production](#)”. *Biohydrogen*. Elsevier, 2019, pp. 187–218 (cit. on p. 29).
- (Kaushal *et al.*, 2017) Priyanka Kaushal and Rakesh Tyagi. “[Advanced Simulation of Biomass Gasification in a Fluidized Bed Reactor Using ASPEN PLUS](#)”. *Renewable Energy* 101 (Feb. 2017), pp. 629–636 (cit. on p. 152).
- (Kemp, 2007) Ian C. Kemp. *Pinch Analysis and Process Integration: A User Guide on Process Integration for the Efficient Use of Energy*. 2nd ed. Amsterdam ; Boston: Butterworth-Heinemann, 2007. 396 pp. (cit. on p. 159).
- (Khalid *et al.*, 2017) Khalidatul Athirah Khalid, Asimi Ana Ahmad, and Tau Len-Kelly Yong. “[Lignin Extraction from Lignocellulosic Biomass Using Sub- and Supercritical Fluid Technology as Precursor for Carbon Fiber Production](#)”. *Journal of the Japan Institute of Energy* 96.8 (2017), pp. 255–260 (cit. on p. 21).
- (Kin Wai Cheah *et al.*, 2022) Kin Wai Cheah, Martin J. Taylor, Geraint Evans, Abby Samson, and Vasiliki Skoulou. “[Overview of Biomass Conversion to Biofuels - ScienceDirect](#)” (cit. on p. 29).
- (Klinghoffer, 2013) Naomi Klinghoffer. “[Utilization of Char from Biomass Gasification in Catalytic Applications](#)”. Columbia University, 2013 (cit. on p. 66).

-
- (Knudsen *et al.*, 2004) Jacob N. Knudsen, Peter A. Jensen, and Kim Dam-Johansen. “Transformation and Release to the Gas Phase of Cl, K, and S during Combustion of Annual Biomass”. *Energy & Fuels* 18.5 (Sept. 1, 2004), pp. 1385–1399 (cit. on p. 143).
- (Kramb *et al.*, 2016) Jason Kramb, Nikolai DeMartini, Magnus Perander, Antero Moilanen, and Jukka Konttinen. “Modeling of the Catalytic Effects of Potassium and Calcium on Spruce Wood Gasification in CO₂”. *Fuel Processing Technology* 148 (July 2016), pp. 50–59 (cit. on p. 114).
- (Hoang Quoc Lam *et al.*, 2001) Hoang Quoc Lam, Yves Le Bigot, Michel Delmas, and et Gérard Avignon. “Formic Acid Pulping of Rice Straw”. *Industrial Crops and Products* 14.1 (July 2001), pp. 65–71 (cit. on pp. 26, 74).
- (Huang Quoc Lam *et al.*, 2005) Huang Quoc Lam, Yves Le Bigot, Denis Ghislain, Vo Huu Thao, and Michel Delmas. “Location and Composition of Silicon Derivatives in Rice Straw Pulp Obtained by Organic Acid Pulping”. 58.3 (May 2005), p. 4 (cit. on p. 76).
- (Larsson *et al.*, 2021) Anton Larsson, Matthias Kuba, Teresa Berdugo Vilches, Martin Seemann, Hermann Hofbauer, and Henrik Thunman. “Steam Gasification of Biomass – Typical Gas Quality and Operational Strategies Derived from Industrial-Scale Plants”. *Fuel Processing Technology* 212 (Feb. 2021), p. 106609 (cit. on p. 143).
- (Le *et al.*, 2015) C.D. Le and S.T. Kolaczkowski. “Steam Gasification of a Refuse Derived Char: Reactivity and Kinetics”. *Chemical Engineering Research and Design* 102 (Oct. 2015), pp. 389–398 (cit. on p. 116).
- (Lersch, 2009) Martin Lersch. “Creating Value from Wood – The Borregaard Biorefinery” (2009), p. 6 (cit. on pp. 3, 14).
- (C. Li *et al.*, 2021) Chao Li, Yifan Sun, Dehua Dong, Guanggang Gao, Shu Zhang, Yi Wang, Jun Xiang, Song Hu, Gholizadeh Mortaza, and Xun Hu. “Co-Pyrolysis of Cellulose/Lignin and Sawdust: Influence of Secondary Condensation of the Volatiles on Characteristics of Biochar”. *Energy* 226 (July 2021), p. 120442 (cit. on pp. 38, 125).
- (Z. Li *et al.*, 2008) Zhengqi Li, Wei Zhao, Baihong Meng, Chunlong Liu, Qunyi Zhu, and Guangbo Zhao. “Kinetic Study of Corn Straw Pyrolysis: Comparison of Two Different Three-Pseudocomponent Models”. *Bioresource Technology* 99.16 (Nov. 2008), pp. 7616–7622 (cit. on p. 91).
- (Lin *et al.*, 2013) Leteng Lin and Michael Strand. “Investigation of the Intrinsic CO₂ Gasification Kinetics of Biomass Char at Medium to High Temperatures”. *Applied Energy* 109 (Sept. 2013), pp. 220–228 (cit. on p. 110).
- (Linde, 2022) Linde. “CO Shift Conversion” () (cit. on pp. 47, 159).
- (Lindemann *et al.*, 2017) Martin Lindemann, Anton Friedl, and Ewald Srebotnik. “Enhanced Cellulose Degradation of Wheat Straw during Aqueous Ethanol Organosolv Treatment”. *BioResources* 12.4 (Oct. 30, 2017), pp. 9407–9419 (cit. on p. 74).

- (Link *et al.*, 2010) Siim Link, Stelios Arvelakis, Mikko Hupa, Patrik Yrjas, Indrek Külaots, and Aadu Paist. “[Reactivity of the Biomass Chars Originating from Reed, Douglas Fir, and Pine](#)”. *Energy & Fuels* 24.12 (Dec. 16, 2010), pp. 6533–6539 (cit. on p. 108).
- (Q. Liu *et al.*, 2017) Qiaoming Liu, Stephen C. Chmely, and Nourredine Abdoulmoumine. “[Biomass Treatment Strategies for Thermochemical Conversion](#)”. *Energy & Fuels* 31.4 (Apr. 20, 2017), pp. 3525–3536 (cit. on pp. 76, 143).
- (T. Liu *et al.*, 2008) T Liu, Y Fang, and Y Wang. “[An Experimental Investigation into the Gasification Reactivity of Chars Prepared at High Temperatures](#)”. *Fuel* 87.4-5 (Apr. 2008), pp. 460–466 (cit. on p. 108).
- (Z. Liu *et al.*, 2022) Zhu Liu, Zhu Deng, Steven J. Davis, Clement Giron, and Philippe Ciais. “[Monitoring Global Carbon Emissions in 2021](#)”. *Nature Reviews Earth & Environment* 3.4 (Apr. 2022), pp. 217–219 (cit. on p. 11).
- (Long *et al.*, 2013) Huiling Long, Xiaobing Li, Hong Wang, and Jingdun Jia. “[Biomass Resources and Their Bioenergy Potential Estimation: A Review](#)”. *Renewable and Sustainable Energy Reviews* 26 (Oct. 2013), pp. 344–352 (cit. on pp. 2, 14).
- (López-González *et al.*, 2014) D. López-González, M. Fernandez-Lopez, J.L. Valverde, and L. Sanchez-Silva. “[Gasification of Lignocellulosic Biomass Char Obtained from Pyrolysis: Kinetic and Evolved Gas Analyses](#)”. *Energy* 71 (July 2014), pp. 456–467 (cit. on pp. 110, 114).
- (Lotfi, 2021) Samira Lotfi. “[Technologies for Tar Removal from Biomass-Derived Syngas](#)”. *Petroleum & Petrochemical Engineering Journal* 5.3 (2021), pp. 1–35 (cit. on p. 45).
- (Lu *et al.*, 2021) Guanghua Lu, Yonghui Bai, Peng Lv, Jiaofei Wang, Xudong Song, Weiguang Su, and Guangsuo Yu. “[Insights into the Role of Calcium during Coal Gasification in the Presence of Silicon and Aluminum](#)”. *Fuel* 302 (Oct. 2021), p. 121134 (cit. on p. 139).
- (Lu *et al.*, 2022) Guanghua Lu, Yonghui Bai, Peng Lv, Jiaofei Wang, Xudong Song, Weiguang Su, and Guangsuo Yu. “[Ca-Si-Al Interactions Induced Char Structure and Active Site Evolution during Gasification—A Comparative Study Based on Different Gasifying Agent](#)”. *Fuel* 316 (May 2022), p. 123382 (cit. on pp. 111, 138, 139).
- (L. Luo *et al.*, 2021) Laipeng Luo, Zhiyi Zhang, Chong Li, Nishu, Fang He, Xingguang Zhang, and Junmeng Cai. “[Insight into Master Plots Method for Kinetic Analysis of Lignocellulosic Biomass Pyrolysis](#)”. *Energy* 233 (Oct. 2021), p. 121194 (cit. on p. 87).
- (S. Luo *et al.*, 2009) S Luo, B Xiao, X Guo, Z Hu, S Liu, and M He. “[Hydrogen-Rich Gas from Catalytic Steam Gasification of Biomass in a Fixed Bed Reactor: Influence of Particle Size on Gasification Performance](#)”. *International Journal of Hydrogen Energy* 34.3 (Feb. 2009), pp. 1260–1264 (cit. on p. 43).

-
- (D. Lv *et al.*, 2010) Dangzhen Lv, Minghou Xu, Xiaowei Liu, Zhonghua Zhan, Zhiyuan Li, and Hong Yao. “Effect of Cellulose, Lignin, Alkali and Alkaline Earth Metallic Species on Biomass Pyrolysis and Gasification”. *Fuel Processing Technology* 91.8 (Aug. 2010), pp. 903–909 (cit. on pp. 37, 88, 125).
- (P. Lv *et al.*, 2018) Peng Lv, Yonghui Bai, Xuhao Yang, Meiqi Gao, Weiren Bao, and Fan Li. “Impacts of Char Structure Evolution and Inherent Alkali and Alkaline Earth Metallic Species Catalysis on Reactivity during the Coal Char Gasification with CO₂/H₂O”. *International Journal of Energy Research* 42.11 (Sept. 2018), pp. 3633–3642 (cit. on p. 139).
- (Lyu *et al.*, 2015) Gaojin Lyu, Shubin Wu, and Hongdan Zhang. “Estimation and Comparison of Bio-Oil Components from Different Pyrolysis Conditions”. *Frontiers in Energy Research* 3 (June 15, 2015) (cit. on p. 125).
- (Ma *et al.*, 2013) Z. Ma, S. Zhang, D. Xie, Y. Yan, and Z. Ren. “Hydrogen Production from Bio-Char via Steam Gasification in a Fluidized-Bed Reactor”. *Chemical Engineering & Technology* 36.9 (Sept. 2013), pp. 1599–1602 (cit. on pp. 132, 133).
- (Magoua Mbeugang *et al.*, 2021) Christian Fabrice Magoua Mbeugang, Bin Li, Dan Lin, Xing Xie, Shuaijun Wang, Shuang Wang, Shu Zhang, Yong Huang, Dongjing Liu, and Qian Wang. “Hydrogen Rich Syngas Production from Sorption Enhanced Gasification of Cellulose in the Presence of Calcium Oxide”. *Energy* 228 (Aug. 2021), p. 120659 (cit. on pp. 40, 43).
- (Malkov, 2001) Sergei Malkov. “Towards Complete Impregnation of Wood Chips with Aqueous Solutions” (2001), p. 14 (cit. on p. 75).
- (Mamleev *et al.*, 2007) Vadim Mamleev, Serge Bourbigot, and Jacques Yvon. “Kinetic Analysis of the Thermal Decomposition of Cellulose: The Main Step of Mass Loss”. *Journal of Analytical and Applied Pyrolysis* 80.1 (Aug. 2007), pp. 151–165 (cit. on p. 97).
- (Mandeep *et al.*, 2019) Mandeep, Guddu Kumar Gupta, Hao Liu, and Pratyosh Shukla. “Pulp and Paper Industry–Based Pollutants, Their Health Hazards and Environmental Risks”. *Current Opinion in Environmental Science & Health* 12 (Dec. 2019), pp. 48–56 (cit. on p. 25).
- (Mandlekar *et al.*, 2018) Neeraj Mandlekar, Aurélie Cayla, François Rault, Stéphane Giraud, Fabine Salaün, Giulio Malucelli, and Jin-Ping Guan. “An Overview on the Use of Lignin and Its Derivatives in Fire Retardant Polymer Systems”. *Lignin - Trends and Applications*. Ed. by Matheus Poletto. InTech, Mar. 21, 2018 (cit. on p. 24).
- (Marquez-Montesinos *et al.*, 2002) F Marquez-Montesinos, T Cordero, J Rodríguez-Mirasol, and J J Rodríguez. “CO₂ and Steam Gasification of a Grapefruit Skin Char” (2002), p. 7 (cit. on p. 119).

- (Mathew *et al.*, 2018) Anil K. Mathew, Amith Abraham, Kiran Kumar Mallapureddy, and Rajeev K. Sukumaran. “Lignocellulosic Biorefinery Wastes, or Resources?” *Waste Biorefinery*. Elsevier, 2018, pp. 267–297 (cit. on p. 24).
- (Matsukata *et al.*, 1988) M. Matsukata, T. Fujikawa, E. Kikuchi, and Y. Morita. “Interaction between Potassium Carbonate and Carbon Substrate at Subgasification Temperatures. Migration of Potassium into the Carbon Matrix”. *Energy & Fuels* 2.6 (Nov. 1, 1988), pp. 750–756 (cit. on p. 138).
- (Mboowa, 2021) Drake Mboowa. “A Review of the Traditional Pulping Methods and the Recent Improvements in the Pulping Processes”. *Biomass Conversion and Biorefinery* (Jan. 3, 2021) (cit. on p. 24).
- (McKee, 1983) Douglas W. McKee. “Mechanisms of the Alkali Metal Catalysed Gasification of Carbon”. *Fuel* 62.2 (Feb. 1983), pp. 170–175 (cit. on p. 138).
- (Mednikov, 2018) A S Mednikov. “A Review of Technologies for Multistage Wood Biomass Gasification”. 65.8 (2018), p. 16 (cit. on pp. 35, 37).
- (Meijden *et al.*, 2010) van der Meijden and C.M. *Development of the MILENA gasification technology for the production of Bio-SNG*. Technische Universiteit Eindhoven, 2010 (cit. on p. 32).
- (Millan, 2018) Lina Maria Romero Millan. “Steam Gasification of Tropical Lignocellulosic Agrowaste : Impact of Biomass Characteristics on the Gaseous and Solid by-Products”. PhD thesis. Ecole des Mines d’Albi-Carmaux ; Universidad nacional de Colombia, Nov. 28, 2018 (cit. on p. 39).
- (Milne *et al.*, 1998) T A Milne, R J Evans, and N Abatzaglou. *Biomass Gasifier "Tars": Their Nature, Formation, and Conversion*. NREL/TP-570-25357, ON: DE00003726, 3726. Nov. 1, 1998, NREL/TP-570–25357, ON: DE00003726, 3726 (cit. on p. 30).
- (Mishra, 2021) Somya Mishra. “Review on Biomass Gasification: Gasifiers, Gasifying Mediums, and Operational Parameters” (2021), p. 12 (cit. on p. 32).
- (Mitsuoka *et al.*, 2011) Keiichirou Mitsuoka, Shigeya Hayashi, Hiroshi Amano, Kenji Kayahara, Eiji Sasaoaka, and Md. Azhar Uddin. “Gasification of Woody Biomass Char with CO₂: The Catalytic Effects of K and Ca Species on Char Gasification Reactivity”. *Fuel Processing Technology* 92.1 (Jan. 2011), pp. 26–31 (cit. on p. 119).
- (Moilanen *et al.*, 2011) Antero Moilanen, Muhammad Nasrullah, and Valtion teknillinen tutkimuskeskus. *Gasification Reactivity and Ash Sintering Behaviour of Biomass Feedstocks*. Kuopio: Kopijyv?? Oy, 2011 (cit. on p. 30).
- (Molino *et al.*, 2016) Antonio Molino, Simeone Chianese, and Dino Musmarra. “Biomass Gasification Technology: The State of the Art Overview”. *Journal of Energy Chemistry* 25.1 (Jan. 2016), pp. 10–25 (cit. on pp. 29, 30, 32, 41).
- (Molino *et al.*, 2018) Antonio Molino, Vincenzo Larocca, Simeone Chianese, and Dino Musmarra. “Biofuels Production by Biomass Gasification: A Review”. *Energies* 11.4 (Mar. 31, 2018), p. 811 (cit. on pp. 32, 39, 44).

-
- (Moreira, 2021) Rui Moreira. “Clean Syngas Production by Gasification of Lignocellulosic Char: State of the Art and Future Prospects”. *Journal of Industrial and Engineering Chemistry* (2021), p. 20 (cit. on p. 34).
- (Morf Philipp Oliver, 2001) Morf Philipp Oliver. “Secondary Reactions of Tar during Thermochemical Biomass Conversion” (2001) (cit. on p. 125).
- (Mortha *et al.*, 2016) Gérard Mortha and Anne-Laurence Dupont. « [Chimie des procédés de fabrication des pâtes lignocellulosiques écrues](#) ». *Bois et papiers* (Jan. 2016) (cit. on p. 76).
- (Muradov *et al.*, 2015) Nazim Muradov, Amit Gujar, Jong Baik, and Ali T-Raissi. “Production of Fischer–Tropsch Hydrocarbons via Oxygen-Blown Gasification of Charred Pinewood Pellets”. *Fuel Processing Technology* 140 (Dec. 2015), pp. 236–244 (cit. on p. 124).
- (Naqvi *et al.*, 2012) M. Naqvi, J. Yan, and E. Dahlquist. “Energy Conversion Performance of Black Liquor Gasification to Hydrogen Production Using Direct Causticization with CO₂ Capture”. *Bioresource Technology* 110 (Apr. 2012), pp. 637–644 (cit. on p. 25).
- (Nikoo *et al.*, 2008) Mehrdokht B. Nikoo and Nader Mahinpey. “Simulation of Biomass Gasification in Fluidized Bed Reactor Using ASPEN PLUS”. *Biomass and Bioenergy* 32.12 (Dec. 2008), pp. 1245–1254 (cit. on p. 152).
- (Ning *et al.*, 2018) Siyun Ning, Shuang Jia, Hao Ying, Yunjuan Sun, Wei Xu, and Hang Yin. “Hydrogen-Rich Syngas Produced by Catalytic Steam Gasification of Corncob Char”. *Biomass and Bioenergy* 117 (Oct. 2018), pp. 131–136 (cit. on pp. 124, 133, 136).
- (Noda *et al.*, 2009) Reiji Noda, Tomoyuki Ito, Nao Tanaka, and Masayuki Horio. “Steam Gasification of Cellulose and Wood in a Fluidized Bed of Porous Clay Particles”. *JOURNAL OF CHEMICAL ENGINEERING OF JAPAN* 42.7 (2009), pp. 490–501 (cit. on p. 41).
- (Novo *et al.*, 2011) Lísias Pereira Novo, Leandro Vinícius Alves Gurgel, Karen Marabezi, and Antonio Aprigio da Silva Curvelo. “Delignification of Sugarcane Bagasse Using Glycerol–Water Mixtures to Produce Pulp for Saccharification”. *Bioresource Technology* 102.21 (Nov. 2011), pp. 10040–10046 (cit. on p. 26).
- (Nutalapati *et al.*, 2007) D Nutalapati, R Gupta, B Moghtaderi, and T F Wall. “Assessing Slagging and Fouling during Biomass Combustion: A Thermodynamic Approach Allowing for Alkali/Ash Reactions”. *Fuel Processing Technology* (2007), p. 9 (cit. on p. 143).
- (Nzihou *et al.*, 2021) Ange Nzihou, María Gonzalez Martinez, Doan Pham Minh, Lina María Romero Millan, and Yves Gourinat. « [L’hydrogène vert en aéronautique - Production](#) ». *Systèmes aéronautiques et spatiaux* (Sept. 2021) (cit. on p. 47).

- (Nzihou *et al.*, 2013a) Ange Nzihou and Brian Stanmore. “[The Fate of Heavy Metals during Combustion and Gasification of Contaminated Biomass—A Brief Review](#)”. *Journal of Hazardous Materials* 256–257 (July 2013), pp. 56–66 (cit. on p. 104).
- (Nzihou *et al.*, 2013b) Ange Nzihou, Brian Stanmore, and Patrick Sharrock. “[A Review of Catalysts for the Gasification of Biomass Char, with Some Reference to Coal](#)”. *Energy* 58 (Sept. 2013), pp. 305–317 (cit. on pp. 80, 108, 138).
- (O’Hayre *et al.*, 2016) Ryan P. O’Hayre, Suk-Won Cha, Whitney G. Colella, and F. B. Prinz. *Fuel Cell Fundamentals*. Third edition. Hoboken, New Jersey: John Wiley & Sons Inc, 2016. 1 p. (cit. on p. 136).
- (Owi *et al.*, 2016) Wei Tieng Owi, Ong Hui Lin, Sung Ting Sam, Chin Hua Chia, Sarani Zakaria, Muhammad Safwan Mohaiyiddin, Al Rey Villagrancia, Gil Nonato Santos, and Hazizan Md Akil. “[Comparative Study of Microcelluloses Isolated From Two Different Biomasses with Commercial Cellulose](#)”. *BioResources* 11.2 (Feb. 22, 2016), pp. 3453–3465 (cit. on p. 89).
- (Paasikallio *et al.*, 2013) Ville Paasikallio, Christian Lindfors, Jani Lehto, Anja Oasmaa, and Matti Reinikainen. “[Short Vapour Residence Time Catalytic Pyrolysis of Spruce Sawdust in a Bubbling Fluidized-Bed Reactor with HZSM-5 Catalysts](#)”. *Topics in Catalysis* 56.9-10 (June 2013), pp. 800–812 (cit. on p. 29).
- (Pala *et al.*, 2017) Laxmi Prasad Rao Pala, Qi Wang, Gunther Kolb, and Volker Hessel. “[Steam Gasification of Biomass with Subsequent Syngas Adjustment Using Shift Reaction for Syngas Production: An Aspen Plus Model](#)”. *Renewable Energy* 101 (Feb. 2017), pp. 484–492 (cit. on p. 152).
- (Pan *et al.*, 2005) Xuejun Pan and Yoshihiro Sano. “[Fractionation of Wheat Straw by Atmospheric Acetic Acid Process](#)”. *Bioresource Technology* 96.11 (July 2005), pp. 1256–1263 (cit. on p. 76).
- (Panshin, 1980) A.J. Panshin. *Textbook of Wood Technology. Structure, Identification, Properties, and Uses of the Commercial Woods of the United States and Canada*. 1980 (cit. on p. 75).
- (Parisi, 2018) Claudia Parisi. “[Research Brief: Biorefineries Distribution in the EU](#)”. *European Commission - Joint Research Centre* (2018) (cit. on p. 23).
- (S. Park *et al.*, 2010) Sunkyu Park, John O Baker, Michael E Himmel, Philip A Parilla, and David K Johnson. “Cellulose Crystallinity Index: Measurement Techniques and Their Impact on Interpreting Cellulase Performance” (2010), p. 10 (cit. on pp. 89, 101).
- (Y.-K. Park *et al.*, 2014) Young-Kwon Park, Kyung Sun Park, Seong-Soo Kim, Sung Hoon Park, Sang-Chul Jung, Sang Chai Kim, Jong-Ki Jeon, and Ki-Joon Jeon. “[Conversion of Cellulose over Ni Loaded Mesoporous MSU-F Catalysts via Air Gasification](#)”. *Bulletin of the Korean Chemical Society* 35.11 (2014), pp. 3205–3208 (cit. on p. 41).

-
- (Parthasarathy *et al.*, 2014) Prakash Parthasarathy and K. Sheeba Narayanan. “Hydrogen Production from Steam Gasification of Biomass: Influence of Process Parameters on Hydrogen Yield – A Review”. *Renewable Energy* 66 (June 2014), pp. 570–579 (cit. on pp. 2, 14, 123).
- (Paszner, 1989) Laszlo Paszner. “Topochemistry of Softwood Delignification by Alkali Earth Metal Salt Catalysed Organosolv Pulping”. *Holzforschung* 43.3 (Jan. 1989), pp. 159–168 (cit. on p. 75).
- (Patel *et al.*, 1991) M. Patel and A. Karera. “SiC Whisker from Rice Husk: Microscopic Study”. *Powder Metallurgy International; (Germany, F.R.)* 23:1 (Jan. 1, 1991) (cit. on p. 76).
- (Pathak *et al.*, 2021) Puneet Pathak, Ankush Gupta, Nishi Kant Bhardwaj, Arun Goyal, and Vijayanand Suryakant Moholkar. “Impact of Mild and Harsh Conditions of Formic Acid-Based Organosolv Pretreatment on Biomass Fractionation of Sugarcane Tops”. *Biomass Conversion and Biorefinery* 11.5 (Oct. 2021), pp. 2027–2040 (cit. on p. 74).
- (Pflieger, 2021) Christin Pflieger. “Catalytic Influence of Mineral Compounds on the Reactivity of Cellulose-Derived Char in O₂-, CO₂-, and H₂O-containing Atmospheres” (2021), p. 11 (cit. on p. 108).
- (Pham Minh *et al.*, 2020) Doan Pham Minh *et al.* “Generic and Advanced Characterization Techniques”. *Handbook on Characterization of Biomass, Biowaste and Related By-products*. Ed. by Ange Nzihou. Cham: Springer International Publishing, 2020, pp. 31–497 (cit. on pp. 57, 86, 106).
- (Phan *et al.*, 2018) Thanh Son Phan, Abdoul Razac Sane, Bruna Rêgo de Vasconcelos, Ange Nzihou, Patrick Sharrock, Didier Grouset, and Doan Pham Minh. “Hydroxyapatite Supported Bimetallic Cobalt and Nickel Catalysts for Syngas Production from Dry Reforming of Methane”. *Applied Catalysis B: Environmental* 224 (May 2018), pp. 310–321 (cit. on p. 141).
- (Phounglamcheik *et al.*, 2017) Aekjuthon Phounglamcheik, Matthaus U. Babler, Pawel Donaj, Marko Amovic, Rolf Ljunggren, and Klas Engvall. “Pyrolysis of Wood in a Rotary Kiln Pyrolyzer: Modeling and Pilot Plant Trials”. *Energy Procedia* 105 (May 2017), pp. 908–913 (cit. on p. 35).
- (Pinto *et al.*, 2003) Filomena Pinto, Carlos Franco, Rui Neto Andre, C Tavares, M Dias, I Gulyurtlu, and I Cabrita. “Effect of Experimental Conditions on Co-Gasification of Coal, Biomass and Plastics Wastes with Air/Steam Mixtures in a Fluidized Bed Systemq” (2003), p. 10 (cit. on p. 133).
- (Popp *et al.*, 2021) József Popp, Sándor Kovács, Judit Oláh, Zoltán Divéki, and Ervin Balázs. “Bioeconomy: Biomass and Biomass-Based Energy Supply and Demand”. *New Biotechnology* 60 (Jan. 2021), pp. 76–84 (cit. on pp. 2, 12).

- (Porbatzki *et al.*, 2011) Dirk Porbatzki, Michael Stemmler, and Michael Müller. “[Release of Inorganic Trace Elements during Gasification of Wood, Straw, and Miscanthus](#)”. *Biomass and Bioenergy* 35 (Oct. 2011), S79–S86 (cit. on p. 143).
- (Prestipino *et al.*, 2018) M. Prestipino, A. Galvagno, O. Karlström, and A. Brink. “[Energy Conversion of Agricultural Biomass Char: Steam Gasification Kinetics](#)”. *Energy* 161 (Oct. 2018), pp. 1055–1063 (cit. on p. 110).
- (Pröll *et al.*, n.d.) Tobias Pröll, Reinhard Rauch, Christian Aichernig, and Hermann Hofbauer. “PERFORMANCE CHARACTERISTICS OF AN 8 MWth Combined heat and power plant based on dual fluidized bed steam gasification of solid biomass” (), p. 9 (cit. on p. 35).
- (Qu *et al.*, 2011) Tingting Qu, Wanjun Guo, Laihong Shen, Jun Xiao, and Kun Zhao. “[Experimental Study of Biomass Pyrolysis Based on Three Major Components: Hemicellulose, Cellulose, and Lignin](#)”. *Industrial & Engineering Chemistry Research* 50.18 (Sept. 21, 2011), pp. 10424–10433 (cit. on pp. 38, 125).
- (Quan *et al.*, 2016) Cui Quan, Ningbo Gao, and Qingbin Song. “[Pyrolysis of Biomass Components in a TGA and a Fixed-Bed Reactor: Thermochemical Behaviors, Kinetics, and Product Characterization](#)”. *Journal of Analytical and Applied Pyrolysis* 121 (Sept. 2016), pp. 84–92 (cit. on pp. 38, 125).
- (Quoc Lam *et al.*, 2001) Hoang Quoc Lam, Yves Le Bigot, Michel Delmas, and Gérard Avignon. “[A New Procedure for the Destructuring of Vegetable Matter at Atmospheric Pressure by a Catalyst/Solvent System of Formic Acid/Acetic Acid. Applied to the Pulping of Triticale Straw](#)”. *Industrial Crops and Products* 14.2 (Sept. 2001), pp. 139–144 (cit. on pp. 74, 76).
- (Qureshi *et al.*, 2021) Khan Muhammad Qureshi, Andrew Ng Kay Lup, Saima Khan, Faisal Abnisa, and Wan Mohd Ashri Wan Daud. “[Optimization of Palm Shell Pyrolysis Parameters in Helical Screw Fluidized Bed Reactor: Effect of Particle Size, Pyrolysis Time and Vapor Residence Time](#)”. *Cleaner Engineering and Technology* 4 (Oct. 2021), p. 100174 (cit. on p. 29).
- (Rauch *et al.*, 2014) Reinhard Rauch, Jitka Hrbek, and Hermann Hofbauer. “[Biomass Gasification for Synthesis Gas Production and Applications of the Syngas: Biomass Gasification for Synthesis Gas Production](#)”. *Wiley Interdisciplinary Reviews: Energy and Environment* 3.4 (July 2014), pp. 343–362 (cit. on pp. 30, 44).
- (Rego de Vasconcelos *et al.*, 2020) Bruna Rego de Vasconcelos, Doan Pham Minh, Emmanuel Martins, Alain Germeau, Patrick Sharrock, and Ange Nzihou. “[Highly-Efficient Hydroxyapatite-Supported Nickel Catalysts for Dry Reforming of Methane](#)”. *International Journal of Hydrogen Energy* 45.36 (July 2020), pp. 18502–18518 (cit. on p. 141).

-
- (Ren *et al.*, 2019) Jie Ren, Jing-Pei Cao, Xiao-Yan Zhao, Fei-Long Yang, and Xian-Yong Wei. “Recent Advances in Syngas Production from Biomass Catalytic Gasification: A Critical Review on Reactors, Catalysts, Catalytic Mechanisms and Mathematical Models”. *Renewable and Sustainable Energy Reviews* 116 (Dec. 2019), p. 109426 (cit. on pp. 32, 33).
- (Richardson *et al.*, 2012) Yohan Richardson, Joël Blin, and Anne Julbe. “A Short Overview on Purification and Conditioning of Syngas Produced by Biomass Gasification: Catalytic Strategies, Process Intensification and New Concepts”. *Progress in Energy and Combustion Science* 38.6 (Dec. 2012), pp. 765–781 (cit. on pp. 3, 14).
- (Rizvi *et al.*, 2015) T. Rizvi, P. Xing, M. Pourkashanian, L.I. Darvell, J.M. Jones, and W. Nimmo. “Prediction of Biomass Ash Fusion Behaviour by the Use of Detailed Characterisation Methods Coupled with Thermodynamic Analysis”. *Fuel* 141 (Feb. 2015), pp. 275–284 (cit. on p. 144).
- (Rocca *et al.*, 1999) P A Della Rocca, E G Cerrella, P R Bonelli, and A L Cukierman. “Pyrolysis of Hardwoods Residues: On Kinetics and Chars Characterization”. *Biomass and Bioenergy* (1999), p. 10 (cit. on p. 112).
- (Romero Millán *et al.*, 2017) Lina María Romero Millán, Fabio Emiro Sierra Vargas, and Ange Nzihou. “Kinetic Analysis of Tropical Lignocellulosic Agrowaste Pyrolysis”. *BioEnergy Research* 10.3 (Sept. 2017), pp. 832–845 (cit. on pp. 85, 91, 93, 99).
- (Romero Millán *et al.*, 2019) Lina María Romero Millán, Fabio Emiro Sierra Vargas, and Ange Nzihou. “Steam Gasification Behavior of Tropical Agrowaste: A New Modeling Approach Based on the Inorganic Composition”. *Fuel* 235 (Jan. 2019), pp. 45–53 (cit. on pp. 109, 110, 114, 116, 117, 121).
- (Romero Millán *et al.*, 2021) Lina María Romero Millán, Fabio Emiro Sierra Vargas, and Ange Nzihou. “Unraveled Mechanisms in Energy Production from Bioresources Using Steam Gasification”. *Fuel* 287 (Mar. 2021), p. 119527 (cit. on p. 133).
- (Ruiz *et al.*, 2011) Héctor A. Ruiz, Denise S. Ruzene, Daniel P. Silva, Fernando F. Macieira da Silva, António A. Vicente, and José A. Teixeira. “Development and Characterization of an Environmentally Friendly Process Sequence (Autohydrolysis and Organosolv) for Wheat Straw Delignification”. *Applied Biochemistry and Biotechnology* 164.5 (July 2011), pp. 629–641 (cit. on p. 25).
- (Salaudeen *et al.*, 2020) Shakirudeen A. Salaudeen, Bishnu Acharya, Mohammad Heidari, Sultan M. Al-Salem, and Animesh Dutta. “Hydrogen-Rich Gas Stream from Steam Gasification of Biomass: Eggshell as a CO₂ Sorbent”. *Energy & Fuels* 34.4 (Apr. 16, 2020), pp. 4828–4836 (cit. on p. 132).
- (Salmén, 2004) Lennart Salmén. “Micromechanical Understanding of the Cell-Wall Structure”. *Comptes Rendus Biologies* 327.9-10 (Sept. 2004), pp. 873–880 (cit. on p. 75).

- (Salmén *et al.*, 2008) Lennart Salmén and Ingo Burgert. “Cell Wall Features with Regard to Mechanical Performance. A Review COST Action E35 2004–2008: Wood Machining–Micromechanics and Fracture” (Sept. 12, 2008) (cit. on p. 75).
- (Samuelsson, 2015) Lina N Samuelsson. “Model-Free Rate Expression for Thermal Decomposition Processes: The Case of Microcrystalline Cellulose Pyrolysis” (2015), p. 10 (cit. on p. 91).
- (Sánchez-Jiménez *et al.*, 2013) Pedro E. Sánchez-Jiménez, Luis A. Pérez-Maqueda, Antonio Perejón, and José M. Criado. “Generalized Master Plots as a Straightforward Approach for Determining the Kinetic Model: The Case of Cellulose Pyrolysis”. *Thermochimica Acta* 552 (Jan. 2013), pp. 54–59 (cit. on pp. 86, 96, 97, 99, 106).
- (Sánchez-Jiménez *et al.*, 2011) Pedro E. Sánchez-Jiménez, Luis A. Pérez-Maqueda, Antonio Perejón, José Pascual-Cosp, Mónica Benítez-Guerrero, and José M. Criado. “An Improved Model for the Kinetic Description of the Thermal Degradation of Cellulose”. *Cellulose* 18.6 (Dec. 2011), pp. 1487–1498 (cit. on pp. 93, 97).
- (Sansaniwal *et al.*, 2017) S.K. Sansaniwal, K. Pal, M.A. Rosen, and S.K. Tyagi. “Recent Advances in the Development of Biomass Gasification Technology: A Comprehensive Review”. *Renewable and Sustainable Energy Reviews* 72 (May 2017), pp. 363–384 (cit. on p. 32).
- (Sattar *et al.*, 2014) Anwar Sattar, Gary A. Leeke, Andreas Hornung, and Joseph Wood. “Steam Gasification of Rapeseed, Wood, Sewage Sludge and Miscanthus Biochars for the Production of a Hydrogen-Rich Syngas”. *Biomass and Bioenergy* 69 (Oct. 2014), pp. 276–286 (cit. on pp. 124, 133).
- (Schmetz *et al.*, 2016) Quentin Schmetz, Guillaume Maniet, Nicolas Jacquet, Hiroshi Teramura, Chiaki Ogino, Akihiko Kondo, and Aurore Richel. “Comprehension of an Organosolv Process for Lignin Extraction on Festuca Arundinacea and Monitoring of the Cellulose Degradation”. *Industrial Crops and Products* 94 (Dec. 2016), pp. 308–317 (cit. on p. 74).
- (Seo *et al.*, 2018) Yong-Chil Seo, Md Tanvir Alam, and Won-Seok Yang. “Gasification of Municipal Solid Waste”. *Gasification for Low-grade Feedstock*. Ed. by Yongseung Yun. InTech, July 11, 2018 (cit. on p. 31).
- (Șerbănescu, 2014) Cristina Șerbănescu. “Kinetic Analysis of Cellulose Pyrolysis: A Short Review”. *Chemical Papers* 68.7 (Jan. 1, 2014) (cit. on pp. 97, 99).
- (Shah, 2021) Minish Shah. “Hydrogen Purification Technologies Overview 2021 ARPA-E Methane Pyrolysis Annual Program Review Virtual Meeting” (2021), p. 9 (cit. on p. 48).
- (Shen *et al.*, 2009) D.K. Shen and S. Gu. “The Mechanism for Thermal Decomposition of Cellulose and Its Main Products”. *Bioresource Technology* 100.24 (Dec. 2009), pp. 6496–6504 (cit. on p. 91).

-
- (Singh *et al.*, 2019) Ajay Kumar Singh and Ram Chandra. “Pollutants Released from the Pulp Paper Industry: Aquatic Toxicity and Their Health Hazards”. *Aquatic Toxicology* 211 (June 2019), pp. 202–216 (cit. on p. 25).
- (Sinha, 2021) Akhouri Sanjay Kumar Sinha. “Formic Acid Pulping Process of Rice Straw for Manufacturing of Cellulosic Fibers with Silica”. *TAPPI Journal* 20.8 (Sept. 1, 2021), pp. 489–496 (cit. on pp. 73, 76).
- (Slopiecka *et al.*, 2012) Katarzyna Slopiecka, Pietro Bartocci, and Francesco Fantozzi. “Thermogravimetric Analysis and Kinetic Study of Poplar Wood Pyrolysis”. *Applied Energy* 97 (Sept. 2012), pp. 491–497 (cit. on p. 91).
- (Solli *et al.*, 2018) Kjell-Arne Solli, Raja Kumar Thapa, and Britt Margrethe Emilie Moldestad. “Screening of Kinetic Rate Equations for Gasification Simulation Models”. Proceedings of The 9th EUROSIM Congress on Modelling and Simulation, EUROSIM 2016, The 57th SIMS Conference on Simulation and Modelling SIMS 2016. Dec. 19, 2018, pp. 105–112 (cit. on p. 158).
- (C. Song *et al.*, 2019) Chunfeng Song, Qingling Liu, Shuai Deng, Hailong Li, and Yutaka Kitamura. “Cryogenic-Based CO₂ Capture Technologies: State-of-the-art Developments and Current Challenges”. *Renewable and Sustainable Energy Reviews* 101 (Mar. 2019), pp. 265–278 (cit. on p. 49).
- (T. Song *et al.*, 2012) Tao Song, Jiahua Wu, Laihong Shen, and Jun Xiao. “Experimental Investigation on Hydrogen Production from Biomass Gasification in Interconnected Fluidized Beds”. *Biomass and Bioenergy* 36 (Jan. 2012), pp. 258–267 (cit. on p. 136).
- (Soomro *et al.*, 2018) Ahsanullah Soomro, Shiyi Chen, Shiwei Ma, Changchun Xu, Zhao Sun, and Wenguo Xiang. “Elucidation of Syngas Composition from Catalytic Steam Gasification of Lignin, Cellulose, Actual and Simulated Biomasses”. *Biomass and Bioenergy* 115 (Aug. 2018), pp. 210–222 (cit. on pp. 39, 40, 42, 43).
- (P. Spath *et al.*, 2005) P Spath, A Aden, T Eggeman, M Ringer, B Wallace, and J Jechura. *Biomass to Hydrogen Production Detailed Design and Economics Utilizing the Battelle Columbus Laboratory Indirectly-Heated Gasifier*. NREL/TP-510-37408, 15016221. May 1, 2005, NREL/TP-510–37408, 15016221 (cit. on p. 160).
- (P. L. Spath *et al.*, 2003) P L Spath and D C Dayton. “Preliminary Screening – Technical and Economic Assessment of Synthesis Gas to Fuels and Chemicals with Emphasis on the Potential for Biomass-Derived Syngas” (2003), p. 160 (cit. on pp. 44, 45).
- (Staffell *et al.*, 2019) Iain Staffell, Daniel Scamman, Anthony Velazquez Abad, Paul Balcombe, Paul E. Dodds, Paul Ekins, Nilay Shah, and Kate R. Ward. “The Role of Hydrogen and Fuel Cells in the Global Energy System”. *Energy & Environmental Science* 12.2 (2019), pp. 463–491 (cit. on p. 166).
- (Stephen Nalley *et al.*, 2021) Stephen Nalley and Angelina LaRose. *International Energy Outlook 2021*. Oct. 2021, p. 21 (cit. on p. 11).

- (Strandberg *et al.*, 2017) Anna Strandberg, Per Holmgren, David R. Wagner, Roger Molinder, Henrik Wiinikka, Kentaro Umeki, and Markus Broström. “Effects of Pyrolysis Conditions and Ash Formation on Gasification Rates of Biomass Char”. *Energy & Fuels* 31.6 (June 15, 2017), pp. 6507–6514 (cit. on p. 104).
- (Su *et al.*, 2008) S Su, W Li, Z Bai, and H Xiang. “A Preliminary Study of a Novel Catalyst $\text{Al}_2\text{O}_3 \cdot \text{Na}_2\text{O} \cdot x\text{H}_2\text{O}/\text{NaOH}/\text{Al}(\text{OH})_3$ for Production of Hydrogen and Hydrogen-Rich Gas by Steam Gasification from Cellulose”. *International Journal of Hydrogen Energy* 33.23 (Dec. 2008), pp. 6947–6952 (cit. on p. 40).
- (Shen Su *et al.*, 2010) Shen Su, Wen Li, Zongqing Bai, Hongwei Xiang, and Jin Bai. “Effects of Ionic Catalysis on Hydrogen Production by the Steam Gasification of Cellulose”. *International Journal of Hydrogen Energy* 35.10 (May 2010), pp. 4459–4465 (cit. on p. 40).
- (Tang *et al.*, 2022a) Genyang Tang, Jing Gu, Zhen Huang, Haoran Yuan, and Yong Chen. “Cellulose Gasification with Ca–Fe Oxygen Carrier in Chemical-Looping Process”. *Energy* 239 (Jan. 2022), p. 122204 (cit. on pp. 40, 41, 43).
- (Tang *et al.*, 2022b) Genyang Tang, Jing Gu, Guoqiang Wei, Zhen Huang, Jiahuan Wu, Haoran Yuan, and Yong Chen. “Syngas Production from Cellulose Solid Waste by Enhanced Chemical Looping Gasification Using Ca-Fe Bimetallic Oxygen Carrier with Porous Structure”. *Fuel* 322 (Aug. 2022), p. 124106 (cit. on pp. 41, 43).
- (Tchini Severin Tanoh, 2021) Tchini Severin Tanoh. “Production d’un Syngaz Par Pyrogazéification de Biomasse En Vue d’une Biométhanation”. Theses. Ecole des Mines d’Albi-Carmaux, Mar. 2021 (cit. on p. 56).
- (Tchini Séverin Tanoh *et al.*, 2020) Tchini Séverin Tanoh, Amina Ait Oumeziane, Jérôme Lemonon, Francisco Javier Escudero Sanz, and Sylvain Salvador. “Green Waste/Wood Pellet Pyrolysis in a Pilot-Scale Rotary Kiln: Effect of Temperature on Product Distribution and Characteristics”. *Energy & Fuels* 34.3 (Mar. 19, 2020), pp. 3336–3345 (cit. on pp. 126, 127).
- (Thengane *et al.*, 2019) Sonal K. Thengane, Ankita Gupta, and Sanjay M. Mahajani. “Co-Gasification of High Ash Biomass and High Ash Coal in Downdraft Gasifier”. *Bioresource Technology* 273 (Feb. 2019), pp. 159–168 (cit. on p. 110).
- (G. Tian *et al.*, 2019) Guoyu Tian, Jiayun Xu, Yingjuan Fu, Yanzhu Guo, Zhaojiang Wang, and Qun Li. “High β -O-4 Polymeric Lignin and Oligomeric Phenols from Flow-through Fractionation of Wheat Straw Using Recyclable Aqueous Formic Acid”. *Industrial Crops and Products* 131 (May 2019), pp. 142–150 (cit. on p. 74).
- (T. Tian *et al.*, 2017) Tian Tian, Qinghai Li, Rong He, Zhongchao Tan, and Yanguo Zhang. “Effects of Biochemical Composition on Hydrogen Production by Biomass Gasification”. *International Journal of Hydrogen Energy* 42.31 (Aug. 2017), pp. 19723–19732 (cit. on pp. 39, 41).

-
- (Timilsina *et al.*, 2010) Govinda R. Timilsina and Jay J. Cheng. *Advanced Biofuel Technologies : Status and Barriers*. Policy Research Working Papers. The World Bank, Sept. 29, 2010 (cit. on p. 21).
- (Tomaszewicz *et al.*, 2017) Martyna Tomaszewicz, Grzegorz Tomaszewicz, and Marek Sciazko. “Experimental Study on Kinetics of Coal Char–CO₂ Reaction by Means of Pressurized Thermogravimetric Analysis”. *Journal of Thermal Analysis and Calorimetry* 130.3 (Dec. 2017), pp. 2315–2330 (cit. on p. 114).
- (Torres *et al.*, 2007) Walter Torres, Sourabh S. Pansare, and James G. Goodwin. “Hot Gas Removal of Tars, Ammonia, and Hydrogen Sulfide from Biomass Gasification Gas”. *Catalysis Reviews* 49.4 (Oct. 2007), pp. 407–456 (cit. on p. 45).
- (Tu *et al.*, 2008) Qiliang Tu, Shiyu Fu, Huaiyu Zhan, Xinsheng Chai, and Lucian A. Lucia. “Kinetic Modeling of Formic Acid Pulping of Bagasse”. *Journal of Agricultural and Food Chemistry* 56.9 (May 2008), pp. 3097–3101 (cit. on p. 73).
- (Turn *et al.*, 2007) S Turn, C Kinoshita, Z ZHANGt, D Ishimura, and J Zhou. “An Experimental Investigation of Hydrogen Production from Biomass Gasification” (Aug. 2007), p. 9 (cit. on p. 132).
- (Uehara, n.d.) Itsuki Uehara. “Separation and Purification of Hydrogen” (), p. 7 (cit. on p. 49).
- (Vallejos *et al.*, 2015) María Evangelina Vallejos, Marcia Dib Zambon, María Cristina Area, and Antonio Aprigio da Silva Curvelo. “Low Liquid-Solid Ratio Fractionation of Sugarcane Bagasse by Hot Water Autohydrolysis and Organosolv Delignification”. *Industrial Crops and Products* 65 (Mar. 2015), pp. 349–353 (cit. on p. 26).
- (Vassilev *et al.*, 2010) Stanislav V. Vassilev, David Baxter, Lars K. Andersen, and Christina G. Vassileva. “An Overview of the Chemical Composition of Biomass”. *Fuel* 89.5 (May 2010), pp. 913–933 (cit. on p. 21).
- (Vyazovkin *et al.*, 2011) Sergey Vyazovkin, Alan K. Burnham, José M. Criado, Luis A. Pérez-Maqueda, Crisan Popescu, and Nicolas Sbirrazzuoli. “ICTAC Kinetics Committee Recommendations for Performing Kinetic Computations on Thermal Analysis Data”. *Thermochimica Acta* 520.1-2 (June 2011), pp. 1–19 (cit. on pp. 84, 96).
- (Q. M. K. Waheed *et al.*, 2013) Qari M. K. Waheed and Paul T. Williams. “Hydrogen Production from High Temperature Pyrolysis/Steam Reforming of Waste Biomass: Rice Husk, Sugar Cane Bagasse, and Wheat Straw”. *Energy & Fuels* 27.11 (Nov. 21, 2013), pp. 6695–6704 (cit. on p. 133).
- (Q. M. Waheed *et al.*, 2016) Qari M.K. Waheed, Chunfei Wu, and Paul T. Williams. “Hydrogen Production from High Temperature Steam Catalytic Gasification of Bio-Char”. *Journal of the Energy Institute* 89.2 (May 2016), pp. 222–230 (cit. on pp. 124, 132, 136).

- (I.-C. Wang *et al.*, 1993) I-Chen Wang, Mon-Lin Kuo, and Yun-Chuan Ku. “[Alcohol Pulping of Plantation Taiwania and Eucalyptus. I. Pulping and Pulp Properties](#)” (1993) (cit. on p. 75).
- (Jianqiao Wang *et al.*, 2019) Jianqiao Wang, Boxiong Shen, Dongrui Kang, Peng Yuan, and Chunfei Wu. “[Investigate the Interactions between Biomass Components during Pyrolysis Using In-Situ DRIFTS and TGA](#)”. *Chemical Engineering Science* 195 (Feb. 2019), pp. 767–776 (cit. on p. 38).
- (Jiawei Wang *et al.*, 2021) Jiawei Wang, Eiji Minami, Mohd Asmadi, and Haruo Kawamoto. “[Effect of Delignification on Thermal Degradation Reactivities of Hemicellulose and Cellulose in Wood Cell Walls](#)”. *Journal of Wood Science* 67.1 (Dec. 2021), p. 19 (cit. on p. 89).
- (Jie Wang *et al.*, 2009) Jie Wang, Mingquan Jiang, Yihong Yao, Yanmei Zhang, and Jianqin Cao. “[Steam Gasification of Coal Char Catalyzed by K₂CO₃ for Enhanced Production of Hydrogen without Formation of Methane](#)”. *Fuel* 88.9 (Sept. 2009), pp. 1572–1579 (cit. on p. 124).
- (Jingbo Wang *et al.*, 2013) Jingbo Wang, Bo Xiao, Shiming Liu, Zhiquan Hu, Piwen He, Dabin Guo, Mian Hu, Fangjie Qi, and Siyi Luo. “[Catalytic Steam Gasification of Pig Compost for Hydrogen-Rich Gas Production in a Fixed Bed Reactor](#)”. *Bioresource Technology* 133 (Apr. 2013), pp. 127–133 (cit. on p. 133).
- (S. Wang *et al.*, 2011) Shurong Wang, Xiujuan Guo, Kaige Wang, and Zhongyang Luo. “[Influence of the Interaction of Components on the Pyrolysis Behavior of Biomass](#)”. *Journal of Analytical and Applied Pyrolysis* 91.1 (May 2011), pp. 183–189 (cit. on p. 38).
- (W. Wang *et al.*, 2022) Weimin Wang, Guanqun Luo, Yuan Zhao, Yuanjun Tang, Kaige Wang, Xuan Li, and Yousheng Xu. “[Kinetic and Thermodynamic Analyses of Co-Pyrolysis of Pine Wood and Polyethylene Plastic Based on Fraser-Suzuki Deconvolution Procedure](#)”. *Fuel* 322 (Aug. 2022), p. 124200 (cit. on p. 91).
- (Wertz *et al.*, 2016) Jean-Luc Wertz, Aurore Richel, and Patrick Gerin. « [Prétraitements de la biomasse lignocellulosique](#) » (Feb. 2016), p. 58 (cit. on p. 27).
- (Wiinikka *et al.*, 2010) Henrik Wiinikka, Per Carlsson, Fredrik Granberg, Johan Löfström, Magnus Marklund, Ragnar Tegman, Mats Lindblom, and Rikard Gebart. “[Design and Methodology of a High Temperature Gas Sampling System for Pressurized Black Liquor Gasification](#)”. *Fuel* 89.9 (Sept. 2010), pp. 2583–2591 (cit. on p. 25).
- (Wildschut *et al.*, 2013) Jelle Wildschut, Arjan T. Smit, Johannes H. Reith, and Wouter J.J. Huijgen. “[Ethanol-Based Organosolv Fractionation of Wheat Straw for the Production of Lignin and Enzymatically Digestible Cellulose](#)”. *Bioresource Technology* 135 (May 2013), pp. 58–66 (cit. on p. 26).

-
- (Williams *et al.*, n.d.) Robert B Williams and Stephen Kaffka. “California Biomass Collaborative / California Renewable Energy Collaborative University of California One Shields Ave. Davis, CA 95616” (), p. 46 (cit. on p. 32).
- (Woolcock *et al.*, 2013) Patrick J. Woolcock and Robert C. Brown. “[A Review of Cleaning Technologies for Biomass-Derived Syngas](#)”. *Biomass and Bioenergy* 52 (May 2013), pp. 54–84 (cit. on p. 45).
- (Wu *et al.*, 2013a) Chunfei Wu, Zichun Wang, Valerie Dupont, Jun Huang, and Paul T. Williams. “[Nickel-Catalysed Pyrolysis/Gasification of Biomass Components](#)”. *Journal of Analytical and Applied Pyrolysis* 99 (Jan. 2013), pp. 143–148 (cit. on p. 43).
- (Wu *et al.*, 2013b) Chunfei Wu, Zichun Wang, Jun Huang, and Paul T. Williams. “[Pyrolysis/Gasification of Cellulose, Hemicellulose and Lignin for Hydrogen Production in the Presence of Various Nickel-Based Catalysts](#)”. *Fuel* 106 (Apr. 2013), pp. 697–706 (cit. on pp. 39, 41–43).
- (Xiao *et al.*, 2017) Yahui Xiao, Shaoping Xu, Yangbo Song, Yiyuan Shan, Chao Wang, and Guangyong Wang. “[Biomass Steam Gasification for Hydrogen-Rich Gas Production in a Decoupled Dual Loop Gasification System](#)”. *Fuel Processing Technology* 165 (Oct. 2017), pp. 54–61 (cit. on p. 130).
- (C. (Xu *et al.*, 2010) Chunbao (Charles) Xu, Jaclyn Donald, Enkhsaruul Byambajav, and Yasuo Ohtsuka. “[Recent Advances in Catalysts for Hot-Gas Removal of Tar and NH₃ from Biomass Gasification](#)”. *Fuel* 89.8 (Aug. 2010), pp. 1784–1795 (cit. on p. 142).
- (J. Xu *et al.*, 2020) Jiayun Xu, Chenyu Li, Lin Dai, Chunlin Xu, Yongda Zhong, Faxin Yu, and Chuanling Si. “[Biomass Fractionation and Lignin Fractionation towards Lignin Valorization](#)”. *ChemSusChem* 13.17 (Sept. 7, 2020), pp. 4284–4295 (cit. on p. 25).
- (Yadav *et al.*, 2021) Sanjeev Yadav, Dharminder Singh, Pravakar Mohanty, and Prakash Kumar Sarangi. “[Biochemical and Thermochemical Routes of H₂ Production from Food Waste: A Comparative Review](#)”. *Chemical Engineering & Technology* (June 28, 2021), ceat.202000526 (cit. on pp. 3, 14).
- (Yan *et al.*, 2010a) Feng Yan, Si-yi Luo, Zhi-quan Hu, Bo Xiao, and Gong Cheng. “[Hydrogen-Rich Gas Production by Steam Gasification of Char from Biomass Fast Pyrolysis in a Fixed-Bed Reactor: Influence of Temperature and Steam on Hydrogen Yield and Syngas Composition](#)”. *Bioresource Technology* 101.14 (July 2010), pp. 5633–5637 (cit. on pp. 130, 132, 136).

- (Yan *et al.*, 2010b) Feng Yan, Leguan Zhang, Zhiquan Hu, Gong Cheng, Chengcheng Jiang, Yanli Zhang, Tao Xu, Piwen He, Siyi Luo, and Bo Xiao. “Hydrogen-Rich Gas Production by Steam Gasification of Char Derived from Cyanobacterial Blooms (CDCB) in a Fixed-Bed Reactor: Influence of Particle Size and Residence Time on Gas Yield and Syngas Composition”. *International Journal of Hydrogen Energy* 35.19 (Oct. 2010), pp. 10212–10217 (cit. on p. 141).
- (Yang *et al.*, 2007) Haiping Yang, Rong Yan, Hanping Chen, Dong Ho Lee, and Chuguang Zheng. “Characteristics of Hemicellulose, Cellulose and Lignin Pyrolysis”. *Fuel* 86.12-13 (Aug. 2007), pp. 1781–1788 (cit. on pp. 37, 38, 88, 91, 125).
- (Yeo *et al.*, 2019) Jun Yi Yeo, Bridgid Lai Fui Chin, Jun Kit Tan, and Ying Sheng Loh. “Comparative Studies on the Pyrolysis of Cellulose, Hemicellulose, and Lignin Based on Combined Kinetics”. *Journal of the Energy Institute* 92.1 (Feb. 2019), pp. 27–37 (cit. on pp. 96, 97, 99).
- (Yip *et al.*, 2010) Kongvui Yip, Fujun Tian, Jun-ichiro Hayashi, and Hongwei Wu. “Effect of Alkali and Alkaline Earth Metallic Species on Biochar Reactivity and Syngas Compositions during Steam Gasification”. *Energy Fuels* (2010), p. 9 (cit. on pp. 119, 139).
- (Yoon *et al.*, 2012) Hyung Chul Yoon, Peter Pozivil, and Aldo Steinfeld. “Thermogravimetric Pyrolysis and Gasification of Lignocellulosic Biomass and Kinetic Summative Law for Parallel Reactions with Cellulose, Xylan, and Lignin”. *Energy & Fuels* 26.1 (Jan. 19, 2012), pp. 357–364 (cit. on p. 39).
- (G. Yu *et al.*, 2013) Guang Yu, Bin Li, Chao Liu, Yuedong Zhang, Haisong Wang, and Xindong Mu. “Fractionation of the Main Components of Corn Stover by Formic Acid and Enzymatic Saccharification of Solid Residue”. *Industrial Crops and Products* 50 (Oct. 2013), pp. 750–757 (cit. on p. 73).
- (H. Yu *et al.*, 2018) Haimiao Yu, Zilu Wu, and Geng Chen. “Catalytic Gasification Characteristics of Cellulose, Hemicellulose and Lignin”. *Renewable Energy* 121 (June 2018), pp. 559–567 (cit. on pp. 37, 39, 40).
- (H. Yu *et al.*, 2014) Haimiao Yu, Ze Zhang, Zeshen Li, and Dezhen Chen. “Characteristics of Tar Formation during Cellulose, Hemicellulose and Lignin Gasification”. *Fuel* 118 (Feb. 2014), pp. 250–256 (cit. on pp. 39, 41).
- (Jie Yu *et al.*, 2017) Jie Yu, Nigel Paterson, John Blamey, and Marcos Millan. “Cellulose, Xylan and Lignin Interactions during Pyrolysis of Lignocellulosic Biomass”. *Fuel* 191 (Mar. 2017), pp. 140–149 (cit. on pp. 38, 39).
- (Junqin Yu *et al.*, 2021) Junqin Yu, Qinghua Guo, Yan Gong, Lu Ding, Jiajian Wang, and Guangsuo Yu. “A Review of the Effects of Alkali and Alkaline Earth Metal Species on Biomass Gasification”. *Fuel Processing Technology* 214 (Apr. 2021), p. 106723 (cit. on p. 138).

-
- (T. Yu *et al.*, 2020) Tao Yu, Abulikemu Abudukeranmu, Aisikaer Anniwaer, Yohanes Andre Situmorang, Akihiro Yoshida, Xiaogang Hao, Yutaka Kasai, Abuliti Abudula, and Guoqing Guan. “[Steam Gasification of Biochars Derived from Pruned Apple Branch with Various Pyrolysis Temperatures](#)”. *International Journal of Hydrogen Energy* 45.36 (July 2020), pp. 18321–18330 (cit. on p. 133).
- (Yukesh Kannah *et al.*, 2021) R. Yukesh Kannah, S. Kavitha, Preethi, O. Parthiba Karthikeyan, Gopalakrishnan Kumar, N. Vo. Dai-Viet, and J. Rajesh Banu. “[Techno-Economic Assessment of Various Hydrogen Production Methods – A Review](#)”. *Biore-source Technology* 319 (Jan. 2021), p. 124175 (cit. on pp. 3, 14).
- (K. Zeng *et al.*, 2015) Kuo Zeng, Doan Pham Minh, Daniel Gauthier, Elsa Weiss-Hortala, Ange Nzihou, and Gilles Flamant. “[The Effect of Temperature and Heating Rate on Char Properties Obtained from Solar Pyrolysis of Beech Wood](#)”. *Biore-source Technology* 182 (Apr. 2015), pp. 114–119 (cit. on p. 112).
- (X. Zeng *et al.*, 2021) Xi Zeng, Mengxiang Fang, Tong Lv, Jianglei Tian, Zhixiang Xia, Jianmeng Cen, and Qinhui Wang. “[Enhanced Hydrogen Production by the Catalytic Alkaline Thermal Gasification of Cellulose with Ni/Fe Dual-Functional CaO Based Catalysts](#)”. *International Journal of Hydrogen Energy* 46.65 (Sept. 2021), pp. 32783–32799 (cit. on pp. 39, 41, 43).
- (K. Zhang *et al.*, 2016) Ke Zhang, Zhijian Pei, and Donghai Wang. “[Organic Solvent Pretreatment of Lignocellulosic Biomass for Biofuels and Biochemicals: A Review](#)”. *Biore-source Technology* 199 (Jan. 2016), pp. 21–33 (cit. on p. 25).
- (M. Zhang *et al.*, 2010) Mingjia Zhang, Wei Qi, Rui Liu, Rongxin Su, Shaomin Wu, and Zhimin He. “[Fractionating Lignocellulose by Formic Acid: Characterization of Major Components](#)”. *Biomass and Bioenergy* 34.4 (Apr. 2010), pp. 525–532 (cit. on p. 74).
- (S. Zhang *et al.*, 2022) Shuming Zhang, Su He, Ningbo Gao, Jianqiao Wang, Yihang Duan, Cui Quan, Boxiong Shen, and Chunfei Wu. “[Hydrogen Production from Autothermal CO₂ Gasification of Cellulose in a Fixed-Bed Reactor: Influence of Thermal Compensation from CaO Carbonation](#)”. *International Journal of Hydrogen Energy* (Feb. 2022), S0360319922005419 (cit. on pp. 40, 43).
- (Zhang *et al.*, 2008) Y Zhang, M Ashizawa, S Kajitani, and K Miura. “Proposal of a Semi-Empirical Kinetic Model to Reconcile with Gasification Reactivity Profiles of Biomass Chars” (2008), p. 7 (cit. on pp. 110, 111, 114).
- (Y.-H. P. Zhang, 2008) Y.-H. Percival Zhang. “[Reviving the Carbohydrate Economy via Multi-Product Lignocellulose Biorefineries](#)”. *Journal of Industrial Microbiology & Biotechnology* 35.5 (May 2008), pp. 367–375 (cit. on p. 25).
- (Yang Zhang *et al.*, 2014) Yang Zhang, Xun Gong, Biao Zhang, Wenqiang Liu, and Minghou Xu. “[Potassium Catalytic Hydrogen Production in Sorption Enhanced Gasification of Biomass with Steam](#)”. *International Journal of Hydrogen Energy* 39.9 (Mar. 2014), pp. 4234–4243 (cit. on p. 138).

- (Yuming Zhang *et al.*, 2020) Yuming Zhang, Lifeng Wan, Juntao Guan, Qing'an Xiong, Shu Zhang, and Xin Jin. “[A Review on Biomass Gasification: Effect of Main Parameters on Char Generation and Reaction](#)”. *Energy & Fuels* 34.11 (Nov. 19, 2020), pp. 13438–13455 (cit. on p. 103).
- (Z. Zhang *et al.*, 2016) Zhanying Zhang, Mark D. Harrison, Darryn W. Rackemann, William O. S. Doherty, and Ian M. O’Hara. “[Organosolv Pretreatment of Plant Biomass for Enhanced Enzymatic Saccharification](#)”. *Green Chemistry* 18.2 (2016), pp. 360–381 (cit. on pp. 26, 27).
- (C. Zhao *et al.*, 2017) Chenxi Zhao, Enchen Jiang, and Aihui Chen. “[Volatile Production from Pyrolysis of Cellulose, Hemicellulose and Lignin](#)”. *Journal of the Energy Institute* 90.6 (Dec. 2017), pp. 902–913 (cit. on pp. 38, 125).
- (X. Zhao *et al.*, 2017) Xuebing Zhao, Siming Li, Ruchun Wu, and Dehua Liu. “[Organosolv Fractionating Pre-treatment of Lignocellulosic Biomass for Efficient Enzymatic Saccharification: Chemistry, Kinetics, and Substrate Structures](#)”. *Biofuels, Bioproducts and Biorefining* 11.3 (May 2017), pp. 567–590 (cit. on pp. 25, 26).
- (Zhou *et al.*, 2013) Hui Zhou, YanQiu Long, AiHong Meng, QingHai Li, and YanGuo Zhang. “[The Pyrolysis Simulation of Five Biomass Species by Hemi-Cellulose, Cellulose and Lignin Based on Thermogravimetric Curves](#)”. *Thermochimica Acta* 566 (Aug. 2013), pp. 36–43 (cit. on p. 88).
- (Zou *et al.*, 2018) Jun Zou, Japhet Oladipo, Shilong Fu, Amal Al-Rahbi, Haiping Yang, Chunfei Wu, Ning Cai, Paul Williams, and Hanping Chen. “[Hydrogen Production from Cellulose Catalytic Gasification on CeO₂/Fe₂O₃ Catalyst](#)”. *Energy Conversion and Management* 171 (Sept. 2018), pp. 241–248 (cit. on pp. 41, 43).
- (Zou *et al.*, 2016) Jun Zou, Haiping Yang, Zhiwei Zeng, Chunfei Wu, Paul T. Williams, and Hanping Chen. “[Hydrogen Production from Pyrolysis Catalytic Reforming of Cellulose in the Presence of K Alkali Metal](#)”. *International Journal of Hydrogen Energy* 41.25 (July 2016), pp. 10598–10607 (cit. on pp. 40, 41, 43).

Glossary

- A** Pre-exponential factor 84, 96, 99, 105, 112, 116
- AAEM** Alkali and alkaline earth metals 6, 38, 40, 76, 80, 103, 108, 109, 111, 117, 120, 129, 138, 139, 142, 143, 169
- ARC** ArboCell JRS 8, 54, 66, 124, 125, 129, 130, 132, 133, 136, 139, 140, 145, 175, 178
- Cell-SS-A** Alkaline Washed cellulose from Cell-SS-P 61, 80, 103, 117, 119
- Cell-SS-L** Cellulose extracted from Softwood Sawdust at a Lab scale 58, 63, 76
- Cell-SS-P** Cellulose extracted from Softwood Sawdust at a Pilot scale 61, 63, 66, 71, 76, 80, 81, 84, 88, 89, 96, 97, 103, 106, 109, 111, 112, 114, 116, 117, 123–125, 127, 129, 130, 132, 133, 136, 138–143, 145, 174, 175, 178
- Cell-WS-L** Cellulose extracted from Wheat Straw at a Lab scale 58, 63, 74, 76, 84, 88, 89, 96, 97, 103, 106, 109, 111, 112, 114, 116, 117
- CGE** Cold Gas Efficiency 132
- CI** Crystallinity Index 89, 101
- DM** Dry Matter 60, 61
- dTG** Difference Thermo Gravimetry 63, 88, 89, 174
- Ea** activation Energy 84, 86, 93, 96, 99, 105, 112, 116, 174
- FA** Formic Acid 58, 60, 72–74, 76, 80, 152, 154
- GC-MS** Gas Chromatography – Mass Spectrometer 69, 125, 140
- HHV** High heating value 56, 132
- KAS** Kissinger–Akahira–Sunose 84, 85, 93, 96
- Kn** Kappa number 58–60, 73

LEEBIO Low Energy Extraction of BIOmass 5–10, 16, 50, 51, 54, 58, 61, 71–74, 84, 103, 120, 123, 127, 139–143, 169–171, 173

MCC Microcrystalline Cellulose 54, 63, 84, 85, 88, 89, 91, 96, 97, 101

PAH Polycyclic aromatic hydrocarbons 30, 39–41

PSA Pressure swing adsorption 47, 152, 159

R^2 Correlation Coefficient 89, 93

RMSE Root Mean Square Error 160

S/C Steam to Carbon ratio 129, 130, 132, 136, 160, 174, 175

S/L solid:liquid ratio 26

SEM Scanning Electron Microscopy 57, 112

SS Softwood Sawdust 6, 8, 54, 58, 60, 61, 63, 66, 71–76, 80, 103, 106, 109, 112, 114, 117, 129, 130, 132, 133, 136, 138–140, 142, 143, 145, 169, 175, 178

TEM Transmission Electron Microscopy 57, 76, 81, 145, 175

TG Thermogravimetry 63, 88, 174

TGA Thermogravimetric Analysis 7, 8, 38, 54, 63, 65, 83, 84, 89, 104, 105, 120, 169–171

WGR Water-gas reaction 127–129, 132, 133, 138, 139

WGSR Water-gas shift reaction 39–41, 45, 127, 128, 132, 133, 139, 140, 156, 158, 159

WS Wheat Straw 6, 54, 58, 63, 66, 71–76, 103, 106, 109, 111, 112, 114, 117, 169

XRD X-ray Diffraction 57, 101

Résumé

Gazéification de la cellulose pour la production d'un syngas riche en hydrogène - Une approche bioraffinerie

Ce travail porte sur la gazéification à la vapeur de la cellulose pour la production de gaz de synthèse riche en hydrogène dans le contexte du développement de bioraffinerie. La paille de blé et de la sciure de bois résineux ont été sélectionnées et fractionnées sous un procédé organosolv utilisant de l'acide formique sous des conditions opératoires modérées à l'échelle laboratoire et pilote. Des différences ont été observées dans la composition minérale de la biomasse et de la cellulose en raison de l'extraction en milieu acide. Si était le principal élément inorganique inhérent présent dans la cellulose.

La cinétique de la gazéification à la vapeur d'eau a été étudiée par analyse thermogravimétrique. La réactivité du char de cellulose était plus faible que celle du char de la biomasse, en raison de leur composition inorganique, en particulier les métaux alcalins et alcalino-terreux et du Si. Le comportement de gazéification du char de cellulose était principalement régi par la teneur en Si. Par la suite, une nouvelle approche de modélisation basée sur la concentration en Si a été proposée pour prédire la cinétique de gazéification de la biomasse et de la cellulose.

La gazéification à la vapeur du biochar a été aussi étudiée dans un réacteur à lit fixe à l'échelle laboratoire. L'augmentation du ratio vapeur/carbone a permis d'augmenter la conversion du carbone et d'améliorer le rendement en gaz. L'ajout de vapeur peut améliorer le rendement et la concentration de H₂ par les réactions gazéification à la vapeur d'eau et de gaz à l'eau. L'augmentation de la température a été bénéfique pour la production de H₂. Cependant, la concentration de H₂ dans le gaz de synthèse diminue à une température plus élevée en raison de la réaction du gaz à l'eau inverse. Par rapport aux chars de la biomasse et de la cellulose commerciale, la conversion du carbone et le rendement en H₂ des chars de cellulose extraite étaient plus faibles à 750 et 850 °C en raison de la teneur élevée en Si qui a fortement entravé les réactions carbone-gaz. A 950 °C, un gaz sans azote contenant plus de 55% de H₂ et plus de 30% de CO a été produit à partir de la cellulose organosolv. Les résultats ont démontré que les composés alcalins, en particulier K, peuvent être capturés par la silice dans le solide, ce qui empêche leur chargement dans le gaz de production. Enfin, les procédés organosolv et de pyrogazéification ont été simulés afin de proposer une intégration énergétique du système global pour une implantation à grande échelle.

Mots-clés : Biomasse lignocellulosique, Organosolv, Cellulose, Gazéification à la vapeur, Cinétique de gazéification, Gaz de synthèse riche en hydrogène

Abstract

Hydrogen-rich syngas from steam gasification of cellulose in a biorefinery approach

This work deals with steam gasification of cellulose for hydrogen-rich syngas production in the context of integrated biorefinery. Wheat straw and softwood sawdust were selected and fractionated using an organosolv pretreatment using formic acid at moderate operating conditions at lab and pilot scales. Drastic differences were displayed in the mineral composition of raw biomass and cellulose due to the acid medium extraction. Silicon was the main inherent inorganic element present in cellulose.

Steam gasification was studied at experimental level with thermogravimetric analysis. The reactivity of cellulose char was lower than that of biomass char, owing to the difference in the inorganic content, in particular alkali and alkaline-earth metals (AAEM) and Si. The gasification behavior of cellulose char was predominantly governed by Si concentration. A new modeling approach based on Si concentration was proposed to predict gasification behavior of lignocellulosic biomass and cellulose chars.

At lab scale, steam gasification experiments of biochar were carried out in a fixed-bed reactor under different experimental conditions. Increasing steam to carbon ratio boosted carbon conversion yielding to an enhancement in gas yield. Adding steam can improve H₂ yield and concentration through water gas and water gas shift reactions. However, excessive steam addition was harmful for gasification process. Higher temperature was beneficial for H₂ production. Nevertheless, H₂ fraction decreased at higher temperature due to the reverse water gas shift reaction. Compared with biomass and commercial cellulose chars, carbon conversion and H₂ yield of extracted cellulose char were lower at 750 and 850 °C due to high content of Si which exhibited severely hampered on carbon-gas reactions. At 950 °C, free-nitrogen gas containing more than 55% of H₂ and more than 30% of CO was produced from organosolv cellulose. The results demonstrated that alkali compounds in particular K can be captured by silica in the solid preventing its loading in the producer gas.

Finally, the integration of organosolv pretreatment and pyrogasification was simulated to validate the overall process and provides an appropriate opportunity for understanding and constructing the optimum design for large scale establishment.

Keywords: Lignocellulosic biomass, Organosolv, Cellulose, Steam gasification, Gasification kinetics, Hydrogen-rich syngas